UNIVERSIDAD AUTONOMA DE BAJA CALIFORNIA
FACULTAD DE CIENCIAS MARINAS
INSTITUTO DE INVESTIGACIONES OCEANOLOGICAS

MORFODINAMICA ESTACIONAL A INTERANUAL DE UNA BARRA SUBMAREAL EN UNA PLAYA INTERMEDIA

SEASONAL AND INTERANNUAL SUBTIDAL SANDBAR MORPHODYNAMICS ON A INTERMEDIATE BEACH

TESIS

QUE PARA OBTENER EL GRADO DE

DOCTOR EN CIENCIAS EN OCEANOGRAFIA COSTERA

PRESENTA

JESÚS ADRIÁN VIDAL RUIZ

ENSENADA, BAJA CALIFORNIA, MEXICO. ENERO 2020

FACULTAD DE CIENCIAS MARINAS
INSTITUTO DE INVESTIGACIONES OCEANOLOGICAS
POSGRADO EN OCEANOGRAFIA COSTERA

"Morfodinámica estacional a interanual de una barra submareal en una playa intermedia"

TESIS

QUE PARA OBTENER EL GRADO DE

DOCTOR EN CIENCIAS EN OCEANOGRAFIA COSTERA

Presenta

Jesús Adrián Vidal Ruiz

Aprobada por:

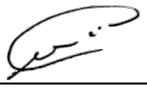

Dra. Amaia Ruíz de Alegría Arzaburu
Director

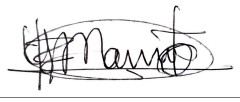

Dr. Ismael de Jesús Mariño Tapia
Co-Director

Dr. Rafael Hernández Walls
Sinodal

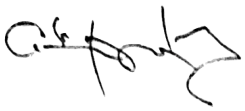

Dr. Adán Mejía Trejo
Sinodal

Dr. David Alberto Rivas Camargo
Sinodal

Agradecimientos

A la Dra. Amaia Ruíz de Alegría Arzaburu por su excepcional dedicación y paciencia al instruirme durante esta importante etapa de mi vida. Por plasmar en mi lo que es ser un investigador comprometido, constante y responsable, que da lo mejor de si en todo momento y ante cualquier circunstancia.

Al Dr. Ismael Mariño por su humildad y objetividad durante las evaluaciones de proyecto y conocimientos. Al Dr. Rafael Hernández por siempre aportar ideas ingeniosas que por tiempo no se pudieron desarrollar, pero quedan pendientes para un futuro. Al Dr. David A. Rivas por su frase: “no concibo la idea de un Dr. que no domine el ingles”, que al principio me intimido y después me motivo. Al Dr. Adán Mejía por su siempre buena disposición en brindarme apoyo, animo y su gran amistad. A todos por su ejemplo como personas integras y profesionales.

Al Super Dream Team: Ernesto Carsolio, Julio Lopez, Eduardo Gil, Angélica Romero, Berenice Soto, Martin Vizcarra, David Gracia, Beatriz Gasalla, Niels van Kuik , Alejandro Domínguez y al sensei Tadashi Kono, por haber hecho posible este trabajo y sobre todo, por su gran amistad y disposición en todo momento que fue requerido.

A mi amada esposa Livier, por ese bello espíritu inquebrantable y perfecto en el amor, por ser mi refugio de paz, mi inspiración y compañera eterna de vida.

A Dios por permitirme nacer de buenos padres, que me han instruido sabiamente y de forma ejemplar: “Y estas palabras que yo te mando hoy estarán sobre tu corazón: amaras a Dios con todo tu corazón y con toda tu alma y con todas tus fuerzas, y se las repetirás a tus hijos y les hablarás de ellas estando en tu casa, y andando por el camino, y cuando te acuestes y cuando te levantes” (Deuteronomio 6: 5-7).

A CONACyT por la beca otorgada y financiamiento de los proyectos de Ciencia Básica y CB-2014-238765, a cargo de la Dra. Amaia Ruíz de Alegría Arzaburu.

Abstract

The primary purpose of this study is to gain a better understanding on the morphodynamic behavior of subtidal sandbars on a single-barred and swell dominated beach. This includes the inter-annual, seasonal and event-driven onshore and offshore sandbar migration patterns, and its relation with the incident wave climate variations. This study was undertaken in Ensenada Beach, located in the Pacific coast of the Baja California peninsula, Mexico, in a mesotidal environment. Monthly measured topographic and bathymetric data were used in combination with nearshore wave measurements collected over a four-year period between August 2014 and September 2018. This research demonstrates that the sandbar moves toward a wave-height dependent equilibrium state in a highly-seasonal manner. The sandbar forms near the shoreline at the beginning of the high wave energy period, it migrates offshore during energetic wave conditions and moves back onshore when calm conditions return. The complete coupling of the sandbar to the shoreline will depend on the offshore location from which it has to migrate onshore. This implies the existence of a dynamic equilibrium position (DEP), offshore of which onshore migration and welding to the shore is not possible. For this beach the DEP was empirically determined to occur at a distance of 150 m from the reference shoreline (equivalent to ~3 m water depth) for an alongshore-averaged maximum sandbar height of 1 m containing up to 100 m^3m^{-1} of sand. Five distinct cross-shore sandbar migration modes were identified, primarily governed by sandbar size (volume and height) and crest location from DEP.

Mode I, after a moderately energetic winter the sandbar is located onshore from DEP and complete sandbar coupling (SC) is possible during the following low wave-energy conditions (summer). Mode II, sandbar to terrace-bar transition (STT): after a highly-energetic winter the sandbar is located offshore from DEP, and during low-energy conditions the sandbar is flattened and turned into a terrace-bar with no onshore attachment. Mode III, terrace-bar to sandbar transition (TST): when located near DEP, the terrace-bar turned into a sandbar after a rebuilding process during moderately energetic conditions. Mode IV, terrace-bar splitting (TS): when located offshore from DEP and under low-energy conditions, the terrace-bar divided into two: the outer section followed a net offshore migration cycle while the inner section migrated towards DEP, and could then follow TST. And Mode V, sandbar and terrace-bar coexistence (STC): it occurred when a new sandbar formed near the shoreline whilst the terrace-bar continued degrading and migrating offshore. These findings contribute to the understanding of onshore sediment transport processes, and the acquired data-set will be further used to validate numerical models and improve their capabilities to predict beach recovery.

Resumen

El objetivo principal de este estudio es obtener un mejor entendimiento sobre el comportamiento morfodinámico de las barras de arena submareales en una playa con una sola barra dominada por el oleaje lejano. Esto incluye los patrones de migración de la barra de arena interanuales, estacionales e impulsados por eventos hacia dentro y fuera de la costa, y su relación con las variaciones del clima del oleaje incidente. Este estudio se realizó en la playa de Ensenada, ubicada en la costa del Pacífico de la península de Baja California, México, en un ambiente mesomareal. Se utilizaron datos topográficos y batimétricos medidos mensualmente en combinación con mediciones de oleaje cerca de la costa recopiladas durante un período de cuatro años entre agosto de 2014 y septiembre de 2018. Esta investigación demuestra que la barra de arena se mueve hacia un estado de equilibrio dependiente de la altura de la ola de manera estacional. La barra de arena se forma cerca de la costa al principio del período de alta energía del oleaje, migra hacia fuera de la costa durante las condiciones de mayor energía y regresa hacia la costa cuando las condiciones de calma vuelven. El completo acoplamiento de la barra de arena a la costa dependerá de la posición mar adentro desde la que tiene que migrar hasta la costa. Esto implica la existencia de una posición de equilibrio dinámico (PED) mar adentro de la cual no es posible la migración hacia tierra y el acoplamiento a la costa. Para esta playa, se determinó empíricamente que la PED ocurría a una distancia de 150 m desde la línea de costa de referencia (equivalente a ~3 profundidad) para una altura máxima de barra promediada a lo largo de la costa

de 1 m que contiene hasta 100 m^3m^{-1} de arena. Se identificaron cinco distintos modos de migración transversal de la barra de arena, gobernados principalmente por el tamaño de la barra (volumen y altura) y la posición de la cresta desde la PED. Modo I, después de un invierno moderadamente enérgico, la barra de arena se encuentra hacia la costa desde la PED y durante las siguientes condiciones de baja energía (verano) es posible el completo acoplamiento de la barra (SC). Modo II, transición de barra a barra tipo terraza (STT): después de un invierno muy enérgico, la barra de arena se encuentra hacia el mar desde la PED, y durante condiciones de baja energía, la barra se aplana y se convierte en una barra tipo terraza sin acoplamiento a la costa. Modo III, transición de barra tipo terraza a barra (TST): cuando se encuentra cerca de la PED, la barra tipo terraza se convirtió en una barra de arena después de un proceso de reconstrucción durante condiciones moderadamente energéticas. Modo IV, división de la barra tipo terraza (TS): cuando se encuentra hacia el mar desde la PED y en condiciones de baja energía, la barra tipo terraza se divide en dos: una sección siguió un ciclo de migración neta mar adentro, mientras la otra sección migró hacia la PED, y después pudo haber continuado con una TST. Y Modo V, coexistencia de barra y terraza-barra (STC): ocurrió cuando se formó una nueva barra de arena cerca de la costa mientras la barra tipo terraza se continuó degradando y migrando hacia mar adentro. Estos hallazgos contribuyen a la comprensión de los procesos de transporte de sedimentos hacia la costa, y el conjunto de datos adquiridos se utilizará para validar modelos numéricos y mejorar sus capacidades para predecir la recuperación de las playas.

ASUNTO: Voto aprobatorio sobre
trabajo de tesis de grado de Doctor.

DRA. IVONE GIFFARD MENA
COORDINADORA DE POSGRADO
E INVESTIGACION, F. C. M.

Presente.-

Después de haber efectuado una revisión minuciosa sobre el trabajo de tesis presentado por el estudiante **Jesús Adrián Vidal Ruiz** para poder presentar la defensa de su examen y obtener el grado de Doctor en Ciencias en Oceanografía Costera, me permito comunicarle que he dado mi voto **Aprobatorio**, sobre su trabajo titulado:

Morfodinámica estacional a interanual de una barra submareal
en una playa intermedia.

Esperando reciba el presente de conformidad, quedo de usted.

Ensenada, B. C., a 24 de enero de 2020

Dra. Amaia Ruíz de Alegría Arzaburu
Director

c. c. p. Expediente

ASUNTO: Voto aprobatorio sobre
trabajo de tesis de grado de Doctor.

DRA. IVONE GIFFARD MENA
COORDINADORA DE POSGRADO
E INVESTIGACION, F. C. M.

Presente.-

Después de haber efectuado una revisión minuciosa sobre el trabajo de tesis presentado por el estudiante **Jesús Adrián Vidal Ruiz** para poder presentar la defensa de su examen y obtener el grado de Doctor en Ciencias en Oceanografía Costera, me permito comunicarle que he dado mi voto **Aprobatorio**, sobre su trabajo titulado:

Morfodinámica estacional a interanual de una barra submareal
en una playa intermedia.

Esperando reciba el presente de conformidad, quedo de usted.

Ensenada, B. C., a 24 de enero de 2020

Dr. Ismael de Jesús Mariño Tapia
Co-director

c. c. p. Expediente

ASUNTO: Voto aprobatorio sobre
trabajo de tesis de grado de Doctor.

DRA. IVONE GIFFARD MENA
COORDINADORA DE POSGRADO
E INVESTIGACION, F. C. M.

Presente.-

Después de haber efectuado una revisión minuciosa sobre el trabajo de tesis presentado por el estudiante **Jesús Adrián Vidal Ruiz** para poder presentar la defensa de su examen y obtener el grado de Doctor en Ciencias en Oceanografía Costera, me permito comunicarle que he dado mi voto **Aprobatorio**, sobre su trabajo titulado:

Morfodinámica estacional a interanual de una barra submareal
en una playa intermedia.

Esperando reciba el presente de conformidad, quedo de usted.

Ensenada, B. C., a 24 de enero de 2020

Dr. Adán Mejía Trejo
Sinodal

c. c. p. Expediente

X

ASUNTO: Voto aprobatorio sobre
trabajo de tesis de grado de Doctor.

DRA. IVONE GIFFARD MENA
COORDINADORA DE POSGRADO
E INVESTIGACION, F. C. M.

Presente.-

Después de haber efectuado una revisión minuciosa sobre el trabajo de tesis presentado por el estudiante **Jesús Adrián Vidal Ruiz** para poder presentar la defensa de su examen y obtener el grado de Doctor en Ciencias en Oceanografía Costera, me permito comunicarle que he dado mi voto **Aprobatorio**, sobre su trabajo titulado:

Morfodinámica estacional a interanual de una barra submareal
en una playa intermedia.

Esperando reciba el presente de conformidad, quedo de usted.

Ensenada, B. C., a 24 de enero de 2020

Dr. David Alberto Rivas Camargo
Sinodal

c. c. p. Expediente

ASUNTO: Voto aprobatorio sobre
trabajo de tesis de grado de Doctor.

DRA. IVONE GIFFARD MENA
COORDINADORA DE POSGRADO
E INVESTIGACION, F. C. M.

Presente.-

Después de haber efectuado una revisión minuciosa sobre el trabajo de tesis presentado por el estudiante **Jesús Adrián Vidal Ruiz** para poder presentar la defensa de su examen y obtener el grado de Doctor en Ciencias en Oceanografía Costera, me permito comunicarle que he dado mi voto **Aprobatorio**, sobre su trabajo titulado:

Morfodinámica estacional a interanual de una barra submareal
en una playa intermedia.

Esperando reciba el presente de conformidad, quedo de usted.

Ensenada, B. C., a 24 de enero de 2020

Dr. Rafael Hernández Walls
Sinodal

c. c. p. Expediente

List of figures

Chapter 1

1 Introduction

1.1 Background

Nearshore morphodynamics refers to the evolution of the land-ocean interface through the interaction between the morphology and hydrodynamics involving sediment transport (Coco and Murray, 2007). Large variety of bedforms results from the constant interaction between sediments, waves and currents at time-scales ranging from intra-wave periods to interannual cycles, and dictated by variations in local environmental settings (Splinter et al., 2018). These morphological features are generally perceived as amplifications on the submerged profile elevation; commonly referred to as sandbars for perturbations of high-amplitude, and terrace-bars for those of low-amplitude, still clearly separated from the shore (Holman and Bowen, 1982; Aagaard et al., 2013). Sandbars are located predominantly inside or just seaward of the surf zone (up to water depths of about 10 m), and thus constitute the first line of natural defense against coastal erosion and flooding on sandy beaches, and contain large amounts of sediment that contribute significantly to the sediment balance on the beach (Senechal et al., 2015).

Beaches can exhibit single or multiple sandbar systems depending on the wave conditions, tidal range, sediment characteristics and topographical gradients (e.g. Masselink and Short, 1993). Most multi-barred beaches sustain a

lack of intra-annual correlation between the incident wave conditions and their seaward movements, and present net offshore migrations (NOM) over periods from a few years to decades (Birkemeier, 1984; Lippmann et al., 1993; Ruessink and Kroon, 1994; Plant et al., 1999; Shand et al., 1999; Aleman et al., 2017). During the interannual migration cycles, sandbars form near the shoreline, migrate offshore until finally decaying at the seaward limit of the surf zone (Ruessink and Kroon, 1994). However, these beaches can present different behaviors. Gently sloping multi-barred beaches have shown continuous landward migration over decades (e.g. Aagaard et al., 2004; Anthony et al. 2006). While sites with NOM dominance presented differences depending on the sandbar volumes; those with large sandbars attained interannual NOM while episodic NOM occurred on beaches with small sandbars (Ruessink et al., 2009).

In contrast to the multi-barred counterparts, single-barred systems have been surprisingly understudied (e.g. Ostrowski et al., 1991; Van de Lageweg et al., 2013; Blossier et al., 2016). Most of the existing knowledge on the behavioral modes of single-barred beaches to the incident wave conditions are based on morphodynamic bar state models, which qualitatively relate observations of bar morphologies at beaches with contrasting environmental conditions (e.g. Wright and Short, 1984; Lippman and Holman, 1990). In general, these models conclude that under highly-energetic wave conditions the sandbar moves seaward and becomes alongshore-uniform, while during subsequent low-energy conditions, the sandbar becomes crescentic and slowly moves shoreward until

welding to the shoreline if low-energy conditions persist (unbarred configuration) (Shepard, 1950; Komar, 1974). This behavior has been documented at a variety of sites in response to both episodic storms and annual wave climate variations (e.g. van de Lageweg et al., 2013; Sénéchal et al., 2015; Ruiz de Alegría-Arzaburu and Vidal-Ruiz, 2018). However high-variability exists in the sandbar behavior during the cross-shore migration process, primarily associated with nearshore slope differences and sandbar volume variations (Aagaard et al., 2004; Van Enckevort et al., 2004).

It is generally accepted that seaward sandbar movements are associated to strong mean offshore currents (bed return flow) occurring under the breaking of highly-energetic waves (e.g. Sallenger et al., 1985; Short, 1999). In contrast, the physical processes behind onshore sandbar migrations are still controversial (Dubarbier et al., 2015; Fernández-Mora et al., 2015). The mechanisms of onshore sandbar migration are associated with weak-to-nonbreaking waves, and induced by wave vertical asymmetry (Hoefel and Elgar, 2003), near-bed wave skewness (Hsu et al., 2006; Ruessink et al., 2007; Fernández-Mora et al., 2015), Stokes drift and/or boundary layer streaming (Henderson et al., 2004). Early attempts to simulate onshore sandbar migration using process-based models under relatively quiescent wave conditions were not completely successful (Roelvink and Brøker, 1993; Van Rijn et al., 2003). Thus, there is a present need to properly integrate these processes into existing models to be able to predict beach recovery and onshore migration of sandbars in time.

Most of the subtidal beach research has focused on the morphodynamics of nearshore bars using video data and/or numerical modelling (Ruessink and Kroon, 1994; Ranasinghe et al., 2004; Sedrati and Anthony, 2007) or short-term beach shape variations during intensive field campaigns (Brander, 1999; Masselink et al., 2008; Coco et al., 2014). Very little effort has been applied to the understanding of the volumetric evolution of the subtidal beach in a time span of months to years, since in situ measurements are expensive and difficult to perform (Aubrey, 1979; Larson and Kraus, 1994; Yates et al., 2009; Roberts et al., 2013; Di Leonardo and Ruggiero, 2015). Consequently, there is a lack of appropriate data (bathymetries) needed for the development and validation of accurate models that could provide a better understanding of generation processes and morphological evolution of sandbars under varying hydrodynamic conditions (e.g. Plant et al., 1999; Hsu et al., 2006; Mariño-Tapia et al., 2007; Walstra et al., 2012; Holman et al., 2016; Ruessink et al., 2016).

The complete understanding of sandbar behavior implies acquiring high-quality morphological data over varying hydrodynamic conditions, concurrently, and over a continuous period of time covering several years. The first studies on sandbar behavior consisted on visual observations focused on understanding changes in two-dimensional (2D) and three-dimensional (3D) sandbar geometry, and these were found to be well correlated to the time-varying wave forcing and/or to preceding morphologic states (Wright et al., 1985; Lippmann and Holman, 1990), which could also result from self-organization patterns (Coco

and Murray, 2007). These studies, however, implied a degree of subjectivity in the process of visually identifying features related to the morphodynamic beach states (Ranasinghe et al., 2004). At present, the studies addressing a quantitative analysis of the sandbar behavior in terms of their position and morphometric characteristics (i.e. sandbar crest depth, distance, height, width and volume) are scarce (Larson and Kraus, 1992; Ruessink and Kroon, 1994; Grunnet and Hoekstra, 2004; Aleman et al., 2017; Cheng and Wang, 2018). Based on monthly measured bathymetric data over a four-year period, this research reports a detailed analysis of sandbar morphometry under varying wave conditions (i.e. calm periods, highly-energetic El Niño winter, extreme storm events) on a single-barred beach located in Ensenada, in the Pacific coast of the Baja California peninsula in Mexico.

1.2 Single sandbar systems

1.2.1 Morphodynamic beach states

For single-barred systems, Wright and Short (1984) developed the most widely accepted and applied beach morphodynamic conceptual model comprising sequential states of bar morphologies based on observations of surf zones with contrasting environmental conditions. Six discrete morphodynamic beach states were described based on field observations: reflective (R); longshore bar and trough (LBT); rhythmic bar and beach (RBB); transverse bar and rip (TBR); low tide terrace (LTT); and, dissipative (D). Further research

efforts demonstrated that the morphodynamic beach transitions from two-dimensional (alongshore-uniform) to three-dimensional (alongshore variability) sandbar morphology were well correlated to the incoming wave forcing and/or to preceding morphologic states (Lippmann and Holman, 1990). Low-energy conditions induce the generation of morphodynamic down-states, characterized by a slow (days to weeks) shoreward sandbar movements that evolve toward a crescentic shape (van Enckvort, 2004; Price and Ruessink, 2011). On the other hand, wave energy increase induces morphodynamic up-states characterized by rapid (hours) seaward sandbar displacements that generate alongshore-uniform (shore-parallel) sandbars and throughs (van Enckvort, 2004; Price and Ruessink, 2011; van de Lageweg et al., 2013) (Fig. 1.1).

1.2.2 Observations on sandbar behavior

Sandbars are very dynamic features studied for many decades due to their relevance on wave energy dissipation and sediment transport processes (e.g. Sallenger et al., 1985; Short, 1999; Hoefel and Elgar, 2003; Hsu et al., 2006; Ruessink et al., 2007). However, detailed investigations on their behavior during their cross-shore displacements are limited (Larson and Kraus, 1992; Ruessink and Kroon, 1994; Grunnet and Hoekstra, 2004; Aleman et al., 2017; Vidal-Ruiz and Ruiz de Alegría-Arzaburu, 2019).

On beaches with high seasonality, cross-shore sandbar displacements are mainly modulated by the incoming wave energy; hence, the beach becomes barred during high-energy conditions and unbarred during periods of low-energy

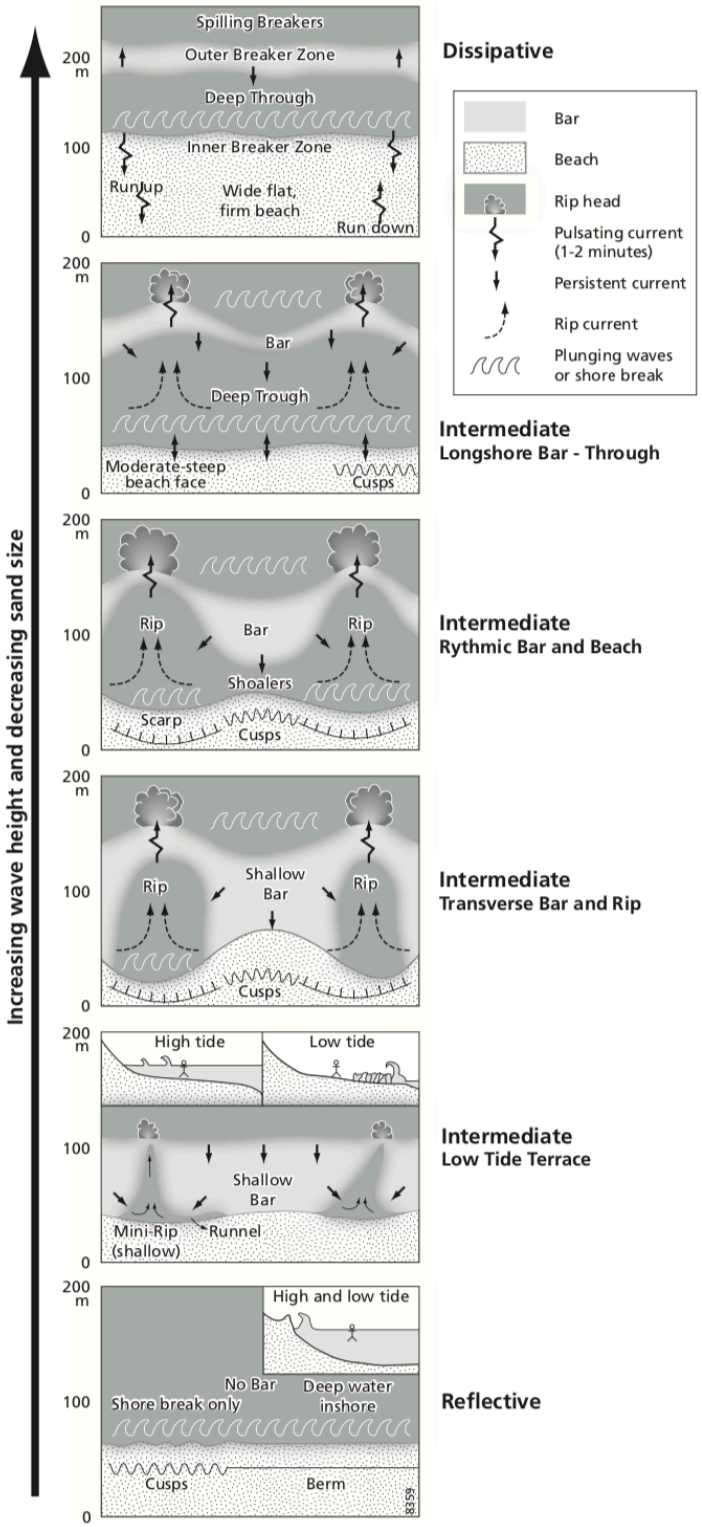

Figure 1.1 Single barred system classification according Wright and Short (1984). Adapted from Wright and Short (1984).

due to the welding of the sandbar to the shoreline (Shepard, 1950; Komar, 1974; Vidal-Ruiz and Ruiz de Alegría-Arzaburu, 2019). Onshore sandbar migrations, however, have also been described on beaches without clear seasonality, during short low-energy periods (e.g. Ostrowski et al., 1991; Larson and Kraus, 1992; Van Maanen et al., 2008; Van de Lageweg et al., 2013; Blossier et al., 2016; Phillips et al., 2017; Cohn et al., 2017; Cheng and Wang, 2018) and on decadal scales (Aagaard et al., 2004; Anthony et al., 2006). But only a few studies have described the morphometric characteristics of the sandbar during the cross-shore migration cycle (Larson and Kraus, 1992; Ruessink and Kroon, 1994; Grunnet and Hoekstra, 2004; Aleman et al., 2017; Cheng and Wang, 2018), which is required to adequately understand the physical processes that induce its behavior under different wave forcing conditions.

Sandbars have been reported to migrate in cycles. Multiple-sandbar systems in sea-wave dominated environments displayed a dominant interannual net offshore migration (NOM) cycle, while similar systems in swell-dominated environments presented onshore and offshore migrations in response to individual wave events (Ruessink et al., 2009). Observations of sandbar variability at different swell-dominated and single-barred beaches (Wright and Short, 1984; Ranasinghe et al., 2004; Holman et al., 2006) have not shown evidences for net offshore migration cycles. Consequently, the same bar formed near the shoreline migrates offshore-onshore in response to the incident wave conditions, and long-term net migration pattern are inexistent (Ojeda et al.,

2011).

Despite the existence of several data-sets with observations on the morphological behavior of sandbars at a variety of environments and time-scales, there is still a need to better understand and parameterize the physical processes associated with onshore sandbar displacements. Short (daily) and long-term (years) data sets of nearshore morphology and hydrodynamic conditions are crucial. Thus, the results of the investigation of these processes are key for improving the capabilities of existing physical and numerical models on predicting sandbar behavior.

1.3 Objectives and thesis outline

The primary purpose of this study is to gain a better understanding on the morphodynamic behavior of the sandbar in a single-barred and swell dominated beach. This research is based on field measurements collected monthly over four years. On one hand, a detailed analysis of the sandbar morphometry is provided during the formation, offshore and onshore seasonal migration cycle. On the other hand, the sandbar behavioral modes during the onshore migration process are described in detailed for a variety of wave conditions.

The structure of the thesis is outlined as follows:

Chapter 2. Describes the field site and presents the data-set and methodology used to quantify the variability in nearshore morphology.

Chapter 3. Describes in detail the cross-shore sandbar migration cycle related to the incoming wave energy, in a seasonal scale, and the perturbations generated by an individual extreme storm and during the highly-energetic El Niño winter.

Chapter 4. Determines the main behavioral modes of the sandbar during its onshore migration process in relation to the dynamic equilibrium position over a range of wave energy conditions.

Chapter 5. Provides a summary of the main research findings and future perspectives.

1.4 References

Aagaard, T., Greenwood, B., & Hughes, M.G. (2013), Sediment transport on dissipative, intermediate and reflective beaches. *Earth-Science Reviews*, 124, 32–50.doi.org/10.1016/j.earscirev.2013.05.002

Aagaard, T., Davidson-Arnott, R., Greenwood, B., & Nielsen, J. (2004), Sediment supply from shoreface to dunes: linking sediment transport measurements and long-term morphological evolution. *Geomorphology*, 60(1), 205–224.doi.org/10.1016/j.geomorph.2003.08.002

Aleman, N., Certain, R., Robin, N., & Barusseau, J.P. (2017), Morphodynamics of slightly oblique nearshore bars and their relationship with the cycle of net offshore migration. *Marine Geology* 392, 41–52.
doi.org/10.1016/j.margeo.2017.08.014

Anthony E.J., Vanhée S., & Ruz, M.H. (2006), Short-term beach-dune sand budgets on the North Sea coast of France: sand supply from shoreface to dunes and the role of wind and fetch. *Geomorphology,* 81, 316–329.
doi.org/10.1016/j.geomorph.2006.04.022

Aubrey, D.G. (1979), Seasonal patterns of onshore/offshore sediment movement. Journal of Geophysical Research 84,6347–6354.

Birkemeier, W.A. (1984), *Time scales of nearshore profile changes.* Paper presented at 19th International Conference on Coastal Engineering, American Society of Civil Engineers, New York.

Blossier, B., Bryan, K. R., Daly, C. J., & Winter, C. (2016), Nearshore sandbar rotation at single-barred embayed beaches. *Journal of Geophysical Research: Oceans*, 121, 2286–2313.doi.org/10.1002/ 2015JC011031.

Brander, R.W. (1999), Field observations on the morphodynamic evolution of low wave energy rip current system. *Marine Geology*, 157, 199–217.

Cheng, J., & Wang, P. (2018), Dynamic equilibrium of sandbar position and height along a low wave energy micro-tidal coast. *Continental Shelf Research*, 165, 120–136.doi.org/10.1016/j.csr.2018.05.004

Cohn, N., Ruggiero, P., de Vries, S., García-Medina, G. (2017), Beach growth driven by intertidal sandbar welding. *Paper Presented at 8th International Conference on Coastal Dynamics*. Denmark, Helsingør.

Coco, G., Murray, A.B. (2007), Patterns in the sand: from forcing templates to self-organization. Geomorphology 91, 271–290.
https://doi.org/10.1016/j.geomorph.2007.04.023.

Coco, G., Senechal, N., Rejas, A., Bryan, K.R., Capo, S., Parisot, J.P., Brown, J.A., MacMahan, J.H.M. (2014), Beach response to a sequence of extreme storms. *Geomorphology* 204:493–501.
http://dx.doi.org/10.1016/j.geomorph.2013.08.028.

Di Leonardo, D., & Ruggiero, P. (2015), Regional scale sandbar variability: Observations from the U.S. Pacific Northwest. *Continental Shelf Research*, 95, 74–88.doi.org/10.1016/j.csr.2014.12.012

Dubabier, B., Castelle, B., Marieu, V., & Ruessink, B.G. (2015), Process-based modeling of cross-shore sandbar behaviour. *Coastal Engineering*, 95, 35–50. doi.org/10.1016/j.coastaleng.2014.09.004

Fernández-Mora, A., Calvete, D., Falqués, A., & de Swart H.E. (2015), Onshore sandbar migration in the surf zone: New insights into the wave-induced sediment transport mechanisms. *Geophysical Research Letters*, 42, 2869–2877. doi.org/10.1002/2014GL063004

Grunnet, N.M., & Hoekstra, P. (2004), Alongshore variability of the multiple barred coast of Terschelling, The Netherlands. *Marine Geology*, 203, 23–41. doi.org/10.1016/S0025-3227(03)00336-0

Henderson, S.M., Allen, J.S., Newberger, P.A. (2004). Nearshore sandbar migration predicted by an eddy-diffusive boundary layer model, Journal of *Geophysical Research*, 109, C06024.

Hoefel, F., & Elgar, S. (2003), Wave-induced sediment transport and sandbar migration. *Science*, 299, 1885–1887.doi.org/10.1126/science.1081448

Holman, R.A. & Bowen, A.J. (1982), Bars, bumps, and holes: Models for the generation of complex beach topography. *Journal of Geophysical Research*, 87, 457-468.doi.org/10.1029/JC087iC01p00457

Holman, R.A., Lalejini, D.M., & Holland, T. (2016), A parametric model for barred equilibrium beach profiles: Two-dimensional implementation. *Coastal Engineering*, 117, 166–175.doi.org/10.1016/j.coastaleng.2016.07.010

Holman, R.A.; Symonds, G.; Thornton, E.B. and Ranasinghe, R. (2006), Rip spacing and persistence on an embayed beach. *Journal of Geohpysical Research* 111, C01006.

Hsu, T. J., Elgar, S., & Guza, R.T. (2006), Wave-induced sediment transport and onshore sandbar migration. *Coastal Engineering*, 53, 817–824. doi.org/10.1016/j.coastaleng.2006.04.003

Komar, P.D. (1974), *Beach Processes and Sedimentation* (429pp). Englewood Cliffs, NJ: Prentice-Hall.

Larson, M., and Kraus N.C. (1994), Temporal and spatial scales of beach profile change, Duck, North Carolina, *Marine Geology*, 117(1), 75–94.

Larson, M., & Kraus, N.C. (1992), *Dynamics of longshore bars*. Paper presented at 23rd International Conference on Coastal Engineering, American Society of Civil Engineers, Venice, Italy.

Lippmann, T.C., Holman, R.A., & Hathaway, K.K. (1993), Episodic, Nonstationary Behavior of a Double Bar System at Duck, North Carolina, U.S.A., 1986–1991. *Journal of Coastal Research* SI, 15, 49–75.

Lippmann, T.C., & Holman, R.A. (1990), The spatial and temporal variability of sand bar morphology. *Journal of Geophysical Research*, 95 (C7), 11575–11590. doi.org/10.1029/JC095iC07p11575

Mariño-Tapia, I. J., O'Hare, T. J., Russell, P. E., Davidson, M. A. & Huntley, D. A. (2007), Cross-shore sediment transport on natural beaches and its relation to sandbar migration patterns: 2. Application of the field transport parameterization. *Journal of Geophysical Research*, 112, C03002. doi.org/10.1029/2005JC002894

Masselink, G., Austin, M., Tinker, J., O´Hare, T., and Russell, P. (2008), Cross-shore sediment transport and morphological response on a macrotidal beach

with intertidal bar morphology, Truc Vert, France. *Marine Geology*, 251, 141–155.

Masselink, G., Short, A.D. (1993), The effect of tide range on beach morphodynamics and morphology: a conceptual beach model. Journal of Coastal Research 9 (3), 785–800.

Ostrowski, R., Pruszak, Z. & Zeidler, R.B. (1991), *Multi-scale nearshore and beach changes*. Paper presented at 22nd International Conference on Coastal Engineering, American Society of Civil Engineers, Delft, The Netherlands. doi.org/10.1061/9780872627765.161

Ojeda, E., Guillén, J., & Ribas, F. (2011), Dynamics of single-barred embayed beaches. *Marine Geology*, 280, 76–90. doi.org/10.1016/j.margeo.2010.12.002

Phillips, M. S., Harley, M. D., Turner, I. L., Splinter, K. D., & Cox, R.J. (2017), Shoreline recovery on wave-dominated sandy coastlines: the role of sandbar morphodynamics and nearshore wave parameters. *Marine Geology*, 385, 146–159.doi.org/10.1016/j.margeo.2017.01.005

Plant, N.C., Holman, R.A., Freilich, M.H. & Birkemeier, W.A. (1999), A simple model for interannual sandbar behaviour. *Journal of Geophysical Research,* 104, 15755–15776.doi.org/10.1029/1999JC900112

Price, T.D. & Ruessink, B.G. (2011), State dynamics of a double sandbar system. *Continental Shelf Research*, 31 (6), 659–674.

Ranasinghe, R., Symonds, G., Black, K. & Holman, R. (2004), Morphodynamics of intermediate beaches: A video imaging and numerical modelling study. *Coastal Engineering*, 51(7), 629–655.doi.org/10.1016/j.coastaleng.2004.07.018

Ruessink, B.G., Blenkinsopp, C., Brinkkemper, J.A., Castelle, B., Dubarbier, B., Grasso, F., Puleo, J.A., & Lanckriet, T. (2016), Sandbar and beach-face evolution on a prototype coarse sandy barrier. *Coastal Engineering*, 113, 19–32. doi.org/10.1016/j.coastaleng.2015.11.005

Ruessink, B.G., Pape, L., & Turner, I.L. (2009), Daily to interannual cross-shore sandbar migration: observation from a multiple sandbar system. *Continental Shelf Research*, 29, 1663–1677.doi.org/10.1016/j.csr.2009.05.011

Ruessink, B.G., Coco, G., Ranasinghe, R., & Turner, I.L. (2007), Coupled and noncoupled behavior of three-dimensional morphological patterns in a double sandbar system. *Journal of Geophysical Research*, 112, C07002. doi.org/10.1029/2006JC003799

Ruessink, B.G., & Kroon, A. (1994), The behaviour of a multiple bar system in the nearshore zone of Terschelling, the Netherlands: 1965–1993. *Marine Geology*, 121, 187–197. doi.org/10.1016/0025-3227(94)90030-2

Ruiz de Alegría-Arzaburu, A. & Vidal-Ruiz, J.A. (2018), Beach recovery capabilities after El Niño 2015–2016 at Ensenada Beach, Northern Baja California. *Ocean Dynamics*, 6, 749–759.doi.org/10.1007/s10236-018-1164-6

Sallenger, A.H., Holman, R.A., & Birkemeier, W.A. (1985), Storm-induced response of a nearshore-bar system. *Marine Geology*, 64, 237–257. doi.org/10.1016/0025-3227(85)90107-0

Sedrati, M., Anthony, E.J. (2007), Storm-generated morphological change and longshore sand transport in the intertidal zone of a multi-barred macrotidal beach. *Marine Geology*, 244, 209–229.

Senechal, N., Coco, G., Castelle, B., & Marieu V. (2015), Storm impact on the seasonal shoreline dynamics of a meso- to macrotidal open sandy beach (Biscarrosse, France). *Geomorphology*, 228, 448–461.

Shand, R.D., Bailey, D.G., & Shepherd, M. J. (1999), An inter-site comparison of net offshore bar migration characteristics and environmental conditions. *Journal of Coastal Research*, 15, 750–765.

Shepard, F.P. (1950), *Beach cycles in southern California. Beach Erosion Board (Technical Memo 20)*. Washington DC: US Army Corps of Engineering.

Short, A. D. (1999), *Handbook of Beach and Shoreface Morphodynamics*. Chichester, UK: John Wiley and Sons.

Splinter, K.D., Gonzalez, M.V.G., Oltman-Shay, J., Rutten, J., & Holman., R. (2018), Observations and modelling of shoreline and multiple sandbar behaviour on a high-energy meso-tidal beach. *Continental Shelf Research*, 159, 33–45. doi.org/10.1016/j.csr.2018.03.010

Van Enckevort, I.M.J., Ruessink, B.G., Coco, G., Suzuki, K., Turner, I.L., Plant, N.G., and Holman, R.A. (2004), Observations of nearshore crescentic sandbars. *Journal of geophysical research,* 109, C06028.
doi:10.1029/2003JC002214.

Van de Lageweg, W. I., Bryan, K. R., Coco, G., & Ruessink, B.G. (2013), Observations of shoreline–sandbar coupling on an embayed beach. *Marine Geology*, 344, 101–114.doi.org/10.1016/j.margeo.2013.07.018

Van Maanen, B., de Ruiter, P.J., Coco, G., Bryan, K.R., & Ruessink, B.G. (2008), Onshore sandbar migration at tairua beach (new zealand): numerical simulations and field measurements. *Marine Geology*, 253, 99–106. doi.org/10.1016/j.margeo.2008.05.007

Vidal-Ruiz, J.A., Ruiz de Alegría-Arzaburu, A. (2019), Variability of sandbar morphometrics over three seasonal cycles on a single-barred beach. Geomorphology, 333, 61–72. doi.org/10.1007/s10236-018-1164-6.

Walstra, D.J.R., Ranasinghe, R., Roelvink, J.A., & Ruessink, B.G. (2012), On bar growth and decay during interannual net offshore migration. *Coastal Engineering*, 60, 190–200.doi.org/10.1016/j.coastaleng.2011.10.002

Wright, L.D., Short, A.D., & Green, M.O. (1985), Short-term changes in the morphodynamics states of beaches and surf zones: an empirical predictive model. *Marine Geology* 62, 339–364.

Wright, L.D. & Short, A.D. (1984), Morphodynamic variability of surf zones and beaches: a synthesis. *Marine Geology*, 56: 93–118. doi.org/10.1016/0025-3227(84)90008-2

Yates, M.L., Guza, R.T., O'Reilly, W.C. (2009), Equilibrium shoreline response: observations and modeling. *Journal of Geophysical Research* 114, C09014.

Chapter 2

2 Nearshore measurements and analytical methods

2.1 Field site

Located in the northwestern coast of the Baja California peninsula, Ensenada is located in Todos Santos Bay (TSB), which is connected with the Pacific Ocean through two main entrances separated by Todos Santos Islands (17 km offshore) (Fig. 2.1). The offshore bathymetry presents a relatively deep canyon next to the Punta Banda headland (more than 400 m depth) and a shallow sandbank located near San Miguel (Fig. 2.1). The coastline in the northern bay contains pocket beaches made of gravel, cobble and mixed sand/gravel, while the beaches in the eastern side are made of siliceous medium sand (D_{50} of 0.25 mm). The sandy stretch of coast has a length of 14 km and is interrupted by the entrance of the Punta Banda estuary (Fig. 2.1).

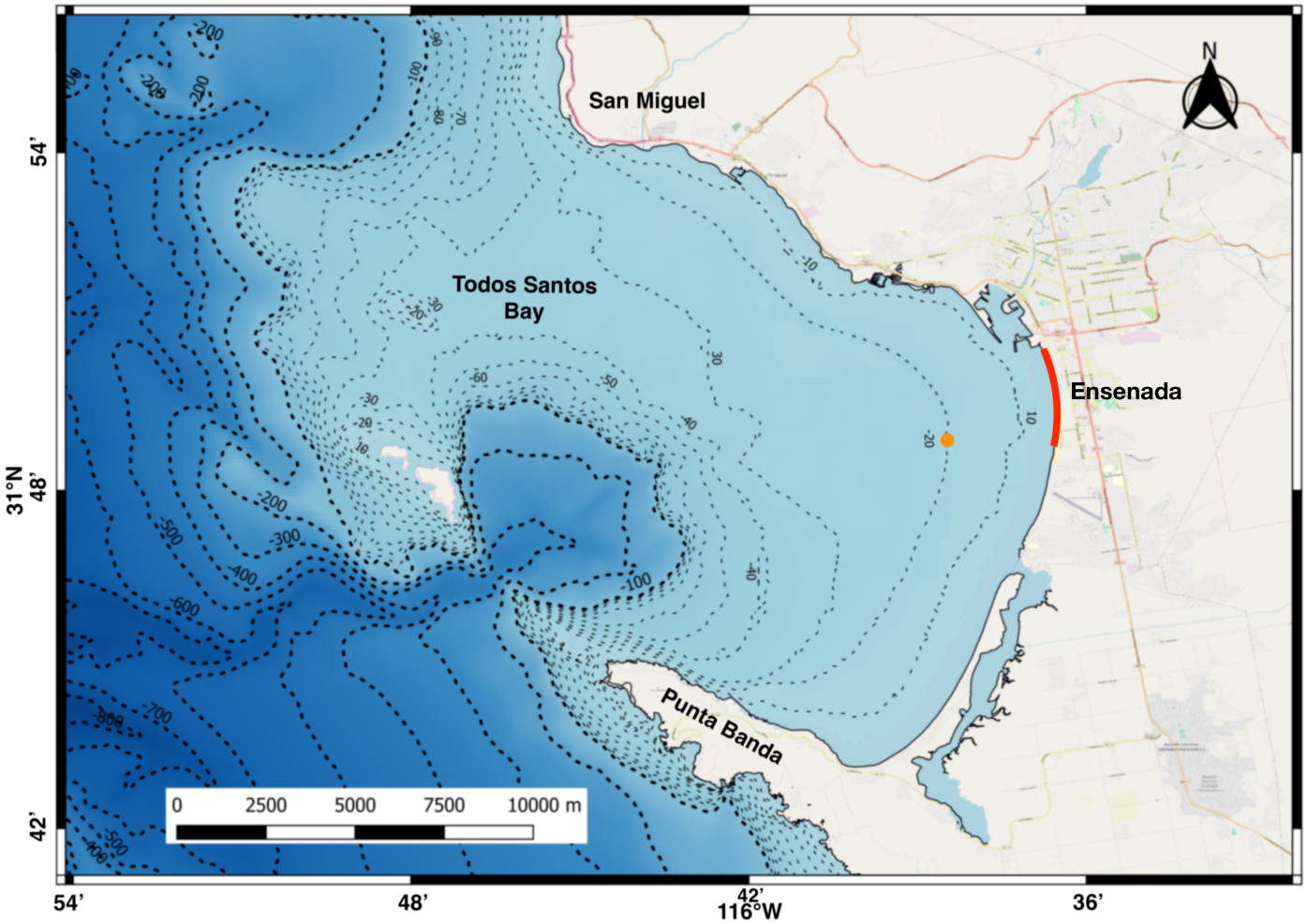

Figure 2.1 Location of Ensenada Beach within Todos Santos Bay in NW Baja California (red line) and approximate location of the bottom-mounted Acoustic Doppler Current Profiler (ADCP; orange dot).

Ensenada is part of the Todos Santos coastal plain within the Coastal Mountain providence, also known as the Ensenada Block (Gastil et al., 1975). Characterized by a rough topography, Ensenada Block stands ~500 m above sea level and extends from the Guadalupe valley to the Agua Blanca fault in the southern end of the bay (Pérez-Flores et al., 2004). The fault is one of the most active in the northern Baja California region, and extends for more than 130 km from El Paso de San Matias to Todos Santos Bay until reaching the intertidal beach (with thermal water upwelling) and extending further offshore (Allen et al., 1960; Rockwell et al., 1987; Ortega, 1988; Suárez et al., 1991; Pérez-Flores et al., 2004).

This research was undertaken in Ensenada Beach, a nearly 3 km long sandy beach located in the northeastern side of the bay. The beach is single-barred and presents a dominant intermediate morphodynamic state over the year, with an average slope (tan β) of 0.025 (Ruiz de Alegría-Arzaburu et al., 2015). Coastal structures are present along the northern 2 km of the beach, such as a promenade (north) and a seawall and rip-rap (middle) (Fig. 2.2). The southern beach preserves a natural dune backed by a shallow and intermittently dry freshwater lagoon (Fig. 2.2). The subaerial beach width varies from 80 to 120 m in the walled section with a supratidal beach elevation of about 6.5 m; and the non-walled section is 220–240 m wide, and 10 m high above mean low water (MLW) (Ruiz de Alegría-Arzaburu et al., 2015). Relatively weak northwesterly winds (~4 ms^{-1}) are dominant in the study area, and sporadic

easterlies known as Santa Ana conditions, which are frequent from October to March, with speeds of up to 10 ms^{-1} and 2–3 days of duration (Alvarez-Sanchez, 1977; Castro and Martínez, 2010). The beach is located in a mesotidal environment, the tides are semi-diurnal, and the average spring and neap tidal ranges are 2.3 m and 0.5 m, respectively.

Figure 2.2 Aerial view of the northern (promenade), middle (rip-rap) and southern (dune and lagoon) beach sections.

The incoming wave conditions are dominantly swell and typically bimodal in direction, with northwesterly waves being common during the winter and southwesterly waves during the summer, generated in northern and southern Pacific extratropical regions, respectively. Associated with the variability in wave energy, the beach exhibits strong seasonal morphological variations (± 70 m^3 m^{-1} cross-shore and ±35 m^3 m^{-1} longshore), reaching maximum and minimum subaerial volumes in September–October and January–February, respectively (Ruiz de Alegría-Arzaburu et al., 2017). The largest subaerial volumetric variations of the past 4 years occurred during the beginning of the 2015–2016 El Niño winter (Ruiz de Alegría-Arzaburu et al. 2017).

2.2 Research background

Previous research indicated that the cross-shore sandbar movement was highly modulated by the incident wave conditions; the sandbar migrated offshore during periods of energetic waves and onshore during calm wave energy (Fig. 2.3) (Ruiz de Alegría-Arzaburu and Vidal-Ruiz, 2018). The seasonal sandbar migration cycle was demonstrated to play an important role in the sediment transfer between the subaerial and subtidal beach (Ruiz de Alegría-Arzaburu and Vidal-Ruiz, 2018). Consequently, the recovery capability of the subaerial beach depended completely on the full attachment of the sandbar to the shoreline over the spring, which did not happen after the energetic El Niño 2015–2016 winter (Ruiz de Alegría- Arzaburu and Vidal-Ruiz, 2018).

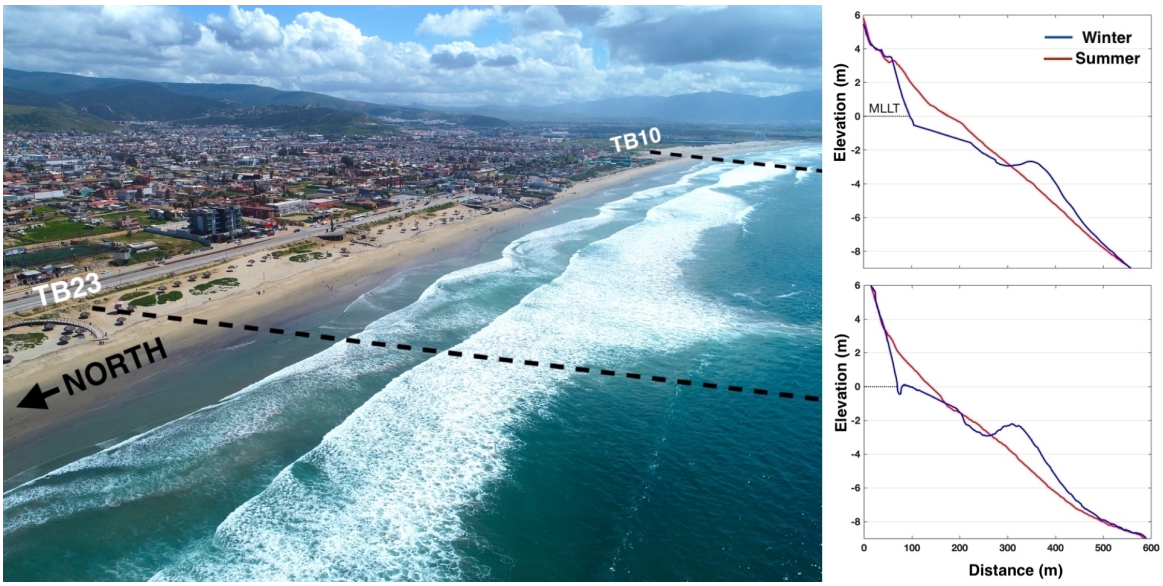

Figure 2.3 Aerial view of the beach (left photo), and example of two beach profiles in summer and winter (right panels). The profile elevations are referred to the mean low low-tide level (MLLT).

Four seasonal sandbar migration stages were identified in Ruiz de Alegría-Arzaburu and Vidal-Ruiz (2018): (1) generation of a sandbar in autumn at depths lower than 1 m; (2) offshore migration during large winter waves; (3) onshore migration during milder waves over the spring; and during May–June: (4a) weld to the subaerial beach resulting in an unbarred summer configuration; or (4b) terrace-bar formation and flattening during the summer. Option (4a) occurred when an offshore sandbar distance of ~110 m and 1.5 m depth was reached, while (4b) took place when the sandbar migrated greater offshore distances of up to ~190 m and located at deeper depths.

2.3 Morphological data

The subaerial morphology of the beach was measured monthly from August 2014 to September 2018 (Fig. 2.4). A total of 46 topographic surveys were conducted following the same transect lines at each survey time, as mapped on the GPS controller. A total of 61 cross-shore profiles (with ~50 m spacing) were consistently measured during low spring tides. All profiles were measured on foot at a frequency of 1 Hz, using a two-wheeled trolley operated by two people performing the survey down to the mean low low-tide level (MLLT) with a real-time kinematic global positioning system (RTK-GPS), with a precision of ±0.03 m. A threshold elevation value of 0.05 m was established to discard post-processed erroneous data as established in other research studies (e.g. Coco et al., 2014). In addition to the regular surveys, pre- and post-storm surveys were also conducted.

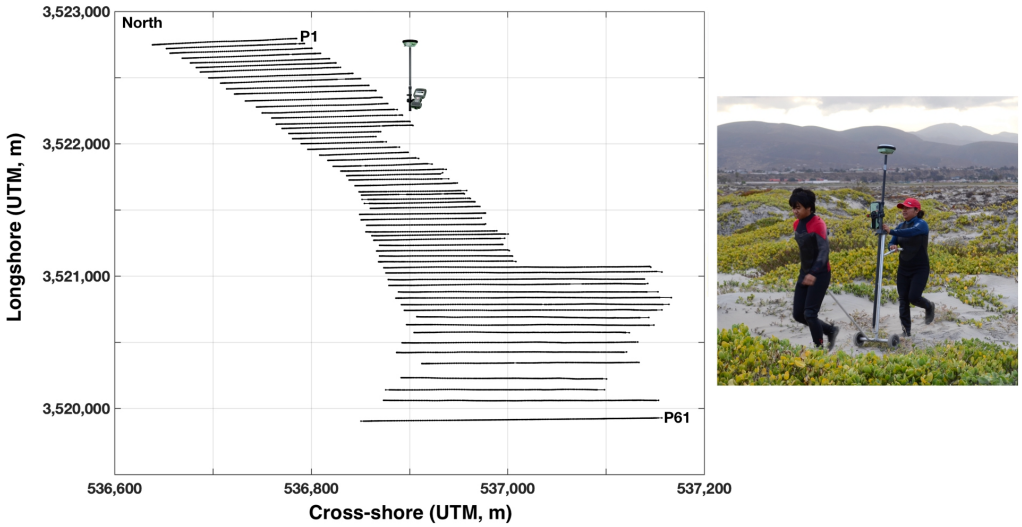

Figure 2.4 Plan view of the 61 topographic profiles (left panel). The right panel shows an example of the performance of a topographic survey on foot using a two-wheeled trolley operated by two people with a real-time kinematic global positioning system (RTK-GPS).

The subtidal morphology was measured monthly from August 2014 to September 2018. A total of 35 bathymetric profiles were measured using a jetski equipped with an Acoustic Doppler Current Profiler (ADCP; Sontek M9 Hydrosurveyor) synchronized to the RTK-GPS (Fig. 2.5). The frequency of 0.5 MHz was used to obtain the bathymetric data with a sound speed corrected depth accuracy of ±0.02 m. Similar to Wijnberg and Terwindt, 1995, an accuracy of ±0.1 m was estimated when ship dependent errors were included.

Figure 2.5 Aerial image of the beach (left panel). The dashed lines represent the first and last bathymetric lines out of 35 surveyed. The equipment used to carry out the measurements is presented in the right panels: jetski equipped with an ADCP and the RTK-GPS.

In all surveys an overlap was obtained between some of the topographic and bathymetric lines. When gaps between the subaerial and subtidal morphology occurred, linear interpolation was applied. The mean cross-shore distance subjected to interpolation was 50 m, corresponding to depths between 0 and 1 m.

Combining topographic and bathymetric data, 30 transects 100-m spaced along the nearly 3,000 m long beach were obtained. These topo-bathymetric transects (TB) comprises the upper subaerial beach (generally over 5 m in elevation) down to a depth of -12 m, beyond the depth of closure of ~ -9m visually estimated (plotting all cross-shore profiles per transect at different times together). Beach volumes were calculated for each TB by integrating the profile upwards from the elevations of 0 to 5.5 m (intertidal and supratidal, IS), −9 to 0 m (subtidal, SUB) and −9 to 5.5 m (total, TOT), and multiplying the corresponding alongshore length represented by each profile. A hypothetical vertical error of 0.1 m across the whole TB profile (from −9 to 5.5 m of elevation) and extending along the studied beach section would imply a total volumetric error of 2%. The loss or gain of volume was determined by subtracting the mean value to each volume in time, which resulted in demeaned (Dem) IS, SUB and TOT volumes. The volumetric evolution of the beach was obtained by calculating the cumulative volumetric differences (Cum ΔV) per beach profile in time.

The TB profiles were interpolated at 0.1 m across-shore to obtain digital elevation models (DEMs) whose spatial coordinates are referred in Universal Transverse Mercator (Easting and Northing in meters), and the elevations were referenced to the local MLLT (Fig. 2.6). Differences were performed from August 2014 to September 2018, which represented seasonal topographic variations. Monthly cumulative differences of the DEMs were calculated to determine the morphological evolution of the studied beach section over the four-year period.

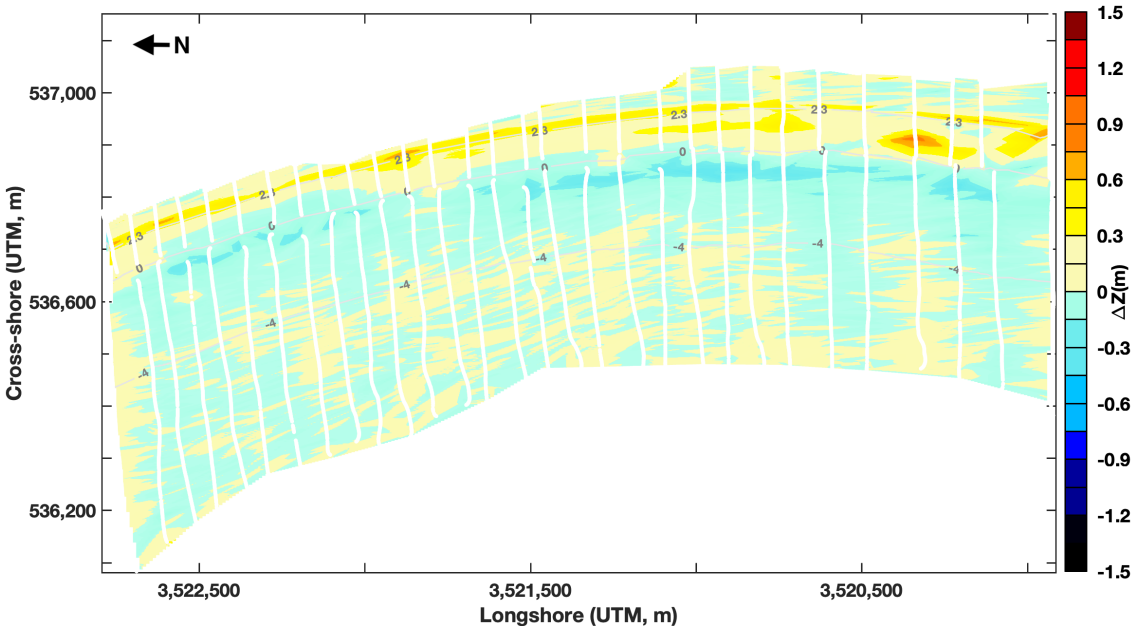

Figure 2.6 An example of a Digital Elevation Model (DEM) calculated from the measured 30 TB profiles (white lines).

2.4 Wave data

Hourly wave data were collected from August 2014 to September 2018 with a 1 MHz Acoustic Doppler Current Profiler (ADCP; Fig. 2.7) located 2.5 km offshore of the study site at a water depth of 20 m (Fig. 2.7). The instrument was installed on the seabed and provided offshore measurements of wave parameters including the significant wave height (H_s), peak wave period (T_p) and wave direction (α). Hence, a time-series of H_s, T_p and α were obtained (Fig. 2.7).

The waves presented a clear seasonal pattern over the study period, although significant interannual variability was encountered. The monthly-averaged waves were typically shorter (T_p of 8 s) and smaller (H_s < 0.7 m)

between May and September, and longer (T_p = 12 s) and larger (H_s = 1.2 m reaching 2 m) between October and April. During El Niño 2015–2016 winter, the high-energy wave condition (H_s > 3 m, T_p > 14 s) lasted longer than during the preceding and succeeding winters (until April rather than February–March) (Ruiz de Alegría-Arzaburu and Vidal-Ruiz, 2018). The most energetic condition on 2016–2017 happened during an individual storm in late January 2017, which lasted three days and presented H_s > 4 m with T_p of 15 s during a high neap tide; thus, this event presented conditions of similar wave energy as during the El Niño winter.

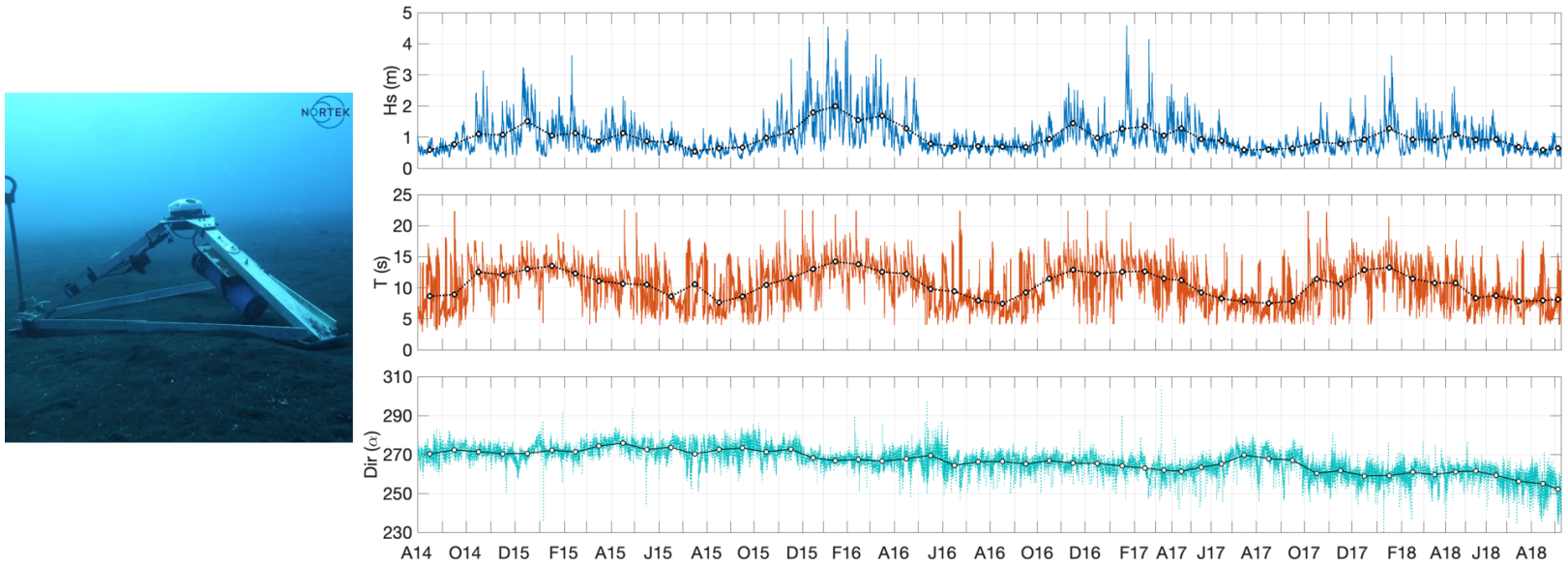

Figure 2.7 Time-series of significant wave heights, H_s, spectral peak wave periods, T_p, and wave directions, Dir, from August 2014 to September 2018 (right panel). A photograph of the bottom-mounted ADCP (AWAC, Nortek) is provided in the left panel.

2.5 References

Allen, C.R., Silver, L.T. and Stehli, F.G. (1960), Agua Blanca fault: A major transverse structure of northen Baja California, Mexico. Bull. Geol. Soc. Am., 71: 457–482.

Alvarez Sanchez, L.G. (1977), Vientos en la Bahía de Todos Santos BajaCalifornia. Ciencias Marinas.

Castro, R. Martínez, A. (2010), Variabilidad espacial y temporal del campo de viento. En: Gaxiola-Castro G, Durazo R (eds.), Dinámica del Ecosistema Pelágico frente a Baja California, 1997–2007: Diez años de Investigaciones Mexicanas de la Corriente de California. 129–147.

Coco, G., Senechal, N., Rejas, A., Bryan, K.R., Capo, S., Parisot, J.P., Brown, J.A., MacMahan, J.H.M. (2014), Beach response to a sequence of extreme storms. *Geomorphology* 204:493–501. http://dx.doi.org/10.1016/j.geomorph.2013.08.028.

Gastil, R.G., Phillips, R.P. and Allison, E.C. (1975), Reconnaissance Geology of the State of Baja California, Mexico. *Geological Society of America*, Memoir 140, Boulder, 170 pp.

Suárez, F., Armijo, R., Morgan, G., Bodin, P. and Gastil, R.G. (1991), Framework of recent and active faulting in northern Baja California. In: P. Dauphin and B. Simoneit (eds.), The Gulf and Peninsular Provinces of the Californias. AAPG Mem., 47: 285–200 pp.

Ortega, M.A. (1988), Neotectónica de un sector de la falla de Agua Blanca, Valle Agua Blanca (Rancho la Cocina–Rancho Agua Blanca), Baja California, Mexico.

Tesis de maestría, Centro de Investigación Científica y de Educación Superior de Ensenada, Baja California, México, 146pp.

Pérez Flores, M. A., Suárez Vidal, F., Gallardo Delgado, L. A., González Fernández, A., & Vázquez González, R. (2004), Structural pattern of the Todos Santos Coastal Plain based upon geophysical data. *Ciencias Marinas*, 30(2), 349-364. (ID: 6183)

Rockwell, K.T., Hatch, E.M. and Schug, L.D. (1987), Late Quaternary rates Agua Blanca and Borderland faults. Final Technical Rep. US Geol. Surv., 122 pp.

Ruiz de Alegria-Arzaburu, A., García-Nava, H., Gil-Silva, E., Desplán-Salinas, G. (2015). A morphodynamic comparison of walled and non- walled beach sections, Ensenada beach, Mexico. World Scientific. The Proceedings of the Coastal Sediments ISBN:978-981-4355-52-0

Ruiz de Alegria-Arzaburu A, Vidal-Ruiz JA, García-Nava H, Romero-Arteaga A (2017), Seasonal morphodynamics of the subaerial and subtidal sections of an intermediate and mesotidal beach. *Geomorphology* 295:383–392

Ruiz de Alegría-Arzaburu, A. & Vidal-Ruiz, J.A. (2018), Beach recovery capabilities after El Niño 2015–2016 at Ensenada Beach, Northern Baja California. *Ocean Dynamics*, 6, 749–759.doi.org/10.1007/s10236-018-1164-6

Wijnberg, K.M., and Terwindt, J.H.J. (1995), Quantification of decadal morphological behavior of the central Dutch coast. *Marine Geology*, 62:339–364.

Chapter 3

3 Variability of sandbar morphometrics over three seasonal cycles[1]

Understanding the morphodynamics of surfzone sandbars is very relevant from a sediment transport perspective. Three complete annual sandbar migration cycles were studied on a single-barred beach. The study period included the 2015–2016 El Niño anomaly and the incidence of a highly energetic swell-storm during winter 2016-2017. The sandbar responded directly to the seasonal wave forcing, thus, it migrated offshore during the energetic winter and onshore during the milder summer conditions. Its seasonal migration cycle comprised four stages: (1) generation in autumn (November) at lower than 1 m depth; (2) offshore migration over the winter (until January/February) while $\overline{H_S}$ > 1.3 m; (3) onshore migration over the early spring (March and April) while $\overline{H_S}$ < 1.0 m; and during May–June: (4a) subaerial beach welding (unbarred beach) when a dynamic equilibrium was reached; or (4b) terrace-bar formation (sandbar flattening) as a consequence of a lack of a dynamic equilibrium. The energetic El Niño winter conditions induced the same amount of offshore sandbar displacement as the individual extreme swell-storm, placing the sandbar at a maximum cross-shore distance of ~190 m, beyond the dynamic equilibrium. During the 2017 winter, a period of mild wave conditions favored the landward migration of the sandbar, locating it near its generation point. The duration of mild wave energy conditions and the offshore sandbar location and volume are considered relevant factors that limit the capabilities of the sandbar to reach shallow waters and weld to the subaerial beach before the summer.

[1] This chapter is based on the article published in *Geomorphology* 2019:

Vidal-Ruiz, J.A., Ruiz de Alegría-Arzaburu, A., 2019. Variability of sandbar morphometrics over three seasonal cycles on a single-barred beach. *Geomorphology* 333, 61–72. https://doi.org/10.1016/j.geomorph.2019.02.034

3.1 Introduction

Surfzone sandbars are very dynamic features that result from a constant feedback between hydrodynamic forcing and morphology. The responsible sediment transport processes occur at time-scales ranging from intra-wave periods to interannual cycles, and are controlled by variations in local environmental forcings (Splinter et al., 2018). A large variety of sandbars exist, and these bedforms are generally perceived as amplifications on the submerged profile elevation, but are commonly referred to as sandbars for perturbations of high-amplitude, and terrace-bars for those of low-amplitude still clearly separated from the shore (Holman and Bowen, 1982; Aagaard et al., 2013). These features constitute the first line of natural defense against coastal erosion and flooding on sandy beaches, and contain large amounts of sediment that contribute significantly to the sediment balance on the beach (Senechal et al., 2015). Quantifying onshore sandbar migrations, and events of welding to the beach face is, therefore, essential to determine the capabilities of the subaerial beach to recover after periods of energetic wave incidence (Ruiz de Alegría-Arzaburu and Vidal-Ruiz, 2018).

The physical processes behind onshore sandbar migrations are, at present, still controversial (Dubarbier et al., 2015; Fernández-Mora et al., 2015). It is generally accepted that seaward sandbar movements are related to intensive mean offshore currents (bed return flow or undertow) that generate during breaking, high-energy waves (e.g. Sallenger et al., 1985; Short, 1999).

Shoreward sandbar migrations, instead, are associated with weak-to-nonbreaking waves, and induced by wave asymmetry (Hoefel and Elgar, 2003), near-bed wave skewness (Hsu et al., 2006; Ruessink et al., 2007; Fernández-Mora et al., 2015), Stokes drift and/or boundary layer streaming (Henderson et al., 2004). Therefore, it is relevant to measure the nearshore bathymetric changes frequently (days-to-weeks) and over periods of years-to-decades to be able to determine the morphological geometry (morphometry) and location of sandbars at event-driven and seasonal scales (e.g. Price et al., 2014; Di Leonardo and Ruggiero, 2015). To date, a few studies have analyzed sandbar behavior in terms of the characteristics of their morphometry (i.e. sandbar crest depth, distance, height, width and volume) (Larson and Kraus, 1992; Ruessink and Kroon, 1994; Grunnet and Hoekstra, 2004; Aleman et al., 2017; Cheng and Wang, 2018). Data are needed to contribute to the development of accurate models that could provide a better understanding of the generation processes and the morphological evolution of sandbars under varying incident hydrodynamic conditions (e.g. Plant et al., 1999; Hsu et al., 2006; Mariño-Tapia et al., 2007; Van Maanen et al., 2008; Thiébot et al., 2012; Walstra et al., 2012; Smit et al., 2012; Holman et al., 2016; Ruessink et al., 2016).

Changes in two-dimensional (alongshore-uniform) and three-dimensional (alongshore variability) sandbar geometry have been found to be well correlated to the incoming wave forcing and/or to preceding morphologic states (Wright et al., 1985; Lippmann and Holman, 1990; Masselink et al., 2014), and these can

also result from self-organization patterns (Coco and Murray, 2007). The first conceptual model of sandbar migrations (Shepard, 1950; Komar, 1974) indicated that beaches evolved from an unbarred shape during periods of low-energy waves to barred after high-energy wave conditions, thus, suggesting seasonal onshore and offshore sandbar movements. Many beaches, however, lack of a clear seasonality on the sandbar migration cycle. While a few beaches describe continuous sandbar landward migrations over decades (e.g. Aagaard et al., 2004; Anthony et al., 2006), other beaches present sporadic net onshore movements over periods of days to months (and sometimes, intertidal beach welding) during weak incident waves (e.g. Ostrowski et al., 1991; Larson and Kraus, 1992; Van Maanen et al., 2008; Ruggiero et al., 2009; Van de Lageweg et al., 2013; Senechal et al., 2015; Blossier et al., 2016; Phillips et al., 2017; Cohn et al., 2017).

Most multi-barred beaches sustain a lack of intra-annual correlation between the incident wave energy and cross-shore sandbar movements, and present net offshore migrations (NOM) over periods from a few years to decades (Birkemeier, 1984; Lippmann et al., 1993; Ruessink and Kroon, 1994; Plant et al., 1999; Shand et al., 1999; Aleman et al., 2017). During interannual migration cycles, sandbars form near the shoreline, migrate offshore across the surf zone and finally degenerate at the outer nearshore margin (Ruessink and Kroon, 1994). But high-variability has been encountered in sandbar behavior in the degeneration zone, primarily associated with nearshore slope differences and

sandbar volume variations (Shand et al., 1999; Tătui et al., 2016). Beaches with large sandbars attained interannual NOM cycles while those with small sandbars were subjected to episodic NOM (Ruessink et al., 2009); thus, highlighting the relevance of sandbar geometry in the characteristics of the migration cycles. However, few research studies have analyzed differences in sandbar morphometry during their migration cycle on time-scales of hours to weeks (Ostrowski et al., 1991; Larson and Kraus, 1992) or years to decades (Ruessink and Kroon, 1994; Ruessink et al., 2003; Grunnet and Hoekstra, 2004; Di Leonardo and Ruggiero, 2015; Aleman et al., 2017; Cheng and Wang, 2018).

Single-barred beaches have been surprisingly understudied compared to their multi-barred counterparts (e.g. Ostrowski et al., 1991; Van de Lageweg et al., 2013; Blossier et al., 2016). Based on monthly bathymetric data collected over three years, this research reports a detailed analysis of sandbar morphometrics before, during and after the 2015–2016 El Niño winter on a single-barred beach.

3.2 Methods

3.2.1 Field measurements

Morphological data consisting of monthly topo-bathymetric profiles (Fig. 3.1) and sandbar morphometrics data were obtained from August 2014 to August 2017 along nearly 2867 m of beach length in Ensenada Beach. Three-year dataset of significant wave heights (H_S), wave peak periods (T_P) and wave

directions (α) were obtained from an ADCP (Nortek AWAC) located 2500 m offshore from the beach (Fig. 3.1).

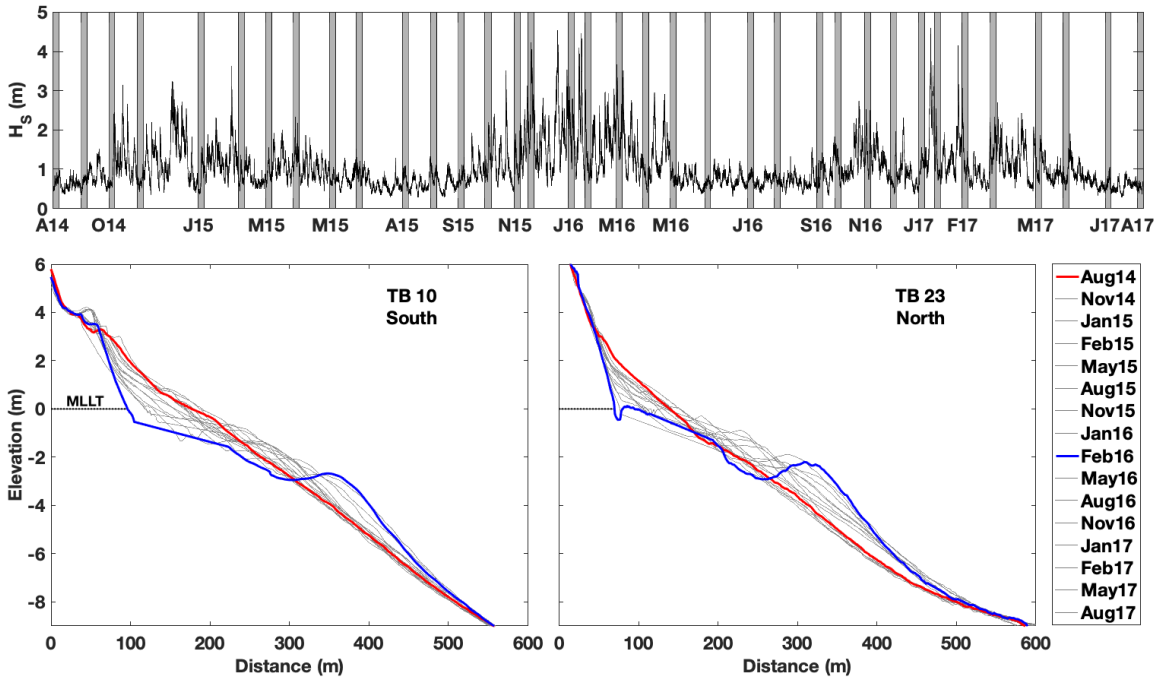

Figure 3.1 The top panel presents the time series of significant wave heights (black lines) and the dates of topo-bathymetric (gray lines) surveys. The bottom panels present the temporal evolution of the TB10 and TB23 topo-bathymetric profiles from August, November, January, February and May (gray profiles) 2014-2017 and the profiles for August 2014 and February 2016 are plotted in red and blue lines respectively. The TB elevations are referred to the mean low low-tide level (MLLT).

3.2.2 Sandbar Morphometrics

In order to analyze the spatio-temporal variability of the subtidal sandbar morphology, five morphometric parameters were extracted from the measured topo-bathymetric (TB) profiles following the works of Ruessink and Kroon (1994) and Di Leonardo and Ruggiero (2015), which were: the sandbar crest height (h_b), depth (d_b) and cross-shore position (P_b), and sandbar width (W_b) and volume per linear meter (V_b) (Fig. 3.2). Each TB profile was first linearly

interpolated at 0.1 m cross-shore and plotted against the unbarred reference profile from September 2014. Thus, all morphometric parameters were defined relative to the position of the reference profile. W_b was defined as the cross-shore distance between the intersecting points of the instantaneous profile with the unbarred reference profile, and V_b corresponds to the area confined between both profiles (Fig. 3.2a and c). A threshold value of $h_b > 0.75$ m was used to define a sandbar; hence, terrace-bars would be features with $h_b \leq 0.75$ m (Fig. 3.2c and d).

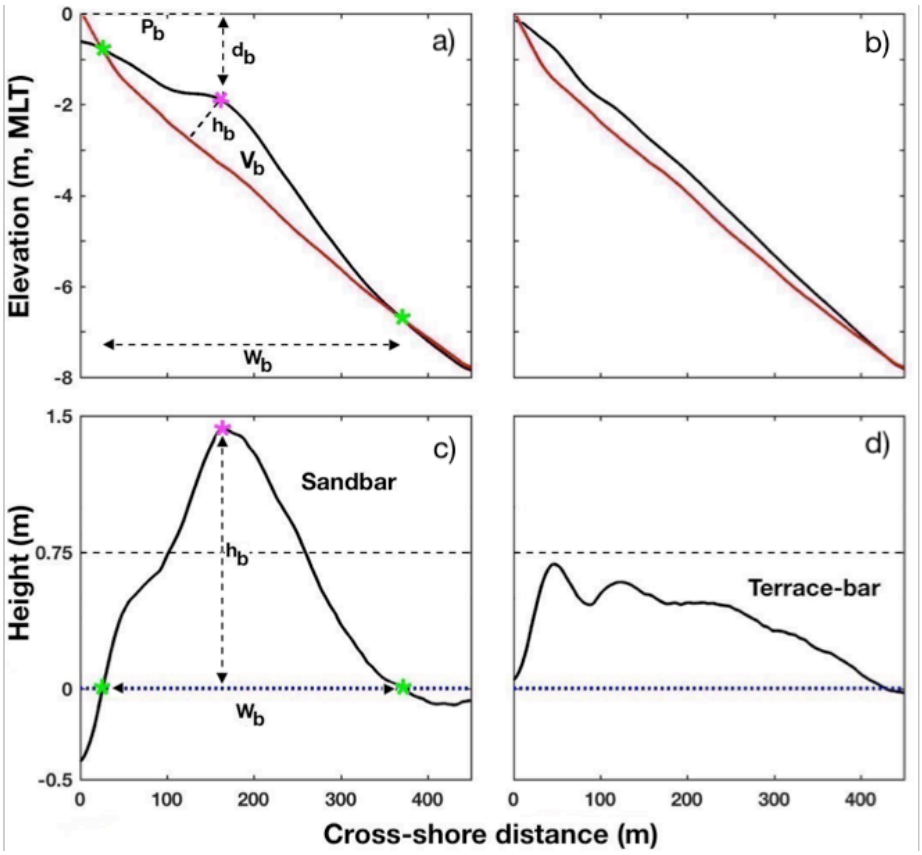

Figure 3.2 (a and c) Schematic diagram of the main morphometric parameters of a sandbar: sandbar crest position (P_b; pink star), depth (d_b), height (h_b) and sandbar width (W_b; distance between the green stars) and volume (V_b), obtained plotting a typical instantaneous profile (black line) against the unbarred reference profile from September 2014 (red line). (b) and (d) panels refer to the terrace-bar case.

3.3 Results

3.3.1 Wave conditions

The waves presented a clear seasonal pattern over the three-year study period, although significant interannual variability was encountered (Fig. 3.3A, B and C). The monthly-averaged waves were typically shorter (T_p of 9 s) and smaller (H_s < 0.7 m) between May and October, and longer (T_p > 13 s) and larger (H_s > 1.3 m reaching 2 m) between November and April. During El Niño 2015–2016 winter, the high-energy wave condition (H_s > 4 m, T_p ≈ 17 s) lasted longer than during the preceding and succeeding winters (till April rather than February–March) (Ruiz de Alegría-Arzaburu and Vidal-Ruiz, 2018). The most energetic condition on 2016–2017 happened during an individual storm in late January 2017, which lasted ≈4 days and reached maximum H_s of 4.6 m and T_p of 17 s during a high neap tide; thus, this event presented conditions of similar wave energy as during the El Niño winter.

The joint PDFs between H_s and T_p for the energetic wave periods from November to April show significant differences between the winters of 2015–2016 and the others, being the most probable conditions of 1.0 m and 12 s in 2014–2015, 1.6 m and 13 s in 2015–2016, and 1.2 m and 12 s in 2016–2017 (Fig. 3.3b', d' and f'). In contrast, and as indicated in Ruiz de Alegría-Arzaburu and Vidal-Ruiz (2018), the low-wave energy periods presented similar joint PDFs over the study period, being the most common waves of 0.7 m and 9 s

(Fig. 3.3a', c', e' and g'). In 2016, however, lesser variations in H_S happened compared to the other periods (Fig. 3.3e'). The wave direction ranged between 260 and 280° over the time series, but a slight shift toward 260–270° occurred after November 2015 (till the 2017 summer), while the dominating wave direction was 270–280° prior to that period (Fig. 3.3C).

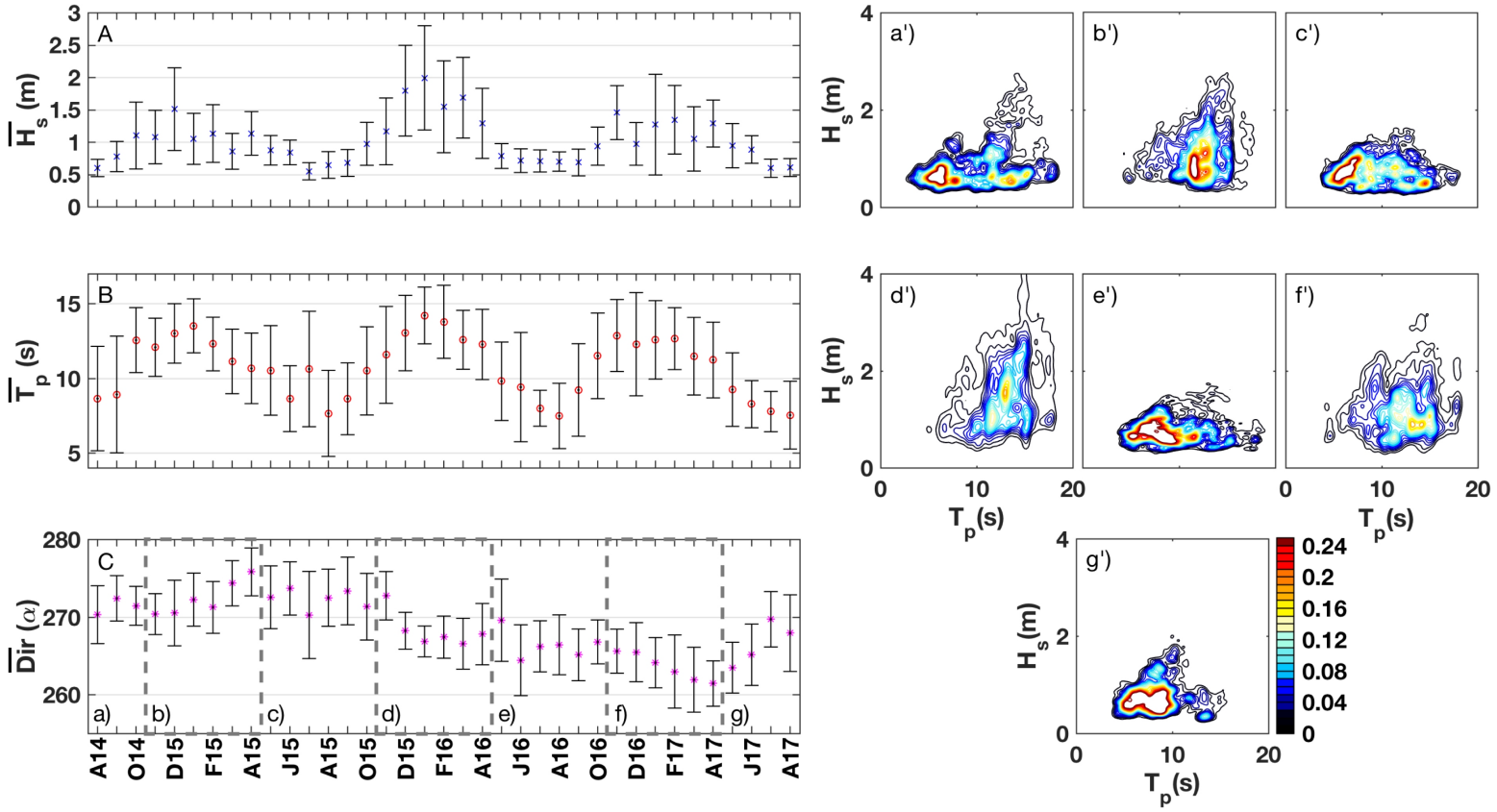

Figure 3.3 Time-series of monthly-averaged significant wave heights, H_S, peak wave periods, T_P, and wave directions, Dir, from August 2014 to August 2017, and their standard deviations (vertical bars) (left panels A to C). The right panels present the joint probability density functions (PDFs) between H_S and T_P for the periods of May–October (a', c', e', g') and November–April (b', d', f') each year (dashed boxes on panel C). Low-energy wave conditions dominate in summer and present little variations, while high-energy waves occur between October and April.

3.3.2 Cross-shore sandbar evolution

Two representative TB profiles were selected from the mid-southern (TB10) and northern (TB23) beach, and their temporal evolution was analyzed between August 2014 and August 2017 using the unbarred September 2014 profile as a reference (Figs. 3.4 and 3.5). During the first year, from August 2014 to August 2015 (previous to El Niño winter), the summer profiles remained unbarred, and a berm was present in the upper beach. In November 2014, a small sandbar was identified slightly below the mean low low-tide level (MLLT; 0 m elevation) in co-existence with a berm. By January 2015 the sandbar was well-developed and located at a depth of 1.7 m, and 150 m and 145 m offshore the reference shoreline in the southern (TB10, Fig. 3.4) and northern (TB23, Fig. 3.5) sections, respectively. The sandbar built-up and spread toward the shore after January, and by May 2015, it welded the shoreline, reincorporating its sediment onto the subaerial beach (Figs. 3.4 and 3.5).

Similar to the previous year, in November 2015 the sandbar formed close to the MLLT level, in co-existence with the berm (Figs. 3.4 and 3.5). The energetic El Niño winter waves between November 2015 and January 2016 (Fig. 3.3) moved the sandbar offshore to depths of 2 m and distances of 145 m and 160 m in the southern and northern sections (Figs. 3.4 and 3.5). Between January and February 2016, the incoming waves were highly energetic (Fig. 3.3), and the sandbar migrated toward deeper depths reaching 2.5 m at a

distance of 190 m in both sections; and presented steeper crests in the northern than in the southern beach (Figs. 3.4 and 3.5).

The milder wave conditions after May and during the 2016 summer (Fig. 3.3) induced the flattening of the sandbar. Part of the sandbar migrated onshore and welded to the shoreline during the spring, while considerable amounts of sediment remained at depths of 2.5–3.5 m (distances of 120–180 m) as a terrace-bar (Figs. 3.4 and 3.5). In November 2016, a subtidal sandbar reformed around 1.7 m depth, and its crest was steeper in the northern than in the southern beach section. During the 2016–2017 winter, the sandbar migrated up to 190 m offshore, gaining sediment, and reaching 3 m depth by January 2017 (Figs. 3.4 and 3.5). During the less energetic wave conditions after February 2017 (Fig. 3.3), the sandbar migrated onshore, partially welding the lower intertidal beach and gradually spreading its sediment toward the subaerial section. By August 2017, a significant amount of sediment remained in the lower subtidal section at the northern beach as a terrace-bar feature (Figs. 3.4 and 3.5).

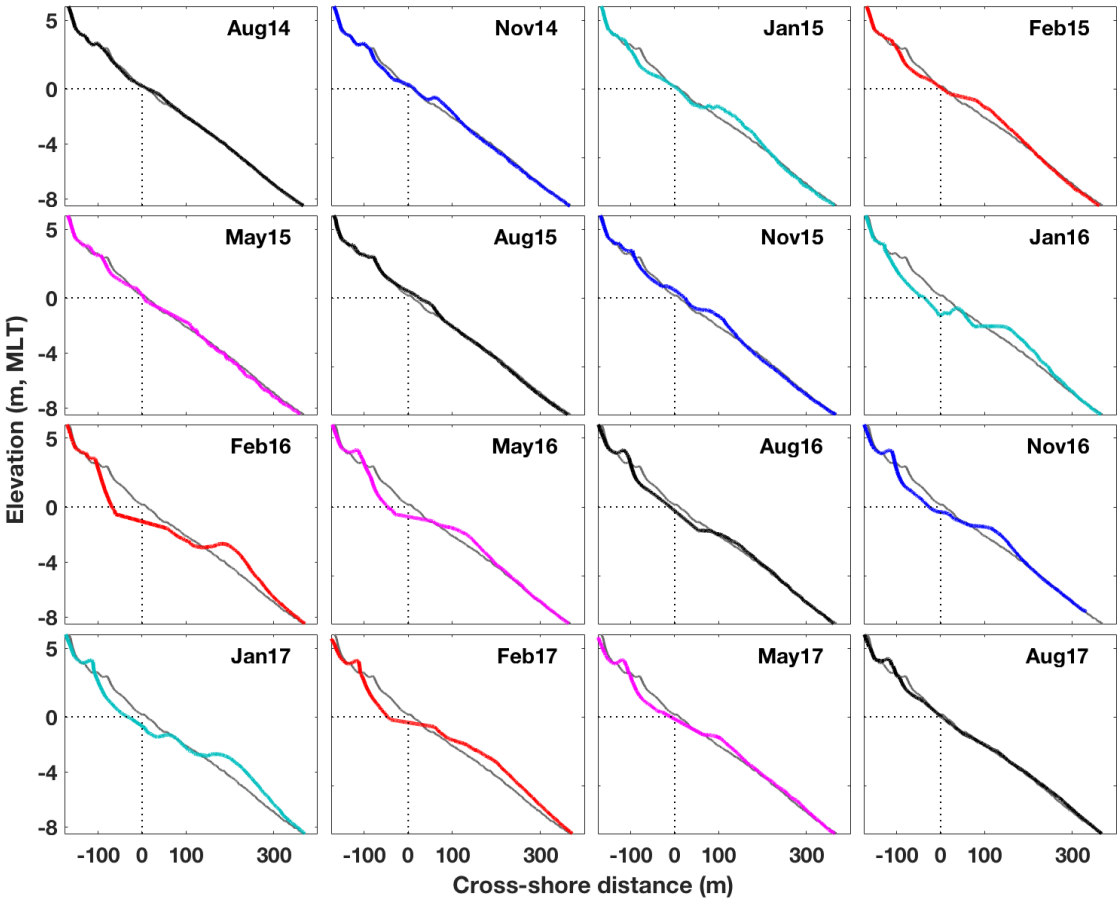

Figure 3.4 Temporal evolution of TB10 (mid-southern beach) from August 2014 to August 2017 (colour profiles) relative to the unbarred September 2014 reference profile (gray profile).

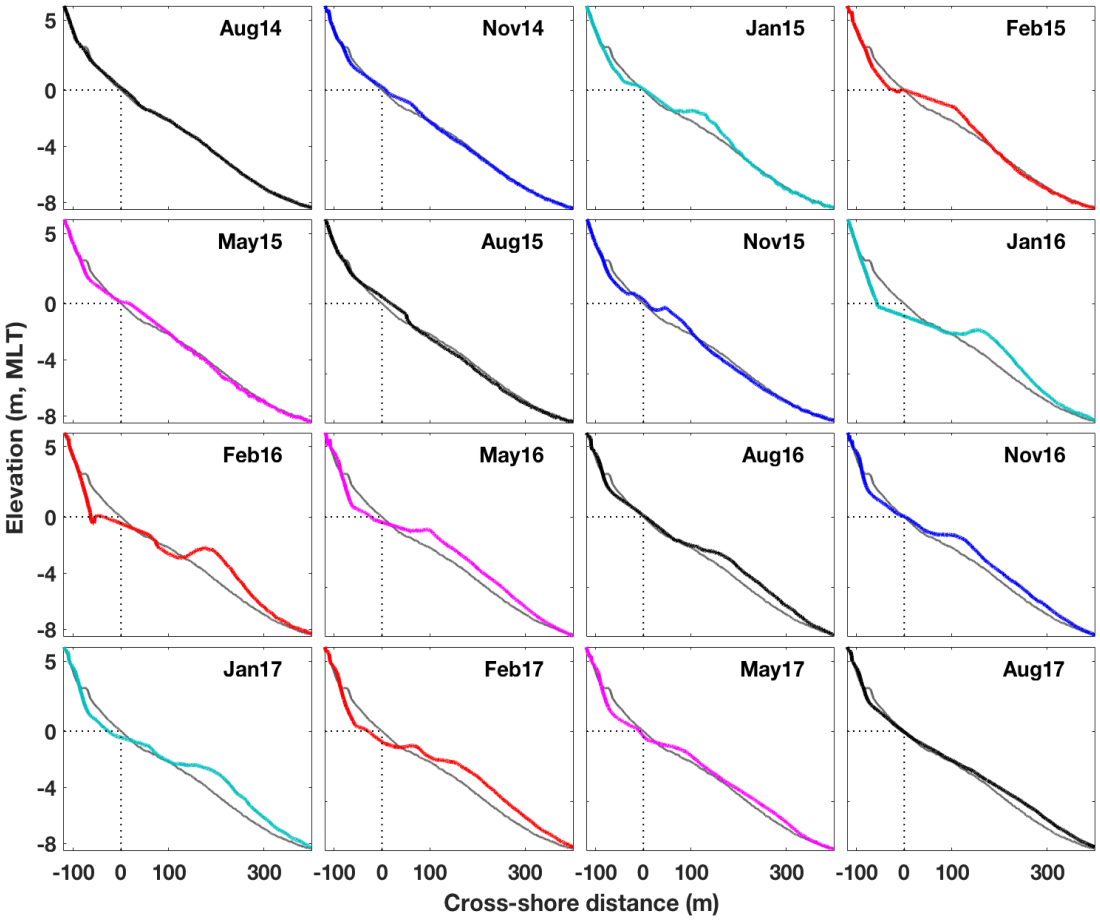

Figure 3.5 Temporal evolution of TB23 (northern beach) from August 2014 to August 2017 (colour profiles) relative to the unbarred September 2014 reference profile (gray profile).

3.3.3 Seasonal sandbar cycles

The beach was unbarred in August 2014, and the subaerial section accreted while the subtidal beach slightly eroded (ΔZ = ±0.3 m). In November 2014, the sandbar formed slightly below MLLT level, associated with partial subaerial erosion (Fig. 3.6). The subaerial erosion continued over the winter (ΔZ = −1 m), and contributed to the sandbar accretion and offshore migration by January 2015. Between January and February 2015, the sandbar became an alongshore-uniform ridge, losing its three-dimensional configuration or

rhythmicity. The sandbar propagated onshore and welded to the intertidal beach by May 2015, reincorporating sediment onto the subaerial section.

Similar to the previous year, the sandbar formed in November 2015 close to the MLLT level in the northern beach, and farther offshore in the southern section. The energetic El Niño 2015–2016 winter waves caused large morphological change (ΔZ = ±1.5 m), eroding the subaerial beach and accreting the subtidal section. This contributed to the sandbar accretion at 1.5–3.9 m depth and its offshore migration till February 2016 (Fig. 3.6). By May 2016, the sandbar migrated onshore and presented alongshore rhythmicity (crest depths varying between 0.8 and 2.5 m alongshore). This contributed to the partial accretion of the inner subtidal beach, but the sandbar was unable to completely weld to the intertidal section. Part of the sandbar welded to the shoreline over the 2016 summer, contributing to partial subaerial recovery. Another part, however, formed a terrace-bar that flattened and propagated offshore up to depths of 2.5–3.6 m (Fig. 3.6).

The sandbar rebuilt in November 2016 around 1–2.5 m depth, partly with the sediment contained in the terrace-bar, and also with sand that eroded from the intertidal beach (Fig. 3.6). During the 2016–2017 winter, the subaerial beach eroded and the subtidal accreted (ΔZ ± 1 m). In January 2017, the sandbar was well formed and alongshore uniform, and after February it started migrating onshore, partially accreting the inner subtidal beach. By May 2017, the sandbar split into two sections: one migrated onshore up to depth of 1.5–2 m, and the

other part remained at 2–4 m depth. Over the summer, the inner part of the sandbar welded to the shoreline and reincorporated its sediment onto the subaerial section, but large amounts of sand persisted at ~5 m depth by August 2017 in the form of a terrace-bar (Fig. 3.6).

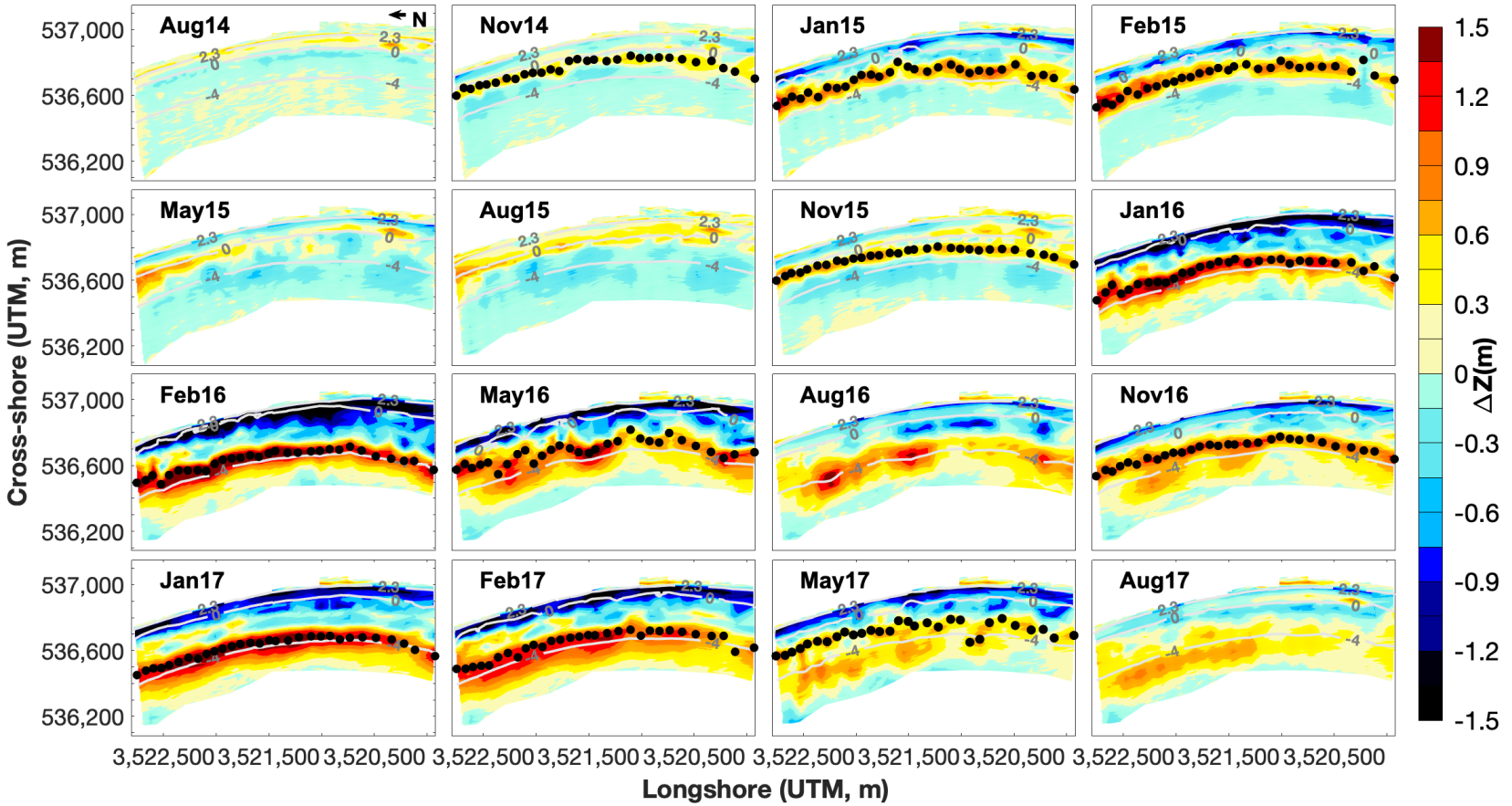

Figure 3.6 Sandbar crest locations (black dots) overlaid the summer (Aug), autumn (Nov), winter (Jan, Feb) and spring (May) cumulative morphological changes from August 2014 to August 2017. The 0-m, 2.3-m and −4-m contour lines correspond to the mean low-tide level, upper intertidal limit and mid-subtidal zone, respectively.

3.3.4 Storm-driven sandbar migration

A single swell storm-event in late January 2017 caused the equivalent magnitude of offshore sandbar movement as during the El Niño 2015–2016 winter (Figs. 3.5 and 3.7). Prior to the storm, the beach presented an unusual morphological condition for January. The sandbar migrated onshore between November 2016 and early January 2017, becoming highly rhythmic and locating near the MLLT level (Fig. 3.7). The storm with maximum H_s of 4.6 m, T_p of 14–17 s and an incident wave angle of 260° hit the beach on the 22nd of January and triggered a rapid offshore sandbar movement. The sandbar migrated a distance of 100 m and 145 m offshore up to 3 m depth in the southern and northern sections, respectively. During the seaward migration, the sandbar reshaped from rhythmic to an alongshore-uniform configuration, and gained significant amounts of sand originated from the subaerial beach erosion.

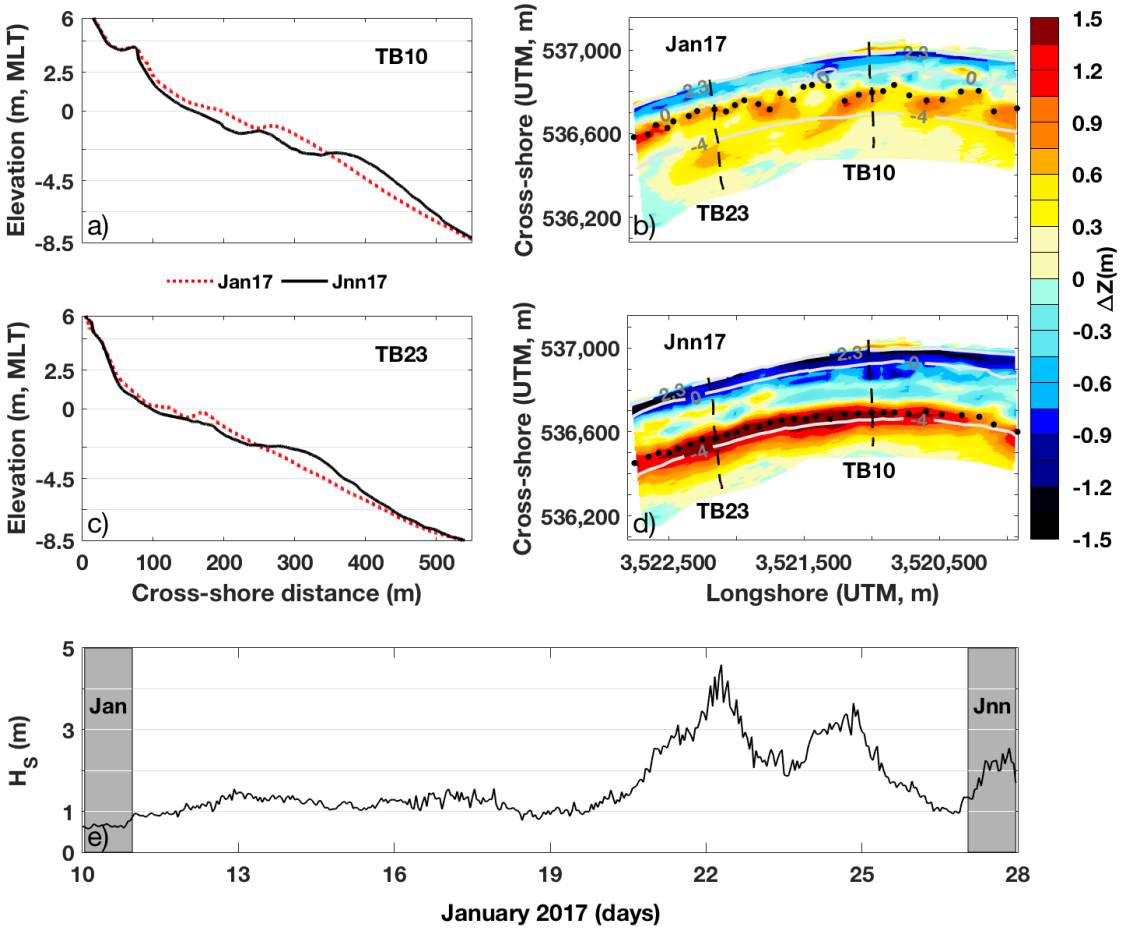

Figure 3.7 Storm-driven offshore sandbar migration during the 21–25 January 2017 event. The top left panels show the profile change before (dashed red lines) and after (full black lines) the storm for TB10 and TB23. The top right panels present the cumulative morphological change before (Jan17) and after (Jnn17) the storm. The time series of significant wave height (H_S) during the storm and between the periods of morphological measurements (in gray) is presented in the bottom panel.

3.3.5 Temporal variability of sandbar morphometrics

Temporal changes of sandbar morphometry were analysed from August 2014 to August 2017 based on alongshore-averaged parameters such as sandbar crest positions, $\overline{P_b}$, depths, $\overline{d_b}$, and heights, $\overline{h_b}$, and sandbar widths, $\overline{W_b}$, and volumes, $\overline{V_b}$. The variability of these parameters was then related to

the averaged significant wave height for the periods between morphological measurements, $\overline{H_S}$. Three complete annual cross-shore sandbar migration cycles are herein described into detail (Fig. 3.8).

Cycle I corresponded to pre-El Niño conditions (August 2014–August 2015). The sandbar formed in November 2014 at a distance of 50 m from the reference shoreline and 0.7 m depth, it was 0.8 m high and 95 m wide and contained ~35 $m^3\,m^{-1}$ of sediment. During the energetic wave conditions (up to $\overline{H_S} \approx$ 1:3 m) it migrated offshore reaching its maximum distance of 109 m and 1.5 m depth by January 2015; and contained ~75 $m^3\,m^{-1}$ of sand and was 1 m high and 150 m wide (Fig. 3.8). Between January and February 2015, the sandbar moved slightly onshore to a distance of 97 m and 1.2 m depth, barely increasing its height to 1.1 m but gaining sediment ($\overline{V_b}$ = 88 $m^3\,m^{-1}$) and reaching its maximum width of 157 m. During the milder wave conditions after February ($\overline{H_S}$ of 1 m), the sandbar migrated onshore to a distance of 62 m from the reference shoreline and a depth of 0.8 m, and gradually decreased its volume (to 62 $m^3\,m^{-1}$) and width (to 140 m), stabilizing its height to 1 m by April, and eventually welded to the shoreline by May 2015. The beach was unbarred over the 2015 summer (Fig. 3.8).

During cycle II (August 2015–August 2016), which included the El Niño winter, the sandbar formed in November near the shoreline, at 0.9 m depth and 72 m offshore from the reference shoreline, it was 0.9 m high, 100 m wide and

contained ~50 $m^3\,m^{-1}$ of sediment. The wave conditions during the winter were more energetic than in the previous year ($\overline{H_S}$ = 1.6–2 m), which induced a larger offshore sandbar migration. Thus, the sandbar reached a maximum distance of 183 m and depth of 2.6 m by February 2016, had a volume of 172 $m^3\,m^{-1}$ and was 1.4 m high and 249 m wide (Fig. 3.8). The wave energy decreased between February and May 2016 (from $\overline{H_S}$ of 2 m to 1 m) favoring the onshore sandbar migration to a distance of 125 m and to shallower depths of 1.8 m, reducing its $\overline{V_b}$ and $\overline{h_b}$ considerably (to 148 $m^3\,m^{-1}$ and 1 m), and increasing its $\overline{W_b}$ to 280 m. In June 2016, the sandbar was 0.8 m high and 288 m wide, and migrated slightly offshore to a distance of 137 m and depth of 2.3 m, decreasing its volume (134 $m^3\,m^{-1}$) and turning into a terrace-bar by July (Fig. 3.8). Over the 2016 summer a terrace-bar existed at distances between 165 and 185 m and depths of 2.5–3.5 m, and gradually decreased its volume (85–110 $m^3\,m^{-1}$), height (0.6–0.7 m) and width (246–275 m) while partially transferring sediment onto the subaerial beach.

In cycle III (August 2016–August 2017), the sandbar reformed in November farther offshore and deeper (distance of 120 m and depth of 1.7m). It was 1 m high, 282 m wide and had 123 $m^3\,m^{-1}$ of sand, which suggested that the sediment contained in the terrace-bar contributed to the sandbar build-up. The first half of the winter (November to early January) presented mild wave conditions ($\overline{H_S}$ < 1.1 m) that favored onshore sandbar migration to a distance of 73 m and depths of 0.9 m, while it widened (from 282 to 305 m) and reduced its

volume (111 $m^3\,m^{-1}$) and height (0.8 m) (Fig. 3.8). A large swell storm in late January (Jnn17; $\overline{H_s}$ of 2 m in Fig. 3.8) induced a rapid offshore sandbar movement of 120 m, placing the sandbar at a distance of 193 m and 3 m depth, and nearly doubling its $\overline{V_b}$ (from 111 to 197 $m^3\,m^{-1}$), increasing its $\overline{h_b}$ to 1.1 m and decreasing its $\overline{W_b}$ to 281 m (steepening). After the storm (in February), the sandbar moved slightly onshore (25 m), to a distance of 168 m and depth of 2.7 m, and widened ($\overline{W_b}$ = 319 m) but decreased its volume ($\overline{V_b}$ = 195 $m^3\,m^{-1}$) and flattened ($\overline{h_b}$ = 0.8 m). During the subsequent mild wave conditions ($\overline{H_s}$ < 1 m), the sandbar reduced its $\overline{V_b}$ (103 $m^3\,m^{-1}$), $\overline{h_b}$ (0.6 m) and $\overline{W_b}$ (270 m) turning the sandbar into a terrace-bar at a depth of 3.9 m and distance of 203 m by March (Fig. 3.8). By May the terrace-bar stabilized its $\overline{V_b}$, $\overline{h_b}$ and $\overline{W_b}$ and moved slightly onshore to a distance of 170 m and 3.2 m depth. The mild wave-energy conditions over the 2017 summer ($\overline{H_s}$ < 0.7 m) placed the terrace-bar at a distance of 220 m and depth of 4.6 m by August, and it became smaller and narrower ($\overline{h_b}$ = 0.4 m; $\overline{V_b}$ = 75 $m^3\,m^{-1}$; $\overline{W_b}$ = 280 m), suggesting that part of its sand was transferred onto the subaerial beach (Fig. 3.8).

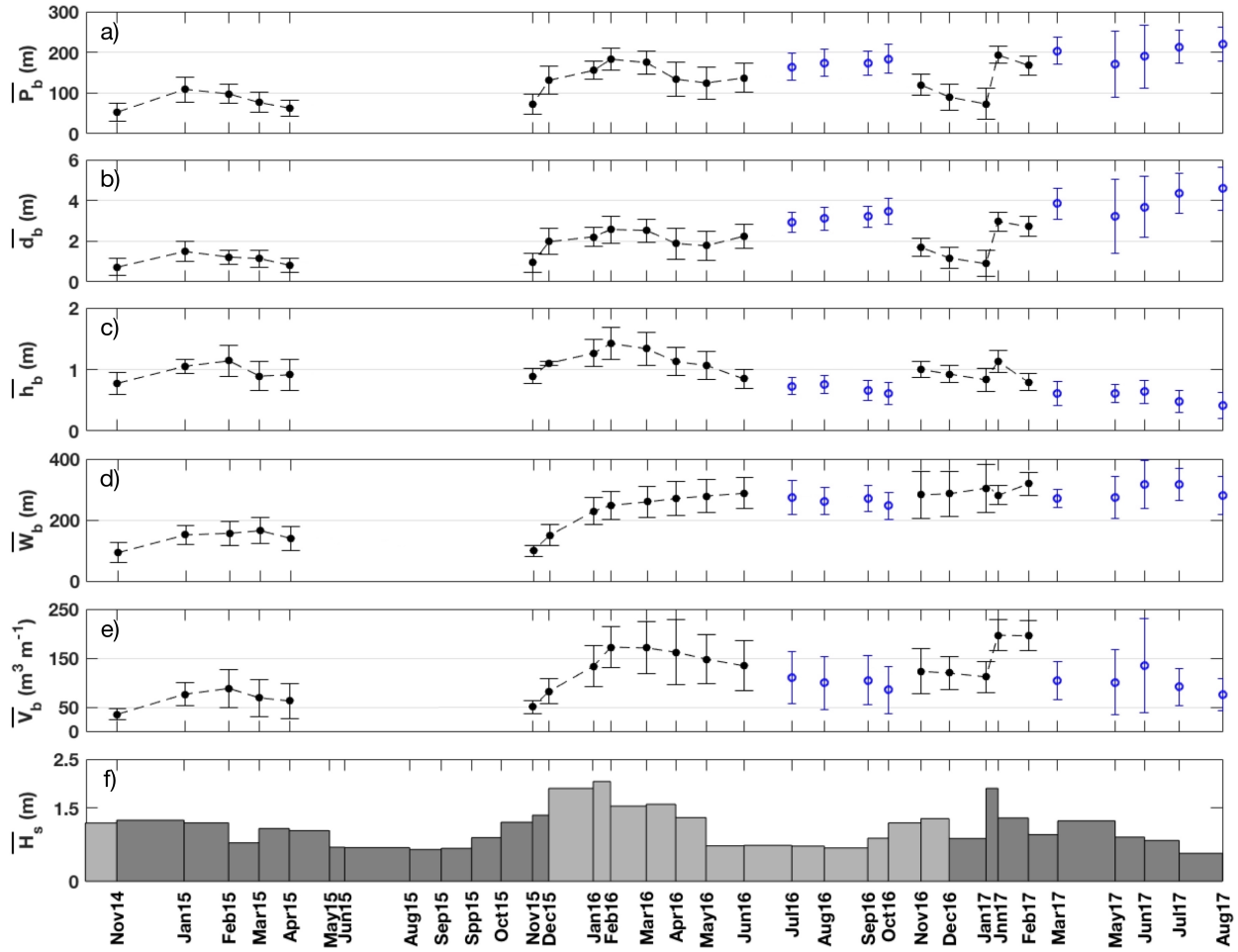

Figure 3.8 Time-series of alongshore averaged sandbar morphometric parameters from October 2014 to August 2017. (a): Sandbar crest positions. (b): Sandbar crest depths. (c): Sandbar crest heights. (d): Sandbar widths. (e): Sandbar volumes. The black dots represent averaged values for sandbars and blue circles for terrace-bars, and the vertical lines are the standard deviations. (e): averaged significant wave height between periods of morphological measurements. The gap between measurements indicates an unbarred beach configuration.

3.3.6 Spatial variability of sandbar morphometry

The cross-shore variability of the alongshore averaged sandbar morphometry was analyzed for the three annual cycles (Fig. 3.9). During cycle I, an increase of all morphometric parameters occurred during the high wave-energy period (November 2014 to February 2015). By January, the sandbar reached maximum distances of 110 m and depths of 1.5 m while the maximum sandbar crest heights (1.2 m) and volumes (75 $m^3 m^{-1}$) ocurred in February. The sandbar migrated landwards near to its location of origin by April, and minimum values of $\overline{d_b}$= 0.8 m, $\overline{h_b}$ = 0.9 m, $\overline{W_b}$ = 140 m and $\overline{V_b}$ = 60 $m^3 m^{-1}$ were obtained (Fig. 3.9). The morphometric parameters also increased linearly with the cross-shore distance during cycle II (November 2015 to February 2016), but at a higher rate than in the previous cycle. The sandbar reached a maximum distance of nearly 190 m by February 2016 and presented $\overline{d_b}$ = 2.6 m, $\overline{h_b}$ = 1.4 m and $\overline{V_b}$ = 172 $m^3 m^{-1}$. The sandbar persisted two months longer than in cycle I (until June rather than April), and in June, it was located at a distance of 140 m, even farther than in January the previous year. Thus, the sandbar was unable to reach a similar position as its origin in November, instead, it stabilized at $\overline{d_b}$ = 1.9–2:3 m, decreasing its volume (and height) and flattening between April and June (Fig. 3.9). During cycle III the sandbar formed in November at a similar depth (1.7 m) and cross-shore distance (120 m) as where it was located in May in cycle II (Fig. 3.9). Contrary to the expected, the sandbar migrated onshore between November and early January, locating it at a similar depth (0.9 m) and

distance (70 m) as its origin in the previous cycles but containing twice as much sand. Associated with the storm in late January (Jnn in Fig. 3.9), the sandbar migrated 120 m seaward, locating at a similar position as in February of cycle II (distance of 190 m) but slightly deeper ($\overline{d_b}$ ≈ 3 m). The sandbar migrated slightly onshore to a distance of 170 m by February but it flattened ($\overline{h_b}$ < 0.75 m) and widened, becoming a terrace-bar after March (Fig. 3.9).

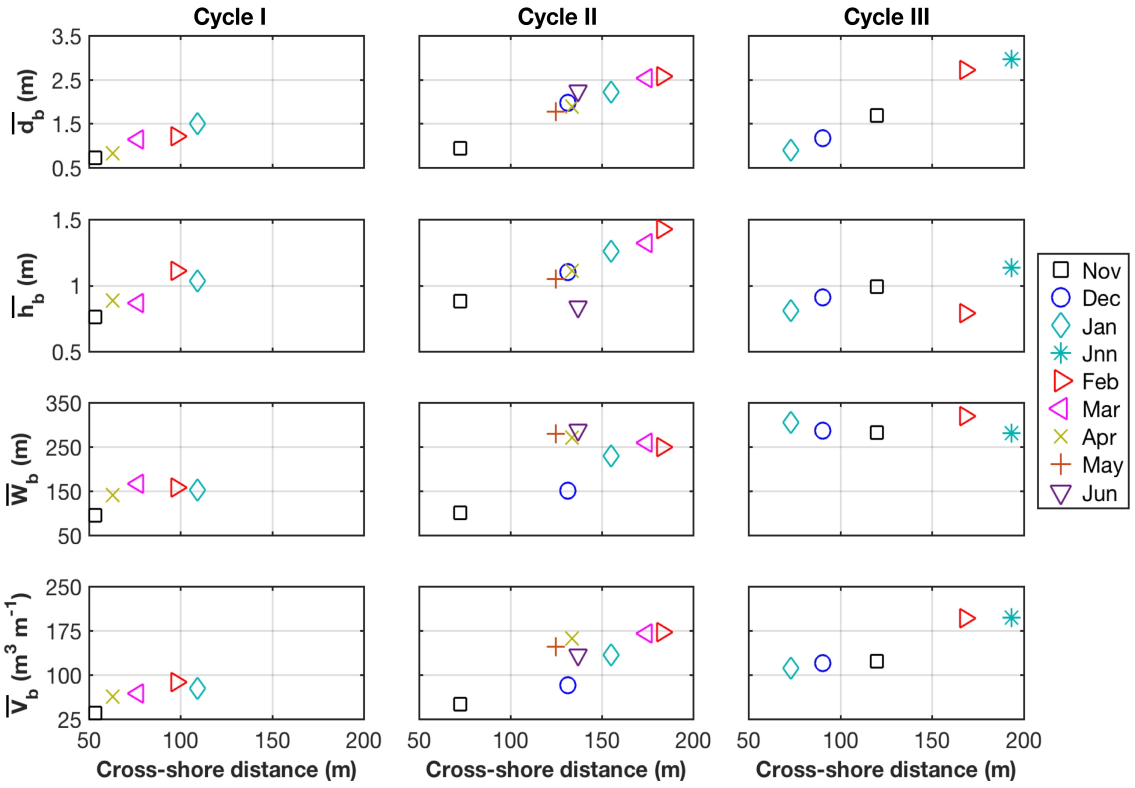

Figure 3.9 Cross-shore distribution of the alongshore averaged morphometric parameters: sandbar crest depths ($\overline{d_b}$; top panels) and heights ($\overline{h_b}$; second top) and, sandbar widths ($\overline{W_b}$; third top panels) and volumes ($\overline{V_b}$; bottom panels) per migration cycle: cycle I (August 2014-August 2015, left panels), cycle II (August 2015-August 2016, middle panels) and cycle III (August 2016-August 2017, right panels).

3.4 Discussion

Monthly morphological measurements collected over three years, from August 2014 to August 2017, allowed a detailed analysis on the variability of sandbar crest positions, depths and heights, and sandbar widths and volumes relative to the incident wave forcing on a single-barred beach in Baja California. Previous studies showed strong seasonality in the morphological beach evolution, directly related to the incoming wave forcing (Ruiz de Alegría-Arzaburu et al., 2017). The cross-shore sandbar movement was highly modulated by the incident wave conditions (Ranasinghe et al., 2004; Ojeda et al., 2011), and in accordance with other studies (Shepard, 1950; Komar, 1974; Van Enckevort and Ruessink, 2003; Di Leonardo and Ruggiero, 2015; Splinter et al., 2018; Cheng and Wang, 2018), the sandbar migrated offshore during periods of energetic waves and onshore during calm wave conditions (Ruiz de Alegría-Arzaburu and Vidal-Ruiz, 2018). The recovery capability of the subaerial beach depended completely on the full attachment of the sandbar to the shoreline over the spring, which did not happen after the energetic El Niño 2015–2016 winter (Ruiz de Alegría- Arzaburu and Vidal-Ruiz, 2018). Here, the morphometric characteristics of the sandbar were analyzed in order to understand its propagating patterns across the beach, prior, during and after the El Niño event.

The beach followed the accretionary morphological beach state sequence described by Wright and Short (1984) during the complete onshore sandbar

migration cycle in 2015, prior to El Niño. At the end of that winter (in February), the beach presented a longshore bar-trough state, which turned into a low-tide terrace by the end of spring (in May). Thus, the beach became unbarred in summer while a berm was built in the upper beach, following the seasonal bar–berm model (Shepard, 1950; Komar, 1974). The sandbar formed in November ($\overline{h_b}$ = 0.8 – 0.9 m) at depths of 0.7–0.9 m and distance of 50–72 m, migrated offshore (to 1.5 m depth and distance of 109 m) during the winter (up to $\overline{H_s} \approx 1.3$ m) and landward during the lower energy conditions over the spring ($\overline{H_s} < 1.0$ m), to a similar location and depth as origin (62 m and $\overline{h_b}$ = 0.8), until it welded to the shoreline by May. These cross-shore migration patterns suggest that the sandbar migrates toward a wave height dependent equilibrium, following the breakpoint hypothesis (Dean, 1973; Sallenger et al., 1985; Dally, 1987; Plant et al., 1999; Mariño-Tapia, et al. 2007b). As wave energy increases, the sandbar migrates offshore in direction of an equilibrium position, very possibly driven by the undertow. However, the accretionary beach state sequence was not repeated in the following two years (after El Niño), and large differences in the geometry (width, height and volume) and magnitude of sandbar displacement (position and depth) were encountered between the different annual cycles.

Sandbars occasionally split into an onshore propagating feature and an offshore migrating feature, and some other times, inner and outer bars merge (Plant et al., 1999). The incidence of higher wave energy during the El Niño winter ($\overline{H_s}$ = 1.6–2 m) propagated the sandbar 74 m farther than in the previous

winter, up to a distance of 183 m and depth of 2.6 m, and with twice the volume (172 $m^3\ m^{-1}$). During the milder wave conditions in spring ($\overline{Hs}$ < 1.0 m), the sandbar migrated onshore, but stabilized at a distance of 125 m and 1.8 m depth, with large amount of sand ($\overline{Vb}$ = 148 $m^3\ m^{-1}$). Thus, the inability of the beach to reach the dynamic equilibrium during the lower wave energy period after the El Niño winter, is attributed to the large amount of sediment contained in the sandbar (twice the amount of the year before). The sandbar volume continuously decreased over the 2016 spring; part of the sandbar propagated landwards, and other part became a terrace-bar (h_b < 0.75 m) that flattened over the summer ($\overline{db}$ = 2.5–3 m). In agreement with Plant et al. (1999), the sandbar divided into a shoreward propagating feature that contributed to partial subaerial recovery, and an offshore migrating and flattening terrace-bar over the summer. These findings suggest that the sandbar rebuilt in November 2016, with the input of terrace-bar sediment, and was located farther offshore (120 m) and deeper (1.7 m) than in previous years.

Although onshore sandbar movements are generally associated with the spring and summer seasons, this behavior can also occur anytime under moderately energetic wave condition (Plant et al., 1999; Pape et al., 2010). Landward sandbar propagation was measured during a low-wave energy period ($\overline{Hs}$ < 1.1 m) at the beginning of the 2016–2017 winter, which placed the sandbar at the location of its origin ($\overline{Pb}$ = 73 m; $\overline{db}$ = 0.9 m; $\overline{hb}$ = 0.8 m; $\overline{Vb}$ = 111 $m^3\ m^{-1}$). Thus, the lowering of wave energy caused the disruption of the

erosional morphological beach state sequence expected during the winter (Wright and Short, 1984). Nevertheless, this morphological beach state reseted with the impact of a subsequent extreme storm (Larson and Kraus, 1992; Ruessink et al., 2007; Ojeda et al., 2011) that caused a rapid seaward sandbar propagation of 120 m, placing it at a distance of 193 m and 3 m depth ($\overline{h_b}$ = 1.1 m; $\overline{V_b}$ = 197 $m^3\,m^{-1}$). Interestingly, the offshore sandbar displacement induced by this extreme storm was of similar magnitude to the reached at the end of the El Niño winter (~190 m from the reference shoreline), and in both cases, the sandbar migrated onshore during the subsequent milder wave period. Contrary to this behavior, many multi-barred beaches lack intra-annual correlation between sandbar migrations and incident wave forcing, and instead, they present interannual variability consisting of a net offshore migration (NOM) over periods from a few years to decades, and a final sandbar degeneration phase at the outer nearshore margin (e.g. Ruessink and Kroon, 1994; Plant et al., 1999; Shand et al., 1999).

Four seasonal sandbar migration stages were identified in the studied single-barred beach: (1) generation in autumn (November) at lower depths than 1 m; (2) offshore migration during large winter waves ($\overline{H_s}$ > 1.3 m; until February); (3) onshore migration during milder waves over the spring ($\overline{H_s}$ < 1.0 m; March to April); and during May–June: (4a) weld to the subaerial beach resulting in an unbarred summer configuration; or (4b) terrace-bar formation and flattening during the summer (sand transference toward the subaerial beach).

Option (4a) occurred when an offshore sandbar equilibrium distance of ~110 m and 1.5 m depth was reached, while (4b) took place when the sandbar migrated greater offshore distances of up to ~190 m and located at deeper depths (2.6–3 m; almost twice than in 4a). The sandbar tended to evolve toward an equilibrium position during the seasonal cycle (e.g. Plant et al., 2001; Cheng and Wang, 2018), but was unable to reach its dynamic equilibrium in (4b). This supports the idea that offshore/onshore sandbar migration distances are not only associated with the incident wave energy, but also with the preceding morphological conditions (Plant et al., 1999; Pape et al., 2010).

3.5 Conclusions

Sandbar morphometric variations were studied over three annual cycles (August 2014 to August 2017) at the single-barred Ensenada Beach, located in the northwestern Baja California peninsula in Mexico. Changes in sandbar migration patterns associated with the 2015–2016 El Niño anomaly and a highly energetic storm were analyzed. The sandbar migrated toward a wave height dependent equilibrium, following the breakpoint hypothesis. After the El Niño winter, the beach was unable to reach the dynamic equilibrium during the low-wave energy period, which was attributed to the large sandbar volume (twice the amount of the year before). Consequently, the sandbar divided into a shoreward propagating feature that contributed to partial subaerial recovery and a terrace-bar feature that flattened and migrated offshore over the summer.

A period of mild wave conditions during the 2017 winter favored the landward migration of the sandbar, placing it at its dynamic equilibrium location onshore (near its generation point). But the impact of a subsequent extreme storm reset the morphology and triggered a rapid offshore sandbar migration. The sandbar displacement of the individual energetic storm was very similar to the observed at the end of the El Niño winter, in both cases, the sandbar reached a maximum cross-shore distance of ~190 m; beyond the dynamic equilibrium. After these events, the sandbar migrated onshore during the subsequent milder wave period, but was unable to weld to the shoreline, and instead, a terrace-bar feature was formed.

In summary, four seasonal sandbar migration stages were identified: (1) generation in November at $\overline{d_b} < 1$ m; (2) offshore migration over the winter until February ($\overline{H_s} > 1.3$ m); (3) onshore migration from March to April ($\overline{H_s} < 1.0$ m); and during May–June: (4a) weld to the subaerial beach (unbarred beach); or (4b) terrace-bar formation and flattening over the summer. Option (4a) occurred when an offshore sandbar equilibrium distance of ~110 m and 1.5 m depth was reached, while (4b) took place when the sandbar migrated greater offshore distances of up to ~190 m and located at deeper depths (2.6–3 m; almost twice than in 4a). Consequently, the capabilities of the sandbar to reach shallow waters ($\overline{d_b} < 1$ m) and weld to the subaerial beach will depend on its distance relative to the dynamic equilibrium point, but also, on the amount of sand contained by the sandbar and the duration of the mild wave condition period.

3.6 References

Aagaard, T., Greenwood, B., & Hughes, M. G. (2013), Sediment transport on dissipative, intermediate and reflective beaches. *Earth-Science Reviews*, 124, 32–50.doi.org/10.1016/j.earscirev.2013.05.002

Aagaard, T., Davidson-Arnott, R., Greenwood, B., & Nielsen, J. (2004), Sediment supply from shoreface to dunes: linking sediment transport measurements and long-term morphological evolution. *Geomorphology*, 60(1), 205–224.doi.org/10.1016/j.geomorph.2003.08.002

Aleman, N., Certain, R., Robin, N., & Barusseau, J. P. (2017), Morphodynamics of slightly oblique nearshore bars and their relationship with the cycle of net offshore migration. *Marine Geology* 392, 41–52.
doi.org/10.1016/j.margeo.2017.08.014

Anthony E .J., Vanhée S., & Ruz, M. H. (2006), Short-term beach-dune sand budgets on the North Sea coast of France: sand supply from shoreface to dunes and the role of wind and fetch. *Geomorphology,* 81, 316-329.
doi.org/10.1016/j.geomorph.2006.04.022

Birkemeier, W.A. (1984), *Time scales of nearshore profile changes.* Paper presented at 19th International Conference on Coastal Engineering, American Society of Civil Engineers, New York.

Blossier, B., Bryan, K. R., Daly, C. J., & Winter, C. (2016), Nearshore sandbar rotation at single-barred embayed beaches. *Journal of Geophysical Research: Oceans*, 121, 2286–2313.doi.org/10.1002/ 2015JC011031.

Cheng, J., & Wang, P. (2018), Dynamic equilibrium of sandbar position and height along a low wave energy micro-tidal coast. *Continental Shelf Research*, 165, 120–136.doi.org/10.1016/j.csr.2018.05.004

Coco, G. & Murray, A.B. (2007), Patterns in the sand: from forcing templates to self-organization. *Geomorphology*, 91, 271–290. doi.org/10.1016/j.geomorph.2007.04.023

Cohn, N., Ruggiero, P., de Vries, S., & García-Medina, G. (2017), *Beach growth driven by intertidal sandbar welding*. Paper presented at 8th International Conference on Coastal Dynamics, Helsingør, Denmark.

Di Leonardo, D., & Ruggiero, P. (2015), Regional scale sandbar variability: Observations from the U.S. Pacific Northwest. *Continental Shelf Research*, 95, 74–88.doi.org/10.1016/j.csr.2014.12.012

Dubabier, B., Castelle, B., Marieu, V., & Ruessink, B. G. (2015), Process-based modeling of cross-shore sandbar behaviour. *Coastal Engineering*, 95, 35–50. doi.org/10.1016/j.coastaleng.2014.09.004

Fernández-Mora, A., Calvete, D., Falqués, A., & de Swart H. E. (2015), Onshore sandbar migration in the surf zone: New insights into the wave-induced sediment transport mechanisms. *Geophysical Research Letters*, 42, 2869–2877. doi.org/10.1002/2014GL063004

Grunnet, N.M., & Hoekstra, P. (2004), Alongshore variability of the multiple barred coast of Terschelling, The Netherlands. *Marine Geology*, 203, 23–41. doi.org/10.1016/S0025-3227(03)00336-0

Henderson, S.M., Allen, J.S., & Newberger, P.A., (2004), Nearshore sandbar migration predicted by an eddy-diffusive boundary layer model. *Journal of Geophysical Research*, 109, C06024.doi.org/10.1029/2003JC002137.

Hoefel, F., & Elgar, S. (2003), Wave-induced sediment transport and sandbar migration. *Science*, 299, 1885–1887.doi.org/10.1126/science.1081448

Holman, R.A., Lalejini, D.M., & Holland, T. (2016), A parametric model for barred equilibrium beach profiles: Two-dimensional implementation. *Coastal Engineering*, 117, 166–175.doi.org/10.1016/j.coastaleng.2016.07.010

Holman, R. A. & Bowen, A. J. (1982), Bars, bumps, and holes: Models for the generation of complex beach topography. *Journal of Geophysical Research*, 87, 457–468.doi.org/10.1029/JC087iC01p00457

Hsu, T. J., Elgar, S., & Guza, R.T. (2006), Wave-induced sediment transport and onshore sandbar migration. *Coastal Engineering*, 53, 817–824. doi.org/10.1016/j.coastaleng.2006.04.003

Komar, P. D. (1974), *Beach Processes and Sedimentation* (429pp). Englewood Cliffs, NJ: Prentice-Hall.

Larson, M., & Kraus, N.C. (1992), *Dynamics of longshore bars*. Paper presented at 23rd International Conference on Coastal Engineering, American Society of Civil Engineers, Venice, Italy.

Lippmann, T.C., Holman, R.A., & Hathaway, K.K. (1993), Episodic, Nonstationary Behavior of a Double Bar System at Duck, North Carolina, U.S.A., 1986–1991. *Journal of Coastal Research* SI, 15, 49–75.

Lippmann, T.C., & Holman, R.A. (1990), The spatial and temporal variability of sand bar morphology. *Journal of Geophysical Research*, 95 (C7), 11575–11590. doi.org/10.1029/JC095iC07p11575

Mariño-Tapia, I. J., O'Hare, T. J., Russell, P. E., Davidson, M. A. & Huntley, D. A. (2007), Cross-shore sediment transport on natural beaches and its relation to sandbar migration patterns: 2. Application of the field transport parameterization. *Journal of Geophysical Research*, 112, C03002. doi.org/10.1029/2005JC002894

Masselink, G., Austin, M., Scott, T., Poate, T., & Russell, P. (2014), Role of wave forcing, storms and NAO in outer bar dynamics on a high-energy, macro-tidal beach. *Geomorphology*, 226, 76–93.
doi.org/10.1016/j.geomorph.2014.07.025

Ostrowski, R., Pruszak, Z. & Zeidler, R.B. (1991), *Multi-scale nearshore and beach changes*. Paper presented at 22nd International Conference on Coastal Engineering, American Society of Civil Engineers, Delft, The Netherlands. doi.org/10.1061/9780872627765.161

Ojeda, E., Guillén, J., & Ribas, F. (2011), Dynamics of single-barred embayed beaches. *Marine Geology*, 280, 76–90. doi.org/10.1016/j.margeo.2010.12.002

Pape, L., Plant, N. G., & Ruessink, B. G. (2010), On cross-shore migration and equilibrium states of nearshore sandbars. *Journal of Geophyscal Research*, 115, F03008.doi.org/10.1029/2009JF001501.

Phillips, M. S., Harley, M. D., Turner, I. L., Splinter, K. D., & Cox, R. J. (2017), Shoreline recovery on wave-dominated sandy coastlines: the role of sandbar morphodynamics and nearshore wave parameters. *Marine Geology*, 385, 146–159.doi.org/10.1016/j.margeo.2017.01.005

Plant, N.G., Freilich, M.H., & Holman, R.A. (2001), Role of morphologic feedback in surf zone sandbar response. *Journal of Geophyscal Research*, 106 (C1), 973–989.doi.org/10.1029/2000JC900144

Plant, N.C., Holman, R.A., Freilich, M.H. & Birkemeier, W.A. (1999), A simple model for interannual sandbar behaviour. *Journal of Geophysical Research,* 104, 15755–15776.doi.org/10.1029/1999JC900112

Price, T. D., Ruessink, B. G. & Castelle, B. (2014), Morphological coupling in multiple sandbar systems – A review. *Earth Surface Dynamics*, 2(1), 309–321. doi.org/10.5194/esurf-2-309-2014

Ranasinghe, R., Symonds, G., Black, K. & Holman, R. (2004), Morphodynamics of intermediate beaches: A video imaging and numerical modelling study. *Coastal Engineering*, 51(7), 629–655.doi.org/10.1016/j.coastaleng.2004.07.018

Ruessink, B.G., Blenkinsopp, C., Brinkkemper, J.A., Castelle, B., Dubarbier, B., Grasso, F., Puleo, J.A., & Lanckriet, T. (2016), Sandbar and beach-face evolution on a prototype coarse sandy barrier. *Coastal Engineering*, 113, 19–32. doi.org/10.1016/j.coastaleng.2015.11.005

Ruessink, B.G., Coco, G., Ranasinghe, R., & Turner, I.L. (2007), Coupled and noncoupled behavior of three-dimensional morphological patterns in a double sandbar system. *Journal of Geophysical Research*, 112, C07002. doi.org/10.1029/2006JC003799

Ruessink, B.G., Pape, L., & Turner, I. L. (2009), Daily to interannual cross-shore sandbar migration: observation from a multiple sandbar system. *Continental Shelf Research*, 29, 1663–1677.doi.org/10.1016/j.csr.2009.05.011

Ruessink, B.G., Wijnberg, K.M., Holman, R.A., Kuriyama, Y., & Van Enckevort, I.M.J. (2003), Intersite comparison of interannual nearshore bar behavior. *Journal of Geophysical Research*, 108, 3249. doi.org/10.1029/2002JC001505

Ruessink, B.G., & Kroon, A. (1994), The behaviour of a multiple bar system in the nearshore zone of Terschelling, the Netherlands: 1965–1993. *Marine Geology*, 121, 187–197. doi.org/10.1016/0025-3227(94)90030-2

Ruggiero, P., Walstra, D.J.R., Gelfenbaum, G., & Van Ormondt M. (2009), Seasonal-scale nearshore morphological evolution: Field observations and numerical modelling. *Coastal Engineering,* 56, 1153–1172. doi.org/10.1016/j.coastaleng.2009.08.003

Ruiz de Alegría-Arzaburu, A., García-Nava, H., Gil-Silva, E., & Desplán-Salinas, G. (2015), *A morphodynamic comparison of walled and non-walled beach sections, Ensenada beach, Mexico*. Paper presented at 8th International Conference on Coastal Sediments, San Diego, California. doi.org/10.1142/9789814689977_0018

Ruiz de Alegría-Arzaburu, A., Vidal-Ruiz, J.A., García-Nava, H., & Romero-Arteaga, A. (2017), Seasonal morphodynamics of the subaerial and subtidal sections of an intermediate and mesotidal beach. *Geomorphology*, 295, 383–392.doi.org/10.1016/j.geomorph.2017.07.021

Ruiz de Alegría-Arzaburu, A. & Vidal-Ruiz, J.A. (2018), Beach recovery capabilities after El Niño 2015–2016 at Ensenada Beach, Northern Baja California. *Ocean Dynamics*, 6, 749–759.doi.org/10.1007/s10236-018-1164-6

Rutten, J., Ruessink, B.G., & Price, T. D. (2018), Observations on sandbar behaviour along a man-made curved coast. *Earth Surface Processes and Landforms*, 43,134–149.doi.org/10.1002/esp.4158

Sallenger, A.H., Holman, R.A., & Birkemeier, W.A. (1985), Storm-induced response of a nearshore-bar system. *Marine Geology*, 64, 237–257. doi.org/10.1016/0025-3227(85)90107-0

Senechal, N., Coco, G., Castelle, B., & Marieu V. (2015), Storm impact on the seasonal shoreline dynamics of a meso- to macrotidal open sandy beach (Biscarrosse, France). *Geomorphology*, 228, 448–461. doi.org/10.1016/j.geomorph.2014.09.025

Shand, R.D., Bailey, D.G., & Shepherd, M. J. (1999), An inter-site comparison of net offshore bar migration characteristics and environmental conditions. *Journal of Coastal Research*, 15, 750–765.

Shepard, F.P. (1950), *Beach cycles in southern California. Beach Erosion Board (Technical Memo 20)*. Washington DC: US Army Corps of Engineering.

Short, A. D. (1999), *Handbook of Beach and Shoreface Morphodynamics*. Chichester, UK: John Wiley and Sons.

Smit, M.W.J., Reniers, A.J.H.M., & Stive, M.J.F. (2012), Role of morphological variability in the evolution of nearshore sandbars. *Coastal Engineering*, 69, 19-28.doi.org/10.1016/j.coastaleng.2012.05.005

Splinter, K.D., Gonzalez, M.V.G., Oltman-Shay, J., Rutten, J., & Holman., R. (2018), Observations and modelling of shoreline and multiple sandbar behaviour

on a high-energy meso-tidal beach. *Continental Shelf Research*, 159, 33–45. doi.org/10.1016/j.csr.2018.03.010

Tătui, F., Vespremeanu-Stroe, A., & Ruessink, B.G. (2016), Alongshore variability of cross-shore bar behavior on a nontidal beach. *Earth Surface Processes and Landforms*, 41(14), 2085–2097.doi.org/10.1002/esp.3974

Thiébot, J., Idier, D., Garnier, R., Falqués, A., & Ruessink, B. G. (2012), The influence of wave direction on the morphological response of a double sandbar system. *Continental Shelf Research*, 32, 71–85.
doi.org/10.1016/j.csr.2011.10.014

Van Enckevort, I.M.J. & Ruessink, B.G. (2003), Video observations of nearshore bar behaviour. Part 1: alongshore uniform variability. *Continental Shelf Research*, 23, 501–512.doi.org/10.1016/S0278-4343(02)00234-0

Van de Lageweg, W. I., Bryan, K. R., Coco, G., & Ruessink, B. G. (2013), Observations of shoreline–sandbar coupling on an embayed beach. *Marine Geology*, 344, 101–114.doi.org/10.1016/j.margeo.2013.07.018

Van Maanen, B., de Ruiter, P.J., Coco, G., Bryan, K.R., & Ruessink, B.G. (2008), Onshore sandbar migration at tairua beach (new zealand): numerical simulations and field measurements. *Marine Geology*, 253, 99–106.
doi.org/10.1016/j.margeo.2008.05.007

Walstra, D.J.R., Ranasinghe, R., Roelvink, J.A., & Ruessink, B.G. (2012), On bar growth and decay during interannual net offshore migration. *Coastal Engineering*, 60, 190–200.doi.org/10.1016/j.coastaleng.2011.10.002

Wright, L.D., Short, A.D., & Green, M.O. (1985), Short-term changes in the morphodynamics states of beaches and surf zones: an empirical predictive model. *Marine Geology* 62, 339–364.

Wright, L.D. & Short, A.D. (1984), Morphodynamic variability of surf zones and beaches: a synthesis. *Marine Geology*, 56: 93–118. doi.org/10.1016/0025-3227(84)90008-2

Chapter 4

4 Modes of sandbar behavior during onshore migration[2,3]

Eroded sediment can return to the subaerial beach through onshore sandbar migration, thus, understanding this process is key for rebuilding coastal morphology. While net offshore sandbar migration processes have been widely studied, detailed investigations into landward migration and subaerial beach welding are currently lacking. In this study, four years of monthly measured topographic and bathymetric data (46 surveys) were analyzed to describe behavioral modes of onshore sandbar migration on a single-barred beach exposed to a variety of wave conditions. The control of sandbar location and morphometric characteristics over the landward migration process was investigated. The sandbar followed a wave-height dependent time-varying equilibrium state. The cross-shore limit for the dynamic equilibrium position (DEP) was empirically determined as 150 m from the reference shoreline, equivalent to ~3 m water depth, for an alongshore-averaged maximum sandbar height of 1 m containing up to 100 m^3m^{-1} of sand. Five distinct cross-shore sandbar migration modes were identified, primarily governed by sandbar size (volume and height) and crest location from DEP. Mode I, complete sandbar coupling (SC): when located onshore from DEP, onshore sandbar migration and welding to the shoreline occurred during low wave-energy conditions after a moderately energetic winter. Mode II, sandbar to terrace-bar transition (STT): when located offshore from DEP, the sandbar flattened and turned into a terrace-bar during low-energy conditions after a highly-energetic winter. Mode III, terrace-bar to sandbar transition (TST): when located near DEP, the terrace-bar turned into a sandbar after a rebuilding process during moderately energetic conditions. Mode IV, terrace-bar splitting (TS): the terrace-bar located offshore from DEP and exposed to low-energy conditions divided into two: the outer section followed a net offshore migration cycle while the inner section migrated towards DEP, and could then follow TST. And Mode V, sandbar and terrace-bar coexistence (STC): it occurred when a new sandbar formed near the shoreline whilst the terrace-bar continued degrading and migrating offshore.

This chapter is based on the article published in the *proceedings of Coastal Sediments 2019*[2], and on the article submitted to the journal *Marine Geology*[3].

[2] Vidal-Ruiz J. A. and Ruiz de Alegría Arzaburu A. 2019, Shoreline variability related to sandbar morphometrics on a single-barred beach in NW Baja California. *International Conference on Coastal Sediments* '19, Florida (for presentation).

[3] Vidal-Ruiz J. A. and Ruiz de Alegría Arzaburu A. (submitted), Modes of sandbar behavior during onshore migration on a single-barred and swell-dominated beach. Journal *Marine Geology*.

4.1 Introduction

Nearshore sandbars are very dynamic morphological features that can contain large amount of sediment, thus, understanding their cross-shore and longshore displacements is relevant from a beach recovery perspective. These bedforms are generally perceived as amplifications on the elevation of the subtidal profile, and while high-amplitude perturbations are identified as sandbars, terrace-bars are often referred to low-amplitude perturbations separated from the shore (Holman and Bowen, 1982; Aagaard et al., 2013). The dynamics of these features has been studied for many decades due to their relevance on wave energy dissipation and sediment transport processes (e.g. Sallenger et al., 1985; Short, 1999; Hoefel and Elgar, 2003; Hsu et al., 2006; Ruessink et al., 2007), but detailed investigations on their behavior during their cross-shore displacements are limited (Larson and Kraus, 1992; Ruessink and Kroon, 1994; Grunnet and Hoekstra, 2004; Aleman et al., 2017; Cheng and Wang, 2018; Vidal-Ruiz and Ruiz de Alegría-Arzaburu, 2019).

The beach equilibrium concept proposed by Dean (1977) referred to the instant when the beach morphology would no further change assuming idealized steady wave conditions. In reality, the beach sustains a dynamic equilibrium, and adapts continuously its morphological shape to the hydrodynamic forcing. The position and geometry of sandbars result from the constant feedback between the hydrodynamic forcing and nearshore morphology (Wright et al.,

1985; Lippmann and Holman, 1990; Wijnberg and Kroon, 2002), and play an important role in the dynamic equilibrium of the beach (Splinter et al., 2018; Cheng and Wang, 2018). Based on this idea, efforts have been made to predict the cross-shore position of nearshore features such as shorelines (Yates et al., 2009; Davidson et al., 2013) and sandbars (Plant et al., 1999; Splinter et al., 2018) based on behavioral equilibrium models, but these have mainly focused on double-barred or multi-barred environments that followed dominant net offshore migration cycles.

On beaches with high seasonality, cross-shore sandbar displacements are mainly modulated by the incoming wave energy; hence, the beach becomes barred during high-energy conditions and unbarred during periods of low-energy due to the welding of the sandbar to the shoreline (Shepard, 1950; Komar, 1974; Vidal-Ruiz and Ruiz de Alegría-Arzaburu, 2019). Onshore sandbar migrations have also been described on beaches without clear seasonality, during short low-energy periods (e.g. Ostrowski et al., 1991; Larson and Kraus, 1992; Van Maanen et al., 2008; Van de Lageweg et al., 2013; Blossier et al., 2016; Phillips et al., 2017; Cohn et al., 2017; Cheng and Wang, 2018) and on decadal scales (Aagaard et al., 2004; Anthony et al., 2006), but only a few studies have described the sandbar morphometric characteristics during the cross-shore migration cycle (Larson and Kraus, 1992; Ruessink and Kroon, 1994; Grunnet and Hoekstra, 2004; Aleman et al., 2017; Cheng and Wang, 2018).

The primary objective of this study is to determine the main behavioral modes of the sandbar during its onshore migration process in relation to the dynamic equilibrium position on a seasonal single-barred beach exposed to a range of wave energy conditions. For that purpose, a detailed analysis on sandbar geometry (i.e. height, volume, depth) and location is undertaken for low-energy and high-energy conditions. A previous study demonstrated that the sandbar position responded directly to the incoming wave energy; hence, the beach formed a sandbar that migrated offshore during the high-energy period and onshore when mild-energy conditions prevailed (Vidal-Ruiz and Ruiz de Alegría-Arzaburu, 2019). The sandbar behavior was different during the onshore migration process over the years, highly depending on the preceeding wave energy. Here, five sandbar behavioral modes are described during the landward migration process, in relation to the sandbar morphometric characteristics and location relative to the dynamic equilibrium position.

4.2 Field measurements

Four years of monthly measured bathymetric data consisting of sandbar location and geometry and shoreline positions data were obtained from August 2014 to September 2018 along nearly 3,000 m of beach length in Ensenada Beach in order to understand the behavioral modes of onshore sandbar migration on a single-barred beach, related to the incident wave energy conditions.

4.2.1 Wave data

The wave data were acquired hourly over 1024 s, and the integral wave parameters such as the significant wave height (H_s), spectral peak wave period (T_p) and wave direction (α) were used to characterize the incident wave conditions. These parameters were also used to calculate the total energy flux (Pt) and, the alongshore (Pl) and cross-shore (Px) components, using the following equations:

$$Pl = \frac{\rho g^2}{64\pi} H_s^2 T_p \sin(\alpha)\cos(\alpha) \quad (1)$$

$$Px = \frac{\rho g^2}{64\pi} H_s^2 T_p \cos^2(\alpha) \quad (2)$$

where *g* is the gravitational acceleration, ρ the water density and α the wave angle. Hourly calculated energy flux values were monthly averaged over the four-year study period in order to determine the seasonal and interannual variability in the incident wave energy. In addition, cumulative total energy fluxes were averaged over specific periods between morphological measurements. The dimensionless fall velocity (Gourlay, 1968; Dean, 1973) was calculated using equation (3), being $\overline{W_s}$ the time-averaged sediment settling velocity for a constant D_{50} of 0.31 mm (highest value obtained for February 2016) and H_b the breaker wave height calculated with the Komar and Gaughan (1973) equation. Ω was averaged between periods of morphological measurements to correlate it with variations in sandbar morphometrics.

$$\Omega = \frac{H_b}{\overline{W_s} T_p} \quad (3)$$

4.2.2 Morphological data

Monthly measurements of the subaerial and subtidal morphology were acquired from August 2014 to September 2018 following the same methodology as the described in Chapter 2.

Shoreline positions were extracted from each topographic profile at an elevation of 0.5 m from mean low low-tide level. Sandbars were extracted following the methodology proposed by Vidal-Ruiz and Ruiz de Alegría-Arzaburu (2019) and four morphometric parameters were obtained from the sandbar identified at each bathymetric profile: sandbar crest height (h_b), sandbar depth (d_b), sandbar volume per linear meter (V_b) and sandbar position (P_b). Terrace-bars were defined as morphological features of $h_b \leq 0.75$ m located offshore from the dynamic equilibrium position (DEP). The shoreline extracted from the unbarred September 2014 profile ($S14_{ref}$) was selected as the benchmark to calculate shoreline and sandbar distances over the time.

4.3 Results

4.3.1 Wave conditions: seasonal and interannual variability

Monthly-averaged wave conditions indicated a clear seasonal signal over the four-year study period, but significant interannual differences were encountered, mostly for the winter periods (Fig. 4.2). Calm wave-energy

conditions occurred between May and September, dominated by shorter ($\overline{T_p}$ = 8 s), smaller ($\overline{H_s}$ = 0.7 m) and less energetic waves. During this period, an average total energy flux ($\overline{Pt}$) of 65 kWm^{-1} took place, with dominance of the cross-shore component over the longshore. In 2018, the longshore energy flux tripled and was mainly northerly directed.

High-energy waves dominated between October and April. The waves were longer ($\overline{T_p}$ =12 s) and higher ($\overline{H_s}$ =1.2 m) than from May to September, and contained more than five times of energy ($\overline{Pt}$ =335 kWm^{-1}). In the 2015–2016 winter, $\overline{Pt}$ doubled ($\overline{Pt}$ =577 kWm^{-1}), due to the presence of several energetic storms of $\overline{H_s}$ > 3 m with associated $\overline{T_p}$ > 14 s. However, the most energetic event occurred at the end of January 2017, which lasted three days and presented Pt=1396 kWm^{-1} associated with $\overline{H_s}$ > 4 m and $\overline{T_p}$ of 15 s (Fig. 4.2). Generally, cross-shore energy fluxes were one order of magnitude larger than the alongshore (Figs. 4.2d and 4.2e), but after the 2017 summer, the incoming wave direction shifted slightly towards the south (270° to 250°) (Fig. 4.2c) inducing an increase in the alongshore energy flux (Fig. 4.2d), particularly during the 2018 winter.

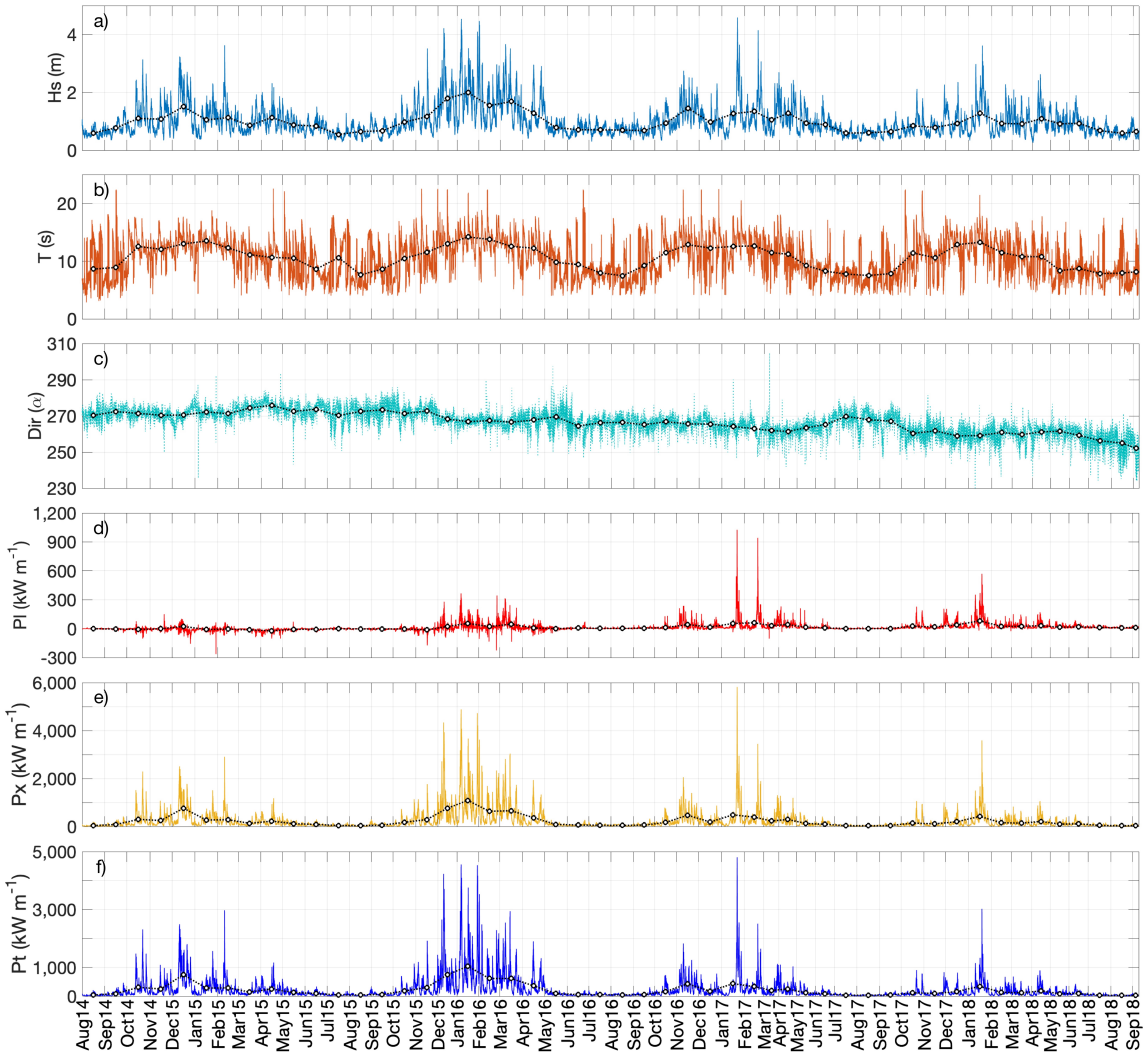

Figure 4.1 Time-series of: (a) significant wave height (H_s); (b) spectral peak wave period (T_p); (c) wave direction (Dir); (d) longshore energy flux (Pl); (e) cross-shore energy flux (Px); and (f) total energy flux (Pt), from August 2014 to September 2018. The dashed-circled lines represent monthly-averaged values for all parameters.

4.3.2 Seasonal and interannual sandbar morphodynamics

The morphological evolution of the beach over the four-year period from August 2014 to September 2018 is presented in Fig. 4.3. Unbarred beach conditions were identified between August and October in 2014, 2015 and 2018, at the end of the calm wave-energy period. In these cases, the preceding

winters were not extremely energetic; hence, the sandbar did not exceed the depth of 3 m during its offshore migration period (Fig. 4.3). After an unbarred condition, the beach formed an alongshore-uniform sandbar near the mean low low-tide level (MLLT) at the beginning of the high wave-energy period in November, and associated with subaerial beach erosion (Fig. 4.3).

The sandbar migrated offshore during the high wave-energy conditions between December and February. The offshore distance and depth reached by the sandbar depended mostly on the incident wave energy. Extremely energetic winters (i.e. El Niño 2015–2016 and 2016–2017) induced the formation of a large sandbar that migrated offshore exceeding the depth of 3 m (Fig. 4.3). While less energetic winters (i.e. 2014–2015 and 2017–2018), contributed to the onshore migration of the sandbar to shallower depths of < 3 m (Fig. 4.3). A decrease in wave energy over the spring (March to June) favored the onshore migration of the sandbar. However, the complete welding of the sandbar to the shoreline happened only when the sandbar was located at a depth < 3 m at the beginning of the spring (i.e. March 2015 and March 2018) (Fig. 4.3).

The sandbar was unable to completely weld to the shoreline during the calm wave-energy conditions (March to June) when located at depths > 3 m at the beginning of the spring. This happened in March 2016 and 2017, and was related to preceding extremely energetic winters (Fig. 4.3). In these cases, the sandbar splitted into two sections: the inner part acted as a sandbar, migrating onshore during the following calm energy period, while the outer part formed a

terrace-bar. In November 2016, the terrace-bar attached partially to the active sandbar and contributed to its formation (Fig. 4.3). After May 2017, however, the terrace-bar migrated offshore slowly degrading over the following months. Subsequent to the formation of new sandbar near the shoreline in December 2017, the coexistence of the new sandbar and the offshore migrating terrace-bar occurred, until the sandbar welded to the shoreline in the summer 2018 (Fig. 4.3).

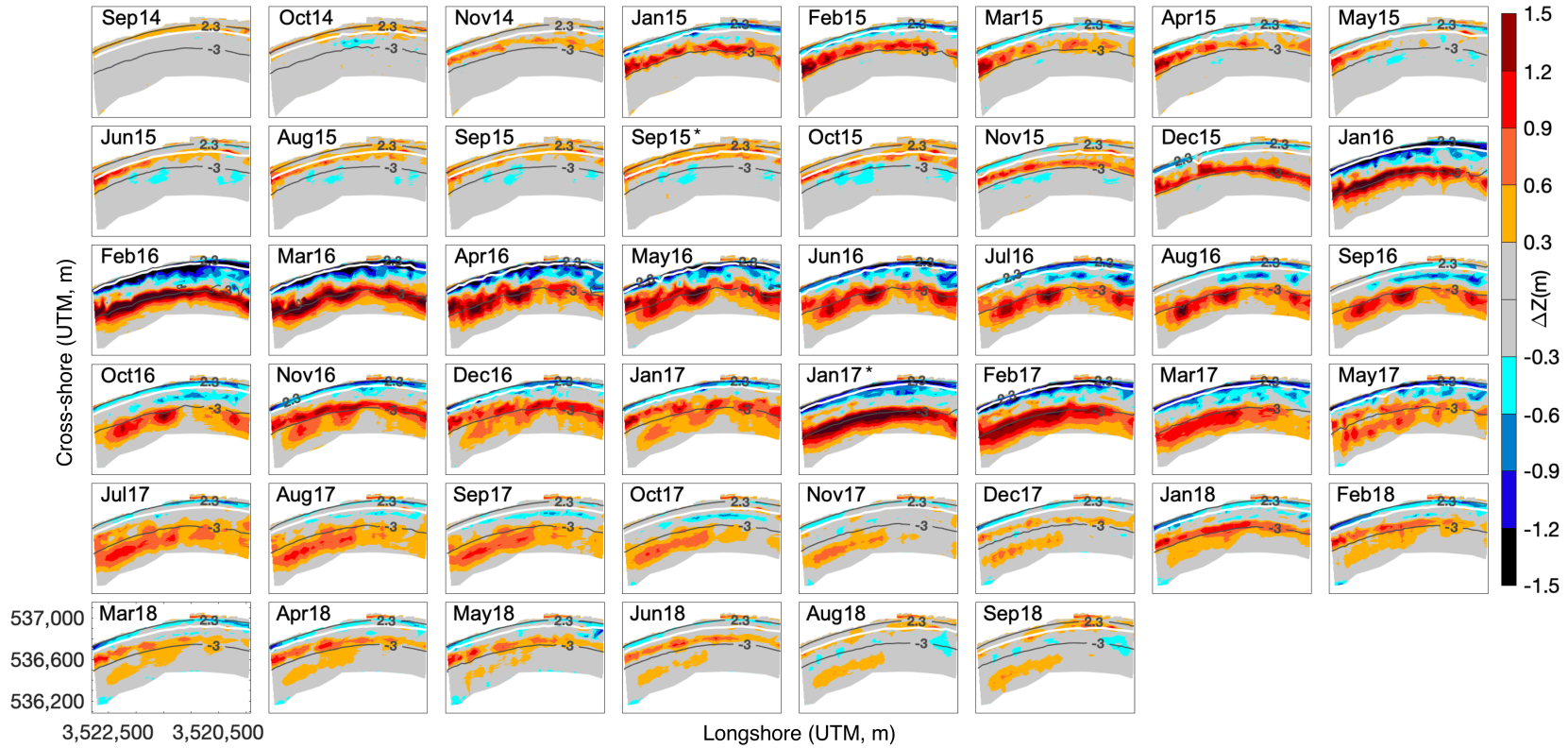

Figure 4.2 Cumulative morphological changes for the subaerial and subtidal beach from August 2014 to September 2018. The 0.5–m shoreline (above mean low low-tide level) is highlighted in white, and the black lines represent the 2.3–m (mean high water spring level) and -3–m (lower limit of the inner-subtidal zone) contourlines. Jan17 * indicates the post-storm survey in late January.

4.3.3 Alongshore-averaged behavior

Spatio-temporal variations in sandbar geometry and location were studied during the different onshore and offshore migration instants identified from August 2014 to September 2018. On one hand, alongshore-averaged sandbar morphometric parameters were related to average total energy flux and morphodynamic beach states (Fig. 4.4). On the other hand, the alongshore variability of sandbar morphometric parameters was analyzed over the four-year study period (Fig. 4.5).

Different onshore sandbar migration patterns were identified over the study period depending on the sandbar location after the incidence of high-energy waves over the winter (see Section 4.3.2). Alongshore-averaged sandbar positions ($\overline{P_b}$), depths ($\overline{d_b}$) and volumes ($\overline{V_b}$) were obtained for the different months when the morphology was measured, and these were correlated with the incident total wave energy flux ($\overline{P}t$) and the dimensionless fall velocity ($\overline{\Omega}$) (Fig. 4.4).

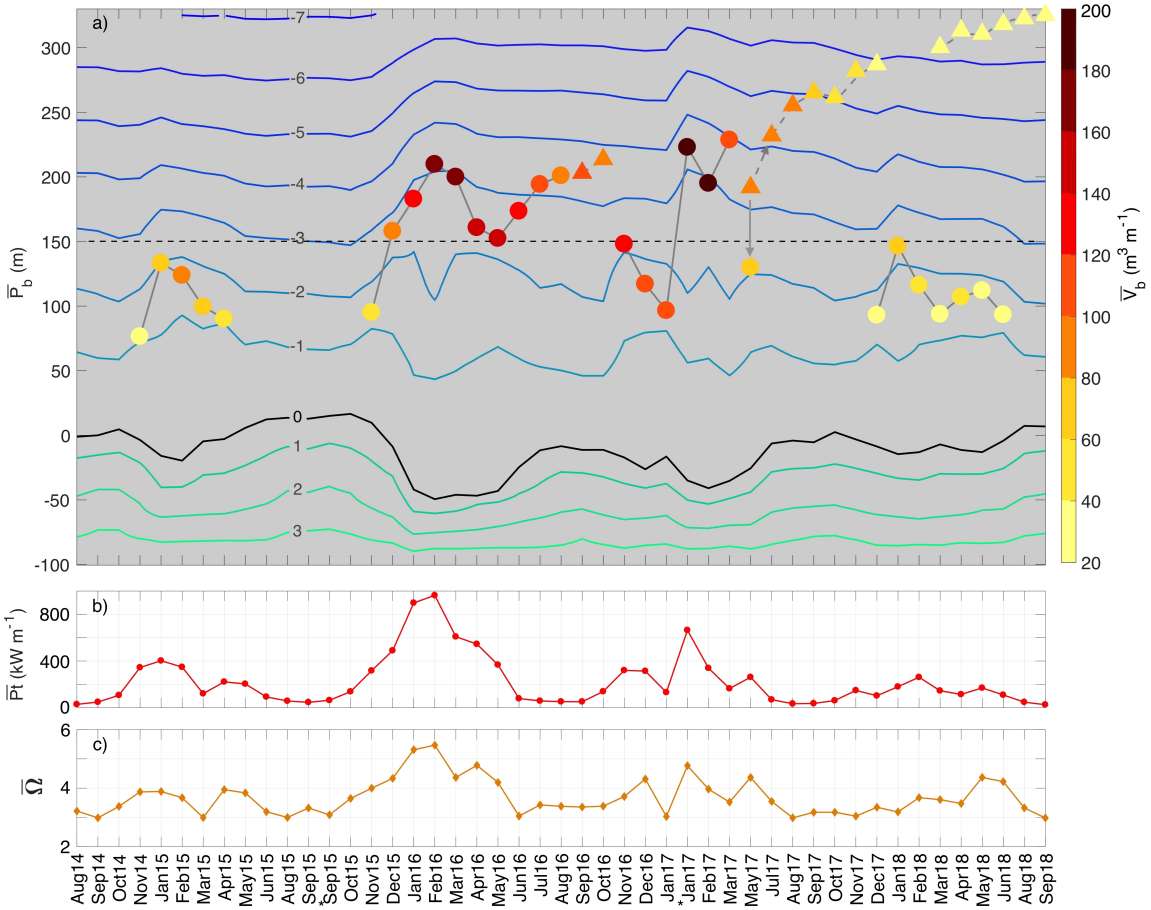

Figure 4.3 (a) Alongshore-averaged sandbar (dots) and terrace-bar (triangles) positions ($\overline{P_b}$), depths (time-averaged bathymetric contourlines in blue) and volumes ($\overline{V_b}$) obtained for each survey from August 2014 to September 2018. (b) Total wave energy flux ($\overline{P_t}$) and (c) dimensionless fall velocity ($\overline{\Omega}$), averaged between survey periods from August 2014 to September 2018. * Indicates additional survey in the same month.

Following an unbarred beach condition, the sandbar formed in November at 1–1.5 m depth and 50–80 m from the shoreline when $\overline{Pt}$ > 200 kWm^{-1}. The new sandbar contained a volume of 20–40 m^3m^{-1}, and the beach transitioned towards a more dissipative state ($\overline{\Omega}$ of 3 to 4) (see November 2014 and 2015 in Fig. 4.4). The distance and depth reached by the sandbar during the winter depended on the amount of incident wave energy. When $\overline{Pt}$ <400 kWm^{-1}

between December and February, the sandbar reached a maximum volume of $\overline{V_b}$ <100 m^3m^{-1} and a maximum depth < 3 m and displaced up to 150 m from the shoreline. In this situation, the sandbar was able of migrating onshore and coupling to the shoreline when $\overline{Pt}$ < 200 kWm^{-1} for a continuous period of a few months in spring (see after April 2015 and June 2018 in Fig. 4.4).

Very energetic winters of $\overline{Pt}$ > 600 kWm^{-1} (i.e. El Niño 2015–2016 and 2016–2017) induced the formation of a large sandbar with $\overline{V_b}$ =180–200 m^3m^{-1} that migrated more than 200 m offshore from the shoreline, reaching depths > 3 m (see February 2016 and end of January 2017 in Fig. 4.4). By the end of the high wave energetic period, the shoreline had retreated around 50 m and the beach was very dissipative ($\overline{\Omega}$ ≥ 5). As soon as the energy decreased over the spring, the beach transitioned towards a more reflective state ($\overline{\Omega}$ ≤ 3) and the shoreline advanced slowly.

In May 2016 and March 2017, the sandbar reached $\overline{d_b}$ < 3 m but contained large amount of sediment ($\overline{V_b}$ >100 m^3m^{-1}), thus, it was unable of displacing onshore during the low-energy period ($\overline{Pt}$ < 200 kWm^{-1}). Consequently, instead of migrating onshore as a single unit, the sandbar split into two sections. The outer part flattened and migrated offshore, later becoming a terrace-bar; while the inner section migrated onshore and contributed to the advancement of the shoreline (Fig. 4.4). Terrace-bars able of migrating onshore up to $\overline{d_b}$ ≤ 3 m over the summer (triangles in Fig. 4.4) contributed to the

reconstruction of a sandbar in November (see November 2016 in Fig. 4.4). Instead, terrace-bars migrating offshore to $\overline{d_b}$ > 3 m and to larger distances (i.e. 300 m from the shoreline) followed a net offshore migration cycle (NOM) towards deeper depths, losing volume gradually (from 120 to 20 m^3m^{-1}). A newly formed sandbar coexisted with the decaying terrace-bar over a few months; hence, the sandbar and terrace-bar coexistence occurred (see November 2017 in Fig. 4.4)

4.3.4 Alongshore-varying behavior

Alongshore differences in onshore sandbar migration patterns existed, and these were related to sandbar locations (distances from the shoreline) and geometry (heights and volumes) (Fig. 4.5). After an unbarred beach condition, alongshore uniformity occurred during the sandbar formation phase (November 2014 and 2015 in Fig. 4.5), but significant variations along the beach took place during the offshore migration and build-up process. The highest (h_b= 1.2–1.5 m) and largest (V_b= 100–175 m^3m^{-1}) sandbars formed in the northern half of the beach. Over the moderate-energy winter ($\overline{Pt}$ <400 kWm^{-1}), however, the sandbar displaced shorter seaward distances in the north (120–160 m) compared to the southern section, where the sandbar was slightly smaller (V_b= 50–100 m^3m^{-1}) and migrated further offshore (160–240 m) (Fig. 4.5).

Highly energetic conditions ($\overline{Pt}$ >600 kWm^{-1}, Fig. 4.4; 2015–2016 winter and 2017 end of January storm) formed very high (h_b= 1.4–2.0 m; Fig. 4.5b) and

large sandbars (V_b= 175–300 m^3m^{-1}; Fig. 4.5c) that displaced further offshore (230–360 m); particularly in the southern beach (Fig. 4.5a). Similar to the moderate-energy winter, the largest and highest sandbars formed in the northern half of the beach, and displaced shorter seaward distances than in the southern section. Rhythmicity in sandbar heights existed at the end of the winter and during the spring, when the incident energy decreased. Smaller sandbars were presented at similar alongshore distances of 600 m apart (i.e. March 2015 and 2018 at locations of y=[400, 1000, 1600, 2250, 2600] m), which were related to the presence of rip channels (Fig. 4.5b).

Low-energy periods ($\overline{P}t$ <200 kWm^{-1}; Fig. 4.4) induced the onshore migration of the sandbar irregularly along the beach (Figs. 4.3 and 4.5) until welding to the shoreline. This occurred typically over the spring and summer, but an unusual period at the beginning of January 2017 favored the onshore migration and flattening (h_b<1.0 m) of the sandbar too. Sandbar coupling to the shoreline occurred at locations of <150 m from the shoreline and contained <100 m^3m^{-1} (h_b<1.2 m) at the beginning of the low-energy period (Fig. 4.5). Overall, these conditions did not accomplish during the spring–summer in 2016 and 2017. At some specific locations (y=[400, 1000, 1600, 2250, 2600] m), the sandbar migrated onshore and welded to the shoreline; while in other locations, it remained offshore, indicative of the alongshore sandbar splitting process (Fig. 4.5).

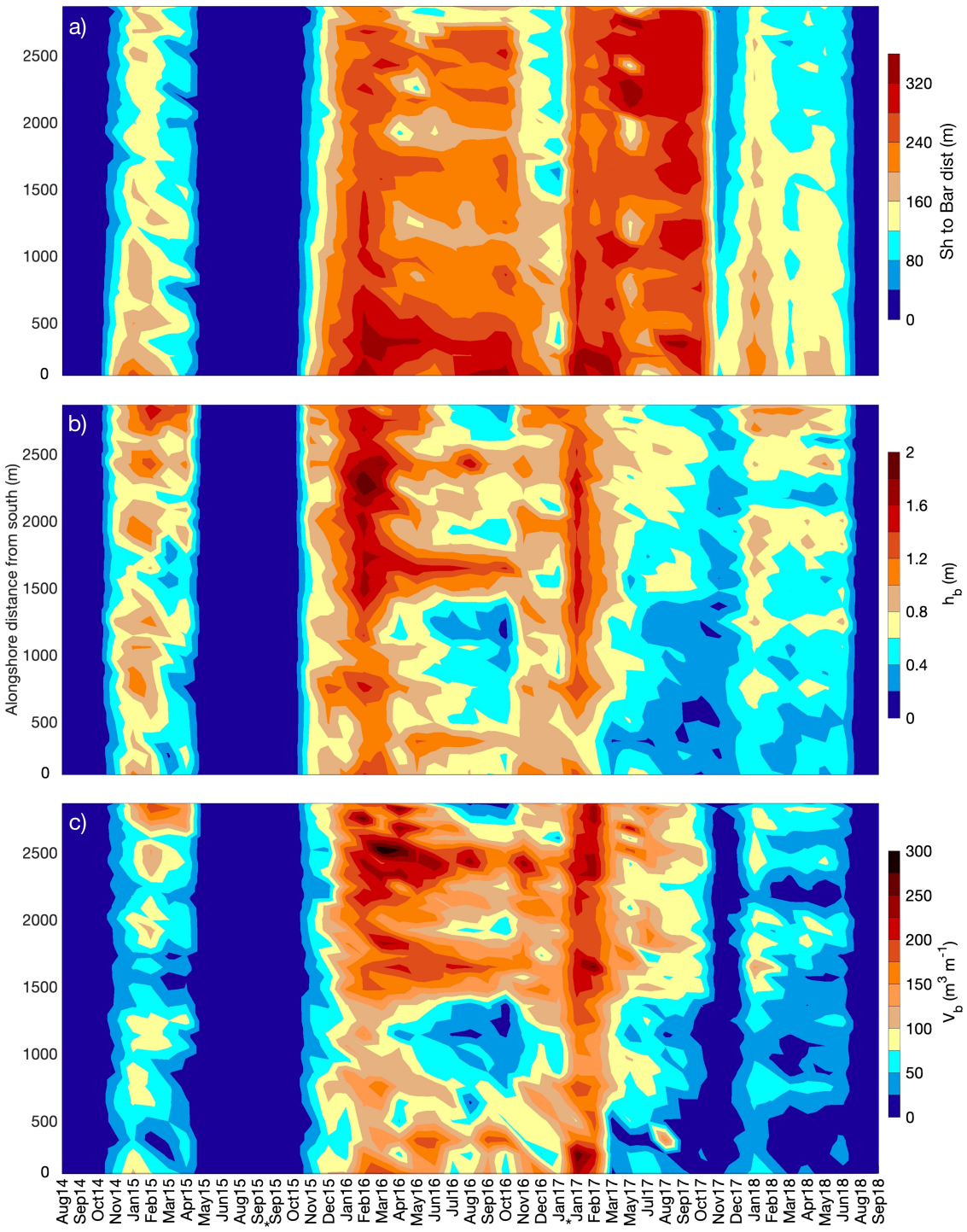

Figure 4.4 Alongshore-varying: (a) shoreline to sandbar distances; (b) sandbar crest heights (h_b); and (c) sandbar volumes (V_b) from August 2014 to September 2018.

The formation and offshore migration of a terrace-bar was very evident in spring and summer 2016 and 2017. At the end of the 2016 summer, the terrace-bar migrated onshore contributing to the reconstruction of the sandbar in November (increasing height and volume; Figs. 4.5b and 4.5c). While the sandbar reformed at a distance of 120 m from the shoreline in the north, this occurred further offshore in the south, at 160–240 m (Fig. 4.5a). In contrast to this behavior, in 2017 the terrace-bar continued displacing offshore over the summer (from 200 to 320 m), losing its volume (V_b< 150 m^3m^{-1}) and height to (h_b<0.8 m) in an alongshore uniform manner (Fig. 4.5). Thus, in that case the terrace-bar degraded offshore following a NOM cycle.

4.3.5 Dynamic equilibrium position

Onshore and offshore sandbar displacements depended primarily on the incident wave energy and the cross-shore sandbar location and geometry (Figs. 4.6 and 4.7). Instants of sandbar formation and offshore and onshore migrations are schematized in Fig. 4.6 for a selected profile (TB01; southern end) over the four-year study period. In 2015 and 2018 (light blue and red in Fig. 4.6), the sandbars welded to the shoreline during the low-energy period, thus, they remained within the dynamic equilibrium position (DEP). Instead, the incidence of excessive wave energy (i.e. January to March 2016) generated a high and large (1.3–1.5 m containing 180–230 m^3m^{-1}) sandbar that overcame DEP and was unable of merging the shoreline over the summer (Fig. 4.6).

The dashed lines on Fig. 4.7, represent a maximum alongshore-averaged cross-shore position of $\overline{P_b}$ = 150 m and a maximum alongshore-averaged sandbar crest height of $\overline{h_b}$ =1 m. The sandbar is capable of migrating onshore and welding to the shoreline if, on average, its volume ≤100 m^3m^{-1} and h_b≤1.0 m (Fig. 4.7). When dynamic equilibrium conditions of $\overline{h_b}$ y $\overline{P_b}$ are overcome due to the incidence of excessive wave energy (i.e. January to March 2016), the sandbar approximates to the DEP during low-energy conditions, but then degrades becoming a terrace-bar (Figs. 4.4 and 4.5). Terrace-bars located at $\overline{P_b}$ ≤ 220 m can still migrate onshore and contribute to the reconstruction of a sandbar at the DEP (in November 2016, Fig. 4.4 and 7), but if located further offshore, the terrace-bar will degrade following a NOM cycle (Fig. 4.7). Instead, when a maximum averaged cumulative total energy flux of 2000 kW m^{-1} is not overcome during the prevailing winter; the terrace-bar is capable of migrating towards DEP becoming an active sandbar when its height is increased (Fig. 4.7).

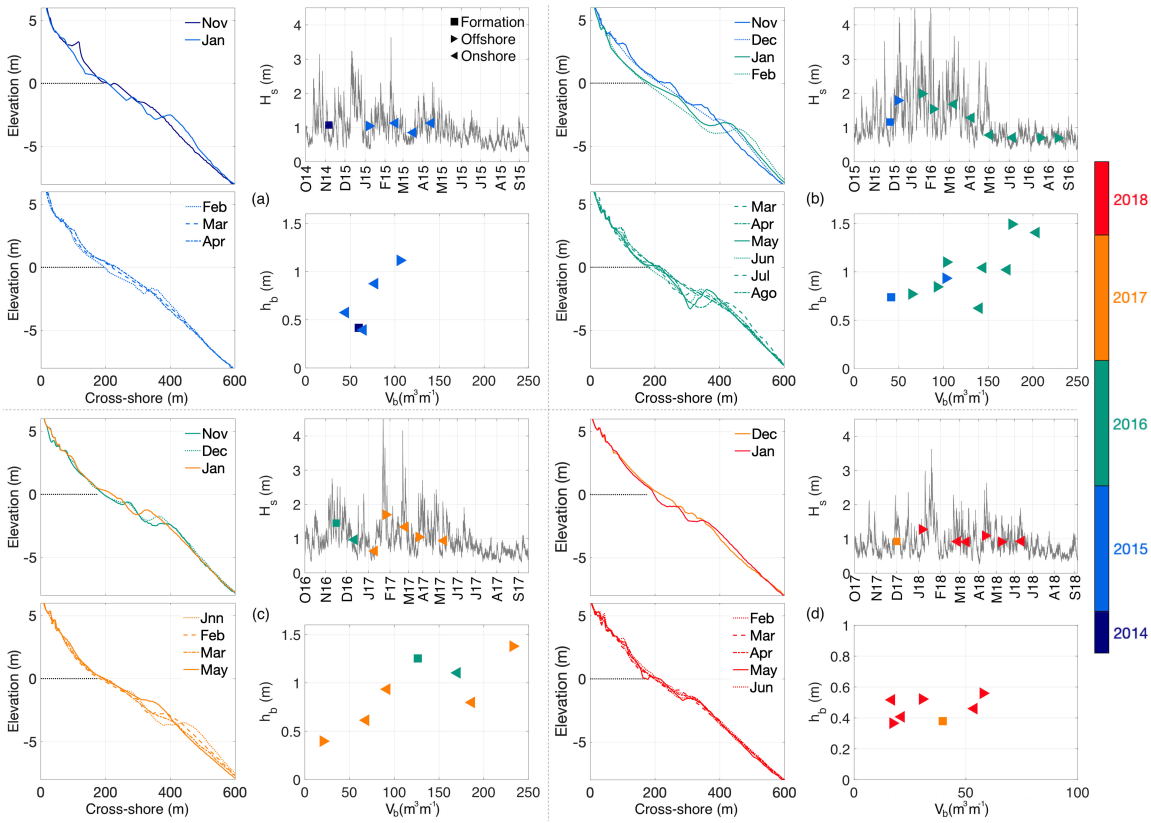

Figure 4.5 Temporal sequence of beach profile TB01 (southern end) during offshore (top) and onshore (bottom) sandbar migrations from November 2014 to June 2018. Instants of sandbar formation (squares) and offshore (>) and onshore (<) migrations are plotted against significant wave heights (H_s; gray). Sandbar crest heights (h_b) are represented versus their cross-shore positions (P_b) for each year (coloured bar). Note a different scale for h_b *vs* P_b in 2018 (bottom right panel).

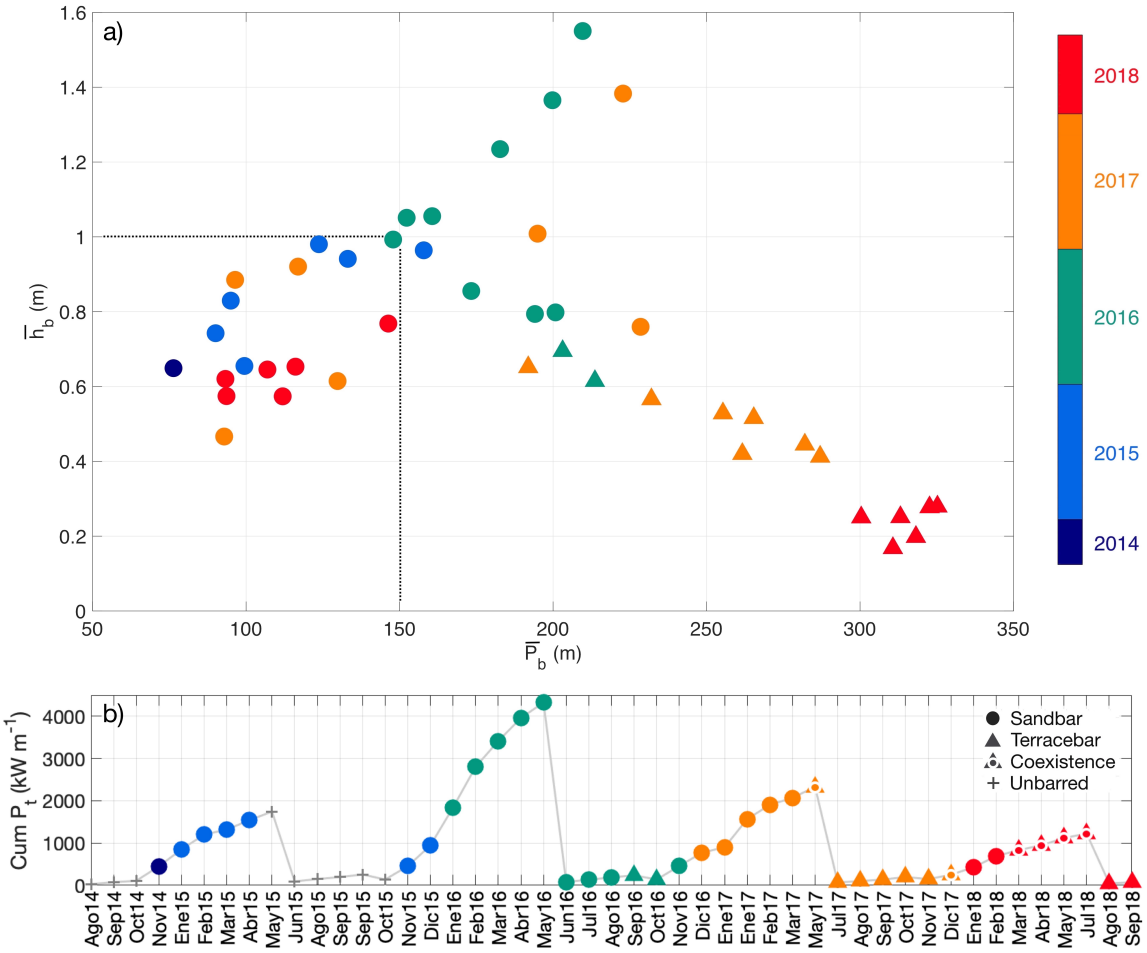

Figure 4.6 (a) Alongshore-averaged sandbar (dots) and terrace-bar (triangles) heights (h_b) versus cross-shore positions (P_b) from August 2014 to September 2018. The dotted line represents the combined cross-shore position and sandbar height limit at the dynamic equilibrium position (DEP). (b) Monthly-averaged cumulative total energy fluxes (Cum $\overline{P}_t$) calculated for different periods comprising low-energy and high-energy conditions. The type of sandbar morphology for each month is presented with different symbols: sandbar (dot), terrace-bar (triangle), sandbar and terrace-bar coexistence (dotted triangle) and unbarred conditions (cross).

4.3.6 Behavioral modes of cross-shore sandbar migration

Five modes of sandbar behavior are identified during the onshore migration process over the study period: (I) sandbar coupling (SC); (II) sandbar to terrace-bar transition (STT); (III) terrace-bar to sandbar transition (TST); (IV) terrace-bar splitting (TS); and (V) sandbar and terrace-bar coexistence (STC).

The SC mode (I in Fig. 4.8) occurs when, at the end of a moderately energetic winter ($\overline{H_s}$=1.1-1.5 m and Pt_{max}≥2000 kWm^{-1}), the sandbar is located onshore from DEP, and it couples to the shoreline during the low-energy period in summer ($\overline{H_s}$<1 m and Pt<500 kWm^{-1}) (Fig. 4.8). May 2015 presents an example of this mode (diamond in Fig. 4.8). The sandbar was located at P_b ≤150 m, at a maximum depth d_b≤ 3 m and the alongshore-averaged sandbar was $\overline{h_b}$≤1 m and contained $\overline{V_b}$≤ 100 m^3m^{-1} (Figs. 4.4 and 4.7). In the specific case of profile TB01 (southern beach end), the sandbar was slightly higher than average (h_b=1.1 m) and contained a little bit more of sand (V_b= 110 m^3m^{-1}) but remained onshore from DEP and followed the SC mode (Fig. 4.6).

The STT mode (II in Fig. 4.8) occurs when highly energetic winter conditions ($\overline{H_s}$>1.5 m and Pt_{max}≥4000 kWm^{-1}) locate the sandbar offshore from DEP and, during the low-energy period, it is unable of migrating onshore, and instead, it flattens turning into a terrace-bar (Fig. 4.8). June 2016 presents an example of this mode. The sandbar was located at P_b >150 m, at a maximum depth d_b> 3 m and the alongshore-averaged sandbar was $\overline{h_b}$>1 m and contained $\overline{V_b}$> 100 m^3m^{-1} (Figs. 4.4 and 4.7). Profile TB01 presented a sandbar of h_b>1.5 m that contained V_b= 180 m^3m^{-1} and was located offshore from DEP, thus, it followed STT over the low-energy period (Fig. 4.6).

A terrace-bar located near DEP can follow the TST mode (III in Fig. 4.8) if moderately energetic waves ($\overline{H_s}$≈ 2 m and Pt<2000 kWm^{-1}) induce it to build up

and turn it into an active sandbar. This occurred in November 2016, when the sandbar was located at P_b <150 m, at a maximum depth d_b< 3 m and the alongshore-averaged sandbar was $\overline{h_b}$<1.5 m and contained $\overline{V_b}$< 150 m^3m^{-1} (Figs. 4.4 and 4.7). With adequate low-energy conditions, the sandbar will continue migrating onshore following SC (Fig. 4.4).

When a terrace-bar located offshore from DEP is exposed to low-energy conditions, it can split into two sections and follow the TS mode (IV, Fig. 4.8). The inner section will migrate onshore towards DEP and, if the right conditions occur, it will follow TST. Instead, the outer section will displace offshore following a net NOM cycle. TS occurred in May 2017 when the terrace-bar was located at d_b> 3 m containing $\overline{V_b}$> 100 m^3m^{-1} (Fig. 4.4). While a terrace-bar migrates offshore following NOM, a new sandbar can be formed, thus, both can coexist in an STC mode (V in Fig. 4.8). This happened in November 2017, a new independent sandbar was formed whilst the offshore terrace-bar continued flattening and displacing offshore; both coexisted over several months (Figs. 4.4 and 4.7).

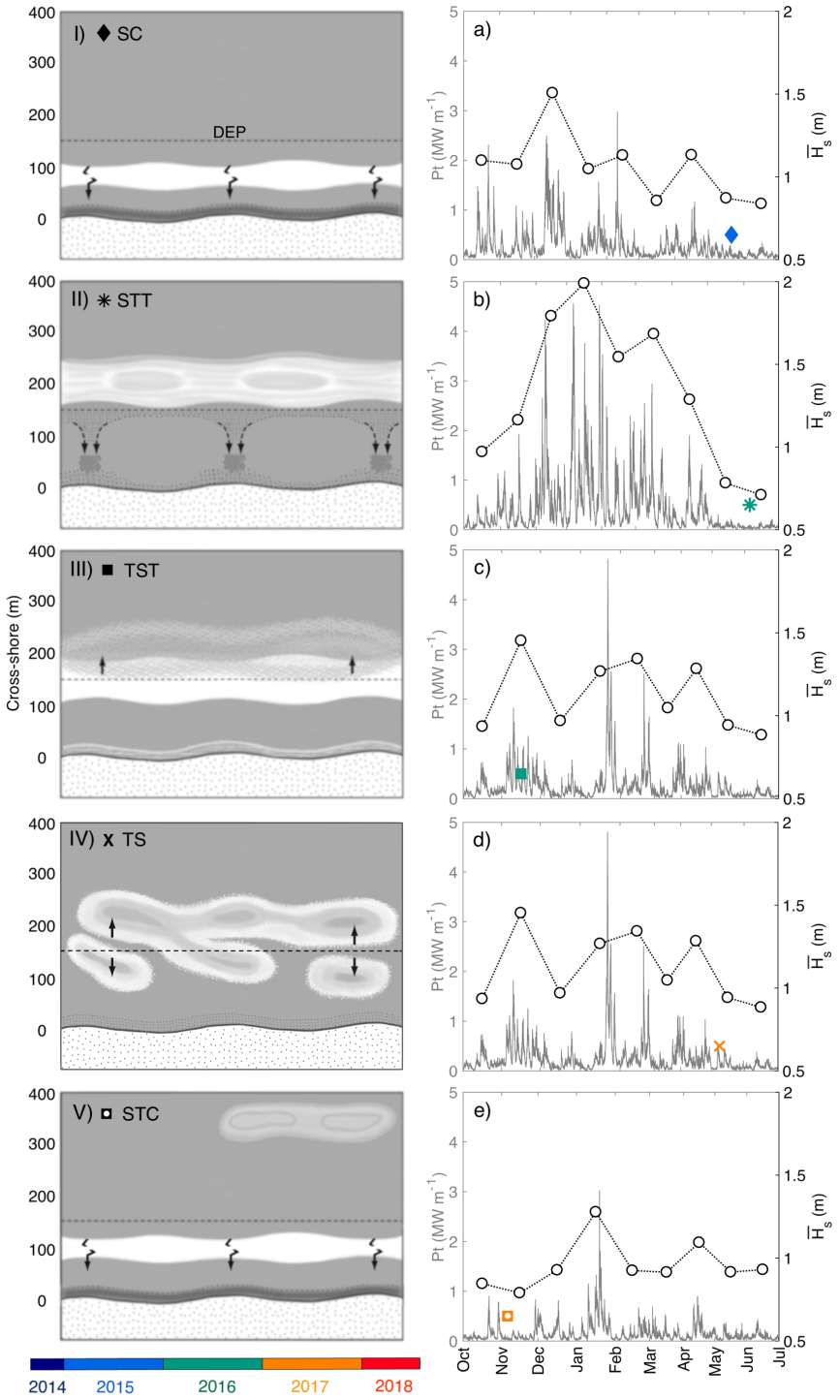

Figure 4.7 Schematized behavioral modes of onshore sandbar migration: I) SD: sandbar coupling (⬥); II) STT: sandbar to terrace bar transition (*); III) TST: terrace-bar to sandbar transition (■); IV) terrace-bar splitting (x); V) STC: sandbar and terrace-bar coexistence (□). Examples are provided for different years (color bar) in relation to the total energy flux (Pt) and monthly-averaged significant wave height ($\overline{H_s}$). DEP refers to the sandbar dynamic equilibrium position.

4.4 Discussion

4.4.1 Role of dynamic equilibrium position

The beach was highly-seasonal (Ruiz de Alegría-Arzaburu et al., 2017) and the sandbar moved constantly toward a wave-height dependent time-varying equilibrium state (Wright et al., 1985; Lippmann and Holman, 1990; Plant et al., 1999, 2001; Pape et al., 2010). After migrating offshore, the sandbar tended to displace onshore toward the location of origin (Sallenger et al., 1985). The sandbar located within the dynamic equilibrium position (DEP) was able of completely welding to the shoreline (*mode I: SC*) during low-energy conditions ($\overline{H_s}$<1 m and Pt_{max}<500 kWm^{-1}); thus, the beach became unbarred in summer and completed the seasonal sandbar migration at a frequency of 1 cycle/yr (Shepard, 1948; Komar, 1974; Wright and Short, 1984).

Sandbar response times to the wave forcing vary significantly at different field sites, but they tend to reach a stable equilibrium location adjusting to the incident wave forcing (Pape et al., 2010). A recent study on the dynamic equilibrium of sandbars on a low-energy microtidal beach indicated up to 80 m of cross-shore displacements during the cross-shore migration cycle (Cheng and Wang, 2018), but the specific characteristics of the dynamic equilibrium were somehow unclear. In this study, DEP was empirically determined at a cross-shore distance of 150 m from the shoreline (depth of ~ 3 m), and the sandbar remained within DEP if moderately energetic winter conditions prevailed ($\overline{H_s}$<1.5

m and max Pt_{max}~ 2000kWm^{-1}). When these conditions were overcome, the sandbar followed a transient behavior (Plant et al., 1999; Pape et al., 2010), displaced offshore from DEP and was unable of migrating onshore during the subsequent low-energy period (at a frequency of 1 cycle/yr).

A sandbar located offshore from DEP would typically erode and transform into a terrace-bar (*mode II: STT*). Several studies described net offshore migration (NOM) cycles of bars that gradually migrated offshore while degrading (Birkemeier, 1984; Lippmann et al., 1993; Ruessink and Kroon, 1994; Plant et al., 1999; Shand et al., 1999; Aleman et al., 2017). In the research site, this process was only observed when the terrace-bar reached a longshore-averaged position of 220 m (~ 3.5 m depth); representing a point of no return. In contrast, a terrace-bar located slightly offshore from DEP could grow during moderately energetic wave conditions ($\overline{H_s}$≈2 m and Pt_{max}< 2000kWm^{-1}) and become an active sandbar (*mode III: TST*).

The splitting of a sandbar has been previously observed during a NOM cycle interrupted by a storm event, and the resulting sections followed different morphological evolutions (Bouvier et al., 2017). Exposed to low-energy conditions, in this study, a terrace-bar located near DEP was observed to divide into two sections (*mode IV: TS*). The outer section continued a NOM cycle, and the inner part followed TST (mode III) when moderately energetic wave conditions prevailed. A terrace-bar following NOM could coexist with a newly formed sandbar, both following independent migration patterns (*mode V: STC*).

4.4.2 Control of sandbar morphometrics

Little attention has been given to the understanding of morphometric variations of nearshore bars during their onshore and offshore displacements in relation to the incident wave energy (Larson and Kraus, 1992; Ruessink and Kroon, 1994; Grunnet and Hoekstra, 2004; Aleman et al., 2017; Vidal-Ruiz and Ruiz de Alegría-Arzaburu, 2019). Several of these studies highlighted the need of characterizing sandbar geometry during the NOM cycle to better understand spatio-temporal variations during the migration process. In the attempt to correlate wave forcing characteristics to sandbar morphometric changes, Ruessink et al. (2003) found large intersite differences in mean sandbar depths on beaches that followed NOM cycles. More recently, Di Leonardo and Ruggiero (2015) indicated limited correlations between sandbar morphometrics and parameters representing incident wave energy and morphodynamic beach states on a regional scale sandbar study. In contrast to previous findings, in this study cross-shore sandbar migration patterns and sandbar geometry were directly correlated to the incident wave energy and morphodynamic beach state transitions.

Contrary to Cheng and Wang (2018), the sandbar height was directly correlated with cross-shore migration distances, and sandbar growth depended on the amount of incident wave energy over the winter. New sandbars ($h_b \leq 0.75$ m) formed typically at water depths of 1–1.5 m (50–80 m from the shoreline) at the beginning of the high-energy period, and contained 20–40 m^3m^{-1} of

sediment. The completion of the full annual cross-shore migration cycle depended on the incident energy conditions that modulated the sandbar growth. During moderately energetic conditions ($\overline{Pt}$ <400 kWm^{-1}), the sandbar was h_b< 1 m and contained up to ~100 m^{3}m^{-1}, and it was able of migrating onshore and completing 1 cycle/yr during the following low-energy period. Instead, highly-energetic winters ($\overline{Pt}$ >400 kWm^{-1}) generated large sandbars (h_b>1 m; $\overline{V_b}$ >100 m^{3}m^{-1}) that located offshore from DEP; hence, these were unable of welding to the shoreline and completing 1 cycle/yr.

4.5 Conclusions

A detailed analysis of four years of monthly measured morphological data in relation to nearshore wave conditions allowed the description of five behavioral modes of the onshore migration of the subtidal sandbar on a single-barred beach. The sandbar followed a wave-height dependent time-varying equilibrium state, it formed near the shoreline and, after migrating offshore, it tended to displace onshore toward the location of origin. While located within the dynamic equilibrium position (DEP) the sandbar was able of completely welding to the shoreline (mode I: SC) during low-energy conditions ($\overline{H_s}$<1 m and Pt_{max}<500 kWm^{-1}), becoming the beach unbarred in summer and completing 1 cycle/yr.

DEP was determined at a cross-shore distance of 150 m from the shoreline (depth of ~3 m), and the sandbar was typically h_b≤ 1 m and contained

up to ~100 m^3m^{-1}. Highly-energetic winters ($\overline{P}t$ >400 kWm^{-1}) induced a larger growth of the sandbar (h_b>1 m; $\overline{V_b}$ >100 m^3m^{-1}) and located it offshore DEP, being unable of welding to the shoreline and completing 1 cycle/yr. Whilst offshore from DEP, the sandbar eroded and turned into a terrace-bar (mode II: STT). If located slightly offshore from DEP, the terrace-bar could grow during moderately energetic wave conditions ($\overline{H_s}$≈2 m and Pt_{max}< 2000kWm^{-1}) and become a sandbar (mode III: TST). Exposed to low-energy conditions, the terrace-bar near DEP could divide into two sections (mode IV: TS). The outer section typically followed a net offshore migration (NOM) cycle, and under moderately energetic wave energy conditions the inner part could follow TST (mode III). The coexistence of a newly formed sandbar and a terrace-bar following NOM could occur (mode V: STC), both following independent migration paths.

4.6 References

Aagaard, T., Davidson-Arnott, R., Greenwood, B., Nielsen, J. (2004), Sediment supply from shoreface to dunes: linking sediment transport measurements and long-term morphological evolution. *Geomorphology* 60 (1), 205–224. https://doi.org/10.1016/j. geomorph.2003.08.002.

Aagaard, T., Greenwood, B., Hughes, M.G. (2013), Sediment transport on dissipative, intermediate and reflective beaches. *Earth-Science Reviegs* 124, 32–50. https://doi.org/10.1016/j.earscirev.2013.05.002.

Aleman, N., Certain, R., Robin, N., Barusseau, J.P. (2017), Morphodynamics of slightly oblique nearshore bars and their relationship with the cycle of net offshore migration. *Marine Geology* 392, 41–52. https://doi.org/10.1016/j.margeo.2017.08.014.

Anthony, E.J., Vanhée, S., Ruz, M.H. (2006), Short-term beach-dune sand budgets on the North Sea coast of France: sand supply from shoreface to dunes and the role of wind and fetch. *Geomorphology* 81, 316–329. https://doi.org/10.1016/j.geomorph.2006.04.022.

Birkemeier, W.A. (1984), Time scales of nearshore profile changes. *Paper Presented at 19th International Conference on Coastal Engineering*. American Society of Civil Engineers, New York.

Blossier, B., Bryan, K. R., Daly, C. J., Winter, C. (2016), Nearshore sandbar rotation at single-barred embayed beaches. *Journal of Geophysical Research: Oceans*, 121, 2286–2313.doi.org/10.1002/ 2015JC011031.

Bouvier, C., Balouin, Y., Castelle, B. (2017), Video monitoring of sandbar-shoreline response to an offshore submerged structure at a microtidal beach. *Geomorphology*, 295, 297-305.

Cheng, J., Wang, P. (2018), Dynamic equilibrium of sandbar position and height along a low wave energy micro-tidal coast. *Continental Shelf Research* 165, 120–136. https://doi.org/ 10.1016/j.csr.2018.05.004.

Cohn, N., Ruggiero, P., de Vries, S., García-Medina, G. (2017), Beach growth driven by inter- tidal sandbar welding. *Paper Presented at 8th International Conference on Coastal Dynamics*. Denmark, Helsingør.

Davidson, M.A., Splinter, K.D., Turner, I.L. (2013), A simple equilibrium model for predicting shoreline change. *Coastal Engineering* 73, 191–202.

Dean, R.G. (1977), *Equilibrium beach profiles: U.S. Atlantic and Gulf coasts*. Department of Civil Engineering. Ocean Engineering Report No. 12, University of Delaware, Newark, DE.

Dean, R.G. (1973), Heuristic models of sand transport in the surf zone. *First Australian Conference on Coastal Engineering: Engineering Dynamics of the Coastal Zone*. Institution of Engineers, Australia, p. 215.

Di Leonardo, D. and Ruggiero, P. (2015), Regional scale sandbar variability: Observations from the U.S. Pacific Northwest. Continental Shelf Research 95, 74–88.

Gourlay, M. (1968), *Beach and dune erosion tests*. Delft Hydraulics Laboratory, Report M, 935.

Grunnet, N.M., Hoekstra, P. (2004), Alongshore variability of the multiple barred coast of Terschelling, The Netherlands. *Marine Geology* 203, 23–41. https://doi.org/10.1016/ S0025-3227(03)00336-0.

Hoefel, F., Elgar, S. (2003), Wave-induced sediment transport and sandbar migration. *Science* 299, 1885–1887. https://doi.org/10.1126/science.1081448.

Holman, R.A., Bowen, A.J. (1982), Bars, bumps, and holes: models for the generation of complex beach topography. *Journal of Geophysical Research* 87, 457–468. https://doi.org/10.1029/ JC087iC01p00457.

Hsu, T.J., Elgar, S., Guza, R.T. (2006), Wave-induced sediment transport and onshore sandbar migration. Coastal Engineering 53, 817–824. https://doi.org/10.1016/j.coastaleng.2006.04.003.

Komar, P. D. (1974), *Beach Processes and Sedimentation* (429pp). Englewood Cliffs, NJ: Prentice-Hall.

Komar, P. D., Gaughan, M. K. 1973. Airy wave theory and breaker height prediction. In: Proceedings of the 13th Coastal Engineering Conference. American Society of Civil Engineers, pp.405–418.

Larson, M., Kraus, N.C. (1992), Dynamics of longshore bars. *Paper Presented at 23rd International Conference on Coastal Engineering.* American Society of Civil Engineers, Venice, Italy.

Lippmann, T.C., Holman, R.A. (1990), The spatial and temporal variability of sand bar morphology. *Journal of Geophysical Research* 95 (C7), 11575–11590. https://doi.org/10.1029/JC095iC07p11575.

Lippmann, T.C., Holman, R.A., Hathaway, K.K. (1993), Episodic, nonstationary behavior of a double bar system at Duck, North Carolina, U.S.A., 1986–1991. J. Coastal Research SI 15, 49–75.

Ostrowski, R., Pruszak, Z., Zeidler, R.B. (1991), Multi-scale nearshore and beach changes. *Paper Presented at 22nd International Conference on Coastal Engineering*. American Society of Civil Engineers, Delft, The Netherlands https://doi.org/10.1061/9780872627765.161.

Pape, L., Plant, N. G., Ruessink, B. G. (2010), On cross-shore migration and equilibrium states of nearshore sandbars. *Journal of Geophysical Research* 115, F03008.doi.org/10. 1029/2009JF001501.

Phillips, M.S., Harley, M.D., Turner, I.L., Splinter, K.D., Cox, R.J. (2017), Shoreline recovery on wave-dominated sandy coastlines: the role of sandbar morphodynamics and nearshore wave parameters. *Marine Geology* 385, 146–159. https://doi.org/10.1016/j. margeo.2017.01.005.

Plant, N.C., Holman, R.A., Freilich, M.H., Birkemeier, W.A. (1999), A simple model for inter- annual sandbar behaviour. *Journal of Geophysical Research* 104, 15755–15776. https://doi.org/ 10.1029/1999JC900112.

Plant, N.G., Freilich, M.H., Holman, R.A. (2001), Role of morphologic feedback in surf zone sandbar response. *Journal of Geophysical Research* 106 (C1), 973–989. https://doi.org/10.1029/2000JC900144.

Ruessink, B.G., Kroon, A. (1994), The behaviour of a multiple bar system in the nearshore zone of Terschelling, the Netherlands: 1965–1993. *Marine Geology* 121, 187–197. doi.org/10.1016/0025-3227(94)90030-2.

Ruessink, B.G., Wijnberg, K.M., Holman, R.A., Kuriyama, Y., Van Enckevort, I.M. (2003), Intersite comparison of interannual nearshore bar behavior. J. Geophys. Res. 108 (C8), http://dx.doi.org/10.1029/2002JC001505.

Ruessink, B.G., Coco, G., Ranasinghe, R., Turner, I.L., (2007). Coupled and noncoupled behavior of three-dimensional morphological patterns in a double sandbar system. *Journal of Geophysical Research* 112, C07002. https://doi.org/10.1029/2006JC003799.

Ruiz de Alegria-Arzaburu, A., Vidal-Ruiz, J.A., García-Nava, H., Romero-Arteaga, A. (2017), Seasonal morphodynamics of the subaerial and subtidal sections of an intermediate and mesotidal beach. *Geomorphology*, 295, 383–392. doi.org/10.1016/j.geomorph.2017.07.021

Ruiz de Alegría-Arzaburu, A., Vidal-Ruiz, J.A. (2018), Beach recovery capabilities after El Niño 2015–2016 at Ensenada Beach, Northern Baja California. *Ocean Dynamics* 6, 749–759. https://doi.org/10.1007/s10236-018-1164-6.

Sallenger, A.H., Holman, R.A., Birkemeier, W.A. (1985), Storm-induced response of a nearshore- bar system. *Marine Geology* 64, 237–257. https://doi.org/10.1016/0025-3227(85)90107-0.

Shand, R.D., Bailey, D.G., Shepherd, M.J. (1999), An inter-site comparison of net offshore bar migration characteristics and environmental conditions. Journal of Coastal Research 15, 750–765.

Shepard, F.P. (1948), *Submarine Geology*, 338 pp., Harper Collins, New York.

Shepard, F.P. (1950), *Beach cycles in southern California*. Beach Erosion Board (Technical Memo 20). Washington DC: US Army Corps of Engineering.

Short, A.D. (1999), *Handbook of Beach and Shoreface Morphodynamics*. John Wiley and Sons, Chichester, UK.

Splinter, K.D., Gonzalez, M.V.G., Oltman-Shay, J., Rutten, J., Holman, R. (2018), Observations and modelling of shoreline and multiple sandbar behaviour on a high-energy meso-tidal beach. *Continental Shelf Research* 159, 33–45. doi.org/10.1016/j.csr.2018.03.010

Van de Lageweg, W. I., Bryan, K. R., Coco, G., & Ruessink, B. G. (2013), Observations of shoreline–sandbar coupling on an embayed beach. *Marine Geology* 344, 101–114. doi.org/10.1016/j.margeo.2013.07.018

Van Maanen, B., de Ruiter, P.J., Coco, G., Bryan, K.R., Ruessink, B.G. (2008), Onshore sandbar migration at Tairua Beach (New Zealand): numerical simulations and field measurements. *Marine Geology* 253, 99–106. https://doi.org/10.1016/j.margeo.2008.05.007.

Vidal-Ruiz, J.A., Ruiz de Alegría-Arzaburu, A. (2019), Variability of sandbar morphometrics over three seasonal cycles on a single-barred beach. *Geomorphology* 333, 61–72. doi.org/10.1007/s10236-018-1164-6.

Wijnberg, K.M., Kroon, A. (2002), Barred beaches. Geomorphology 48 (1–3), 103–120.

Wright, L.D. Short, A.D. (1984), Morphodynamic variability of surf zones and beaches: a synthesis. *Marine Geology* 56, 93–118. doi.org/10.1016/0025-3227(84)90008-2

Wright, L.D., Short, A.D., Green, M.O. (1985), Short-term changes in the morphodynamics states of beaches and surf zones: an empirical predictive model. Marine Geology 62, 339–364.

Yates, M.L., Guza, R.T., O'Reilly, W.C. (2009), Equilibrium shoreline response: observations and modeling. *Journal of Geophysical Research* 114, C09014.

Chapter 5

5 Conclusions and perspectives

The primary purpose of this thesis was to improve the understanding of the morphodynamics of the subtidal sandbar in a single-barred and swell dominated beach. Four years of monthly measured morphological data and hourly collected wave measurements were used to study cross-shore sandbar migration patterns at Ensenada Beach in Baja California, Mexico.

First of all, the morphodynamic state transitions of the sandbar system were studied based on the Wright and Short (1984) conceptual bar-state model. Following this framework, two-dimensional (2D) and three-dimensional (3D) sandbar shapes were analyzed in relation to incident wave energy. It was encountered that the beach became barred and unbarred after the incidence of high and low wave energy conditions, respectively. During reflective beach states the sandbar welded to the shoreline resulting in a low-tide terrace associated with sandbar flattening. As a result of the detailed analysis on sandbar morphometrics, a threshold value of sandbar crest height of $h_b > 0.75$ m was determined to define a sandbar; hence, features with heights of $h_b \leq 0.75$ were considered terrace-bars if located farther than 150 m offshore from the reference shoreline (out of the dynamic equilibrium position).

The sandbar morphodynamic analysis demonstrated the importance of sandbar coupling to the shoreline for the complete rebuilding of the subaerial beach. Thus, the morphological variability of the subaerial beach was controlled by the cross-shore exchange of sediment through the sandbar migration, which was highly modulated by the incident wave conditions. In this context, the sandbar played a key role on the transfer of sediment between the subtidal and subaerial beach; the sediment contained in the sandbar was crucial to assure a complete build-up of the subaerial beach over the mild wave-energy period.

The four annual cross-shore sandbar migration cycles were described into detail with especial attention on spatio-temporal changes in relation sandbar shape variations. Five morphometric parameters were extracted from the bathymetric dataset: sandbar crest position, P_b, depth, d_b, and height, h_b, and sandbar width, W_b, and volume, V_b. The cross-shore migrations of the sandbar were highly modulated by the preceding wave conditions. In general terms, the sandbar formed at the beginning of the high-energy period (i.e. November) near the shoreline at $\overline{d_b}$<1 m, it migrated offshore over the highly energetic wave conditions (i.e. $\overline{H_s}$>1.3 m; until January/February) and onshore when the wave energy decreased (i.e. $\overline{H_s}$<1.0 m; from March to April). During some years the sandbar welded to the subaerial beach between May and June and the beach became unbarred, but in other times a terrace-bar was formed and remained offshore flattening over the summer.

The differences during the onshore sandbar migration were attributed to the presence of extremely energetic wave conditions during El Niño 2015–2016 winter ($\overline{H_S}$ >1.6 m). During that winter the sandbar moved seaward reaching larger distances than in the previous winter and gained large amount of sediment. Over the subsequent milder wave conditions ($\overline{H_S}$ = 1 m), the sandbar displaced onshore but was unable of welding to the shoreline in summer, it contained large amount of sediment, and the sandbar flattened becoming a terrace-bar.

A single highly-energetic swell storm event caused the equivalent offshore sandbar displacement to the captured during the El Niño winter. Prior to the storm, the sandbar was located close to the shoreline and was highly rhythmic, associated with a decrease in the incident wave energy. The incidence of waves of up to H_s of 4.6 m and T_p of 17 s (wave direction of 260°) triggered a rapid offshore sandbar movement that reshaped the sandbar from rhythmic to an alongshore-uniform configuration.

With the idea of getting a better understanding of the onshore sandbar migration process, the final section of this study focused on explaining the main behavioral modes of the sandbar during the landward movement. The sandbar followed a wave-height dependent time varying equilibrium state; during low energy conditions it tended to displace onshore toward the location of origin. The capabilities of the sandbar to migrate onshore and couple to the shoreline depended on its location relative to the dynamic equilibrium position (DEP) and it

height or volume of sediment contained. DEP was determined as the cross-shore distance of 150 m from the shoreline (depth of ~3 m), and the sandbar was typically $h_b \leq 1$ m and contained up to ~100 m^3m^{-1}.

Five sandbar behavioral modes were defined during the onshore migration process. While located within DEP the sandbar was able of completely welding to the shoreline (mode I: SC) during low-energy conditions (Hs<1 m and Pt_{max}<500 kWm^{-1}), becoming the beach unbarred in summer and completing 1 cycle/yr. Highly-energetic winters (Pt>400 kWm^{-1}) induced a larger growth of the sandbar (hb>1 m; Vb>100 m^3m^{-1}) and located it offshore DEP, being unable of welding to the shoreline and completing 1 cycle/yr. Whilst offshore from DEP, the sandbar eroded and turned into a terrace-bar (mode II: STT). If located slightly offshore from DEP, the terrace-bar could grow during moderately energetic wave conditions (Hs≈2 m and Pt_{max}<2000 kWm^{-1}) and become a sandbar (mode III: TST). Exposed to low-energy conditions, the terrace-bar near DEP could divide into two sections (mode IV: TS). The outer section typically followed a net offshore migration (NOM) cycle, and under moderately energetic wave energy conditions the inner part could follow TST (mode III). The coexistence of a newly formed sandbar and a terrace-bar following NOM could occur (mode V: STC), both following an independent migration path.

The findings of this research can be applied to parameterize the physical processes associated with onshore sandbar displacements. The developed methodology and obtained results provide a framework for studying similar data

sets on single-barred beaches. It would be desirable to obtain similar datasets in other sites in order to carry out intersite comparisons on the magnitude of sandbar displacements and geometric characteristics. These datasets are needed to improve the capabilities of existing physical and numerical models on predicting sandbar behavior.

Bound copies of published papers

Geomorphology 295 (2017) 383–392

Contents lists available at ScienceDirect

Geomorphology

journal homepage: www.elsevier.com/locate/geomorph

Invited review

Seasonal morphodynamics of the subaerial and subtidal sections of an intermediate and mesotidal beach

Amaia Ruiz de Alegría-Arzaburu*, Jesús Adrián Vidal-Ruiz, Héctor García-Nava, Angélica Romero-Arteaga

Instituto de Investigaciones Oceanológicas, Universidad Autónoma de Baja California (UABC), km 103 Carretera Tijuana-Ensenada, 22860 Ensenada, Mexico

ARTICLE INFO

Keywords:
Intertidal beach
Supratidal beach
Morphological variations
Beach volumes
El Niño

ABSTRACT

This study provides a detailed insight into the seasonal morphological evolution of the subaerial and subtidal sections of an intermediate and mesotidal beach in relation to the nearshore wave conditions. For this purpose, fortnightly – to – monthly topographic and bathymetric measurements were collected on Ensenada Beach (Baja California, Mexico) from November 2012 to February 2016. Wave data were concurrently measured at 20 m water depth, enabling the correlation of the observed morphological changes to the hydrodynamic forcing. The seasonal morphological variability of the beach comprised $\pm 200{,}000\ m^3$ ($\pm 70\ m^3\ m^{-1}$) and resulted primarily from the cross-shore exchange of sediment. The volumetric fluctuations alongshore were up to $\pm 100{,}000\ m^3$ and event-driven, and played an inportant role in the overall sediment balance. In association with the incoming wave conditions, the subaerial and subtidal beach sections experienced a strong seasonal variability. The subaerial beach reached the maximum volumes in the end of summer (September – October) and minimum in winter (January – February) while the opposite response was obtained for the subtidal beach, with the largest and smallest volumes occurring during the same months in winter and summer, respectively. The morphological fluctuations of the upper and lower beach sections were associated with the preceding monthly averaged wave conditions. The subtidal volume variations were highly and positively correlated to the wave height and period, while the subaerial section was highly but negatively correlated to the same variables. The morphological beach response to energetic waves was more rapid than to low-energy conditions. The largest subaerial erosion and subtidal accretion happened in three months (October – January) while the subaerial accretion and subtidal erosion occurred smoothly over nine months (January – October). The total beach volume (subaerial and subtidal) lacked of seasonal variability, and an annual loss of $50{,}000\ m^3$ ($17\ m^3\ m^{-1}$) occurred from August 2014 to August 2015, indicating that the beach remained fairly stable over that period of time. The largest volumetric variations of $300{,}000\ m^3$ ($105\ m^3\ m^{-1}$) occurred during the beginning of the 2015–2016 El Niño winter.

1. Introduction

Beaches can display dramatic spatio-temporal changes at different scales (Wright and Short, 1984; Larson and Kraus, 1994; Ranasinghe et al., 2004; Ruggiero et al., 2016) and significant efforts have been conducted to construct conceptual models that predict the morphological variations in relation to the prevailing hydrodynamic conditions. Identifying the physical mechanisms that cause the morphological changes is critical to enable accurate predictions of these variations, and in the mid- to long-term (days to years) this has been largely achieved for the subaerial beach.

Most of the subtidal beach research has focused on the morphodynamics of nearshore bars using video data and/or numerical modelling (Ruessink and Kroon, 1994; Ranasinghe et al., 2004; Sedrati and Anthony, 2007) or short-term beach shape variations during intensive field campaigns (Brander, 1999; Masselink et al., 2008; Coco et al., 2014). Very little effort has been applied to the understanding of the volumetric evolution of the subtidal beach in a time span of months to years (Aubrey, 1979; Larson and Kraus, 1994; Yates et al., 2009; Roberts et al., 2013). And this is related to the lack of measurements that can resolve the relationship of sediment gains and losses between the subaerial and submerged sections (e.g. Harley et al., 2015).

On wave-dominated environments beaches typically exhibit subaerial erosion during high-energy wave periods and accretion in the presence of low-energy waves, and this is generally attributed to a seasonal variability (Shepard, 1950; Winant et al., 1975; Aubrey, 1979;

* Corresponding author.
E-mail address: amaia@uabc.edu.mx (A. Ruiz de Alegría-Arzaburu).

http://dx.doi.org/10.1016/j.geomorph.2017.07.021
Received 29 August 2016; Received in revised form 20 June 2017; Accepted 25 July 2017
Available online 27 July 2017
0169-555X/

Wright and Short, 1984; Wright et al., 1985). From a morphological perspective, the average seasonal extreme beach states are the summer and the winter, while the spring and autumn represent transitionary periods, both with similar morphological characteristics (Larson and Kraus, 1994). During the summer low-to-moderate wave energy conditions a net onshore sediment transport is generated inducing the onshore migration of the nearshore bars and contributing to the subaerial beach accretion. Instead, a net offshore sediment transport is dominant during the energetic winter waves, causing erosion on the subaerial beach, and as consequence, the formation of nearshore bars that supply sediment to the subtidal section.

Recent observations on intermediate microtidal (Quartel et al., 2008) and meso-to-macrotidal beaches (Senechal et al., 2009; Ruiz de Alegria-Arzaburu and Masselink, 2010; Bird et al., 2017) restate the strong association between the subaerial beach morphological variability in response to the incoming wave conditions, and usually responding to the 'bar-berm' and 'storm-post-storm' models. It is overall accepted that the accretionary phase of the subaerial beach results primarily from the welding of subtidal bars to the intertidal beach (e.g. Masselink et al., 2006). While storms induce rapid subaerial beach erosion, the recovery during calm wave conditions is slower due to the need of a minimum period of low-to-moderate wave energy that ensure onshore-directed cross-shore sediment transport. The physical processes responsible for the beach recovery are, however, still poorly understood (Senechal et al., 2009; Ruggiero et al., 2016), and this is particularly relevant after extreme energetic events such as El Niño (Allan and Komar, 2002; Storlazzi and Griggs, 2000; Barnard et al., 2011; Dingler and Reiss, 2002; Sallenger et al., 2002; Barnard et al., 2017).

This study contributes to the understanding of the spatio-temporal volumetric evolution of the subtidal and supratidal sections of an intermediate mesotidal beach located on the Pacific coast of the Baja California peninsula in a time span of months to years. First, the morphological and volumetric variability of the subaerial beach is studied over three years. Then, the subaerial response is compared to the subtidal and total beach change over a year and a half. The cross-shore and alongshore morphological variations are evaluated through a sediment balance and the seasonality of the beach is discussed. The volumetric changes on the subaerial, subtidal and total beach are finally related to different wave parameters to determine their relevance on the cross-shore or longshore exchange of sediment between the foreshore and the nearshore.

2. Study site

Located in the northwestern coast of the Baja California peninsula, Todos Santos Bay (TSB) comprises sandy, gravel, mixed and cobble beaches (Fig. 1). The bathymetry within TSB is fairly shallow (depths of up to 50 m) but a deep canyon of over 400 m is present between Todos Santos Islands and the Punta Banda headland. The coastline in northern TSB (between the San Miguel headland and Ensenada city) contains pocket beaches made of gravel, cobble and mixed sand/gravel, while the beaches in central TSB are made of siliceous medium sand (D_{50} of 0.25 mm). The sandy stretch of coast has a length of 14 km and is interrupted by the mouth of the Punta Banda Estuary (Fig. 1).

Ensenada beach comprises the northern half of the sandy coastline within BTS and is partly protected from the western Pacific swell by Todos Santos Islands (17 km offshore). It is a single-barred intermediate beach with an average slope of tan β of 0.025 (Ruiz de Alegria-Arzaburu et al., 2015). Coastal structures are present along the northern 2 km of the beach, such as a promenade in the northern end and a seawall and rip-rap further south. The southern beach preserves a natural dune backed by a shallow and intermittently dry freshwater lagoon. The subaerial beach width varies from 80 to 120 m to 220–240 m in the walled and non-walled sections, and the supratidal beach elevations are up to 6.5 m and 10 m above mean low water (MLW) along both sections, respectively (Ruiz de Alegria-Arzaburu et al., 2015).

The semi-diurnal tides in the study area are mesotidal with spring and neap tidal ranges of 2.3 m and 0.5 m (http://oceanografia.cicese.mx/predmar). Northwesterly winds of 4 ms^{-1} are dominant in the study area, and sporadic easterly winds known as Santa Ana are frequent from October to March, with speeds of up to 10 ms^{-1} and 2–3 days of duration (Alvarez-Sanchez, 1977; Castro and Martínez, 2010).

The incoming swell is bimodal, northwesterly waves are common during the winter, originating in the north Pacific extratropical zone, and southwesterly waves are frequent during the summer, originating in the south Pacific extratropical region. The annual nearshore waves (measured at 20 m depth) are characterised by mean significant wave height (H_s) of 1 m, mean maximum significant wave height of 1.5 m and a peak wave period of 11 s (Ruiz de Alegria-Arzaburu et al., 2016). The incidence of storms is common between October and April with H_s exceeding 4 m, and calm wave conditions dominate from June to September with an average H_s of 0.7 m (Ruiz de Alegria-Arzaburu et al., 2016). The convergence of energetic waves during the winter have been found to induce significant morphological changes along the beaches within TSB, such as the reported for the Punta Banda estuary mouth during the 1998 El Niño year (Delgado-Gonzalez et al., 2005).

3. Methodology

3.1. Morphological measurements

The subaerial morphology of the beach was measured fortnightly to monthly from November 2012 to February 2016 (Fig. 2). A beach section with a length of 2867 m was studied, and a total of 45 topographic surveys were conducted (except from April to August 2013) measuring ~50 m spaced cross-shore profiles during low spring tides. The profiles were measured using a differential GPS (Global Positioning System) with a precision of ± 0.03 m, and a threshold elevation value of 0.05 m was established to discard post-processed erroneous data as established in other research studies (e.g. Coco et al., 2014). In addition to the regular surveys, pre- and post-storm surveys were also conducted. All profiles were measured down to the mean low tide level (MLT) at a frequency of 1 Hz using a two-wheeled trolley operated by two people on foot. The same transect lines were followed at each survey time, as mapped on the GPS controller, and a total of 61 topographic profiles were consistently measured. The measurements were referred in Universal Transverse Mercator (Easting and Northing coordinates in metres), and the elevations were referenced to the local MLT (+ 36.135 m from ellipsoidal heights).

The subtidal morphology was measured monthly from August 2014 to February 2016 (Fig. 2). Bathymetric data were acquired using the Sontek M9 Hydrosurveyor Accoustic Doppler Current Profiler (ADCP) synchronized to the differential GPS and fixed to a small boat. The frequency of 0.5 MHz was used to obtain the bathymetric data with a sound speed corrected depth accuracy of ± 0.02 m. Similar to Wijnberg and Terwindt, 1995, an accuracy of ± 0.1 m was estimated when ship-dependent errors were included. In all surveys an overlap with a few topographic lines was obtained, and it was used to verify the adjustment of the submerged elevations to the subaerial. Due to limitations on data acquisition across the surf zone, linear interpolation was applied when required. A full survey consisted of 100 m spaced 30 cross-sectional transects and comprised depths ranging from 1 to 12 m, beyond the visually estimated depth of closure of ~9 m (see Fig. 2). The combination of the topographic and bathymetric measurements resulted in a total of 100 m spaced 30 topo-bathymetric (TB) transect lines. An example of the temporal evolution of two of the TB profiles (for the northern and southern beach ends) is shown in Fig. 2.

Beach volumes were calculated for each TB by integrating the profile upwards from the elevations of 0 to 5.5 m (subaerial, or

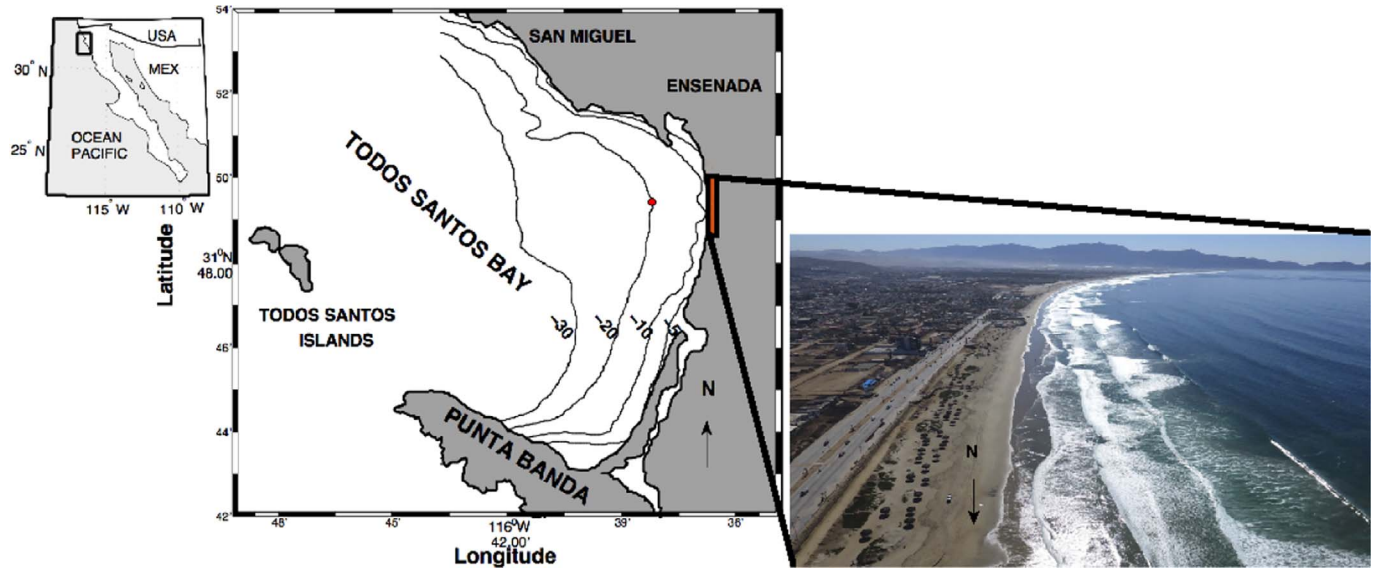

Fig. 1. Location of Ensenada Beach (orange rectangle) within Todos Santos Bay in Baja California, Mexico. An aerial view of the beach is presented on the right panel. The position of the acoustic Doppler profiler (AWAC) is indicated with the red dot on the bathymetric map. (For interpretation of the references to colour in this figure legend, the reader is referred to the web version of this article.)

intertidal and supratidal, IS), − 9 to 0 m (subtidal, SUB) and − 9 to 5.5 m (total, TOT), and multiplying the corresponding alongshore length represented by each profile. A hypothetical vertical error of 0.1 m across the whole TB profile (from − 9 to 5.5 m of elevation) and extending along the studied beach section would imply a total volumetric error of 2%. The loss or gain of volume was determined subtracting the mean value to each volume in time, which resulted in demeaned (Dem) IS, SUB and TOT volumes. The volumetric evolution of the beach was obtained calculating the cumulative volumetric differences (Cum ΔV) per beach profile in time.

The TB profiles were interpolated at 0.1 m across-shore to obtain digital elevation models (DEMs) per survey period. The three-dimensional morphological variations for the subaerial beach (IS) were obtained subtracting the DEMs from 0 to 5.5 m of elevation. DEM differences (referred as *D*) were performed for periods between minimum and maximum IS volumes from November 2012 to February 2016 (D1 to D7 in Table 1), which represented seasonal topographic variations. The three-dimensional morphological variations for the whole beach (TOT) were calculated subtracting the DEMs from − 9 to 5.5 m of elevation for the available periods of minimum and maximum IS volumes.

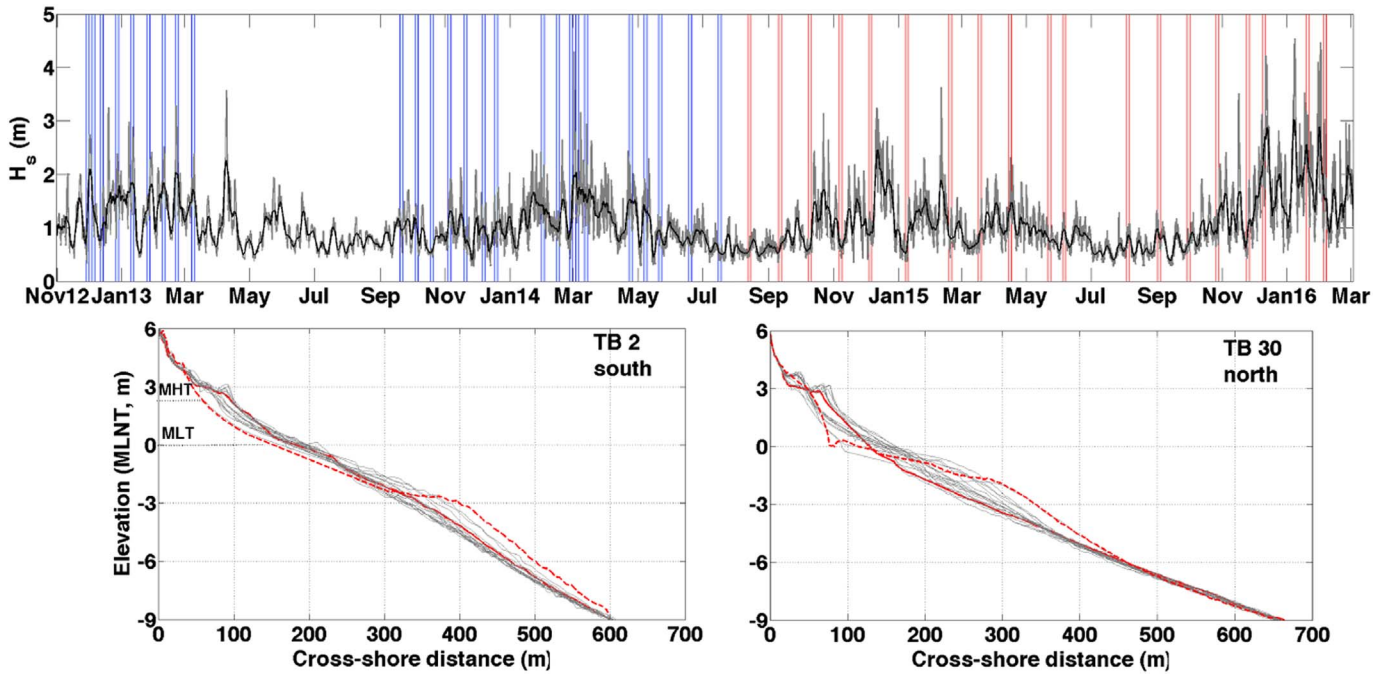

Fig. 2. The top panel presents the time series of hourly and 100-h averaged significant wave heights (gray and black lines) and the dates of topographic (blue lines) and topo-bathymetric (red lines) surveys. The bottom panels present the temporal evolution of the TB2 and TB30 topo-bathymetric profiles from August 2016 to February 2016 (gray profiles) and the profiles for August 2014 and February 2016 are plotted in red with full and dashed lines, respectively. The TB elevations are referred to the mean low tide level (MLT), and MHT refers to the mean high tide level. (For interpretation of the references to colour in this figure legend, the reader is referred to the web version of this article.)

Table 1
Periods of topographic differences (D1 to D7) and their initial and final dates, subaerial volumetric difference for the studied beach length (ΔV) and the wave conditions (significant wave height, H_s, peak period, T_p and wave direction, α) for each period of time.

D	Initial (dd-mm-yy)	Final (dd-mm-yy)	ΔV (m^3)	H_s (m)	T_p (s)	α (deg)
D1	28-Nov-12	07-Mar-13	− 138,655	1.37	12.5	262
D2	07-Mar-13	03-Nov-13	196,192	0.89	11.5	262
D3	03-Nov-13	11-Mar-14	− 201,550	1.10	12.4	268
D4	11-Mar-14	08-Oct-14	224,282	0.86	9.5	270
D5	08-Oct-14	17-Feb-15	− 164,925	1.22	12.8	271
D6	17-Feb-15	29-Sep-15	199,467	0.80	9.8	273
D7	29-Sep-15	05-Feb-16	− 330,787	1.46	12.1	270

3.2. Nearshore wave measurements

Hourly wave data were collected from October 2013 to February 2016 with a 1 MHz ADCP (Nortek AWAC) located 2.5 km off the study site at a water depth of 20 m (Fig. 1). The instrument was installed on the seabed and provided offshore measurements of wave parameters including the significant wave height (H_s), wave peak period (T_p) and wave direction (α). In the absence of measurements from November 2012 to October 2013, wave data were obtained applying the SWAN spectral wave model (Booij et al., 1999). The model domain included Todos Santos Bay and extended 18 km offshore, and it was implemented using a non-structured mesh with variable spatial resolution ranging from 1000 m (offshore) to 100 m in the nearshore. The model boundaries were updated every 3 h with directional wave data obtained from the WW3 global model though the IOWAGA program (Rascle and Ardhuin, 2013).

The SWAN model results for the significant wave height were compared with the ADCP measurements for the period from October 2013 to December 2014, and a correlation coefficient of 0.85 and a bias of 0.27 m were obtained. The model underestimated the wave heights, so the outputs were readjusted with a linear correlation; the results were considered adequate to characterise the wave forcing from November 2012 to October 2013 when measurements were absent. The time series of the modelled and measured significant wave height is presented in Fig. 2 for the study period from November 2012 to February 2016.

The amount of wave energy transferred along and across the beach was determined with the longshore (P_l) and cross-shore (C_x) components of the energy flux, which were calculated in Eqs. (1) and (2), respectively, using the measured offshore wave parameters (Komar and Inman, 1970; Ruessink et al., 2000);

$$Pl = \frac{\rho g^2}{64\pi} H_s^2 T_p \sin(\alpha)\cos(\alpha) \quad (1)$$

$$Cx = \frac{\rho g^2}{64\pi} H_s^2 T_p \cos^2(\alpha) \quad (2)$$

where g is the gravitational acceleration, ρ the water density, α angle of wave incidence to the shore, H_s the significant wave height and T_p its associated peak period.

In order to characterise the wave conditions between the periods of morphological measurements, the wave parameters and the cross-shore and longshore energy fluxes were averaged, and then correlated to the time series of IS, SUB and TOT volumes.

4. Results

4.1. Subaerial beach

The subaerial beach volume (IS) exhibited large seasonality, and a total variability of ± 200,000 m^3 or ± 70 $m^3\ m^{-1}$ from November 2012 to February 2016 (Fig. 3). Erosive conditions dominated from December to May, and the beach gained sediment between June and November. The maximum IS volumes were attained in September – October, while the minimum values were in February – March (top panel Fig. 3). The most erosive events occurred between December 2015 and January 2016 with the loss of 200,000 m^3 (second panel Fig. 3) associated to large storms (H_s > 4 m; Fig. 2). The bottom panel on Fig. 3 shows the cumulative volumetric differences along the beach and indicates that the southern end (from 0 to 1350 m) was more dynamic that the northern half (from 1350 to 2867 m).

Periods of larger subaerial morphological differences were identified based on the minimum and maximum annual volumes (top panel in Fig. 3) between November 2012 and February 2016 (Table 1). During the winter wave conditions characterised by larger and longer waves with H_s of 1.2–1.5 m and T_p of 12 s (D1, D3, D5, D7; Table 1), a sediment loss of 130,000 – 330,000 m^3 took place. Instead, subaerial beach accretion of 200,000 m^3 occurred during the shorter and smaller summer wave conditions with H_s of 0.8–0.9 m and T_p of 10 s (D2, D4, D6; Table 1). The amount of sediment gain was similar during the three accretive periods, on the contrary, the volume of eroded sand varied significantly and it doubled in the last winter 2015 – 2016 (D7; Table 1).

Fig. 4 represents the alongshore morphological and volumetric variations of the subaerial beach related to the significant wave height for each period identified in Table 1 (D1 to D7). The largest morphological changes took place along the southern beach, while the northern 1500 m sustained relatively small and alongshore homogeneous variability for the accretive and erosive periods. Overall, the subaerial beach exhibited a very strong seasonal response to the incoming wave conditions, eroding during the winter and accreting in the summer. The eroded sediment during the winter fully recovered in the following summer (Table 1). The most erosive period happened during the 2015 – 2016 winter, which was associated to the occurrence of a sequence of highly energetic storms of large duration (D7; Fig. 4).

4.2. Subaerial and subtidal beach

With the aim of understanding the association between the subaerial (IS) and subtidal (SUB) volumes, and ultimately, with the total volume (TOT), Fig. 5 represents the volumetric variability for each beach section from August 2014 to February 2016. The subaerial beach represented around 14% of the total beach volume, meaning that the remaining 86% was located on the subtidal beach. Thus, the morphological variability of the whole beach was largely dominated by the changes captured along and across the subtidal section (bottom panels Fig. 5).

The largest and smallest IS volumes took place in the end of the summer (September – October) and winter (January – February), respectively (Figs. 3, 5). Opposing IS, the subtidal beach (SUB) presented the largest and smallest volumes at the end of the winter (January – February) and summer (September – October), respectively (Fig. 5). Thus, IS and SUB sustained opposing volumetric responses, and the variability was ± 200,000 m^3 (middle panels Fig. 5). On a seasonal scale, the amount of cross-shore sediment exchange between IS and SUB was of similar magnitude. For example, SUB gained ~400,000 m^3 between October 2015 and February 2016 while IS lost ~350,000 m^3, suggesting that the sediment exchange on the beach was predominantly cross-shore. The times series of TOT volume, however, shows a variability of ± 100,000 m^3, suggesting the presence of events of substantial longshore sediment exchange such as the loss in May 2015 and gain in December 2015 (left panels in Fig. 5). This indicates the significance of the alongshore contributions to the overall sediment budget.

The winter volumetric change was more abrupt than the summer for both the subaerial and subtidal beach. It took three months for IS to erode and SUB to accrete (October – January) while the accretive phase on IS and the erosive on SUB was slower and occurred over nine months (January – October) (top panels Fig. 5). The beach exhibits alongshore

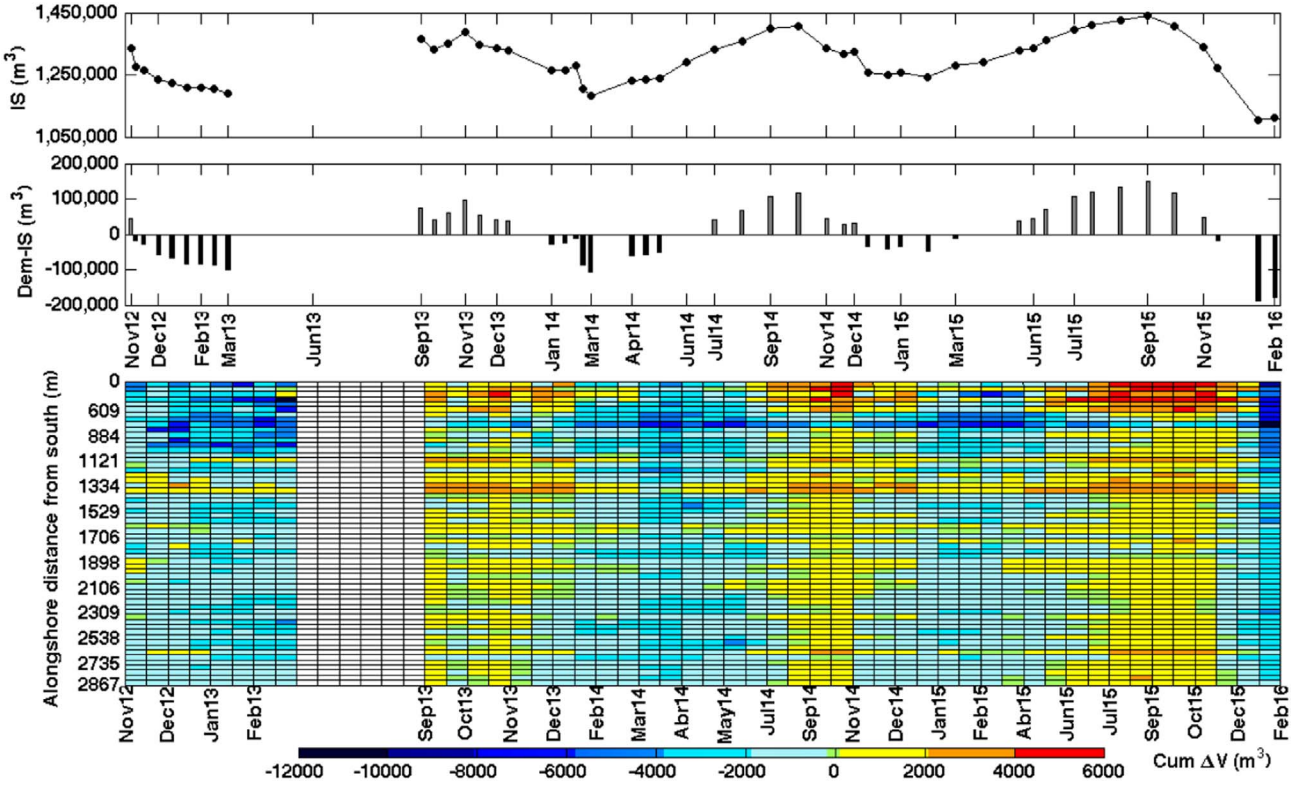

Fig. 3. Subaerial volumes from November 2012 to February 2016 (IS; top panel), de-meaned volumes (Dem-IS; middle panel) and cumulative volumetric differences (Cum ΔV) along the beach (per beach profile) (bottom panel). Note the data gap between April and August 2013.

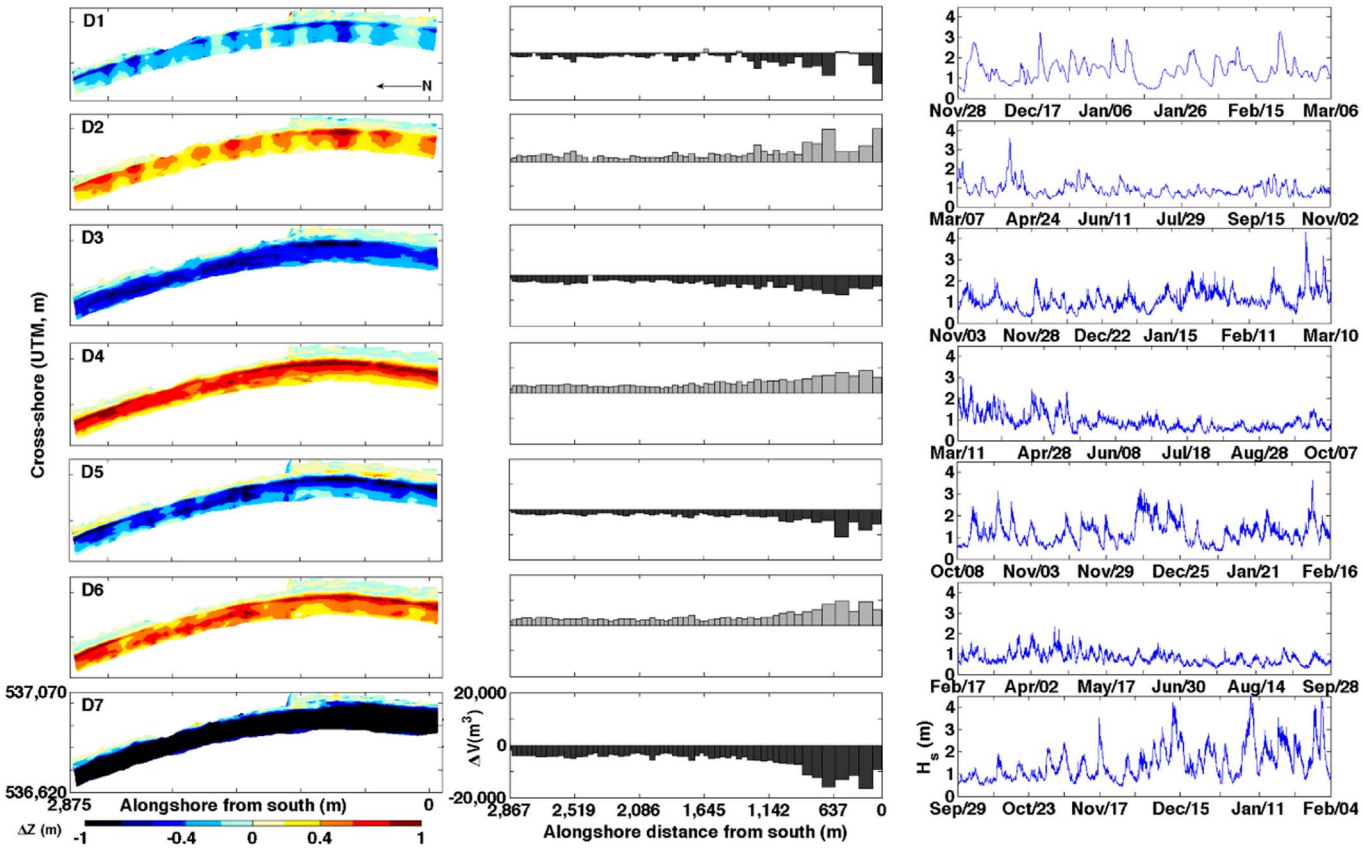

Fig. 4. Subaerial topographic differences for periods of time (from D1 to D7, Table 1) (left panels), volumetric differences per beach profile (ΔV; mid panels) and time series of significant wave heights (H_S) for each period of time.

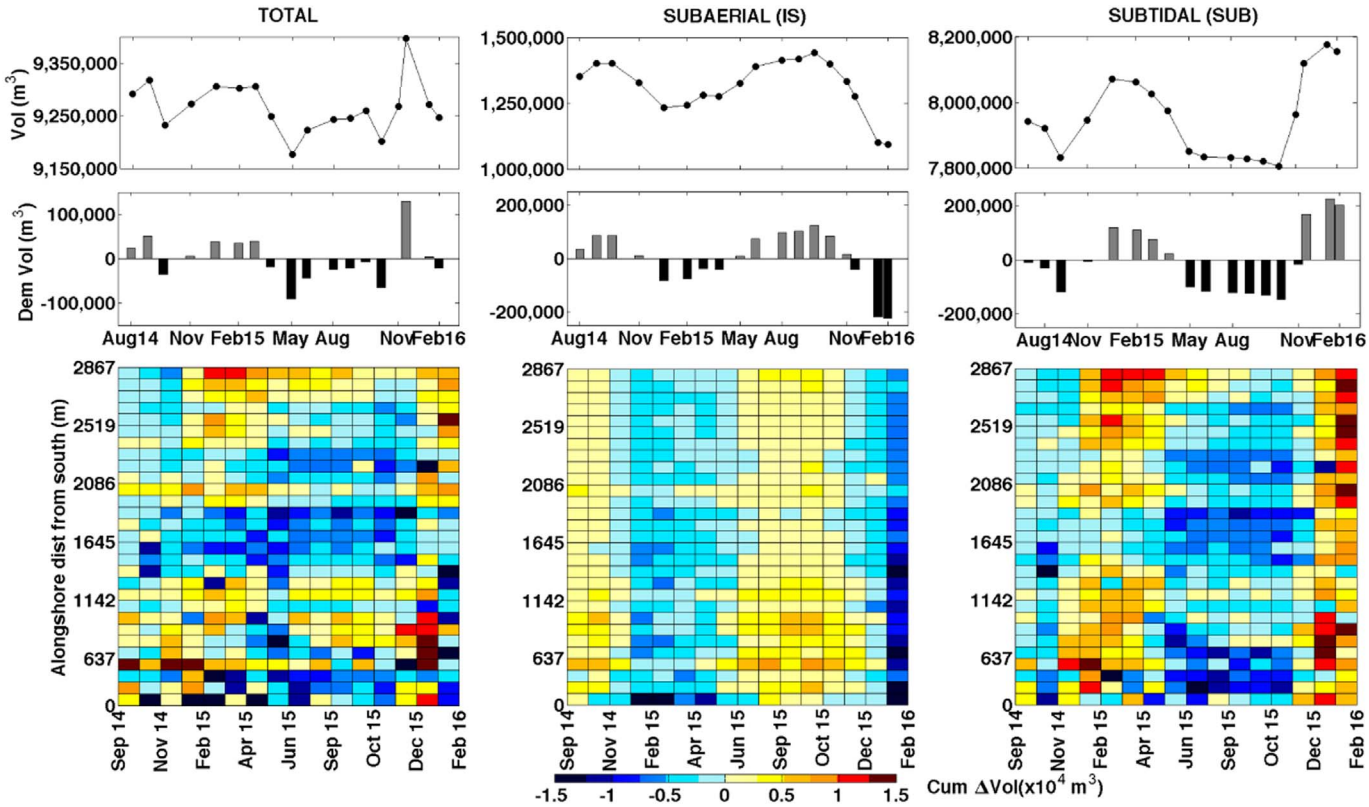

Fig. 5. Total (left column), subaerial (middle column), and subtidal (right column) volumes from August 2014 to February 2016 for the studied beach section (top panels) and de-meaned volumes (Dem; middle panels). The bottom panels represent the cumulative volumetric differences (Cum ΔV) along the beach.

disparities on the morphological response. For instance, SUB gained sediment in the summer of 2015 at an alongshore distance between 700 and 1300 m and lost large amounts of sediment further south (bottom right panel Fig. 5). Moreover, there is continuous erosion between 1500 m and 2000 m from the south, and accretion further north and south (bottom panels Fig. 5); this possibly represents the division of two alongshore sediment transport cells.

The total beach volume fluctuations represent longshore sediment exchange, and in contrast to the subaerial and subtidal sections, it did not exhibit a clear seasonal variability. In 2014, the volume decreased significantly from September to October and increased in a similar amount (60,000 m^3) by the end of the year and the beginning of 2015. Over the spring in 2015, significant erosion occurred (130,000 m^3), which slightly recovered during the summer. During the beginning of the winter in 2015 the beach significantly accreted (200,000 m^3), but most of the sediment eroded by the end of that winter (150,000 m^3). The minimum total volume occurred in October 2014 – 2015 and May 2015, coinciding with the minimum SUB volume (left panels Fig. 5). Thus, the beach exhibits significant volumetric variability alongshore that occurs in a different temporal scale to the clearly seasonal cross-shore exchange.

The foreshore (IS) eroded and deposited offshore in the form of a sandbar during energetic wave conditions (Figs. 2, 6), and the sediment returned to the subaerial beach during calm wave conditions. A maximum vertical morphological variability of ± 2.5 m was captured between the subaerial and subtidal beach and the winter and summer seasons (Fig. 6). During the winter, IS eroded and SUB accreted, with a net difference of 69,375 m^3 and − 13,600 m^3 for D5 and D7. During the summer, IS accreted and SUB eroded, and a net difference of − 41,600 m^3 occurred for D6. The main sediment exchange occurred across-shore between IS and SUB, and it was of similar magnitude (± 200,000 m^3), while the net annual alongshore sediment exchange comprised on average < 20% of the cross-shore exchange (Fig. 6).

Alongshore volumetric differences occurred between the northern and southern beach ends (Fig. 6). The subaerial beach lost and gained more sediment on the southern end, while the northern end was more dynamic than the southern end for the subtidal beach. Overall, these results suggest that during the summer calm wave conditions the main sediment exchange was north-to-south, resulting on erosion of the northern half and accretion of the southern half of the beach (D6 Fig. 6). The opposing pattern was captured for the energetic winter wave conditions when the sediment moved south-to-north, causing erosion of the southern beach half and accretion of the northern half (D7 Fig. 6). The differences on the longshore sediment transport were related to *Pl*, which was relatively small (3 kNs^{-1}) and negative (southerly directed) for D6 and larger (10 kNs^{-1}) and positive (northerly directed) for D7 (bottom panels, Fig. 6).

4.3. Wave forcing vs beach volumes

The beach morphology is best related to wave conditions averaged over an antecedent period, rather than the immediately preceding conditions (Wright et al., 1985; Masselink et al., 2014). Thus, the IS, SUB and TOT volume evolution was compared to average values of H_s, T_p, P_l and C_X for the periods between the morphological surveys (Fig. 7). The variability of SUB volumes were found to be highly and positively correlated to H_s and T_p ($0.6 \leq r \leq 0.66$ at 95% of significance) while IS volumes were highly but negatively correlated to the same variables ($r = -0.78$ at 95% of significance). The correlation of TOT volumes to H_s and T_p were not significant, instead, these were highly and positively ($r = 0.61$) and negatively ($r = -0.71$ at 95% of significance) correlated to P_l and C_x, respectively (Fig. 7).

5. Discussion

The seasonal morphological changes of the subaerial and subtidal

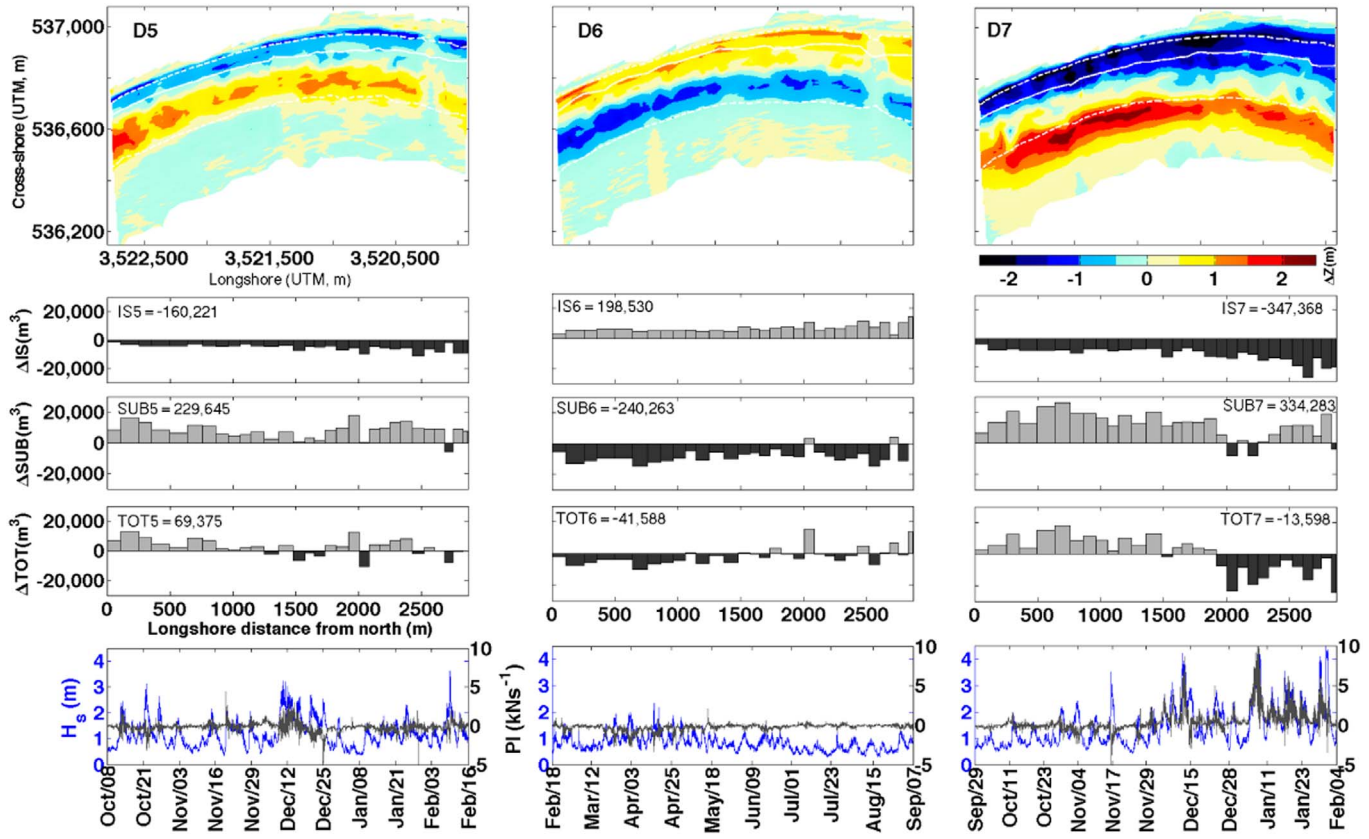

Fig. 6. Topo-bathymetric changes (top panels) and the alongshore volumetric differences for the subaerial (IS), subtidal (SUB) and total (TOT) beach sections (middle panels) for the periods of time D5 (left column), D6 (middle column) and D7 (right column). A time series of significant wave height (H_s) and longshore energy flux is presented in the bottom panels for each period of time (D5, D6 and D7, see Table 1).

sections were investigated over a 3-year period on Ensenada Beach. Morphological data of high spatio-temporal resolution enabled the general understanding of the wave controls on the cross-shore sediment exchange and total volume variations, and the relative importance of cross-shore versus alongshore processes. The subaerial beach represented 14% of the total beach volume while the subaerial section contained the remaining 86% of the total; thus, understanding the morphodynamics of the subtidal section was considered essential (Senechal et al., 2009; Harley et al., 2011).

5.1. Morphological variability

The beach experienced strong cross-shore seasonal variability driven by shoreface erosion and offshore deposition in the form of a sandbar during energetic waves, and the return of the sediment to the subaerial beach during calm wave conditions. These findings agreed with the described by Lizarraga-Arciniega (1976) and with the dominant seasonal cross-shore sediment exchange reported for the southern California beaches (Shepard, 1950; Winant et al., 1975; Aubrey, 1979; Yates et al., 2009). It has been previously stated that the morphodynamics of compartment or embayed beaches is primarily controlled by the cross-shore exchange of sediment, being the longshore transport a comparatively minor contribution (Wright et al., 1985; Harley et al., 2015). In contrast, this study highlights the relevance of the longshore sediment exchange on the overall sediment balance, which occurs on a non-seasonal scale on a beach with limited incidence of oblique waves.

The vertical seasonal morphological variations were up to ± 2.5 m from August 2014 to February 2016, slightly over to the changes of ± 2.0 m reported by Shepard (1950) and Winant et al. (1975) for the southern California beaches. These variations may have been higher than the reported due to the inclusion of the 2015–2016 El Niño winter, which is expected to cause larger morphological variability (Allan and Komar, 2002; Storlazzi and Griggs, 2000; Barnard et al., 2011). The 2015–2016 winter led the subaerial beach to its lower level with a loss of 105 $m^3\ m^{-1}$ or 300,000 m^3, which was within the range of the volume change reported by Aubrey (1979) for storm conditions (100 $m^3\ m^{-1}$). After such energetic winter the recovery may take a few years to occur (Dingler and Reiss, 2002; Sallenger et al., 2002; Doria et al., 2016; Barnard et al., 2017).

5.2. Volumetric variability

Individually, the subaerial and subtidal beach volumes presented a very strong opposing seasonal variability of ± 200,000 m^3. A similar amount of cross-shore sediment exchange between the subaerial and subtidal sections was reported for the southern California beaches (Yates et al., 2009), and this was four times larger than the measured on microtidal and storm-dominated beaches (Quartel et al., 2008). The subaerial beach attained accretion between June and October during small-amplitude and short-period summer waves (H_s = 0.8–0.9 m; T_p = 10 s) and erosive conditions from November to May with the incoming of larger and longer waves (H_s = 1.2–1.5 m; T_p = 12 s). The maximum volumes were reached in September – October and the minimum in January – February. Opposite to the subaerial section, the subtidal beach presented the largest and smallest volumes in the winter (January – February) and end of summer (September – October), respectively.

Despite the relatively large cross-shore sediment exchange between the subaerial and subtidal beach sections (± 200,000 m^3), the total beach volume exhibited significant fluctuations of ± 100,000 m^3. The variations of the total beach volume were indicative of the longshore exchange of sediment, and were relevant in defining sediment balance

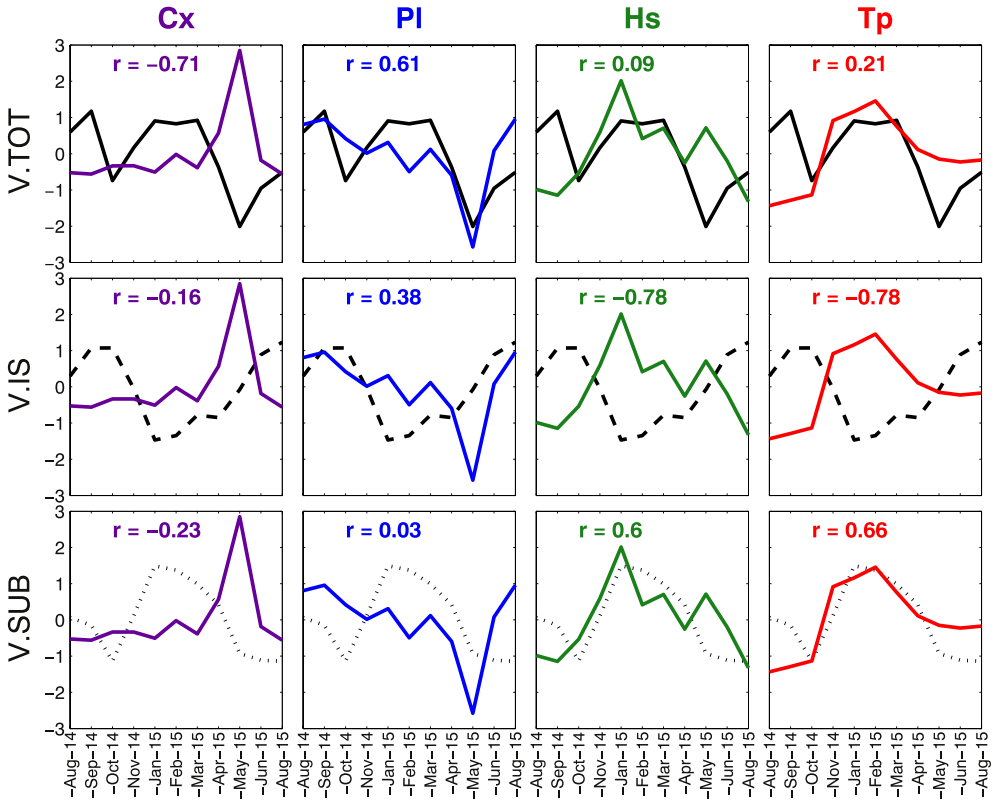

Fig. 7. Standardised anomalies from the monthly averaged cross-shore and longshore energy fluxes, *Cx* and *Pl*, significant wave height, H_s, peak wave period, T_p, (coloured lines in columns) and the beach volumes: total (TOT; black full line), subaerial (IS; black dashed line) and subtidal (SUB, black dotted line), from August 2014 to August 2015. The correlation coefficients at 95% of significance are shown on each panel. (For interpretation of the references to colour in this figure legend, the reader is referred to the web version of this article.)

on the studied beach section. The total volume did not exhibit seasonal fluctuations; instead, these were related to periods of energetic events with dominant northerly or southerly-directed energy fluxes. For instance, from November to December 2015, the beach gained around 100,000 m^3, and during that period strong northerly longshore fluxes were present. Perhaps due to the limited incidence of oblique wave along Ensenada Beach, the alongshore volume variations were significantly smaller than the reported by Yates et al., 2009 for Torrey Pines Beach in California, who measured a loss of 350,000 m^3 over a two-year period (2005–2007).

In addition to the temporal total beach volume fluctuations, there are significant spatial variations along the studied beach section. In particular, the middle section (1500 to 2000 m from the south) seems to lose sediment systematically, while the northern beach end and a section further south (700 to 1200 m from the south) gain sediment regularly. This suggests the existence of two main sediment transport cells (perhaps with sub-cells) along the studied beach, which agrees with the previously reported alongshore differences in the magnitude of nearshore currents that were related to variations in the underlying beach morphology (Ruiz de Alegria-Arzaburu et al., 2016).

The sediment supply along the beach is nearly negligible from neighbouring creeks due to the lack of regular rain and the inexistence of cliffs along the supratidal beach. In terms of sediment balance, the studied beach section is considered stable for the analysed period of time. A total loss of 17 $m^3\,m^{-1}$ (50,000 m^3) occurred over the year from August 2014 to August 2015, and it barely varied until February 2016. These findings disagree with Peynador and Mendez-Sanchez (2010) who suggested an erosive rate of 2100 m^2 per year for the studied beach section based on the analysis of four shorelines between 1985 and 2005.

5.3. Beach morphodynamics

The morphological fluctuations of the subaerial and subtidal beach sections were in direct association with the wave energy conditions (Aubrey, 1979; Yates et al., 2009). The subtidal volumetric change was found to be highly and positively correlated to the wave height and period, while the subaerial section was highly but negatively correlated to the same variables. The morphological beach response to energetic wave conditions was more rapid than to low-energy conditions (Wright and Short, 1984: Sallenger et al., 2002; Doria et al., 2016), the largest subaerial erosion and subtidal accretion happened in three months (October – January) while the subaerial beach recovery and subtidal erosion occurred smoothly over nine months (January – October).

Large volumetric variations occurred along the subaerial and subtidal sections. Overall, the subaerial morphology varied more in the southern end, while the subtidal beach was more dynamic in the northern end. The sediment exchange happened north-to-south in the summer and south-to-north in winter, and this was associated to the longshore component of the energy flux; which was relatively small (3 kNs^{-1}) and negative, indicating southern direction in summer, and larger (10 kNs^{-1}) and positive, indicating northern direction in winter. The longshore energy flux was small compared, for example, to the measured by Senechal et al. (2009) for the same depth (40 kNs^{-1}), and this was attained to the predominantly shore-normal incidence of the nearshore waves on the beach.

In contrast with the subaerial and subtidal sections, the total beach volume did not exhibit a clear seasonal variability. The total volume variations were positively and negatively correlated to the longshore and cross-shore components of the energy flux, indicating that the beach primarily gained sediment associated to a longshore flux and lost sediment in the cross-shore direction. In coincidence with the findings of Yates et al. (2009), the total beach volume did not show large seasonal changes, and instead, the largest fluctuations were associated to events of energetic southerly/northerly directed longshore energy fluxes. The largest volumetric fluctuations for the whole beach occurred during the transitional periods (spring and autumn) and the 2015–2016 El Niño winter, which was reported as one of the strongest of the last 145 years (Barnard et al., 2017).

6. Conclusions

Beach seasonality is commonly referred to as the morphological variability of the subaerial beach in direct association with the incoming wave energy; being the response typically erosive in winter and accretive in summer. The seasonal morphological variability of the subaerial and subtidal zones was investigated over a 3-year period on a single-barred intermediate beach in the northwestern Baja California peninsula. Results indicated that the seasonal morphological variability of the beach was primarily controlled by the cross-shore exchange of sediment. The subaerial and subtidal beach sections experienced a strong seasonal variability in association to the wave conditions. The subaerial section accreted in summer, reaching maximum volumes in September – October, and eroded in winter exhiibiting minimum volumes in January – February. The subtidal section presented the opposite response with the largest and smallest volumes occurring in the same months in winter and summer, respectively. Both beach sections exchanged $\pm 200{,}000\ m^3$ in the cross-shore over the period from August 2014 to February 2016.

Despite the nearly shore-normal incidence of nearshore waves, the total volume fluctuated up to $\pm 100{,}000\ m^3$ and represented the alongshore exchange of sediment. The largest alongshore sediment fluctuations were event-driven, thus, they were not associated to the typical summer/winter wave conditions and lacked of a seasonal variability. The beach presented a total annual loss of $50{,}000\ m^3$ or $17\ m^3\ m^{-1}$ from August 2014 to August 2015, which represented $< 20\%$ of the change; therefore, the beach remained stable for that period. The largest volumetric variations occurred during the beginning of the 2015–2016 El Niño winter, i.e. $300{,}000\ m^3$ or $105\ m^3\ m^{-1}$, which was considered one of the strongest events of the past 145 years.

Acknowledgements

The authors are grateful to CONACyT for the funding provided through CB-2014-238765 and INFR-2013-01I005 with the projects 205020 and 205022. Thanks are extended to F-PROMEP-38/Rev.-03 SEP-23-005 and UABC for the support with UABC-PTC-418 and 18th projects 636 (IMTENS) and 634 (EOCiS). We are very thankful to all field assistants, especially to Eduardo Gil and Ernesto Carsolio for the technical support provided in the field.

References

Allan, J.C., Komar, P.D., 2002. Extreme storms on the Pacific Northwest Coast during the 1997–98 El Niño and 1998–99 La Niña. J. Coast. Res. 18 (1), 175–193.

Alvarez-Sanchez, L.G., 1977. Vientos en la Bahia de Todos Santos, Baja California. Ciencias Marinas 4, 81–89.

Aubrey, D.G., 1979. Seasonal patterns of onshore/offshore sediment movement. J. Geophys. Res. 84, 6347–6354.

Barnard, P.L., Allan, J., Hansen, J.E., Kaminsky, G.M., Ruggiero, P., Doria, A., 2011. The impact of the 2009–10 El Niño Modoki on U.S. West Coast beaches. Geophys. Res. Lett. 38 (13). http://dx.doi.org/10.1029/2011GL047707.

Barnard, P.L., Hoover, D., Hubbard, D.M., Snyder, A., Ludka, B.C., Allan, J., Kaminsky, G.M., Ruggiero, P., Gallien, T.W., Gabel, L., McCandless, D., Weiner, H.M., Cohn, N., Anderson, D.L., Serafin, K.A., 2017. Extreme oceanographic forcing and coastal response due to the 2015–2016 El Niño. Nat. Commun. 8 (14365) Doi:10.1038.

Bird, C.O., Bell, P.S., Plater, A.J., 2017. Application of marine radar to monitoring seasonal and event-base changes in intertidal morphology. Geomorphology 285, 1–15.

Booij, N., Ris, R.C., Holthuijsen, L.H., 1999. A third-generation wave model for coastal regions, part I: model description and validation. J. Geophys. Res. 104 (C4), 7649–7666.

Brander, R.W., 1999. Field observations on the morphodynamic evolution of low wave energy rip current system. Mar. Geol. 157, 199–217.

Castro, R., Martínez, A., 2010. Variabilidad espacial y temporal del campo de viento. In: Gaxiola-Castro, G., Durazo, R. (Eds.), Dinámica del Ecosistema Pelágico frente a Baja California, 1997–2007: Diez años de Investigaciones Mexicanas de la Corriente de California, pp. 129–147.

Coco, G., Senechal, N., Rejas, A., Bryan, K.R., Capo, S., Paristo, J.P., Brown, J.A., MacMahan, J.H.M., 2014. Beach responses to a sequence of extreme storms. Geomorphology 204, 493–501.

Delgado-Gonzalez, O., Lizarraga-Arciniega, R., Martinez-Diaz-de-Leon, A., Galindo-Bect, L., Ferman-Almada, J.L., Sanchez-Arcilla, A., Mosso, C., Perez-Higuera, R., Cruz-Varela, A., 2005. Beach-line changes at the mouth of Punta Banda Estuary, Baja California, during 1972–2003. Ciencias Marinas 31 (4), 707–717.

Dingler, J.R., Reiss, R.E., 2002. Changes to Monterey Bay beaches from the end of the 1982–83 El Niño through the 1997–98 El Niño. Mar. Geol. 181, 249–263.

Doria, A., Guza, R.T., O'Reilly, W.C., Yates, M.L., 2016. Observations and modeling of San Diego beaches during El Niño. Cont. Shelf Res. 124, 153–164.

Harley, M.D., Turner, I.L., Short, A.D., Ranasinghe, R., 2011. A reevaluation of coastal embayment rotation: The dominance of cross-shore versus alongshore sediment transport processes, Collaroy-Narrabeen Beach, southeast Australia. J. Geophys. Res. 116 (F04033). doi:10.102972011JF001989.

Harley, M.D., Turner, I.L., Short, A.D., 2015. New insights into embayed beach rotation: the importance of wave exposure and cross-shore processes. J. Geophys. Res. Earth Surf. 120, 1470–1484. Vol. http://dx.doi.org/10.1002/2014JF003390.

Komar, P.D., Inman, D.L., 1970. Longshore sand transport on beaches. J. Geophys. Res. 75 (30), 5914–5927.

Larson, M., Kraus, N.C., 1994. Temporal and spatial scales of beach profile change, Duck, North Carolina. Mar. Geol. 117, 75–94.

Lizarraga-Arciniega, J.R., 1976. Variaciones estacionales de la playa de Bahía de Todos los Santos, Baja California. Ciencias Marinas 3 (1), 30–50.

Masselink, G., Kroon, A., Davidson-Arnott, R.G.D., 2006. Morphodynamics of intertidal bars in wave – dominated coastal settings — a review. Geomorphology 73, 33–49.

Masselink, G., Austin, M., Tinker, J., O'Hara, J., Russell, P., 2008. Cross-shore sediment transport and morphological response on a macrotidal beach with intertidal bar morphology, Truc Vert, France. Mar. Geol. 251, 141–155.

Masselink, G., Austin, M., Scott, T., Poate, T., Russell, P., 2014. Role of wave forcing, storms and NAO in outer bar dynamics on a high-energy macro-tidal beach. Geomorphology 226, 76–93.

Peynador, C., Mendez-Sanchez, F., 2010. Managing coastal erosion: a management proposal for a littoral cell in Todos Santos Bay, Ensenada, Baja California, Mexico. Ocean Coast. Manag. 53, 350–357.

Quartel, S., Kroon, A., Ruessink, B.G., 2008. Seasonal accretion and erosion patterns of a microtidal sandy beach. Mar. Geol. 250, 19–33.

Ranasinghe, R., Symonds, G., Black, K., Holman, R., 2004. Morphodynamics of intermediate beaches: a video imaging and numerical modeling study. Coast. Eng. 51, 629–655.

Rascle, N., Ardhuin, F., 2013. A global wave parameter database for geophysical applications. Part 2: model validation with improved source term parameterization. Ocean Model 70, 174–188.

Roberts, T.M., Wang, P., Puleo, J.A., 2013. Storm-driven cyclic beach morphodynamics of a mixed sand and gravel beach along the Mid-Atlantic Coast, USA. Mar. Geol. 346, 403–421.

Ruessink, B.G., Kroon, A., 1994. The behaviour of a multiple bar system in the nearshore zone of Terschelling: 1965–1993. Mar. Geol. 121, 187–197.

Ruessink, B.G., van Enckevort, I.M.J., Kingston, K.S., Davidson, M.A., 2000. Analysis of observed two- and three-dimensional nearshore bar behaviour. Mar. Geol. 169 161–18.

Ruggiero, P., Kaminsky, G.M., Gelfenbaum, G., Cohn, N., 2016. Morphodynamics of prograding beaches: a synthesis of seasonal-to-century-scale observations of the Columbia River littoral cell. Mar. Geol. 376, 51–68.

Ruiz de Alegria-Arzaburu, A., Masselink, G., 2010. Storm response and beach rotation on a gravel beach, Slapton Sands, UK. Mar. Geol. 278, 77–99.

Ruiz de Alegria-Arzaburu, A., García-Nava, H., Gil-Silva, E., Desplán-Salinas, G., 2015. A morphodynamic comparison of walled and non-walled beach sections, Ensenada beach, Mexico. In: World Scientific. The Proceedings of the Coastal Sediments, ISBN:978-981-4355-52-0.

Ruiz de Alegria-Arzaburu, A., Arreola-Cortez, M.A., García-Nava, H., Hernández-Walls, R., Mejía-Trejo, A., 2016. The effects of beach morphology variations on the profile of nearshore currents on a gently sloping mesotidal beach. In: Vila-Concejo, A., Bruce, E., Kennedy, D.M., McCarroll, R.J. (Eds.), Proceedings of the 14th International Coastal Symposium (Sydney, Australia), pp. 257–261 (Journal of Coastal Research,

Special Issue, No. 75, Coconut Creek (Florida), ISSN 0749-0208).
Sallenger Jr., A.H., Krabill, W., Brock, J., Swift, R., Manizade, S., Stockdon, H., 2002. Sea-cliff erosion as a function of beach changes and extreme runup during 1997-1998 El Niño. Mar. Geol. 187, 279–297.
Sedrati, M., Anthony, E.J., 2007. Storm-generated morphological change and longshore sand transport in the intertidal zone of a multi-barred macrotidal beach. Mar. Geol. 244, 209–229.
Senechal, N., Gouriou, T., Castelle, B., Parisot, J.-P., Capo, S., Bujan, S., Howa, H., 2009. Morphodynamic response of a meso-to-macro-tidal intermediate beach based on a long-term data set. Geomorphology 107, 263–274.
Shepard, F.P., 1950. Beach cycles in Southern California. In: Beach Erosion Board Technical Memo No. 20. U.S. Army Corps of Eningeers.
Storlazzi, C., Griggs, G., 2000. Influence of El Nino-Southern Oscillation (ENSO) events on the evolution of central California's shoreline. Geol. Soc. Am. Bull. 111, 236–249.
Wijnberg, K.M., Terwindt, J.H.J., 1995. Extracting decadal morphological behaviour from high-resolution, long-term bathymetric surveys along the Holland coast using eigenfunction analysis. Mar. Geol. 126, 301–330.
Winant, C.D., Inman, D.L., Nordstrom, C.E., 1975. Description of seasonal beach changes using empirical eigenfunctions. J. Geophys. Res. 80, 1979–1986.
Wright, L.D., Short, A.D., 1984. Morphodynamic variability of surf zones and beaches: a synthesis. Mar. Geol. 56, 93–118.
Wright, L.D., Short, A.D., Green, M.O., 1985. Short-term changes in the morphodynamics states of beaches and surf zones: an empirical predictive model. Mar. Geol. 62, 339–364.
Yates, M.L., Guza, R.T., O'Reilly, W.C., Seymour, R.J., 2009. Seasonal persistence of a small Southern California beach fill. Coast. Eng. 56, 559–564.

Coastal Dynamics 2017
Paper No. 124

POST-STORM BEACH RECOVERY CAPABILITIES AFTER EL NIÑO WINTER AT ENSENADA BEACH, MEXICO.

Amaia Ruiz de Alegría-Arzaburu[1] and Jesús Adrián Vidal-Ruiz[1]

Abstract

This study investigates the recovery capabilities of a single-barred mesotidal beach located in the Pacific Mexican coast before and after the 2015–2016 El Niño winter. Morphological data from August 2014 to December 2016 were analyzed from monthly measured topographic and bathymetric profiles to determine the cross-shore volumetric exchange in relation to the incident wave forcing. Before the 2015–2016 El Niño winter, the subaerial beach successfully recovered from the erosion during the mild wave conditions from June to October, which induced onshore transport from the subtidal beach. After the 2015–2016 El Niño winter, however, the subaerial beach erosion was much larger, and the eroded sediment moved further offshore to deeper waters of 3–4 m. Thus, the beach was unable of transporting onshore the full amount of sediment during the 2016 summer, and consequently, preventing the subaerial beach from fully recovering. It is concluded that the onshore sandbar migration during the summer wave conditions is critical to ensure a full subaerial beach recovery, and that the capabilities of the beach to recover will depend on the wave conditions during the summer and the cross-shore distance and depth at which the sandbar is located.

Key words: sandbars, morphodynamics, sediment transport, climate change.

1. Introduction

Sandbars contain large amounts of sediment that move cross-shore and alongshore, thus, quantifying their migration rates and directions is essential to determine the capabilities of the subaerial beach for post-winter recovery. The offshore sandbar migrations are generally associated to strong mean offshore currents (undertow) occurring under breaking large wave conditions, while the onshore movement takes place during weak-to-nonbreaking waves and is primarily related to near-bed wave skewness (e.g. Ruessink et al., 2007), wave asymmetry (Hoefel and Elgar, 2003) and/or boundary layer streaming and Stokes drift (Henderson et al., 2004).

Most of the sandbar studies have been focused on multi-barred beaches, and single-barred beaches have been surprisingly understudied (e.g. van de Lageweg et al., 2013; Blossier et al., 2016). The most comprehensive studies on sandbar dynamics were undertaken over decades along the multi-barred beaches of Duck (USA), Terschelling and the Holland Coast (The Netherlands) and Wanganui (New Zealand) (e.g. Lippmann et al., 1993; Ruessink and Kroon, 1994; Shand et al., 1999; Plant et al., 1999). These beaches however, lacked of seasonal sandbar movements and presented interannual migration cycles of bar generation near the shoreline, offshore migration across the surf zone and final stage of sandbar disappearance at the outer nearshore zone (Ruessink and Kroon, 1994).

During El Niño years, the track of Pacific storms move farther to the south than usual, thus inducing unusually energetic waves along the southern part of the Pacific US coast (Seymour, 1998; Allan and Komar, 2002; Storlazzi and Griggs, 2000). Previous studies looking at the morphological change caused by El Niño winters indicated extreme subaerial beach erosion during 1982–1983 and a full beach recovery by 1985 along the California coast (Dingler and Reiss, 2002). During the 1997–1998 El Niño winter Sallenger et al. (2002) demonstrated an inversion on the net longshore sediment transport direction resulting in significant subaerial beach and sea-cliff erosion on the southern side of the central California beaches. More recently, during the 1997–1998 and 2009–2010 El Niño winters severe erosion was reported along the subaerial part of the US Pacific beaches (Barnard et al., 2011) and Doria et al. (2016) reported a

[1]Institute of Oceanographic Research, University of Baja California, Mexico. amaia@uabc.edu.mx

subaerial beach recovery over several years from the 1997–1998 winter while the recovery after the less erosive 2009–2010 winter happened over a season.

Despite all these studies, the association between the seasonal sandbar migration and beach recovery capabilities is still poorly understood. These studies require long-term bathymetric measurements of high spatio-temporal resolution to be able to accurately determine to sandbar shape and position (e.g. Grunnet and Hoekstra, 2004; Di Leonardo and Ruggiero, 2015), and enable the correlation between the sandbar movement and the sediment exchange between the subaerial and subtidal beach. This study aims to quantify the volumetric exchange between the subaerial and subtidal beach before and after El Niño winter 2015–2016 on Ensenada beach, located in a swell-dominated mesotidal environment in the Pacific coast of the Baja California peninsula in Mexico.

2. Field site

The study site comprises the northern 3 km of Ensenada beach, located in the northwestern coast of the Baja California peninsula, within Todos Santos Bay (TSB) (Figure 1). The beach is single-barred and intermediate, with an average slope of 0.025, and is partly protected from the western Pacific swell by Todos Santos Islands (17 km offshore) (Ruiz de Alegria-Arzaburu et al., 2015). The bathymetry within TSB is fairly shallow (depths of up to 50 m) but a deep canyon of over 400 m is present between Todos Santos Islands and the Punta Banda headland.

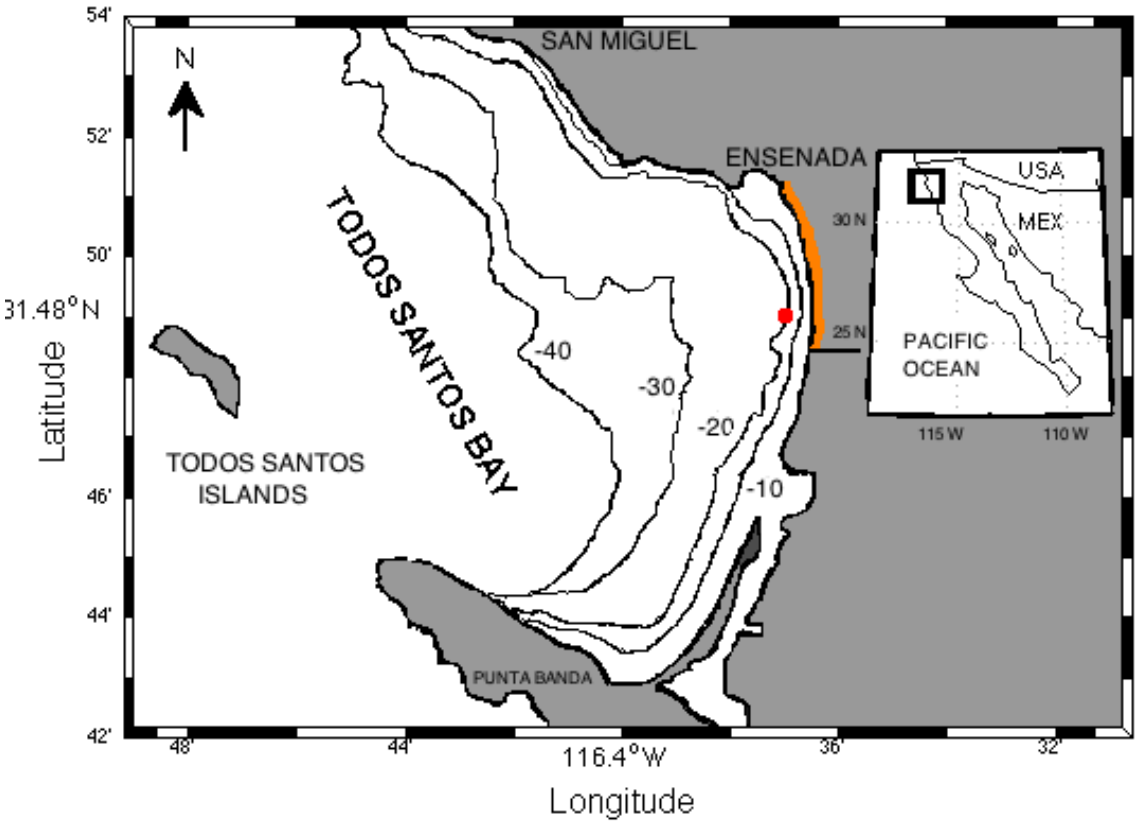

Figure 1. Location of Ensenada Beach (orange line) within Todos Santos Bay in the Mexican Pacific coast. The red dot shows the location of the acoustic Doppler current profiler (AWAC) at 20 m depth.

The subaerial beach width varies from 80–120 m to 220–240 m in the walled and non-walled sections, and the supratidal beach elevations are up to 6.5 m and 10 m above mean low water (MLW) along both sections, respectively (Figure 2; Ruiz de Alegria-Arzaburu et al., 2015). The beach is mesotidal, and the tides are semi-diurnal with spring to neap tidal ranges of 2.3 m and 0.5 m (http://oceanografia.cicese.mx/predmar). Northwesterly winds are dominant in TSB, and sporadic easterly winds known as Santa Ana are frequent between October and March, with speeds of up to 10 ms^{-1} and 2–3 days of duration. The mean significant wave height of 1 m, mean maximum significant wave height of 1.5 m and a peak wave period of 11 s, and the incidence of swell-driven storms is common between October and April with waves exceeding 4 m, while calm waves dominate from June to September with an average height of 0.7 m.

Figure 2. Aerial view of Ensenada Beach on the 6th of October 2016.

3. Methods

Morphological measurements were monthly collected over a 2.5 year period (August 2014 to December 2016) across the subaerial and subtidal sections of nearly 3 km of beach length. The morphological evolution of the beach was determined and related to the incoming wave forcing. Digital elevation models and beach volumes were calculated from the measured topographic-bathymetric profiles.

3.1. *Wave measurements*

Hourly nearshore wave data were collected from August 2014 to December 2016 with a 1MHz ADCP (Nortek AWAC) located 2.5 km off the southern end of the study site at a water depth of 20 m (Figure 1). The instrument was installed on the seabed and provided continuous measurements of wave parameters including the significant wave height (H_s), wave peak period (T_p) and wave direction (α). The monthly averaged wave heights were calculated for the years 2014, 2015 and 2016.

3.2. *Topographic and bathymetric measurements*

The subaerial beach morphology was measured monthly from August 2014 to December 2016 along a beach section of 2,867 m measuring a total o ~50 m spaced 61 cross-shore profiles during low spring tides (top lines in Figure 3). The profiles were measured using a differential GPS (Global Positioning System) with a precision of ± 0.03 m, and a threshold elevation value of 0.05 m was established to discard post-processed erroneous data as established in other research studies (e.g. Coco et al., 2014). All profiles were measured down to the mean low tide level (MLT) at a frequency of 1Hz using a two-wheeled trolley operated by two people on foot. The measurements were referred in Universal Transverse Mercator (Easting and Northing coordinates in metres), and the elevations were referenced to the local MLT (+36.135 m from ellipsoidal heights). The same transect lines were followed at each survey, as these were mapped on the GPS controller.

The subtidal morphology was measured monthly from August 2014 to December 2016, right after or before the topographic measurements. The bathymetric data were acquired using the Sontek M9 Hydrosurveyor Accoustic Doppler Current Profiler (ADCP) synchronized to the differential GPS and fixed to a small boat or to a jetski. The frequency of 0.5 MHz was used to obtain the bathymetric data with a sound speed corrected depth accuracy of ± 0.02 m. Similar to Wijnberg et al. (1995), an accuracy of ± 0.1 m was estimated when ship-dependent errors were included. In all surveys an overlap with a few topographic lines was obtained, and it was used to verify the adjustment of the submerged elevations to the subaerial. Due to limitations on data acquisition across the surf zone, when required, linear interpolation was applied. A full survey consisted of 100 m spaced 30 cross-sectional transects (TB in Figure 3) and comprised depths ranging from 1 to 12 m, beyond the depth of closure (~ 8 m).

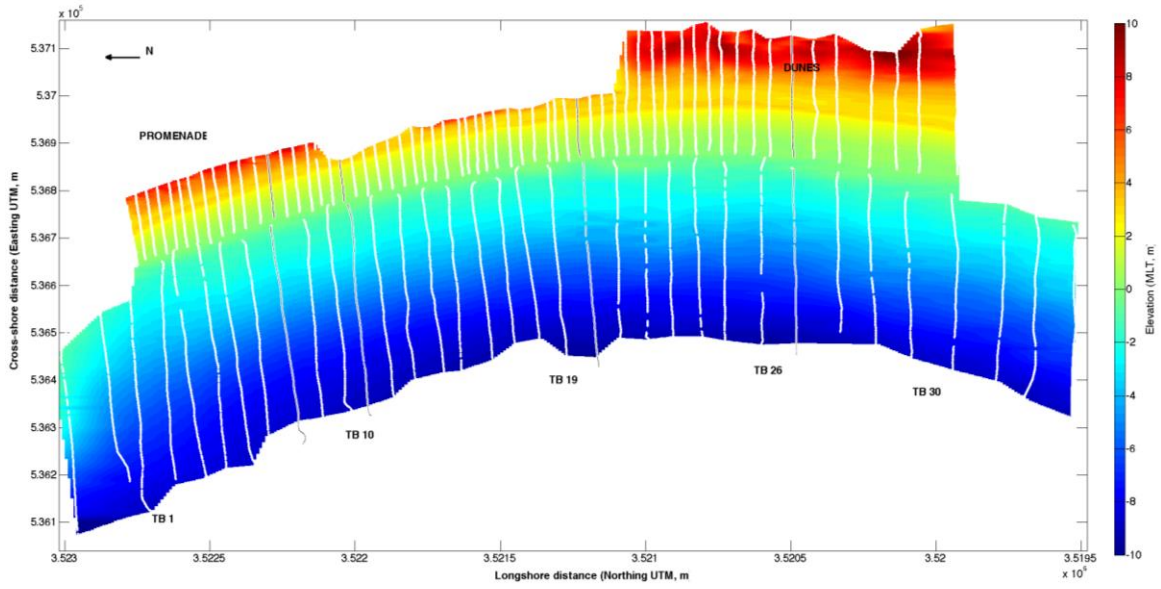

Figure 3. An example of a Digital Elevation Model (DEM) obtained from interpolating topographic (onshore lines) and bathymetric (offshore lines) profiles.

3.3. *Volumes and digital elevation models (DEMs)*

The combination of the topographic and bathymetric measurements resulted in a total of 100 m spaced 30 topo-bathymetric (TB) transect lines. The TB profiles were interpolated at 0.1 m across-shore to obtain digital elevation models (DEMs) per survey period (Figure 3). The three-dimensional morphological variations for the subaerial beach (IS) were obtained subtracting the DEMs from 0 to 5.5 m of elevation; differences for periods between minimum and maximum IS volumes were performed. The three-

dimensional morphological variations for the whole beach (TOT) were calculated subtracting the DEMs from -9 to 5.5 m of elevation for the available periods of minimum and maximum IS volumes.

Beach volumes were calculated for each TB by integrating the profile upwards from the elevations of 0 to 5.5 m (subaerial, or intertidal and supratidal, IS), -9 to 0 m (subtidal, SUB) and -9 to 5.5 m (total, TOT), and multiplying the corresponding alongshore length represented by each profile. A hypothetical vertical error of 0.1 m across the whole TB profile (from -9 to 5.5 m of elevation) and extending along the studied beach section would imply a total volumetric error of 2 %. The loss or gain of volume was determined subtracting the mean value to each volume in time, which resulted in de-meaned (Dem) IS, SUB and TOT volumes. The volumetric evolution of the beach was obtained calculating the cumulative volumetric differences (Cum ΔV) per beach profile in time.

4. Results

4.1 Hydrodynamic conditions

Significant seasonal and interannual differences were encountered in the wave conditions between the years 2014, 2015 and 2016 (Figure 4). The waves were significantly more energetic during the 2015–2016 winter than during the previous winters in 2013 and 2014. The average H_s exceeded 1.5 m from December 2015 to March 2016 and the waves were of longer period (sometimes over 20 s) during some of the energetic events than in the previous winters.

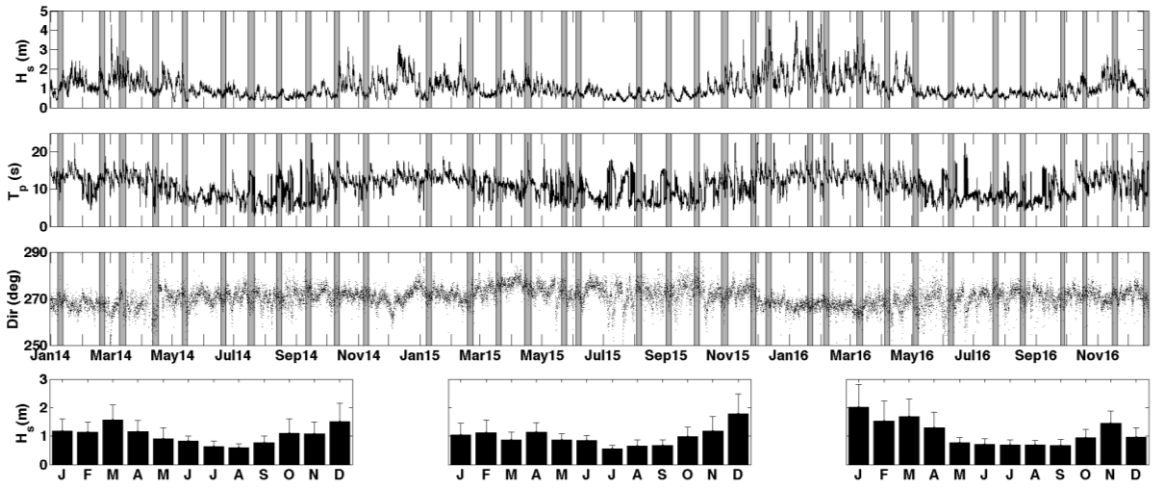

Figure 4. Time series of significant wave height (H_s), peak period (T_p) and wave direction (Dir) from January 2014 to December 2016 (top three panels) and monthly averaged H_s for 2014, 2015 and 2016 (left to right bottom panels). The vertical gray bars indicate the times when the morphological measurements (topography and bathymetry) were undertaken.

4.2 Morphological variability

The subaerial and subtidal morphological variability was determined for the summer and winter seasons in 2014, 2015 and 2016 in order to evaluate the beach erosion and recovery over the study period. The cumulative morphological change for the winter period from December to March in 2015 and 2016 is shown in Figure 5. And Figure 6 represents the cumulative morphological change during the summer periods from August to November 2014, 2015 and 2016.

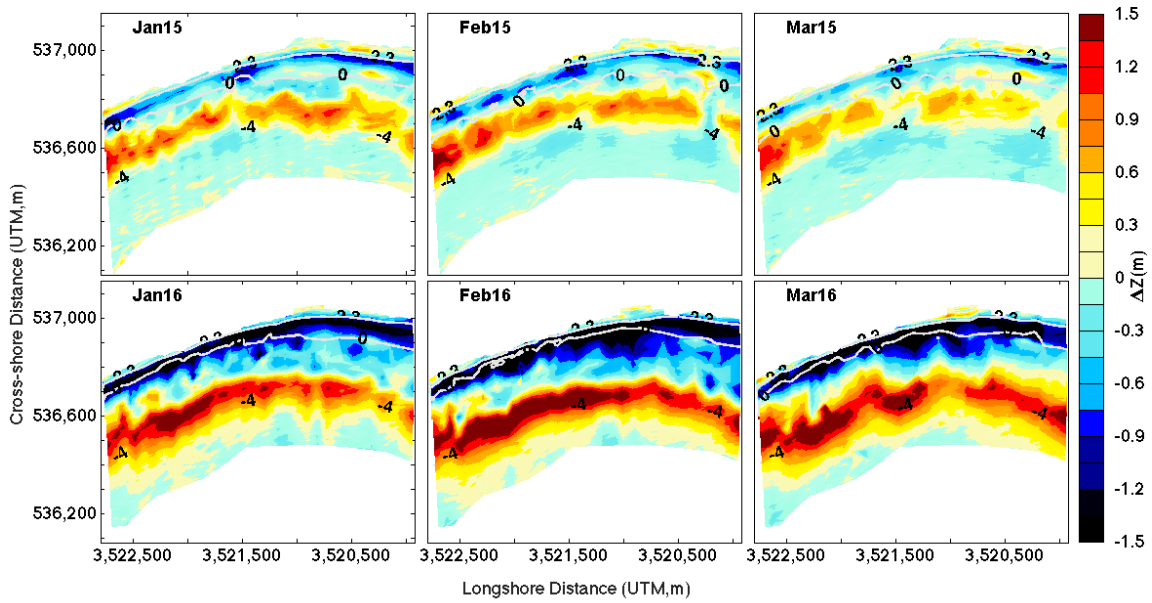

Figure 5. Cumulative morphological differences from December to March 2015 (top panels) and 2016 (bottom panels) for the subaerial and subtidal beach sections. The intertidal beach is defined between the 0 m and 2.3 m contourlines.

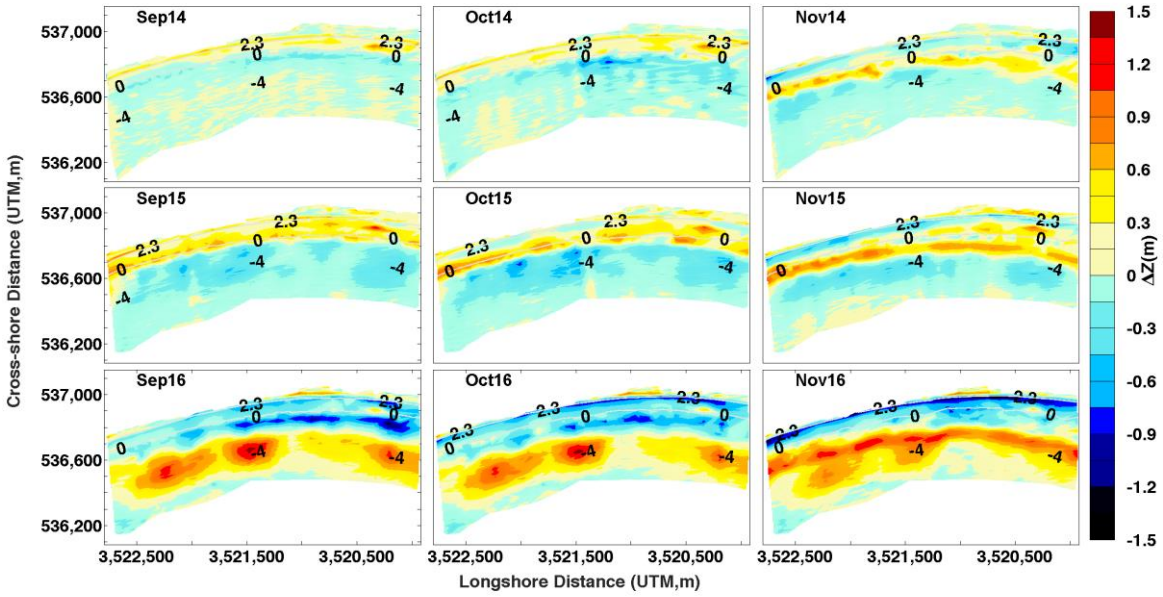

Figure 6. Cumulative morphological differences from August to November 2014 (top panels), 2015 (middle panels) and 2016 (bottom panels) for the subaerial and subtidal beach sections. The intertidal beach is defined between the 0 m and 2.3 m contourlines.

The beach presented very different morphological variability from the winter of 2015 to the 2016. From December 2014 to February 2015 the subaerial beach eroded up to 1 m, and the eroded sediment migrated offshore forming an alongshore sandbar at 2–3 m depth. Between February and March 2015 the sediment

started moving onshore and redistributing along the inner subtidal beach (top panels Figure 5). The cumulative morphological change during the 2015–2016 winter was significantly larger than in 2014–2015 with a vertical morphological change of over ± 1.5 m. From December 2015 to February 2016 the subaerial beach eroded over 1.5 m and the eroded sediment was transported offshore as a form of a nearshore bar located at a depth of 3–4 m. From February to March 2016 the sediment from the sandbar started moving onshore but in contrast to the observed in March 2015, the sediment did not reach the intertidal beach.

The subaerial beach accreted from August to October in 2014 and 2015, and it started eroding between October and November, resulting in the formation of an inner subtidal bar near the shoreline (0 m contourline) (top and middle panels in Figure 6). During the summer in 2016, however, the beach was unable of accreting the subaerial section. From August to October 2016 most of the sediment was located in the subtidal section, subsequently, the subaerial beach was unable of recovering (left and central panels in Figure 6). Between October and November 2016 the subaerial beach eroded up to 1m and the eroded sediment moved offshore accumulating at a depth of 2 to 3 m.

4.3 Volumetric change

Figure 7 presents the cumulative volumetric change from August 2014 to December 2016 along the subtidal and subaerial (intertidal and supratidal) beach sections. These results indicate that the subaerial beach successfully recovered after the 2013–2014 and 2014–2015 winters during the summer months from June to October; the subtidal beach erosion was of similar magnitude to the subaerial accretion. Thus, the subaerial beach recovery is attributed to the cross-shore exchange of sediment from the subtidal beach, associated to the onshore sandbar migration.

After January 2016 the subaerial beach presented severe erosion that lasted till June 2016 and contributed to the significant build up of the subtidal section, mostly along the southern half of the beach. During the summer in 2015 the subtidal beach eroded from June to October, and the eroded sediment contributed to the build up of the subaerial section (Figure 7). During the 2016 summer, however, the subtidal beach did not erode but accreted, and mostly along the southern beach. Between August and October 2016 the subaerial section decreased the volumetric deficit slightly at the same time as the subtidal beach vaguely eroded; indicative of a minor subaerial beach recovery but far from a full recovery (Figure 7).

5. Discussion

The studied 2015–2016 El Niño winter was characterized by the presence of more energetic waves that lasted for a month or two longer than in previous years. This agrees with previous findings along the southern Pacific US coast (Seymour, 1998; Allan and Komar, 2002; Storlazzi and Griggs, 2000) which indicated the presence of unusually energetic waves during the El Niño winters.

Ensenada Beach was unable of fully recovering the subaerial beach volume after the 2015–2016 El Niño winter, and this agrees with previous studies on beaches along the California coast, which indicated that the beaches took a few years to fully recover from extreme subaerial erosion during the energetic 1982–1983 and 1997–1998 El Niño winters (Dingler and Reiss, 2002; Barnard et al., 2011; Doria et al. 2016).

The capability of the beach to fully recover was attributed to the onshore sandbar migration during the summer mild wave conditions. In contrast to studies in multi-barred beaches (Lippmann et al., 1993; Ruessink and Kroon, 1994; Shand et al., 1999; Plant et al., 1999), this single-barred beach presented a very strong seasonal response. The sandbar in Ensenada Beach usually migrates offshore reaching 2–3 m depth from November to February and moves onshore during the post-winter milder waves after February completely welding the beachface by May, and incorporating the eroded sediment back onto the subaerial beach. During the 2015–2016 El Niño winter, however, the sandbar moved further offshore to deeper depths of 3–4 m and the winter waves lasted for a month or two longer (till April 2016). Thus, the beach was unable of transporting the sediment onshore over the shorter summer, and the subaerial beach did not fully recover.

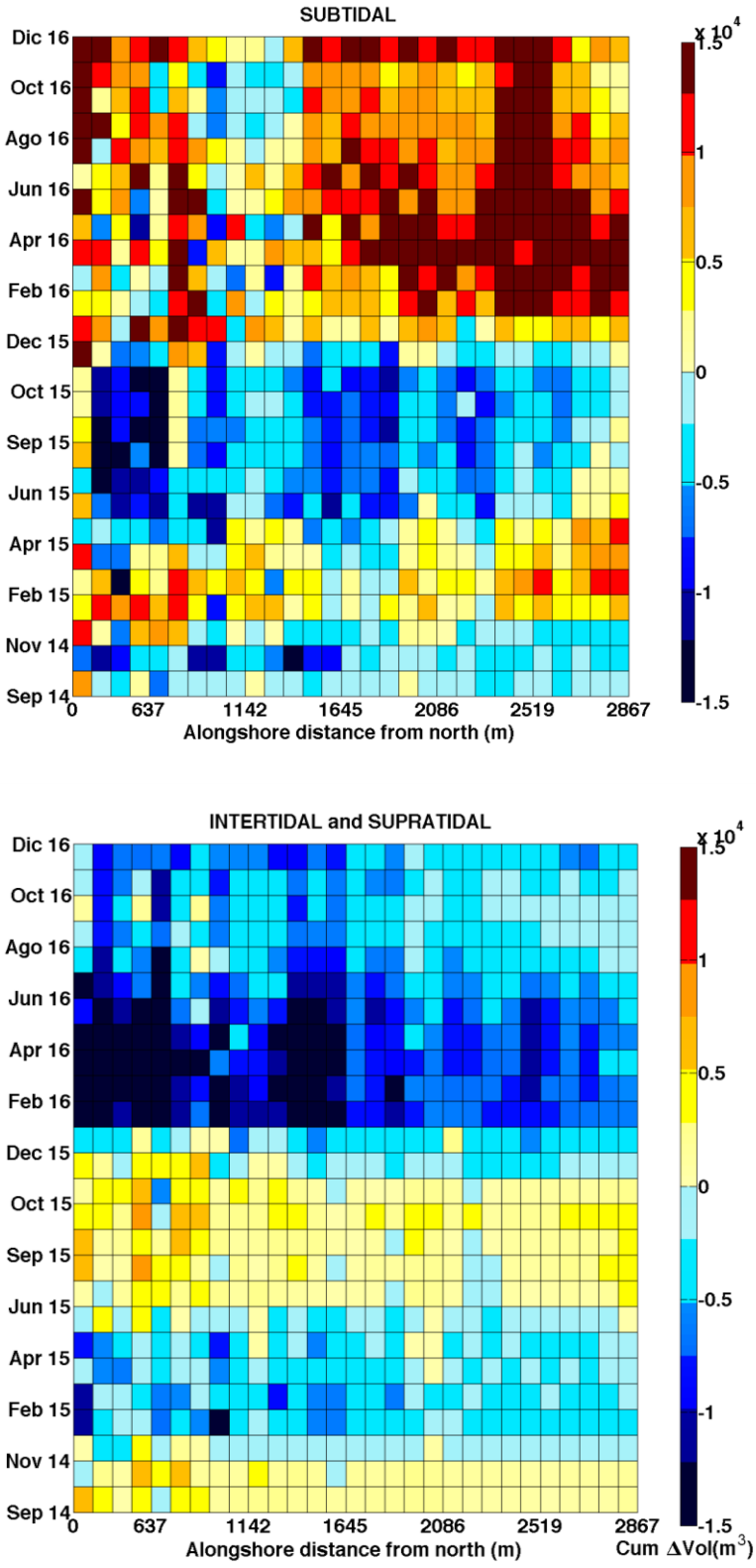

Figure 7. Cumulative volumetric differences for the subtidal beach (top panel) and the intertidal and supratidal or subaerial beach (bottom panel) from August 2014 to December 2016 (bottom to top in the *y* axis).

6. Conclusions

Based on monthly morphological measurements collected over a 2.5 year period, this study investigated the recovery capabilities of a single-barred mesotidal beach located in the Pacific Mexican coast before and after the 2015–2016 El Niño winter. Before the 2015–2016 El Niño winter, the subaerial beach successfully recovered from the erosion during the summer mild wave conditions from June to October that induced onshore sediment transport from the subaerial beach. After the El Niño winter, however, the subaerial beach erosion was much larger, and the eroded sediment moved further offshore to deeper waters of 3–4 m. Consequently, the beach was unable of transporting the full amount of sediment onshore during the 2016 summer, preventing the subaerial beach from fully recovering. It is concluded that the onshore sandbar migration during the summer is critical to ensure a full subaerial beach recovery, since the sediment contained on the sandbar will contribute to the complete build up of the subaerial beach during the accretive phase.

Acknowledgements

The authors are grateful to CONACyT for the funding provided through CB-2014-238765 and INFR-2013-01I005 with the projects 205020 and 205022. Thanks are extended to F-PROMEP-38/Rev-03 SEP-23-005 and UABC for the support with UABC-PTC-418 and 18th project 636 (IMTENS). We are very thankful to all field assistants, especially to Eduardo Gil and Ernesto Carsolio for the technical support provided in the field, and to Angélica Romero for her support on some of the data processing.

References

Allan, J.C., Komar, P.D., 2002. Extreme storms on the Pacific Northwest Coast during the 1997–98 El Niño and 1998–99 La Niña. Journal of Coastal Research 18 (1), 175–193.

Barnard, P.L., Allan, J., Hansen, J.E., Kaminsky, G.M., Ruggiero, P., Doria, A., 2011. The impact of the 2009–10 El Niño Modoki on U.S. West Coast beaches. Geophysical Research Letters 38 (13). http://dx.doi.org/10.1029/2011GL047707.

Coco, G., Senechal, N., Rejas, A., Bryan, K.R., Capo, S., Paristo, J.P., Brown, J.A., MacMahan, J.H.M., 2014. Beach responses to a sequence of extreme storms. Geomorphology 204, 493–501.

Di Leonardo, D. and Ruggiero, P., 2015. Regional scale sandbar variability: Observations from the U.S. Pacific Northwest, *Continental Shelf Research*, 95: 74–88.

Dingler, J.R. and Reiss, R.E., 2002. Changes to Monterey Bay beaches from the end of the 1982-83 El Niño through the 1997-98 El Niño. Marine Geology 181, 249–263.

Doria, A., Guza, R.T., O'Reilly, W.C., Yates, M.L., 2016. Observations and modeling of San Diego beaches during El Niño. Continental Shelf Research 124, 153–164.

Grunnet, N.M., and Hoekstra, P., 2004. Alongshore variability of the multiple barred coast of Terschelling, The Netherlands. *Marine Geology*, 203: 23–41, ISSN 0025-3227.

Blossier, B., Bryan, K.R., Daly, C.J., Winter, C., 2016. Nearshore sandbar rotation at single-barred embayed beaches, *Journal of Geophysical Research*, 121(4), 2286–2313.

Henderson, S.M., Allen, J.S., Newberger, P.A., 2004. Nearshore sandbar migration predicted by an eddy-diffusive boundary layer model, *Journal of Geophysical Research*, 109, C06024.

Hoefel, F., and Elgar, S., 2003. Wave-induced sediment transport and sandbar migration, *Science*, 299: 1885–1887.

Lippmann, T.C., Holman, R.A., Hathaway, K.K., 1993. Episodic, Nonstationary Behavior of a Double Bar System at Duck, North Carolina, U.S.A., 1986-1991, *Journal of Coastal Research* SI 15: 49–75.

Plant, N.C., Holman, R.A., Freilich, M.H., Birkemeier W.A., 1999. A simple model for interannual sandbar behavior, *Journal of Geophysical Research* 104: 15755–15776.

Ruessink, B.G., Kuriyama, Y., Reniers, A.J.H.M., Roelvink, J.A., Walstra, D.J.R., 2007. Modeling cross-shore sandbar behavior on the timescale of weeks. *Journal of Geophysical Research*, 112, F0310.

Ruessink, B.G., Kroon, A., 1994. The behaviour of a multiple bar system in the nearshore zone of Terschelling: 1965–1993. Marine Geology 121, 187–197.

Ruiz de Alegria-Arzaburu, A., García-Nava, H., Gil-Silva, E., Desplán-Salinas, G. 2015. A morphodynamic comparison of walled and non-walled beach sections, Ensenada beach, Mexico. World Scientific. The Proceedings of the Coastal Sediments ISBN:978-981-4355-52-0.Shand et al., 1999

Seymour, R.J., 1998. Effects of El Niños on the West Coast wave climate. Shore Beach 66, 3–6.

Sallenger Jr, A.H., Krabill, W., Brock, J., Swift, R., Manizade, S., Stockdon, H., 2002. Sea-cliff erosion as a function of

beach changes and extreme runup during 1997-1998 El Niño. Marine Geology 187, 279–297.

Storlazzi, C., Griggs, G., 2000. Influence of El Nino-Southern Oscillation (ENSO) events on the evolution of central California's shoreline. Geological Society American Bulletin 111, 236–249.

Van de Lageweg, W.I., Bryan, K.R., Coco, G., Ruessink, B.G., 2013. Observations of shoreline-sandbar coupling on an embayed beach. *Marine Geology*, 344, 101–114.

Wijnberg, K.M., and Terwindt, J.H.J., 1995. Extracting decadal morphological behavior from high-resolution long-term bathymetric surveys along the Holland coast using eigenfunction analysis. Marine Geology 126, 301–330.

Coastal Dynamics 2017
Paper No. 223

AN ANNUAL CYCLE OF SANDBAR MIGRATION ON AN INTERMEDIATE MESOTIDAL BEACH: ENSENADA, MEXICO.

Jesús Adrian Vidal-Ruíz [1], Amaia Ruiz de Alegría-Arzaburu[1]

Abstract

Cross-shore sandbar migration has been studied on a single-barred beach based on monthly measured bathymetric surveys from August 2014 to August 2016. A continuous time-series of nearshore wave measurements allowed the correlation of the onshore and offshore sandbar movement to the incoming wave conditions. The sandbar formed near the shoreline by October 2014, and built up and moved offshore during the 2014–2015 winter from November to February, as a result of the subaerial beach erosion. During that winter the sandbar crest migrated 150–200 m offshore reaching an average depth of 2–2.5 m. The sandbar moved onshore after February 2015, merging the inner intertidal beach by May; from March to April the sandbar and berm coexisted. The beach was unbarred during the 2015 summer waves from June to September, and a berm was built along the upper intertidal beach. The sandbar formed again by October 2015 and migrated 190–250 m offshore during the 2015–2016 El Niño winter, reaching depths of 3–3.5 m. Despite the onshore movement of the sandbar from February to April 2016, it was unable of welding the intertidal beach, thus, the beach was barred from June to August 2016. This study highlights the presence of a strong seasonal sandbar migration cycle in Ensenada Beach, which was interrupted during the 2015–2016 El Niño winter.

Key words: beach, morphodynamics, sediment transport, erosion, accretion, El Niño.

1. Introduction

Sandbars are subaerial features usually located in water depths of less than 10 m, across and just seaward of the surf zone. Sandbars play an important role in the morphodynamics of sandy beaches, since they comprise large amounts of sediment and can dissipate up to 80% of the incident wave energy; consequently acting as a natural defense against shoreline erosion and flooding (Walstra, 2016; Yuhi et al., 2016). These features may have a profound impact on the nearshore hydrodynamics depending on their geometry and cross-shore location (Ruessink and Ranasinghe, 2014; Walstra, 2016). The offshore sandbar migrations are generally associated to strong mean offshore currents (undertow) occurring under breaking large wave conditions, while the onshore movement takes place during weak-to-nonbreaking waves and is primarily related to near-bed wave skewness (e.g. Plant et al., 2001; Ruessink et al., 2007; Cohn et al., 2014), wave asymmetry (Plant et al., 2001; Hoefel and Elgar, 2003) and/or boundary layer streaming and Stokes drift (Henderson et al., 2004; Aagaard et al., 2013). The net onshore sandbar migration results from the gradual sediment transport towards the beachface during calm wave periods, and episodic strong offshore sediment transport during high-energy wave conditions cause the net offshore migration (Ojeda et al., 2011; Sénéchal et al., 2015; Walstra, 2016).

Most of the sandbar studies have been focused on multi-barred beaches, and single-barred beaches have been surprisingly understudied (e.g. van de Lageweg et al., 2013; Blossier et al., 2016). The most comprehensive studies on sandbar dynamics were undertaken over decades along the multi-barred beaches of Duck (USA), Terschelling and the Holland Coast (The Netherlands) and Wanganui (New Zealand) (e.g. Lippmann et al., 1993; Ruessink and Kroon, 1994; Shand et al., 1999; Plant et al., 1999). These beaches however, lacked of seasonal sandbar movements and presented interannual migration cycles of bar generation near the shoreline, offshore migration across the surf zone and final stage of sandbar disappearance at the outer nearshore zone (Ruessink and Kroon, 1994).

[1] Institute of Oceanographic Research, University of Baja California, Km 103 Tijuana-Ensenada Road, 22860, Ensenada, México. avidal@uabc.edu.mx; amaia@uabc.edu.mx

Despite all these studies, the seasonal sandbar migration is still poorly understood given the expense and difficulties of collecting *in-situ* measurements of sandbars (Di Leonardo and Ruggiero, 2015). These studies require long-term bathymetric measurements of high spatio-temporal resolution to be able to accurately determine to sandbar shape and cross-shore position (e.g. Grunnet and Hoekstra, 2004; Di Leonardo and Ruggiero, 2015), and enable the understanding their spatial variability in response to the storm-driven or seasonal wave forcing (Pape et al., 2010).

2. Field site

The study site comprises the northern 3 km of Ensenada beach, located in the northwestern coast of the Baja California peninsula, within Todos Santos Bay (TSB) (Figure 1). The beach is partly protected from the western Pacific swell by Todos Santos Islands (17 km offshore). Ensenada is a single-barred and intermediate beach, made of siliceous medium sand (D_{50} of 0.25 mm) and with an average slope of tan β of 0.025 (Ruiz de Alegria-Arzaburu et al., 2015). The beach is mesotidal, and the tides are semi-diurnal with spring to neap tidal ranges of 2.3 m and 0.5 m (http://oceanografia.cicese.mx/predmar). The bathymetry within TSB is fairly shallow (depths of up to 50 m) but a deep canyon of over 400 m is present between Todos Santos Islands and the Punta Banda headland.

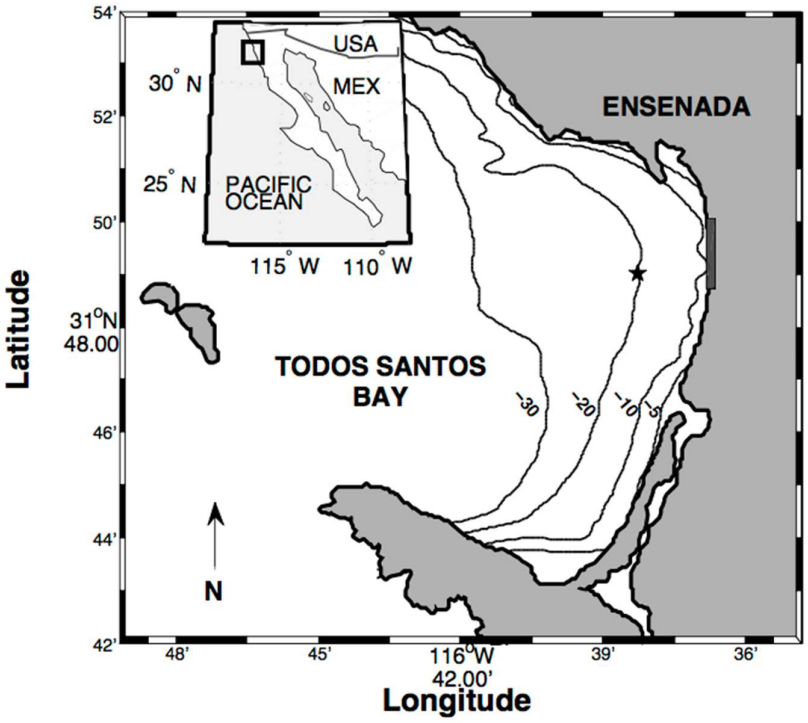

Figure 1. Location of Ensenada Beach (grey longshore rectabnel) within Todos Santos Bay, and the northwestern Baja California peninsula in Mexico. The position of the acoustic Doppler profiler (AWAC) at 20 m depth is indicated with a grey star.

Coastal structures exist along the beach, such as a promenade in the northern section and a seawall and rip-rap in the middle section (Figure 2). The southern beach preserves a natural dune backed by a shallow and intermittently dry freshwater lagoon. The walled subaerial beach is 80–120 m wide, whereas the non-walled section has a subaerial width of 220–240 m (Ruiz de Alegria-Arzaburu et al., 2015). The supratidal beach fronting the promenade is up to 6.5 m above mean low water (MLW) and up to 3.5 m on rip- rap and seawall protected sections, while the dunes have a maximum elevation of 10 m above MLW (Figure 2

Figure 2. View on the study area: (a) beach with a promenade in the northern section, (b) seawall and rip-rap in the middle section, (c) natural dune backed by a freshwater lagoon in the southern section, and (d) southern limit of the study area.

The beach is exposed to the north Pacific and south Pacific swell waves during the winter and summer, respectively. The annual nearshore waves have a mean significant wave height (H_s) of 1 m and an average period of 11 s. The mean winter H_s is 1.5 m (from December to February) with an associated period of 12.5 s. The summer waves (June to August) have an average H_s of 0.7 m with a shorter wave period of 8 s. Significant wave heights above 4 m represent less than 2% of the annual waves and occur mainly during fall and winter seasons.

3. Methods

Morphological measurements were monthly collected over a 2 years period (August 2014 to August 2016) across the subaerial and subtidal sections of nearly 3 km of beach length. The sandbar crest positions were determined and related to the incoming wave forcing.

3.1. Wave measurements

Hourly nearshore wave data were collected from August 2014 to August 2016 with a 1MHz ADCP (Nortek AWAC) located 2.5 km off the beach at a water depth of 20 m (Figure 1). The instrument was installed on the seabed and provided continuous measurements of wave parameters including the significant wave height (H_s), wave peak period (T_p) and wave direction (α). The monthly averaged wave heights were calculated for the years 2014, 2015 and 2016.

3.2. Topographic and bathymetric measurements

The subaerial beach morphology (topography) was measured monthly from August 2014 to December 2016 along a beach section of 2,867 m measuring a total o ~50 m spaced 61 cross-shore profiles during low spring tides. The profiles were measured using a differential GPS (Global Positioning System) with a precision of ± 0.03 m, and a threshold elevation value of 0.05 m was established to discard post-processed erroneous data as established in other research studies (e.g. Coco et al., 2014). All profiles were measured down to the mean low tide level (MLT) at a frequency of 1Hz using a two-wheeled trolley operated by two people on foot. The measurements were referred in Universal Transverse Mercator (Easting and Northing coordinates in meters), and the elevations were referenced to the local MLT (+36.135 m from ellipsoidal heights). The same transect lines were followed at each survey, as these were mapped on the GPS controller.

The subtidal morphology (bathymetry) was monthly measured from August 2014 to December 2016, right after or before the topographic measurements. The bathymetric data were acquired using the Sontek M9 Hydrosurveyor Accoustic Doppler Current Profiler (ADCP) synchronized to the differential GPS and fixed to a small boat or to a jetski. The frequency of 0.5 MHz was used to obtain the bathymetric data with a sound speed corrected depth accuracy of ± 0.02 m. Similar to Wijnberg et al. (1995), an accuracy of ± 0.1 m was estimated when ship-dependent errors were included. In all surveys an overlap with a few topographic lines was obtained, and it was used to verify the adjustment of the submerged elevations to the subaerial. A full survey consisted of 100 m spaced 30 cross-sectional topographic-and-bathymetric profiles (TB), (Figure 3) and comprised depths ranging from 1 to 12 m, beyond the depth of closure (~ 8 m).

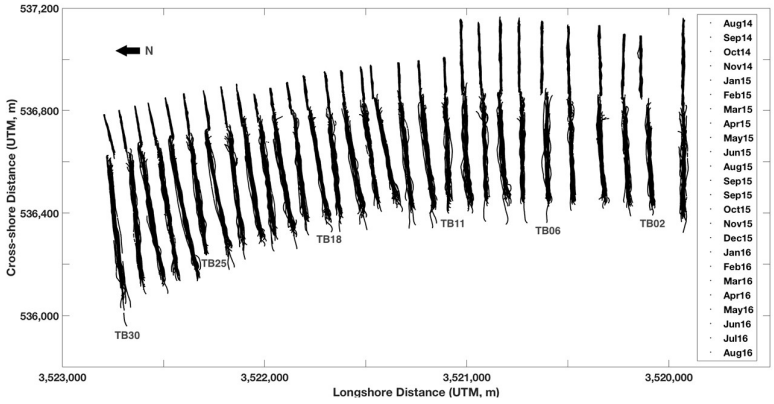

Figure 3. Plan view of the topographic and bathymetric profiles (TB) from August 2014 to August 2016. The cross-shore and longshore distances are in Universal Transverse Mercator (UTM, m).

3.3. Sandbar extraction

The sandbar crest positions were extracted from each of the monthly measured TB profiles. The sandbar crests were defined as the positions of maximum vertical differences relative to the August 2014 unbarred profile (circle in Figure 4). The cross-shore sandbar position was determined as the cross-shore distance between the bar crest and the reference shoreline (x_C - x_S), and the depths were calculated as the vertical differences from the crest to the reference shoreline ($z_C - z_S$).

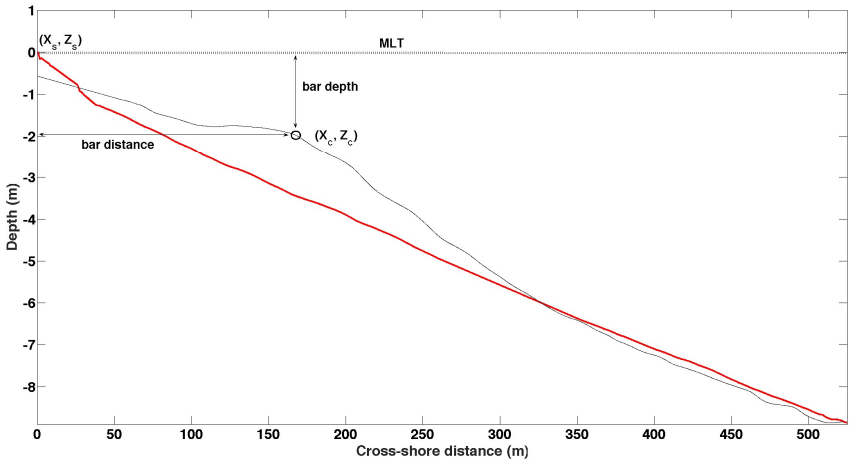

Figure 4. Sandbar crest location (black circle, x_C, z_C) for a typical profile (black profile) relative to the August 2014 unbarred profile (red profile) (modified from Di Leonardo and Ruggiero, 2015). The profile elevations are referred to the mean low tide level (MLT).

4. Results

4.1. Wave conditions

Significant seasonal and interannual differences were encountered in the wave conditions between the years 2014, 2015 and 2016 (Figure 5). The waves were significantly more energetic during the 2015–2016 winter than during the previous winters in 2014 and 2015. The average H_s exceeded 1.5 m from December 2015 to March 2016 and the waves were of longer period (sometimes over 20 s) during some of the energetic events than in the previous winters.

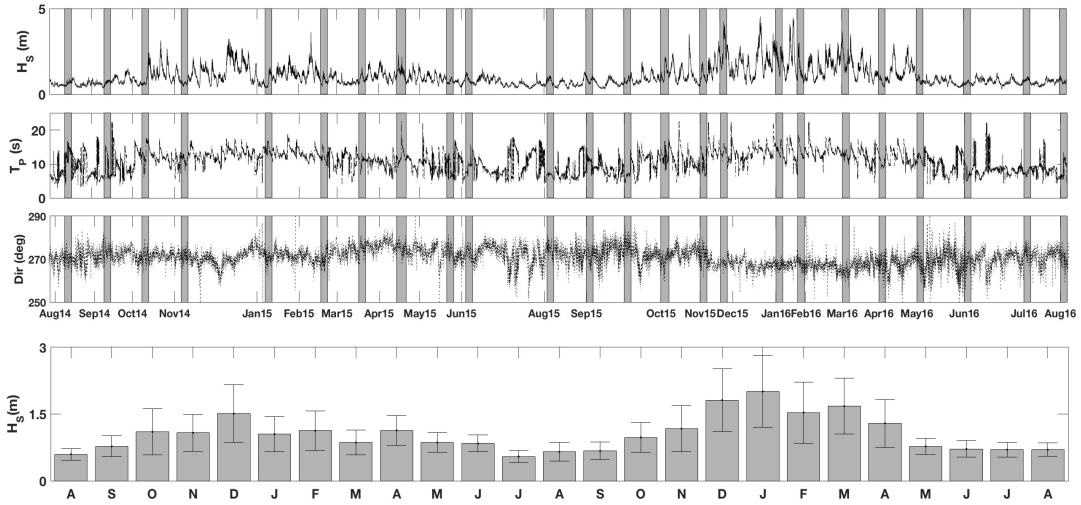

Figure 5. Time series of significant wave height (H_s), peak period (T_p), wave direction (Dir) (top three panels) and monthly averaged H_s from August 2014 to August 2016 and their standard deviations (bottom panel). The vertical gray bars indicate the times when the morphological measurements (topography and bathymetry) were undertaken.

4.2. Beach profile evolution

The topographic-and-bathymetric profile (TB) evolution was studied over a two-year period from August 2014 to August 2016 (Figures 6, 7 and 8) and related to the incident wave conditions. TB 02, 18 and 30 were selected as being the most representative for the southern, middle and northern beach sections. The summer profiles represented by August show an unbarred profile and subaerial beach recovery in 2014 and 2015 with the presence of a berm. In August 2016, however, the subaerial beach does not show a full recovery, and a sandbar is observed at 2.5 m depth, mostly at the southern and middle beach sections (red and cyan profiles in Figures 6, 7 and 8).

In November the beach presents an inner sandbar in co-existence with a berm. The sandbar is located further offshore in the southern and middle beach section (1 to 2 m depth) than in the northern beach end (0.2 m depth), (black profiles in Figures 6, 7 and 8). The sandbar is fully developed and located further offshore by February (blue profiles in Figures 6, 7 and 8) and associated to subaerial beach erosion. The sandbar moved to deeper water in the southern and middle beach sections (3 and 2 m, respectively; Figures 6 and 7) than in the northern section (1.5–2 m, Figure 8), and mostly by February 2016, after El Niño winter.

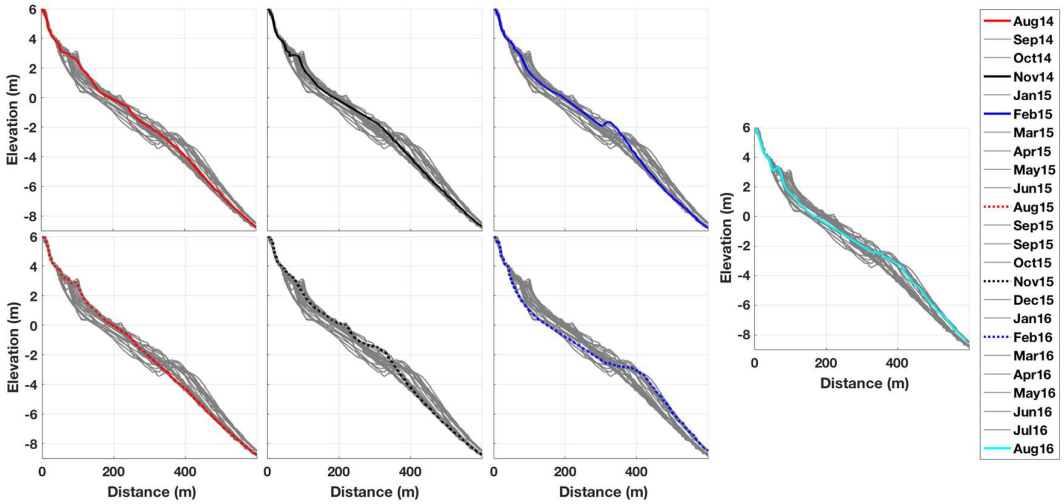

Figure 6. Temporal evolution of TB02 (southern beach) from August 2014 to August 2016 (gray profiles). The August, November and February profiles are highlighted in red, black and blue, respectively. The August 2016 profile is highlighted in cyan.

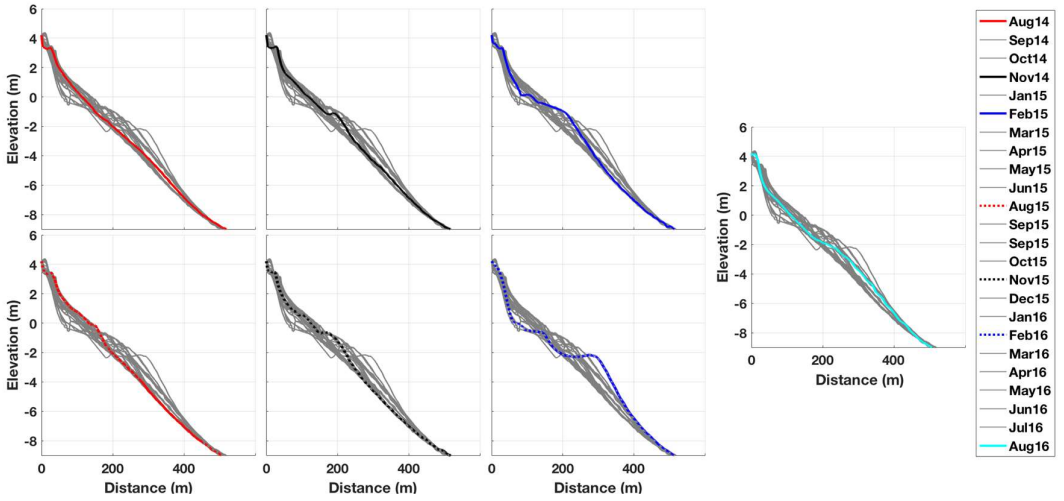

Figure 7. Temporal evolution of TB18 (middle beach) from August 2014 to August 2016 (gray profiles). The August, November and February profiles are highlighted in red, black and blue, respectively. The August 2016 profile is highlighted in cyan.

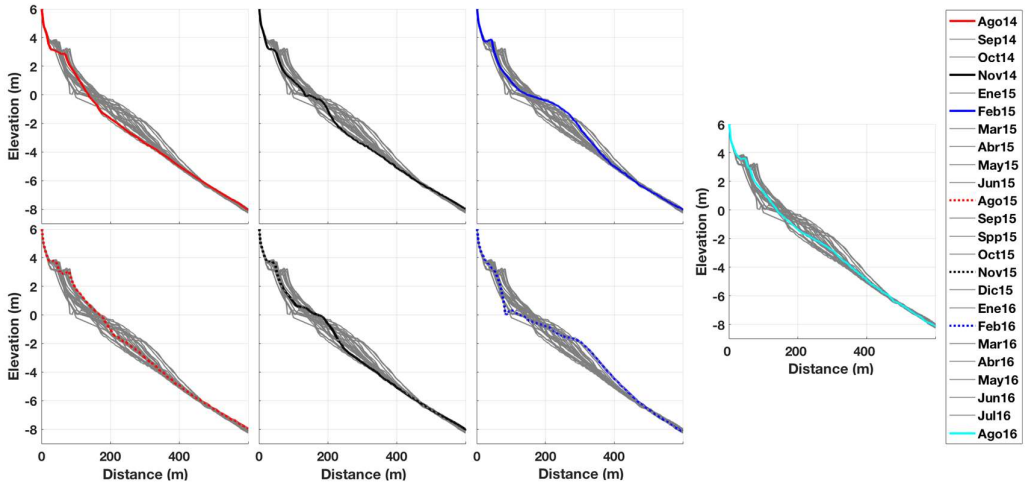

Figure 8. Temporal evolution of TB30 (northern beach) from August 2014 to August 2016 (gray profiles). The August, November and February profiles are highlighted in red, black and blue, respectively. The August 2016 profile is highlighted in cyan.

4.3. Sandbar migration

The sandbar crest positions were obtained for the 02, 06, 11, 18, 25 and 30 TB profiles in order to determine the cross-shore sandbar migration in relation to the different wave conditions (Figures 9, 10 and 11). In 2014 and 2015, the sandbar was formed near the shoreline in September and reached 0.5 to 1 m depth at a distance of 50 to 100 m from the shore by October. Then it migrated 140–190 m offshore between October and February reaching a depth of 2 m, and back onshore between February and April, and being the profile unbarred between May and September (Figures 9, 10 and 11).

The largest offshore migration occurred during 2015–2016 El Niño winter, reaching displacements of 190–200 m from the reference shoreline and maximum depths of 3–3.5 m, mostly in the southern half of the beach (Figures 9, 10 and 11). After the winter, from February to May, the sandbar moved 50–60 m onshore in the southern end (Figure 9) and 80–120 m onshore in the middle and northern ends (Figures 10 and 11). The sandbar maintained in the same cross-shore position between April and July 2016 in the southern end profiles (TB02 and TB06, Figure 9) while the sandbar in the northern end moved further offshore between May and August 2016. The beach maintained barred during the summer period from June to August 2016.

5. Discussion

In accordance with previous findings along the southern Pacific US coast indicating the presence of unusually energetic waves related to the El Niño climatic anomaly (Allan and Komar, 2002; Storlazzi and Griggs, 2000; Adams et al., 2008), in Todos Santos Bay the 2015–2016 El Niño winter was characterized by the presence of more energetic waves that lasted for a month or two longer than in previous years. The average significant wave height exceeded 1.5 m from December 2015 to March 2016 and the waves were of longer period (sometimes over 20 s) during some of the energetic events than in the previous winters in 2014 and 2015.

After the energetic 2015–2016 El Niño winter, the sandbar migrated further offshore (190–250 m) than in the previous winters (150–200 m), and reached a depth of 3–3.5 m compared to 2–2.5 m. These findings agree with Ruggiero et al., (2009) in that energetic incident waves generate strong offshore-directed cross-shore mean flows that induce sandbars to migrate further offshore. Moreover, the sandbars did not weld the shore during the 2016 summer, possibly as a consequence of longer energetic winter (till April) that impeded onshore migration due to the lack of long enough fair weather conditions (Ruggiero et al., 2016).

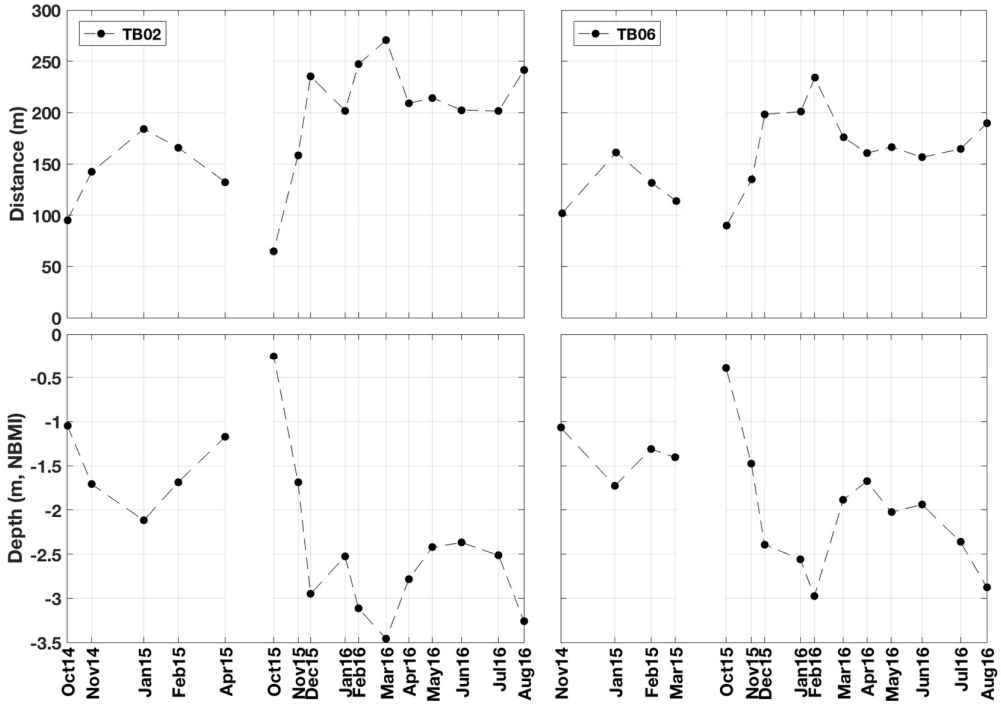

Figure 9. Cross-shore sandbar crest migrations (top panels) at TB02 and TB06 (southern beach) and their associated depths (bottom panels) from October 2014 to August 2016.

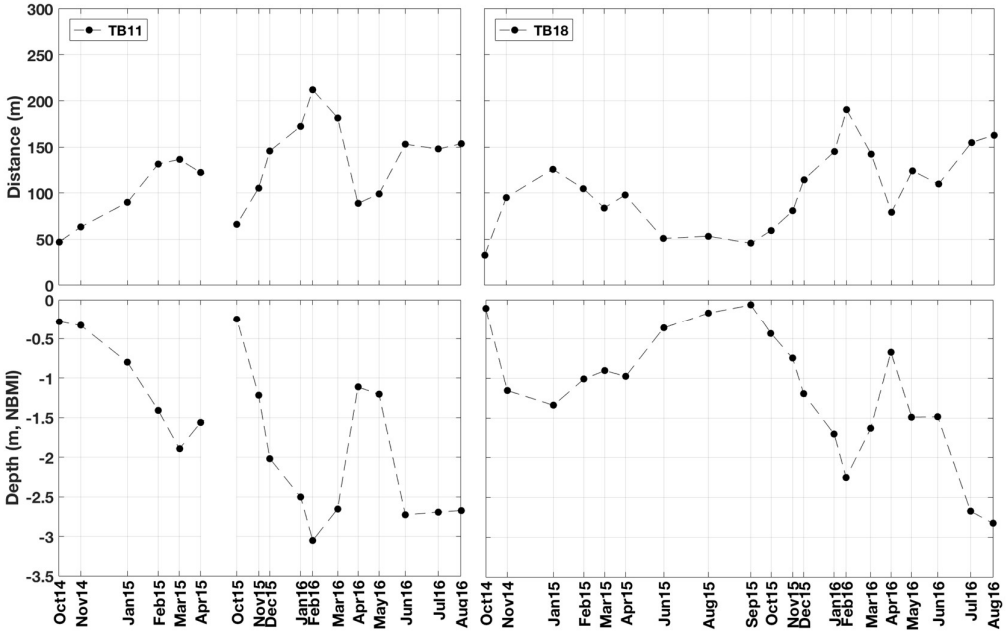

Figure 10. Cross-shore sandbar crest migrations (top panels) at TB11 and TB18 (middle beach) and their associated depths (bottom panels) from October 2014 to August 2016.

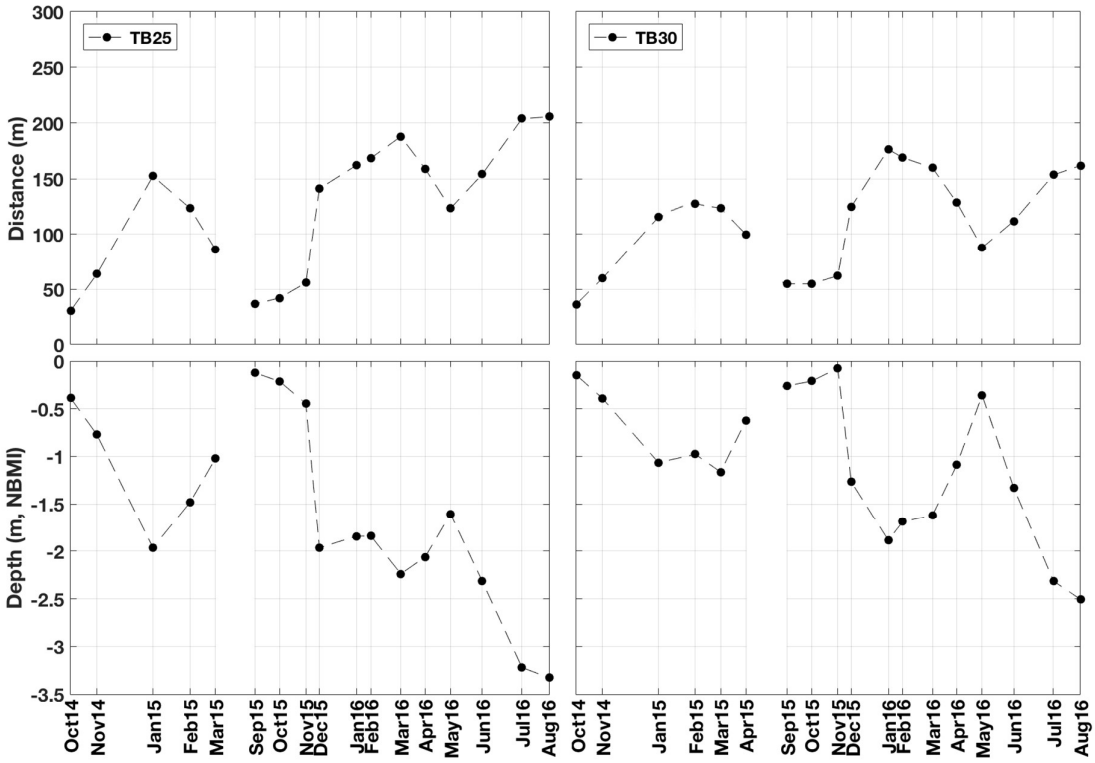

Figure 11. Cross-shore sandbar crest migrations (top panels) at TB25 and TB30 (northern beach) and their associated depths (bottom panels) from October 2014 to August 2016.

Periods of accretion and erosion are generally associated to low and high-energy wave conditions but they also exhibit strong site-specific variations (Sénéchal et al., 2015). In Ensenada beach the sandbars followed a cyclic morphological behavior, associated to periods of high and low wave energy (Ojeda et al., 2011; Ruessink et al., 2003). In contrast to studies in multi-barred beaches (Lippmann et al., 1993; Ruessink and Kroon, 1994; Shand et al., 1999; Plant et al., 1999), this single-barred beach presented a very strong seasonal response. The seasonal morphological variability and sandbar migration cycle of Ensenada beach for 2014 and 2015 coincides with the model proposed by Shepard (1950). In addition, the seasonal morphological changes agree with the suggested by Aagaard et al., (2013) and Sénéchal et al., (2015) for intermediate beaches.

The capability of the subaerial beach to fully recover from the winter erosion was attributed to the onshore sandbar migration during the summer mild wave conditions, which did not occur during the energetic 2015–2016 El Niño winter. In the winters before El Niño, the sandbar migrated offshore reaching 2 m depth from October to February. After February, it moved onshore during the post-winter milder waves welding the beachface by June, and incorporating the eroded sediment back onto the subaerial beach. During the 2015–2016 winter, however, the sandbar moved further offshore to deeper waters and the winter waves lasted for a month or two longer (till April 2016). The lack of long enough fair wave conditions from March to May is considered to be the cause of the inability of the sandbar to migrate onshore and weld the shoreline by June 2016.

6. Conclusions

Based on monthly measured bathymetric surveys from August 2014 to August 2016, this study investigated the cross-shore sandbar migration on the single-barred beach of Ensenada, Baja California. The sandbar for med near the shoreline by October 2014, and built up and moved offshore during the 2014–2015 winter fro m November to February, as a result of the subaerial beach erosion. During that winter the sandbar crest mi grated 150–200 m offshore reaching an average depth of 2–2.5 m. The sandbar moved onshore after Februa ry 2015, merging the inner intertidal beach by May, and the sandbar and berm coexisted from March to Apr il. The beach was unbarred during the 2015 summer waves from June to September, and a berm was built a long the upper intertidal beach. The sandbar formed again by October 2015 and migrated 190–250 m offsh ore during the 2015–2016 El Niño winter, reaching depths of 3–3.5 m. Despite the onshore movement of th e sandbar from February to April 2016, it was unable of welding the intertidal beach, thus, the beach was b arred from June to August 2016. This study highlights the presence of a strong seasonal sandbar migration cycle in Ensenada Beach, which was interrupted during the 2015–2016 El Niño winter. The lack of long enough fair wave conditions in April and May 2016 is considered to be the cause of the inability of the sandbar to migrate onshore and weld the shoreline by June as it happened in 2014 and 2015.

Acknowledgements

The authors are grateful to CONACyT for the funding provided through CB-2014-238765 and INFR-2013-01I005 with the projects 205020 and 205022. Thanks are extended to F-PROMEP-38/Rev-03 SEP-23-005 and UABC for the support with UABC-PTC-418 and 18th project 636 (IMTENS). We are very thankful to all field assistants, especially to Eduardo Gil, Julio Lopez and Ernesto Carsolio for the technical support provided in the field, and to Angélica Romero for her support on some of the data processing.

References

Aagaard, T., Greenwood, B. and Hughes, M.G., 2013. Sediment transport on dissipative, inter- mediate and reflective beaches. *Earth-Science Reviews*, 124: 32–50.

Adams, P.N., Inman, D.L. and Graham, N.E., 2008. Soutern California deep-water wave climate: characterization and a pplication to coastal processes. *Journal of Coastal Research*, 24:1022–1035.

Allan, J.C., Komar, P.D., 2002. Extreme storms on the Pacific Northwest Coast during the 1997–98 El Niño and 1998–99 La Niña. *Journal of Coastal Research* 18 (1): 175–193.

Coco, G., Sénéchal, N., Rejas, A., Bryan, K.R., Capo, S., Paristo, J.P., Brown, J.A., MacMahan, J.H.M., 2014. Beach responses to a sequence of extreme storms. *Geomorphology* 204:493–501.

Di Leonardo, D. and Ruggiero, P., 2015. Regional scale sandbar variability: Observations from the U.S. Pacific Northwest, *Continental Shelf Research*, 95: 74–88.

Grunnet, N.M. and Hoekstra, P., 2004. Alongshore variability of the multiple barred coast of Terschelling, The Netherlands. *Marine Geology*, 203: 23–41, ISSN 0025-3227.

Blossier, B., Bryan, K.R., Daly, C.J., Winter, C., 2016. Nearshore sandbar rotation at single-barred embayed beaches, *Journal of Geophysical Research*, 121(4), 2286–2313.

Henderson, S.M., Allen, J.S., Newberger, P.A., 2004. Nearshore sandbar migration predicted by an eddy-diffusive boundary layer model, *Journal of Geophysical Research*, 109, C06024.

Hoefel, F. and Elgar, S., 2003. Wave-induced sediment transport and sandbar migration, *Science*, 299: 1885–1887.

Lippmann, T.C., Holman, R.A., Hathaway, K.K., 1993. Episodic, Nonstationary Behavior of a Double Bar System at Duck, North Carolina, U.S.A., 1986-1991, *Journal of Coastal Research* SI 15: 49–75.

Ojeda, E., Guillén, J., Ribas, F., 2011. Dynamics of single-barred embayed beaches. *Marine Geolgy*, 280: 76–90.

Pape, L., Y. Kuriyama, y B.G. Ruessink, 2010. Models and scales for cross-shore sandbar migration, *Journal of Geoph yical Research*, 115.

Plant, N.G., Freilich, M.H., Holman, R.A., 2001. Role of morphologic feedback in surf zone sandbar response. *Journal of Geophyical Research,* 106: 973–989.

Plant, N.C., Holman, R.A., Freilich, M.H., Birkemeier W.A., 1999. A simple model for interannual sandbar behavior, *Journal of Geophysical Research* 104: 15755–15776.

Ruessink, B.G. and Ranasinghe R., 2014. *Beaches*. In: Masselink, G., and Gehrels R. (ed.), *Coastal Environments & Global Change*. American Geophysical Union: Wiley. Hardcover, 7: 149–176.

Ruessink, B.G., Kuriyama, Y., Reniers, A.J.H.M., Roelvink, J.A., Walstra, D.J.R., 2007. Modeling cross-shore sandbar behavior on the timescale of weeks. *Journal of Geophysical Research*, 112, F0310.

Ruessink, B.G., Wijnberg, K.M., Holman, R.A., Kuriyama, Y. and van Enckevort, I. M. J., 2003. Intersite comparison of interannual nearshore bar behavior. *Journal of Geophysical Research*, 108: C8 3249.

Ruessink, B.G., Kroon, A., 1994. The behaviour of a multiple bar system in the nearshore zone of Terschelling: 1965–1 993. *Marine Geology* 121, 187–197.

Ruggiero P., Kaminsky G.M., Gelfenbaum G. and Cohn N., 2016. Morphodynamics of prograding beaches: A synthesis of seasonal- to century-scale observations of the Columbia River littoral cell. *Marine Geology,* 376: 51–68.

Ruggiero P., Walstra D.J.R., Gelfenbaum G., 2009. Seasonal-scale nearshore morphological evolution: field observations and numerical modeling. Coast Eng., 56: 1153–1172.

Ruiz de Alegria-Arzaburu, A., García-Nava, H., Gil-Silva, E., Desplán-Salinas, G., 2015. A morphodynamic comparison of walled and non-walled beach sections, Ensenada beach, Mexico. World Scientific. *The Proceedings of the Coastal Sediments* ISBN: 978-981-4355-52-0.Shand et al., 1999

Sénéchal, N., Coco G., Castelle B. and Marieu V., 2015. Storm impact on the seasonal shoreline dynamics of a meso- to macrotidal open sandy beach (Biscarrosse, France), *Geomorphology,* 228: 448–461.

Storlazzi, C., Griggs, G., 2000. Influence of El Nino-Southern Oscillation (ENSO) events on the evolution of central California's shoreline. *Geological Society American Bulletin* 111, 236–249.

Van de Lageweg, W.I., Bryan, K.R., Coco, G., Ruessink, B.G., 2013. Observations of shoreline-sandbar coupling on an embayed beach. *Marine Geology*, 344, 101–114.

Walstra, D.J.R., 2016. On the anatomy of nearshore sandbars: A systematic exposition of inter-annual sandbar dynamics (*Doctoral thesis*, Delft University of Technology).

Wijnberg, K.M., and Terwindt, J.H.J., 1995. Extracting decadal morphological behavior from high-resolution long-term bathymetric surveys along the Holland coast using eigenfunction analysis. Marine Geology 126, 301–330.

Yuhi, M., Matsuyama, M., Hayakawa, K., 2016. Sandbar Migration and Shoreline Change on the Chirihama Coast, Japan. *Journal of Marine Science and Engineering,* 4:40.

Ocean Dynamics
https://doi.org/10.1007/s10236-018-1164-6

Beach recovery capabilities after El Niño 2015–2016 at Ensenada Beach, Northern Baja California

Amaia Ruiz de Alegría-Arzaburu[1] · Jesús Adrián Vidal-Ruiz[1]

Received: 13 October 2017 / Accepted: 8 May 2018

Abstract
This study investigates the recovery capabilities of a single-barred beach in the Pacific Mexican coast before and after the 2015–2016 El Niño winter. Concurrent hydrodynamic and morphological data collected over a 3-year period (August 2014–2017) were analysed to determine the subaerial-subtidal volumetric exchange and cross-shore subtidal sandbar migrations, in relation to the incident wave forcing. The beach presented a seasonal seaward and landward sandbar migration cycle. The sandbar migrated offshore during the energetic waves between November and February, and onshore during the milder wave period in spring, until welding to the subaerial beach around May. The transfer of sediment towards the subaerial section continued over the summer, reaching a complete recovery by September/October. Prior to El Niño, the subaerial beach successfully recovered by the end of summer 2015 through the landward sandbar migration process. The 2015–2016 energetic winter waves caused a subaerial volume loss of ~ 140 m^3 m^{-1} (from October 2015 to March 2016), more than twice the amount eroded in the other winters, and the sandbar moved further offshore and to deeper depths (3–4 m) than the winter before. In addition, the energetic 2015–2016 winter waves lasted for 2 months longer than in other years, making the 2016 spring shorter. Consequently, during the onshore migration, the sandbar was unable of reaching shallow depths, and a large portion of sand remained in the subtidal beach. The subaerial beach recovered 60 and 65% of the loss in the 2016 and 2017 summers, respectively. It is concluded that the landward migration process of the sandbar during the spring is critical to ensure a full subaerial beach recovery over the mild wave period in summer. The recovery capabilities of the subaerial beach will depend on the cross-shore distance and depth where the sandbar is located, and on the duration of mild wave conditions required for the sandbar to migrate onshore.

Keywords Subtidal sandbars · Cross-shore migration · Subaerial beach · Subtidal beach · Sediment transport · Climate change

1 Introduction

Recent studies report an increasing frequency of extreme El Niño events associated to greenhouse warming, which causes a faster increase in sea surface temperature (SST) over the eastern equatorial Pacific than in the adjacent ocean waters (Cai et al. 2014). The El Niño-Southern Oscillation (ENSO) originates in the tropical Indo-Pacific as a result from the ocean-atmosphere interactions. Depending on the location of the SST anomaly, the El Niño phase of ENSO can be located in the eastern Pacific or in the central equatorial Pacific, resulting in Classic El Niño or El Niño Modoki events, respectively (Ashok et al. 2007). During major El Niño climatic conditions, the track of winter extratropical storms over the Pacific Northwest shifts further to the south than usual, and uncommonly energetic waves occur along the southern part of the Pacific US coast (Seymour 1998; Storlazzi and Griggs 2000; Allan and Komar 2002; Barnard et al. 2015). In addition, the incoming waves shift to a more southerly angle relative to the shore, causing reversals on the longshore sediment transport patterns and unusual erosion along the littoral cells (Sallenger et al. 2002).

Extreme ENSOs are the dominant interannual climate variability across the Pacific Ocean. During the warm phase of El Niño, significant subaerial beach erosion was detected along the eastern Pacific coast (Ludka et al. 2016; Barnard et al. 2017), while these events allowed the gradual recovery of

This article is part of the Topical Collection on *the 8th International conference on Coastal Dynamics, Helsingør, Denmark, 12–16 June 2017*

Responsible Editor: Troels Aagaard

✉ Amaia Ruiz de Alegría-Arzaburu
amaia@uabc.edu.mx

[1] Instituto de Investigaciones Oceanológicas, Universidad Autónoma de Baja California, km 103 Carretera Tijuana-Ensenada, 22860 Ensenada, Mexico

Published online: 16 May 2018

beaches along the western Pacific (Barnard et al. 2015). The morphological alterations caused by the El Niño events along the eastern Pacific coast are substantially different from event to event; consequently, the recovery capabilities vary considerably. A full beach recovery was documented by 1985 along the California coast after the 1982–1983 event (Dingler and Reiss 2002). During the 1997–1998 El Niño winter, significant subaerial beach and sea-cliff erosion occurred on the Oregon (Revell et al. 2002), southern California (Sallenger et al. 2002) and northern Baja California (Lizarraga-Arciniega et al. 2003) beaches, and the subaerial recovery in California took place over several years (Doria et al. 2016). Significant coastal erosion occurred along the California coast during the 2009–2010 El Niño Modoki, and the persistence of energetic waves during the spring and summer limited the beaches from recovering in 2010 (Barnard et al. 2011). A recent study by Barnard et al. (2017) indicates that the El Niño 2015–2016 was one of the most powerful events in the past 145 years and that beaches eroded beyond historical records.

Sandbars contain large amounts of sediment that move cross-shore and alongshore, thus, quantifying their migration rates and directions is essential to determine the capabilities of the subaerial beach for post-winter recovery. Offshore sandbar migrations are generally associated to strong mean offshore currents (undertow) occurring under breaking large wave conditions, while onshore movements take place during weak-to-nonbreaking waves and are primarily related to near-bed wave skewness (e.g. Ruessink et al. 2007), wave asymmetry (Hoefel and Elgar 2003) and/or boundary layer streaming and Stokes drift (Henderson et al. 2004). Thus, understanding the periods and durations of onshore sandbar migrations is critical from a beach recovery perspective.

Many studies on multi-barred beaches reported subtidal sandbar formations at the shoreline and net offshore migrations over the years until their disappearance on the outer shoreface (e.g. Lippmann et al. 1993; Ruessink and Kroon 1994; Shand et al. 1999; Plant et al. 1999; Aleman et al. 2017). In contrast, continuous landward migrations have been described in other gently sloping multi-barred beaches on yearly scales (e.g. Aagaard et al. 2004; Anthony et al. 2006). In particular, a sandbar migration study over three decades demonstrated its generation at the outer shoreface, and disappearance through subaerial beach welding during high-energy conditions over an average 8-year period (Aagaard et al. 2004). While some studies on multi-barred beaches reported landward migration and welding of the innermost subtidal sandbar during a storm (Houser and Barrett 2010), others demonstrated onshore migrations during calm wave conditions (Cohn et al. 2017), exhibiting a similar behaviour to intertidal bar systems (Masselink et al. 2006). The physical processes associated to seasonal cross-shore sandbar migrations and subaerial beach welding are still poorly understood, and this is essential to determine the recovery capabilities of beaches.

Long-term bathymetric and hydrodynamic measurements of high spatio-temporal resolution are required to be able to accurately determine subtidal sandbar shapes and positions (e.g. Grunnet and Hoekstra 2004; Di Leonardo and Ruggiero 2015), and to improve the present understanding of the sediment transport processes during their cross-shore migrations. This study investigates the contribution of onshore sandbar migration and subaerial welding on the recovery capabilities of a single-barred beach before and after the 2015–2016 El Niño winter in NW Baja California.

2 Study site

Ensenada Beach is located within Todos Santos Bay (TSB), in the northwestern coast of the Baja California peninsula in Mexico (Fig. 1). The beach is made of siliceous medium sand (D_{50} of 0.25 mm), is single-barred and is low sloping (tanβ of 0.025). The length of the beach is of ~ 3 km, and is part of a 14-km sandy stretch of coast interrupted by the mouth of the Punta Banda Estuary. TSB presents a deep canyon of over 400 m between Todos Santos Islands and the Punta Banda headland, but overall, is fairly shallow with depths of up to 50 m (Fig. 1). The southern half of the beach preserves natural dunes backed by a shallow and intermittently dry freshwater lagoon while the northern half presents a promenade and the remains of coastal structures (seawall and rip-rap) (Ruiz de Alegria-Arzaburu et al. 2015).

The beach is located in a mesotidal regime, and the tides are semi-diurnal with spring and neap tidal ranges of 2.3 and 0.5 m (http://predmar.cicese.mx/). The offshore waves are typically swell of bimodal direction. In winter, northwesterly waves originated in the north Pacific extratropical zone are common, while south-westerly waves generated in the south Pacific extratropical region are frequent in summer. The wave incidence is shore-normal on the beach due to wave refraction, and the mean annual nearshore waves are characterised by 1 m of significant wave height, 1.5 m of maximum significant wave height and 11-s peak wave period (Ruiz de Alegria-Arzaburu et al. 2015).

The beach presents a clear seasonal morphological variability with volumetric changes of ± 70 m^3 m^{-1} cross-shore and ±35 m^3 m^{-1} longshore, and with the maximum and minimum subaerial volumes occurring by September–October and January–February, respectively. The largest subaerial volumetric variations of the past 5 years were over 100 m^3 m^{-1} and occurred during the beginning of the 2015–2016 El Niño winter (Ruiz de Alegria-Arzaburu et al. 2015). Motivated by this previous finding, this study will analyse into detail the recovery capabilities of the beach after the energetic 2015–

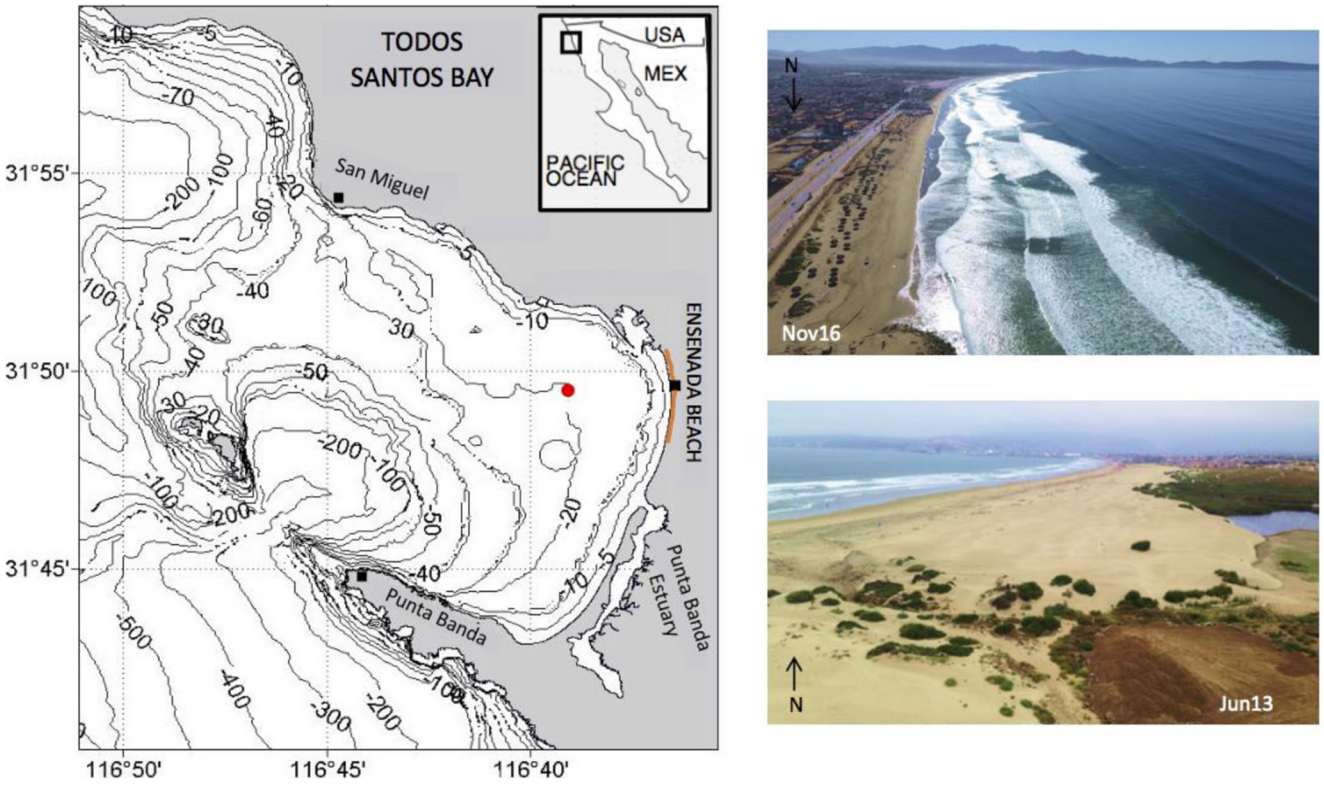

Fig. 1 Location of Ensenada Beach (orange line) within Todos Santos Bay, in the NW Mexican Pacific coast. The red dot shows the location of the acoustic Doppler current profiler (ADCP) in 20-m water depth. Aerial views from the northern and southern beach ends are presented in the top and bottom photos, respectively

2016 El Niño event, specifically examining the volumetric variations associated to cross-shore sandbar migrations.

3 Methodology

Morphological measurements were collected monthly over a 3-year period across the subaerial and subtidal sections of nearly 3 km of beach length (Fig. 1). Beach volumes and digital elevation models were calculated from the measured topographic-bathymetric profiles in order to quantify the morphological beach change, and this was related to the incoming wave forcing. The methods presented in this section are detailed in Ruiz de Alegria-Arzaburu et al. (2017).

3.1 Nearshore wave measurements

Wave measurements were collected hourly from August 2014 to August 2017 with a 1-MHz acoustic Doppler current profiler (ADCP; AWAC type) located 2.5 km offshore of the study site at a water depth of 20 m (Fig. 1). The instrument was installed on the seabed and provided measurements of wave parameters including the significant wave height (H_s), wave peak period (T_p) and wave direction (α). In order to characterise the wave energy variability over the measurement period, averaged wave heights and standard deviations were calculated for each month. In addition, joint probability density functions (PDF) between H_s and T_p were calculated for the low (May to October) and high wave energy (November to April) periods in 2015, 2016 and 2017.

3.2 Topographic and bathymetric measurements

Morphologic measurements were collected monthly from August 2014 to August 2017, and comprised a total of 36 surveys. A full topographic and bathymetric survey consisted of 100-m spaced 30 cross-sectional profiles (TB), covering ~ 3000 m of beach length from the upper subaerial beach down to a depth of 12 m, beyond the depth of closure (Ruiz de Alegria-Arzaburu et al. 2017). The spatial coordinates were referred in Universal Transverse Mercator (Easting and Northing in metres), and the elevations were referenced to the local mean low tide level (MLT; + 36.135 m from ellipsoidal heights).

A real-time kinematic global positioning system (RTK GPS) was used to measure topographic profiles with vertical accuracies of a few centimetres. A threshold elevation value of 0.05 m was established to discard erroneous data during the data post-processing. All profiles were measured on foot at a frequency of 1 Hz using a two-wheeled trolley operated by two people performing the survey down to MLT. The subtidal morphology was measured using a waverunner equipped with

the Sontek Hydrosurveyor ADCP and synchronised to the RTK GPS. The frequency of 0.5 MHz was used to measure the relative depth. The bathymetric measurements were not always able of reaching MLT due to limitations on data acquisition across the surf zone, thus, linear interpolation was applied. The mean cross-shore distance subjected to interpolation was of 50 m, corresponding to depths between 0 and 1 m.

3.3 Volumes and digital elevation models

The measured TB profiles were interpolated onto a 0.2-m cross-shore grid. The areas represented by each TB were obtained integrating the interpolated profile upwards from the elevations of 0 to 5.5 m (subaerial, IS), − 9 to 0 m (subtidal, SUB) and − 9 to 5.5 m (total, TOT). Beach volumes were obtained multiplying the calculated areas by the alongshore lengths represented by each profile. The beach volume variability (loss or gain) was determined by subtracting the mean value over the 3-year period (36 surveys) to each calculated volume (per profile) in time, which resulted in de-meaned (Dem) IS, SUB and TOT volumes. The volumetric evolution of the beach was obtained adding up the volumetric differences per beach profile in time, which resulted in cumulative volumetric changes (Cum ΔV). A total volumetric error of 2% was estimated assuming a hypothetical vertical error of 0.1 m across all TB profiles along the studied beach section (Ruiz de Alegria-Arzaburu et al. 2017).

Digital elevation models (DEMs) were obtained per survey period interpolating the measured TB profiles onto a 0.2 m (cross-shore) by 10 m (longshore) grid. The three-dimensional morphological evolution of the beach was obtained calculating cumulative differences of the DEMs from August 2014 to August 2017 and from − 9 to 5.5 m of elevation. The DEM evolution was determined for the fall/winter (November to February), spring (March to May) and summer (June to September/October) periods. The sandbar positions were identified from the individual TB profiles following the method proposed by Ruessink and Kroon (1994), and these positions were plotted on the DEMs.

4 Results

4.1 Nearshore wave conditions

The time series of wave conditions shows a very clear seasonal variability, but significant interannual differences are encountered between 2014, 2015, 2016 and 2017 (Fig. 2). The waves were significantly more energetic during the 2015–2016 winter and the energetic events ($H_s > 2$ m) lasted longer (until April rather than February) than in the other winters in 2014–15 and 2016–17 (top panel in Fig. 2). The average H_s exceeded 1.5 m from December 2015 to March 2016, and the waves were of longer period than those in the other winters (over 20 s) during some of the energetic events. In contrast, the calm wave conditions from May to October remained fairly similar in all the years.

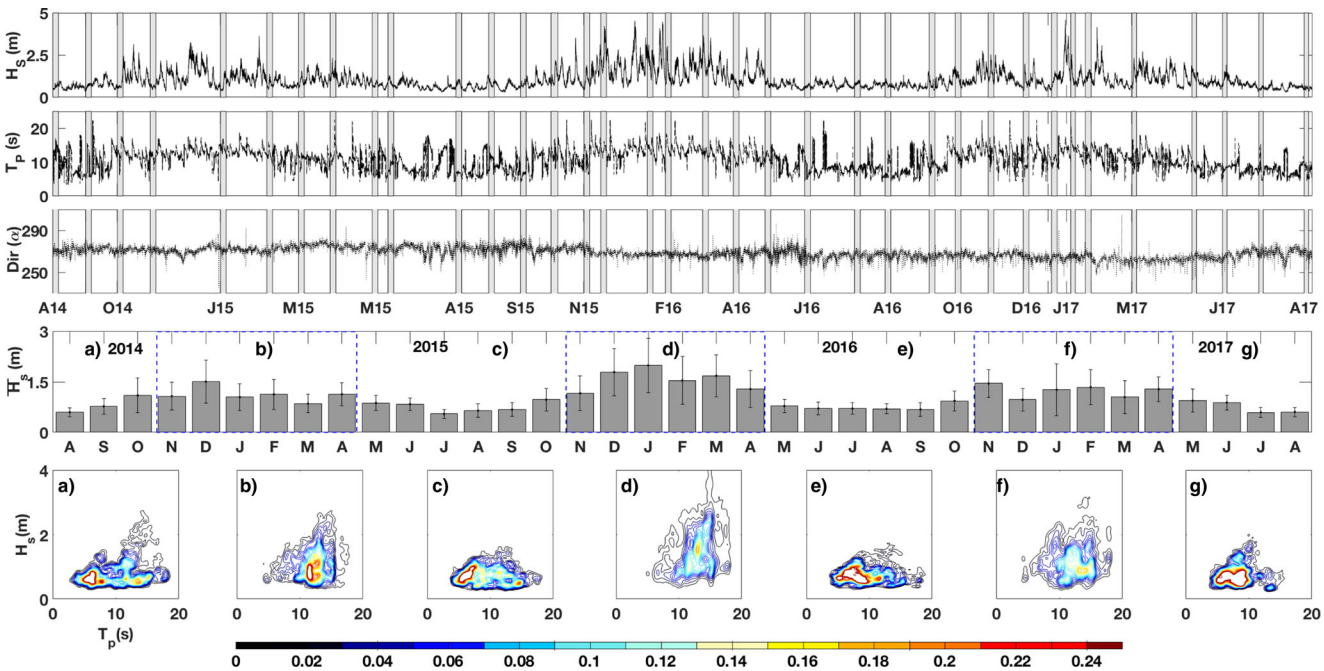

Fig. 2 Time series of significant wave height (H_s), peak period (T_p) and wave direction (Dir) from August 2014 to August 2017 (top three panels); the vertical grey bars indicate the times of morphological measurements. Monthly averaged H_s and standard deviations for 2014, 2015 and 2016 (fourth panel), and joint probability density functions of H_s and T_p for low (a, c, e, g) and high (b, d, f) wave energy periods (bottom panels)

Seasonal and interannual differences in wave conditions are reflected in the joint probability density functions (PDF) calculated for low- and high-energy periods (bottom panel in Fig. 2). Very similar patterns are observed for the two complete summer periods (May to October) in 2015 and 2016 (c and e in Fig. 2), but the waves were shorter in 2016 than those in 2015. Large differences are encountered between the three winters, with 2015–2016 being the most energetic, with a clear shift towards larger waves. The most probable winter wave conditions for 2014–2015 were H_s of 1 m and T_p of 11–12 s, while the waves were slightly longer (13 s) and larger (1.2–2 m) in 2015–2016. The 2016–2017 winter presented less energetic waves compared to the previous winter, but these were longer (14–15 s).

4.2 Morphological variability

The cumulative morphological variability of the beach (subaerial and subtidal sections) was analysed for the autumn/winter, spring and summer seasons in 2014, 2015, 2016 and 2017 to provide an insight into the erosive and accretive patterns along and across the beach (Figs. 3, 4 and 5).

The beach presented a very similar morphological condition in November 2014 and 2015; a sandbar was present at 1.5–2-m depth associated to partial subaerial erosion. In November 2016, however, the subaerial beach presented larger erosion, the sandbar was located further offshore (2.5- to 3-m depth) and the subtidal beach contained significant amounts of sediment (Figs. 3 and 7). The magnitude of subaerial beach erosion by February 2016 was enormous (~ 130 m^3 m^{-1}), more than double that of February 2015 and 2017 (~ 55 m^3 m^{-1}) from the maximum reference value in October (Figs. 3 and 8); and the eroded material moved offshore spreading around 3–4-m depth (Fig. 3).

The morphological evolution of the beach during the spring is critical from a subaerial beach recovery perspective, as it is when the onshore transfer of sediment occurs (Fig. 4). In 2015, the sandbar migrated onshore between February and March, and distributed its sediment landwards between April and May, contributing to the partial subaerial beach recovery (Figs. 4 and 7). The sandbar persisted over the spring in 2016, it migrated from depths of 3 to 2 m between March and May and the amount of sediment transferred onto the subaerial beach was relatively small (Figs. 4 and 7). In March 2017, the sandbar was alongshore lineal and located at a depth of 3 m, and became rhythmic and intersected by May (Fig. 4), transferring part of the sediment towards water depths of 1–1.5 m in some alongshore locations (i.e. TB01, Fig. 7).

The beach was unbarred during the 2015 summer, and the subaerial section accreted due to the incorporation of sand from the inner subtidal zone through onshore sediment transport (Figs. 5 and 7). In June 2016, the subaerial beach was severely eroded, and significant amounts of sediment were contained at ~2-m depth in the form of a sandbar. By August 2016, the sediment contained in the sandbar spread between depths of 2 and 5 m (Figs. 5 and 6). Some of this

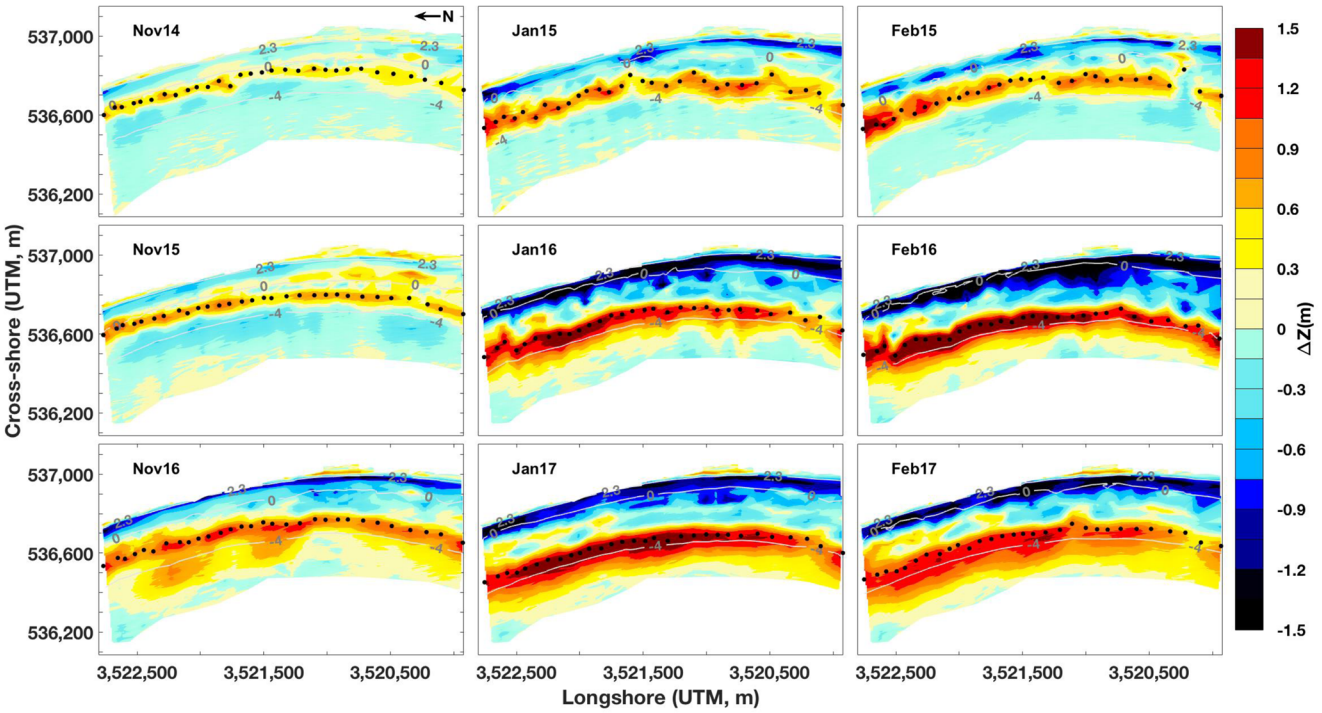

Fig. 3 Cumulative morphological differences for the high wave energy period between November and February (autumn/winter) in 2014–2015 (top), 2015–2016 (middle) and 2016–2017 (bottom). The intertidal beach is delimited between the 0- and 2.3-m contour lines. The black dots represent the sandbar locations extracted from the beach profiles

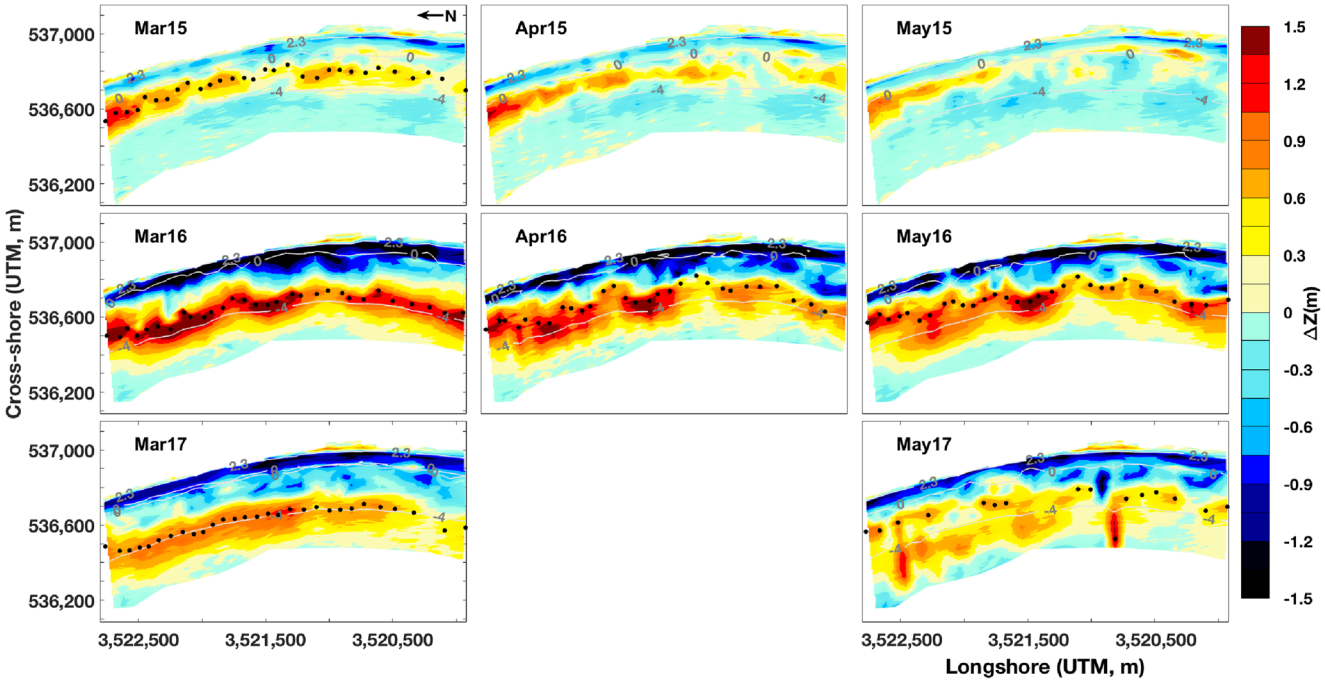

Fig. 4 Cumulative morphological differences for the springs in 2015 (top), 2016 (middle) and 2017 (bottom). The intertidal beach is delimited between the 0- and 2.3-m contour lines. The black dots represent the sandbar locations extracted from the beach profiles

sediment incorporated into the subaerial beach by September 2016, but the subaerial section was unable of reaching the elevations of September 2015 (Fig. 5). By June 2017, the sediment contained in the subtidal sandbar was spread, and by August, the subaerial beach partially recovered (mostly the south), but significant amounts of sediment were located at depths of 2–5 m (Fig. 5).

4.3 Cross-shore sandbar migration

The seasonal beach profile evolution from August 2014 to August 2017 is depicted in Fig. 6. The data indicate that before and after the El Niño winter (August 2014–2015 and August 2016–2017), the beach was unbarred in summer (August) and it formed a nearshore sandbar by autumn (November), which

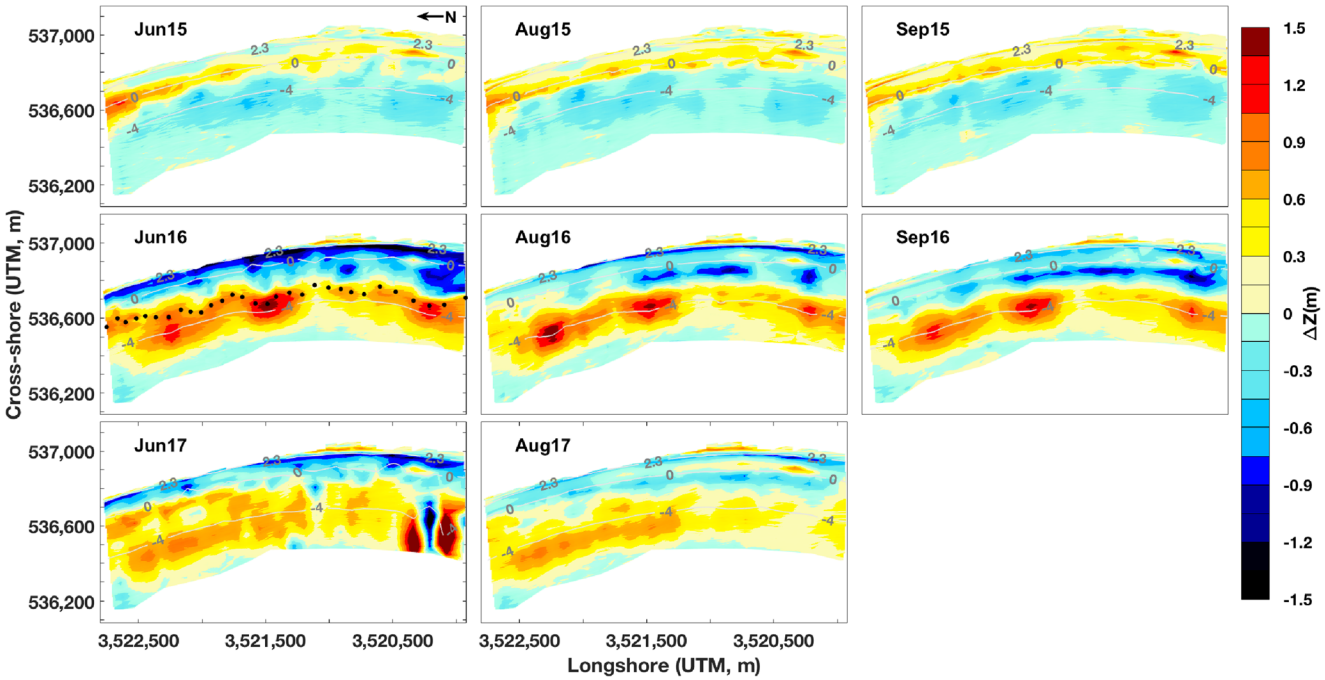

Fig. 5 Cumulative morphological differences for the summers in 2015 (top), 2016 (middle) and 2017 (bottom). The intertidal beach is delimited between the 0- and 2.3-m contour lines. The black dots represent the sandbar locations extracted from the beach profiles

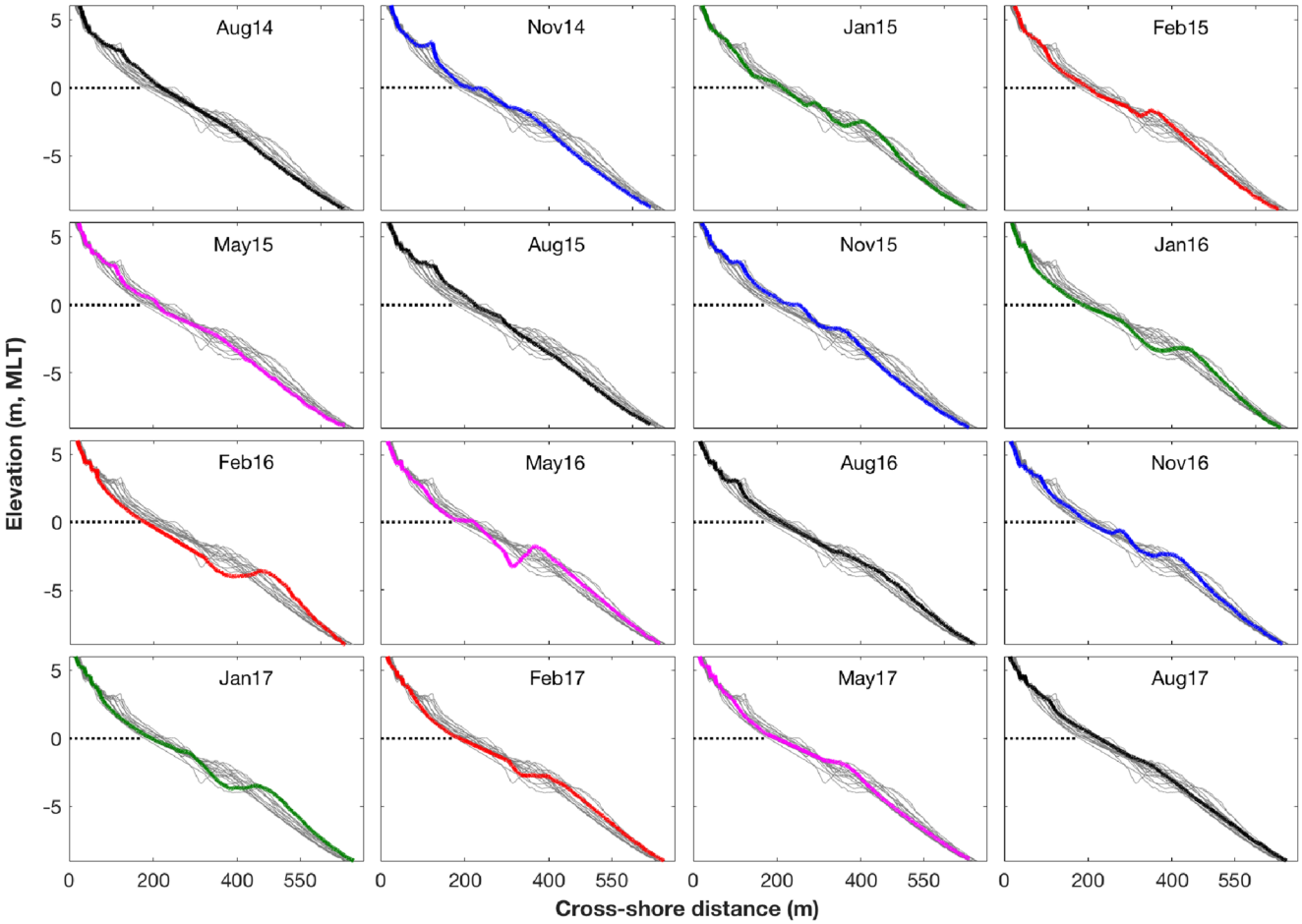

Fig. 6 Seasonal topo-bathymetric profile (TB) evolution from August 2014 to August 2017 for a representative profile in the southern beach end (TB01)

migrated offshore during the winter, reaching its maximum depth by January (2–3 m), and moving onshore after February, until partially/completely welding the subaerial beach by May. The sandbar moved further offshore and to deeper depths (3–4 m) by February 2016, associated to El Niño wave conditions, and it was unable of completely welding the subaerial beach by May 2016. Instead, large part of the sediment was spread across the subtidal beach, and some was transported to the subaerial beach by August 2016 (Figs. 5 and 6).

The seaward and landward sandbar migration cycle over the 3-year period is presented in detail (month-by-month) in Fig. 7. From October to February, prior to El Niño, the sandbar progressively migrated offshore associated to subaerial erosion, reaching its maximum depth by January 2015 (2.5 m). It migrated onshore after February until completely welding the subaerial beach by June 2015, and contributing to the recovery of the subaerial beach (left panels in Fig. 7).

During the El Niño winter, the subaerial beach eroded much more than in the other years (Figs. 8 and 9), and the sandbar moved further offshore and to deeper depths, reaching 3.5–4 m by February 2016. The sandbar migrated onshore after February, partially welding the subaerial section, but was present (as a terrace bar) in July (middle panels in Fig. 7) and flattered spreading its sediment by August 2016 (Fig. 6). In November 2016, after El Niño summer, the sandbar built-up deeper than in previous years (2.5 m rather than 1 m), and in late January 2017 (Jnn), it moved offshore to a similar location than in February 2016 (right panels in Fig. 7). During the 2017 spring and summer, the sandbar migrated onshore, welding partially the subaerial beach by July/August (Figs. 6 and 7), and leaving some sediment spread in the subtidal beach (Fig. 5).

4.4 Volumetric variability

The volumetric variability from August 2014 to August 2017 is presented in Figs. 8 and 9 for the total beach (TOT; −9 to 5.5 m of elevation), subaerial section (IS; 0 to 5.5 m of elevation) and subtidal section (SUB; −9 to 0 m of elevation) and for the whole beach length. IS successfully recovered from the 2014–2015 winter, between April and October 2015, and the SUB erosion was of similar magnitude to the IS accretion (61 m^3 m^{-1}) (Fig. 8). Both beach sections (IS and SUB) reached equilibrium at the beginning of December 2015

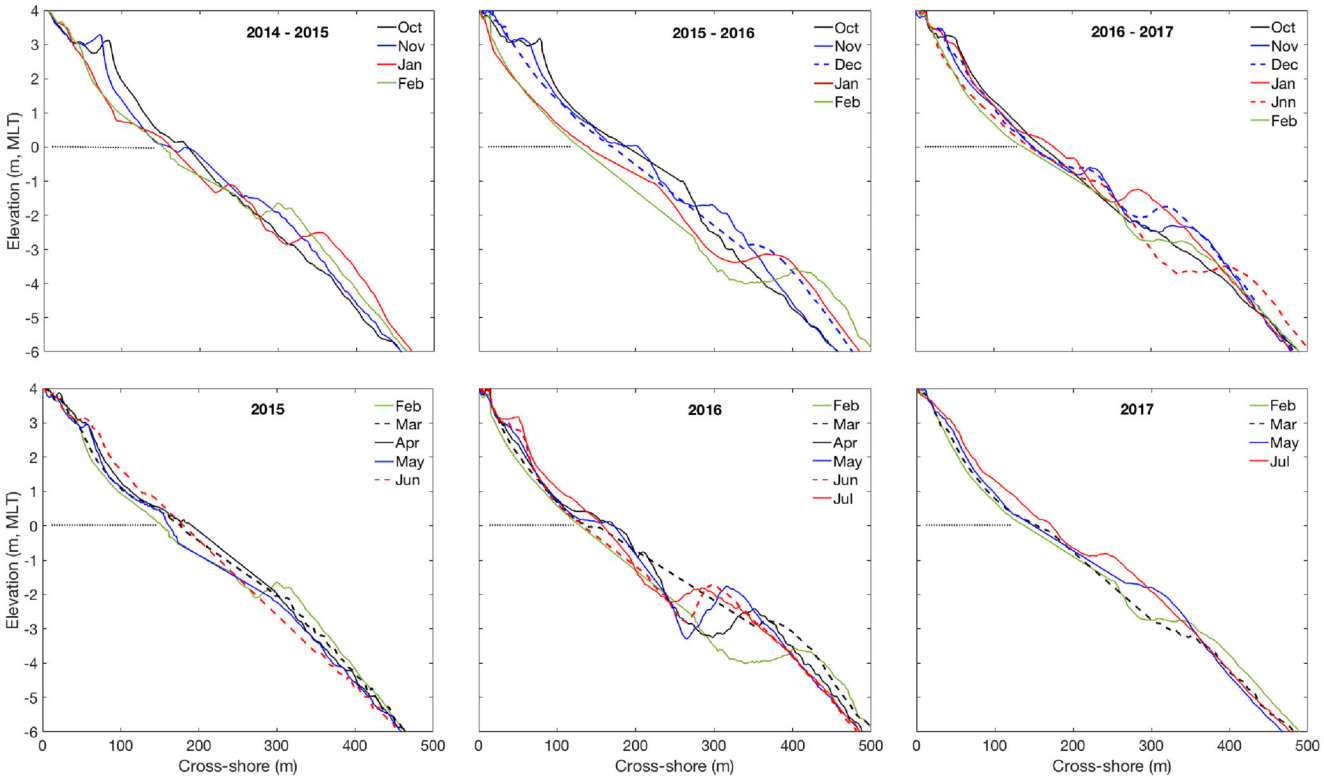

Fig. 7 Offshore (top) and onshore (bottom) sandbar migration for TB01 for the years 2014–2015 (left panels), 2015–2016 (central panels) and 2016–2017 (right panels). Jnn refers to late January in the top righ panel

(Figs. 8 and 9), before the beginning of the energetic 2015 winter waves.

The largest IS volumetric loss was of ~ 140 m^3 m^{-1} (400,000 m^3), occurred between October 2015 and March 2016, and contributed to the significant build-up of the SUB beach (Fig. 8). Between March and October 2016, the SUB beach eroded significantly, contributing to the 60% of IS recovery, with an accretion of 85 m^3 m^{-1} (243,000 m^3). By October 2016, the IS beach reached its maximum volume, but ~ 61 m^3 m^{-1} (175,000 m^3) less than in October of 2014 and 2015.

From December 2016 to March 2017, the IS section lost 20 m^3 m^{-1} (56,000 m^3), and by March 2017, it contained 40 m^3 m^{-1} (114,000 m^3) less than in March 2015 and 30 m^3 m^{-1} (80,000 m^3) more than in March 2016 (Fig. 8). By August 2017, the IS beach gained 90 m^3 m^{-1} (260,000 m^3), which indicated a 65% of recovery since the erosion caused by El Niño winter. It contained 25 and 45 m^3 m^{-1} less than in August 2014 and August 2015, but 13 m^3 m^{-1} more than in August 2016 (Fig. 8).

In terms of total volume, the beach presented a similar amount of sand in August 2014 and May 2017, and had an increase of 40 m^3 m^{-1} between August 2014 and August 2017 (bottom panel in Fig. 8). Overall, there is a clear cross-shore sediment exchange between the subaerial and subtidal sections, but the volumetric imbalance between both sections at different periods indicates the existence of relevant longshore sediment exchange (Figs. 8 and 9). While the southern beach end sustains the largest volumetric variability, the northern beach accretes the most. During the energetic winter waves between November and April (Fig. 2), the largest erosion occurred in the southern subaerial (IS) section and, in all years, the eroded sand was transported northwards to the subtidal (SUB) section (Fig. 9).

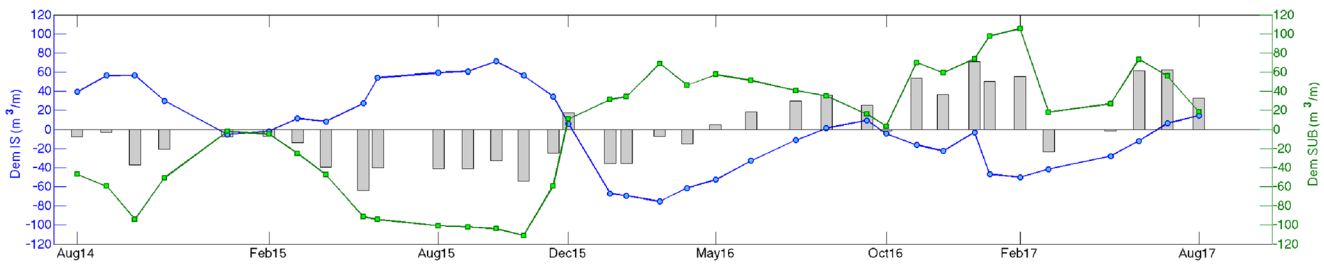

Fig. 8 De-meaned total (TOT; grey bars), subaerial (IS; blue) and subtidal (SUB; green) volumes in m^3/m from August 2014 to August 2017

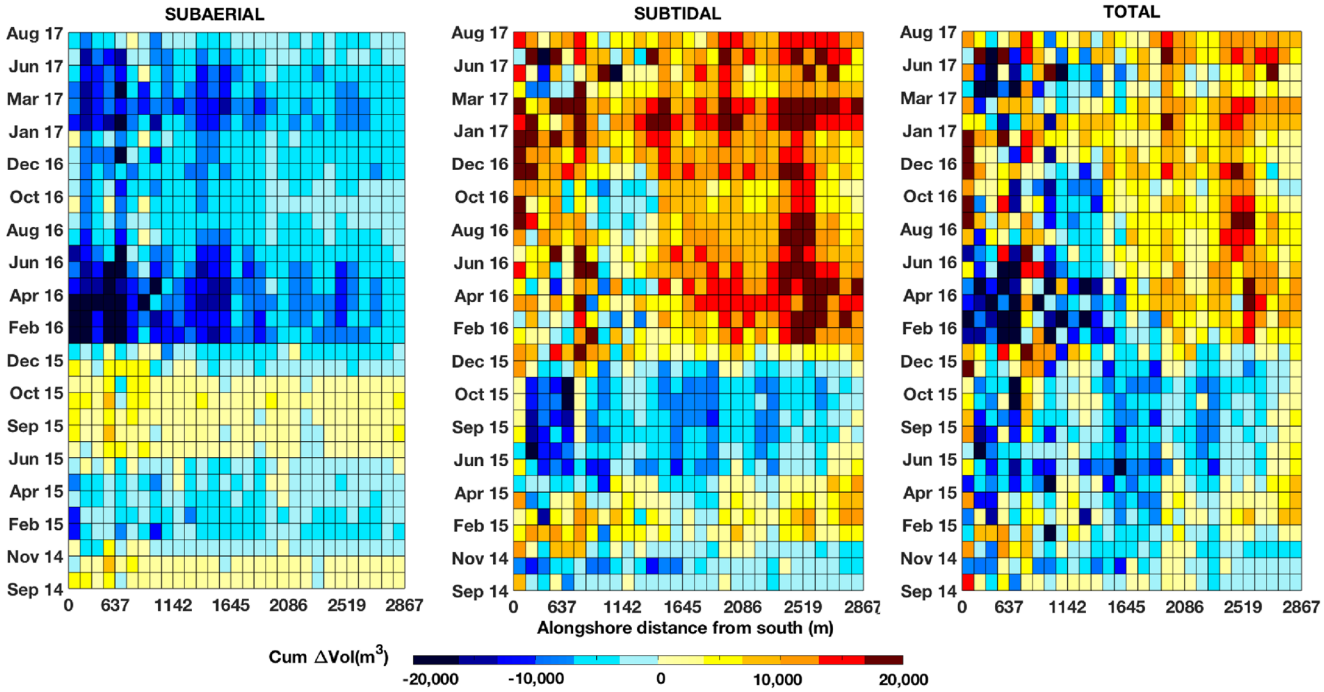

Fig. 9 Cumulative volumetric differences for the total, subaerial (IS) and subtidal (SUB) beach sections (left to right) from August 2014 to August 2017 (y axis) and along the nearly 3-km beach length (x axis). Each longshore box represents the value obtained from a beach profile

5 Discussion

The single-barred Ensenada Beach presented a clear seasonal morphological variability (Ruiz de Alegria-Arzaburu et al. 2015) dominated by an offshore and onshore sandbar migration cycle. The morphological response of the beach was very different to the behaviour observed in other multi-barred beaches dominated by seaward (e.g. Lippmann et al. 1993; Ruessink and Kroon 1994; Shand et al. 1999; Plant et al. 1999) or landward (e.g. Aagaard et al. 2004; Anthony et al. 2006) sandbar movements occurring on yearly scales.

The studied beach presented a nearshore sandbar by November (1–1.5-m depth), associated to the subaerial erosion triggered by the first incoming energetic waves. The sandbar migrated offshore induced by high wave conditions in winter, reaching its maximum depth (2–4 m) by January/February. Previous studies have reported onshore migrations of subtidal sandbars and subaerial welding during storm (Houser and Barrett 2010) and calm (Cohn et al. 2017) wave conditions. In Ensenada, the sandbar started migrating onshore right after the end of the high wave energy period (usually in February), and continued over the spring, until welding the subaerial beach, typically by May. The complete subaerial beach recovery process continued over the milder wave period in summer, through the transfer of sediment onshore from a shallow terrace bar, reaching the maximum subaerial volume by September/October (Ruiz de Alegria-Arzaburu et al. 2017) and resulting in an unbarred summer beach. This behaviour agrees with the common view of cross-shore beach recovery occurring during milder swell wave conditions (Komar 1999).

The landward sandbar migration process transferred 61 m^3 m^{-1} of sand onto the upper beach, allowing a full subaerial recovery after the 2014–2015 winter in Ensenada Beach. The beach remained unbarred in summer, but the sandbar (re)formed near the shoreline by autumn (November). Associated to the impact of larger than usual waves during the El Niño year (Seymour 1998; Allan and Komar 2002; Storlazzi and Griggs 2000), by the end of the 2015–2016 winter, the sandbar moved further offshore and to deeper depths (3–4 m) than in the previous winter. Moreover, in 2016, the energetic waves lasted for 2 months longer than those in other years (until April rather than February), making the spring mild wave period shorter. The sandbar migrated onshore during the shorter spring (from 4- to 2-m depth), but was unable of reaching shallow depths (1–1.5 m). Instead, the sandbar flattened during the summer, spreading the sediment across the subtidal beach (depths of 2–5 m). Consequently, the subaerial beach recovered 60% (85 m^3 m^{-1}) of the sediment lost over the energetic winter.

The 2015–2016 El Niño winter was catalogued as one of the most powerful events in the past 145 years, and beaches along the US Pacific coast eroded beyond historical records (Ludka et al. 2016; Barnard et al. 2017). The subaerial erosion after the very energetic 2015–2016 winter was very large (140 m^3 m^{-1}) in Ensenada, and of similar magnitude to the erosion reported in the European Atlantic coast after the

impact of energetic storms in the 2013–2014 winter (> 200 m^3 m^{-1}) (Scott et al. 2016). Beaches can take several years to fully recover from the impact of highly energetic waves, but a partial recovery can be relatively fast (Senechal et al. 2016; Scott et al. 2016). This was the case in Ensenada, which gained 60% of the eroded subaerial volume over the following summer. Many beaches in California took multiple years to completely build-up after the extreme subaerial erosion induced by the energetic 1982–1983 and 1997–1998 El Niño winters (Dingler and Reiss 2002; Barnard et al. 2011; Doria et al. 2016). Ensenada Beach recovered 65% (90 m^3 m^{-1}) of the subaerial volume lost over the 2015–2016 winter by the 2017 summer (August), and large amounts of sediment were still spread across the subtidal beach (2–5-m depths).

6 Conclusions

The recovery capabilities of a single-barred beach located in the Pacific Mexican coast were investigated before and after the 2015–2016 El Niño winter, based on morphological measurements collected monthly from August 2014 to August 2017. The El Niño 2015–2016 was classified as one of the most energetic events in the past 145 years; the nearshore waves exceeded H_s of 2 m over most of the period, and the high wave period extended until the end of April 2016 in the field site.

Before the 2015–2016 El Niño winter, the subaerial beach successfully recovered from the winter erosion induced by onshore sandbar migration during the spring, and intertidal welding over the summer mild wave conditions. The 2015–2016 El Niño winter caused very large subaerial erosion (140 m^3 m^{-1}), and the eroded sediment moved as a sandbar further offshore and to deeper depths (3–4 m) than in the other winter. During the 2016 spring, the sandbar was unable of reaching shallow water depths, thus, a large portion of the sand was left in the subtidal beach, and only 60% of the previously eroded sediment was transferred to the subaerial beach. During the 2017 summer, the subaerial beach recovered 65% of the 2015–2016 volume loss, and large amounts of sediment were still present in the subtidal beach.

This study highlights that the sediment contained on the sandbar is critical to assure a complete build-up of the subaerial beach during the accretive phase. The single-barred beach presented a clear seasonal seaward and landward sandbar migration cycle, which played the key role on the transfer of sediment between the subtidal and subaerial beach. The capability of the subaerial beach to fully recover was attributed to the landward sandbar migration and subaerial welding during the spring, and the complete accretion through the onshore transfer of sediment from a shallow terrace bar over the summer mild wave period. But the amount of sand transferred to the subaerial beach will depend on the distance and depth of the sandbar location, and also, on the duration of the low wave energy period needed for the sandbar to migrate onshore.

Acknowledgements The contribution of all field assistants and the MORDICS research group (www.mordics.org) is acknowledged, especially the technical support provided in the field by Ernesto Carsolio, Julio López and Eduardo Gil. We would like to thank the anonymous reviewers for their constructive comments and suggestions.

Funding information The authors are grateful to CONACyT for the funding provided through CB-2014-238765 and INFR-2013-01I005 with the projects 238765 and 205020.

References

Aagaard T, Davidson-Arnott R, Greenwood B, Nielsen J (2004) Sediment supply from shoreface to dunes: linking sediment transport measurements and long-term morphological evolution. Geomorphology 60(1):205–224

Aleman N, Certain R, Robin N, Barusseau J-P (2017) Morphodynamics of slightly oblique nearshore bars and their relationship with the cycle of net offshore migration. Mar Geol 392:41–52

Allan JC, Komar PD (2002) Extreme storms on the Pacific Northwest coast during the 1997–98 El Niño and 1998–99 La Niña. J Coast Res 18(1):175–193

Anthony E, Vanhee S, Ruz M-H (2006) Short-term beach-dune sand budgets on the north sea coast of France: sand supply from shoreface to dunes, and the role of wind and fetch. Geomorphology 81:316–329

Ashok K, Behera SK, Rao SA, Weng H, Yamagata T (2007) El Niño Modoki and its possible teleconnection. J Geophys Res 112:C11007

Barnard PL, Allan J, Hansen JE, Kaminsky GM, Ruggiero P, Doria A (2011) The impact of the 2009–10 El Niño Modoki on U.S. West Coast beaches. Geophys Res Lett 38(13). https://doi.org/10.1029/2011GL047707

Barnard PL, Short AD, Harley MD, Splinter KD, Vitousek S, Turner IL, Allan J, Banno M, Bryan KR, Doria A, Hansen JE, Kato S, Kuriyama Y, Randall-Goodwin E, Ruggiero P, Walker IJ, Heathfield D (2015) Coastal vulnerability across the Pacific dominated by El Niño/Southern Oscillation. Nat Geosci 8:801–807

Barnard PL, Hoover D, Hubbard DM, Snyder A, Ludka BC, Allan J, Kaminsky GM, Ruggiero P, Gallien TW, Gabel L, McCandless D, Weiner HM, Cohn N, Anderson DL, Serafin KA (2017) Extreme oceanographic forcing and coastal response due to the 2015–2016 El Niño. Nat Commun 8. https://doi.org/10.1038/ncomms14365

Cai W, Borlace S, Lengaigne M, van Rensch P, Collins M, Vecchi G, Timmermann A, Santoso A, McPhaden MJ, Wu L, England MH, Wang G, Guilyardi E, Jin F-F (2014) Increasing frequency of extreme El Niño events due to greenhouse warming. Nat Climate Change Lett 4:1–6. https://doi.org/10.1038/NCLIMATE2100

Cohn N, Ruggiero P, de Vries S, Garcia-Medina G (2017) Beach growth driven by intertidal sandbar welding. Proc Coast Dyn 199:1059–1069

Di Leonardo D, Ruggiero P (2015) Regional scale sandbar variability: observations from the U.S. Pacific Northwest. Cont Shelf Res 95:74–88

Dingler JR, Reiss RE (2002) Changes to Monterey Bay beaches from the end of the 1982-83 El Niño through the 1997-98 El Niño. Mar Geol 181:249–263

Doria A, Guza RT, O'Reilly WC, Yates ML (2016) Observations and modeling of San Diego beaches during El Niño. Cont Shelf Res 124:153–164

Grunnet NM, Hoekstra P (2004) Alongshore variability of the multiple barred coast of Terschelling, The Netherlands. Mar Geol 203:23–41

Henderson SM, Allen JS, Newberger PA (2004) Nearshore sandbar migration predicted by an eddy-diffusive boundary layer model. J Geophys Res 109:C06024

Hoefel F, Elgar S (2003) Wave-induced sediment transport and sandbar migration. Science 299:1885–1887

Houser C, Barrett G (2010) Divergent behaviour of the swash zone in response to different foreshore slopes and nearshore states. Mar Geol 271:106–118

Komar PD (1999) Beach processes and sedimentation. Prentice-Hall, Upper Saddle River, NJ, p 544

Lippmann TC, Holman RA, Hathaway KK (1993) Episodic, nonstationary behavior of a double bar system at duck, North Carolina, U.S.A., 1986-1991. J Coast Res SI 15:49–75

Lizarraga-Arciniega R, Chee-Barragan A, Gil-Silva E, Mendoza-Ponce T, Martínez-Díaz de León A (2003) Effect of El Niño on the subaerial beach Playas de Rosarito, B.C., Mexico. Geofis Int 42(3): 419–428

Ludka BC, Gallien TW, Crosby SC, Guza RT (2016) Mid-El Niño erosion at nourished and unnourished Southern California beaches. Geophys Res Lett 43:4510–4516. https://doi.org/10.1002/2016GL068612

Masselink G, Kroon A, Davidson-Arnott RGD (2006) Morphometrics of intertidal bars in wave-dominated coastal settings—a review. Geomorphology 73:33–49

Plant NC, Holman RA, Freilich MH, Birkemeier WA (1999) A simple model for interannual sandbar behaviour. J Geophys Res 104: 15755–15776

Revell DL, Komar PD, Sallenger AH (2002) An application of LIDAR to analyses of El Niño erosion in the Netarts littoral cell, Oregon. J Coast Res 18(4):792–801

Ruessink BG, Kroon A (1994) The behaviour of a multiple bar system in the nearshore zone of Terschelling: 1965–1993. Mar Geol 121:187–197

Ruessink BG, Kuriyama Y, Reniers AJHM, Roelvink JA, Walstra DJR (2007) Modeling cross-shore sandbar behavior on the timescale of weeks. J Geophys Res 112:F0310

Ruiz de Alegria-Arzaburu, A., García-Nava, H., Gil-Silva, E., Desplán-Salinas, G. 2015. A morphodynamic comparison of walled and non-walled beach sections, Ensenada beach, Mexico. World Scientific. The Proceedings of the Coastal Sediments ISBN:978-981-4355-52-0

Ruiz de Alegria-Arzaburu A, Vidal-Ruiz JA, García-Nava H, Romero-Arteaga A (2017) Seasonal morphodynamics of the subaerial and subtidal sections of an intermediate and mesotidal beach. Geomorphology 295:383–392

Sallenger Jr AH, Krabill W, Brock J, Swift R, Manizade S, Stockdon H (2002) Sea-cliff erosion as a function of beach changes and extreme runup during 1997-1998 El Niño. Mar Geol 187:279–297

Scott T, Masselink G, O'Hare T, Saulter A, Poate T, Russell P, Davidson M, Conley D (2016) The extreme 2013/2014 winter storms: beach recovery along the southwest coast of England. Mar Geol 382:224–241

Senechal N, Pavon J, Asselot R, Castelle B, Taaouati M, Ferreira S, Bujan S (2016) Recovery assessment of two nearby sandy beaches with contrasting anthropogenic and sediment supply settings. In: Vila-Concejo A, Bruce E, Kennedy DM, MacCarroll RJ (eds.), Proceedings of the 14th International Coastal Symposium (Sydney, Australia). Journal of Coastal Research, Special Issue, No. 75, pp.462–466. Coconut Creek (Florida), ISSN 0749-0208

Seymour RJ (1998) Effects of El Niños on the west coast wave climate. Shore Beach 66:3–6

Shand RD, Bailey DG, Shepherd MJ (1999) An inter-site comparison of net offshore bar migration characteristics and environmental conditions. J Coast Res 15:750–765

Storlazzi C, Griggs G (2000) Influence of El Nino-Southern Oscillation (ENSO) events on the evolution of central California's shoreline. Geol Soc Am Bull 111:236–249

Geomorphology 333 (2019) 61–72

Contents lists available at ScienceDirect

Geomorphology

journal homepage: www.elsevier.com/locate/geomorph

Variability of sandbar morphometrics over three seasonal cycles on a single-barred beach

Jesús Adrián Vidal-Ruiz, Amaia Ruiz de Alegría-Arzaburu *

Instituto de Investigaciones Oceanológicas, Universidad Autónoma de Baja California, Ensenada, Baja California, Mexico

ARTICLE INFO

Article history:
Received 5 October 2018
Received in revised form 23 February 2019
Accepted 23 February 2019
Available online 28 February 2019

Keywords:
Morphodynamics
ENSO
Storms
Sandbar migration

ABSTRACT

Understanding the morphodynamics of surfzone sandbars is very relevant from a sediment transport perspective. Three complete annual sandbar migration cycles were studied on a single-barred beach. The study period included the 2015–2016 El Niño anomaly and the incidence of a highly energetic swell-storm. The sandbar responded directly to the seasonal wave forcing, thus, it migrated offshore during the energetic winter and onshore during the milder summer conditions. Its seasonal migration cycle comprised four stages: (1) generation in autumn (November) at lower than 1 m depth; (2) offshore migration over the winter (until January/February) while $\overline{Hs} > 1.3$ m; (3) onshore migration over the early spring (March and April) while $\overline{Hs} < 1.0$ m; and during May–June: (4a) subaerial beach welding (unbarred beach) when a dynamic equilibrium reached; or (4b) terrace-bar formation (sandbar flattening) as a consequence of a lack of a dynamic equilibrium. The energetic El Niño winter conditions induced the same amount of offshore sandbar displacement as the individual extreme swell-storm, placing the sandbar at a maximum cross-shore distance of ~190 m, beyond the dynamic equilibrium. Contrary to the expected, a period of mild wave conditions during the 2017 winter favored the landward migration of the sandbar, locating it near its generation point. The duration of mild wave energy conditions and the offshore sandbar location and volume are considered relevant factors that limit the capabilities of the sandbar to reach shallow waters and weld to the subaerial beach before the summer.

1. Introduction

Surfzone sandbars are very dynamic features that result from a constant feedback between hydrodynamic forcing and morphology, at time-scales ranging from intra-wave periods to interannual cycles, and dictated by variations in local environmental settings (Splinter et al., 2018). A large variety of sandbars exist, and these bedforms are generally perceived as amplifications on the submerged profile elevation, but are commonly referred to as sandbars for perturbations of high-amplitude, and terrace-bars for those of low-amplitude still clearly separated from the shore (Holman and Bowen, 1982; Aagaard et al., 2013). These features constitute the first line of natural defense against coastal erosion and flooding on sandy beaches, and contain large amounts of sediment that contribute significantly to the sediment balance on the beach (Senechal et al., 2015). Quantifying onshore sandbar migrations, and events of welding to the beach face is, therefore, essential to determine the capabilities of the subaerial beach to recover after periods of energetic wave incidence (Ruiz de Alegría-Arzaburu and Vidal-Ruiz, 2018).

The physical processes behind onshore sandbar migrations are, at present, still controversial (Dubarbier et al., 2015; Fernández-Mora et al., 2015). It is generally accepted that seaward sandbar movements are related to intensive mean offshore currents (bed return flow) that generate during breaking, high-energy waves (e.g. Sallenger et al., 1985; Short, 1999). Shoreward sandbar migrations, instead, are associated with weak-to-nonbreaking waves, and induced by wave asymmetry (Hoefel and Elgar, 2003), near-bed wave skewness (Hsu et al., 2006; Ruessink et al., 2007; Fernández-Mora et al., 2015), Stokes drift and/or boundary layer streaming (Henderson et al., 2004). Therefore, it is relevant to measure the nearshore frequently (days-to-weeks) and over periods of years-to-decades to be able to determine the morphological geometry (morphometry) and location of sandbars at event-driven and seasonal scales (e.g. Price et al., 2014; Di Leonardo and Ruggiero, 2015). To date, a few studies have analysed sandbar behaviour in terms of the characteristics of their morphometry (i.e. sandbar crest depth, distance, height, width and volume) (Larson and Kraus, 1992; Ruessink and Kroon, 1994; Grunnet and Hoekstra, 2004; Aleman et al., 2017; Cheng and Wang, 2018). Data are needed to contribute to the development of accurate models that could provide a better understanding of the generation processes and the morphological evolution of sandbars under varying incident hydrodynamic conditions (e.g. Plant et al., 1999; Hsu et al., 2006; Mariño-Tapia et al., 2007; Van Maanen et al., 2008;

* Corresponding author.
E-mail address: amaia@uabc.edu.mx (A. Ruiz de Alegría-Arzaburu).

https://doi.org/10.1016/j.geomorph.2019.02.034
0169-555X/

Thiébot et al., 2012; Walstra et al., 2012; Smit et al., 2012; Holman et al., 2016; Ruessink et al., 2016).

Changes in two-dimensional (alongshore-uniform) and three-dimensional (alongshore variability) sandbar geometry have been found to be well correlated to the incoming wave forcing and/or to preceding morphologic states (Wright et al., 1985; Lippmann and Holman, 1990; Masselink et al., 2014), and these can also result from self-organization patterns (Coco and Murray, 2007). The first conceptual model of sandbar migrations (Shepard, 1950; Komar, 1974) indicated that beaches evolved from an unbarred shape during periods of low-energy waves to barred after high-energy wave conditions, thus, suggesting seasonal onshore and offshore sandbar movements. Many beaches, however, lack of a clear seasonality on the sandbar migration cycle. While a few beaches describe continuous sandbar landward migrations over decades (e.g. Aagaard et al., 2004; Anthony et al., 2006), other beaches present sporadic net onshore movements over periods of days to months (and sometimes, intertidal beach welding) during weak incident waves (e.g. Ostrowski et al., 1991; Larson and Kraus, 1992; Van Maanen et al., 2008; Ruggiero et al., 2009; Van de Lageweg et al., 2013; Senechal et al., 2015; Blossier et al., 2016; Phillips et al., 2017; Cohn et al., 2017).

Most multi-barred beaches sustain a lack of intra-annual correlation between the incident wave energy and cross-shore sandbar movements, and present net offshore migrations (NOM) over periods from a few years to decades (Birkemeier, 1984; Lippmann et al., 1993; Ruessink and Kroon, 1994; Plant et al., 1999; Shand et al., 1999; Aleman et al., 2017). During interannual migration cycles, sandbars form near the shoreline, migrate offshore across the surf zone and finally degenerate at the outer nearshore margin (Ruessink and Kroon, 1994). But high-variability has been encountered in sandbar behaviour in the degeneration zone, primarily associated with nearshore slope differences and sandbar volume variations (Shand et al., 1999; Tătui et al., 2016). Beaches with large sandbars attained interannual NOM cycles while those with small sandbars were subjected to episodic NOM (Ruessink et al., 2009); thus, highlighting the relevance of sandbar geometry in the characteristics of the migration cycles. However, few research studies have analysed differences in sandbar morphometry during their migration cycle on time-scales of hours to weeks (Ostrowski et al., 1991; Larson and Kraus, 1992) or years to decades (Ruessink and Kroon, 1994; Ruessink et al., 2003; Grunnet and Hoekstra, 2004; Di Leonardo and Ruggiero, 2015; Aleman et al., 2017; Cheng and Wang, 2018).

Single-barred beaches have been surprisingly understudied compared to their multi-barred counterparts (e.g. Ostrowski et al., 1991; Van de Lageweg et al., 2013; Blossier et al., 2016). Based on monthly bathymetric data collected over three years, this research reports a detailed analysis of sandbar morphometrics before, during and after the 2015–2016 El Niño winter on a single-barred beach. In Section 2 the field site is described, and the wave and morphological data are presented. Section 3 includes results on the characterization of the incident wave conditions, a quantitative description of the onshore/offshore sandbar migration, and the temporal variability of sandbar morphometrics. The sandbar migration rates and temporal changes in the morphometrics are related to the incident wave forcing in Section 4, and the main findings are discussed. Finally, Section 5 summarises the most relevant results.

2. Measurements and methods

2.1. Field site

This research was undertaken in Ensenada Beach, located within Todos Santos Bay in the Pacific coast of the northwestern Baja California peninsula (Fig. 1). The beach is made of siliceous medium sand (D_{50} of 0.25 mm), has a length of nearly 3000 m and an average slope tanβ of 0.025 (Ruiz de Alegria-Arzaburu et al., 2015). The field site is predominantly exposed to southwesterly and northwesterly swell waves in summer and winter, respectively, and the mean annual nearshore waves are characterised by a significant wave height of 1 m with an associated peak period of 11 s. While the incidence of swell-driven storms is common between October and April with waves exceeding heights of 3 m, low-energy waves dominate from May to September with an average height of 0.7 m (Ruiz de Alegria-Arzaburu et al., 2017). Associated with the variability in wave energy, the beach exhibits strong seasonal morphological variations (Ruiz de Alegria-Arzaburu et al., 2017). The sandbar migrates seaward during energetic wave conditions and landward with low-energy waves, and the seasonal cycle of sandbar migration plays an important role in the sediment transfer between the subaerial and subtidal beach (Ruiz de Alegría-Arzaburu and Vidal-Ruiz, 2018).

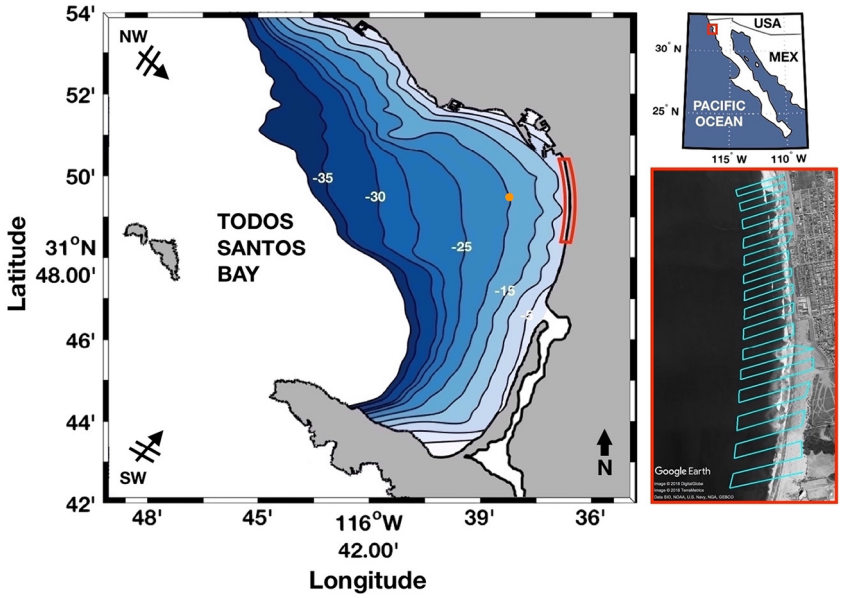

Fig. 1. Location of Ensenada Beach (red rectangle) within Todos Santos Bay in NW Baja California (left panel). The orange dot over the bathymetric map shows the location of the bottom-mounted ADCP. An aerial view of the beach with the monthly measured topo-bathymetric lines (in light blue) is presented in the bottom right panel.

2.2. Morphological measurements

Morphological data were collected monthly over a three-year period, from August 2014 to August 2017, along a beach length of 2867 m. The subaerial morphology was measured with a real-time kinematic global positioning system (RTK-GPS), operated on foot collecting data at 1 Hz. The subtidal morphology was measured using the 0.5 MHz frequency of an Accoustic Doppler Current Profiler (ADCP; Sontek M9 Hydrosurveyor) synchronized to an RTK-GPS and fixed to a jetski. Combining topographic and bathymetric data, 30 topo-bathymetric (TB) transects were collected every 100-m alongshore (Fig. 1), from the upper subaerial beach (generally over 5 m in elevation) down to a depth of 12 m, beyond the depth of closure. All TB profiles were linearly interpolated onto a 0.2 m cross-shore by 10 m alongshore grid to obtain digital elevation models (DEMs) (Fig. 2a). Monthly cumulative differences of the DEMs were calculated to determine the morphological evolution of the studied beach section over the three-year period. Further methodological details on the spatial coordinate system, accounted

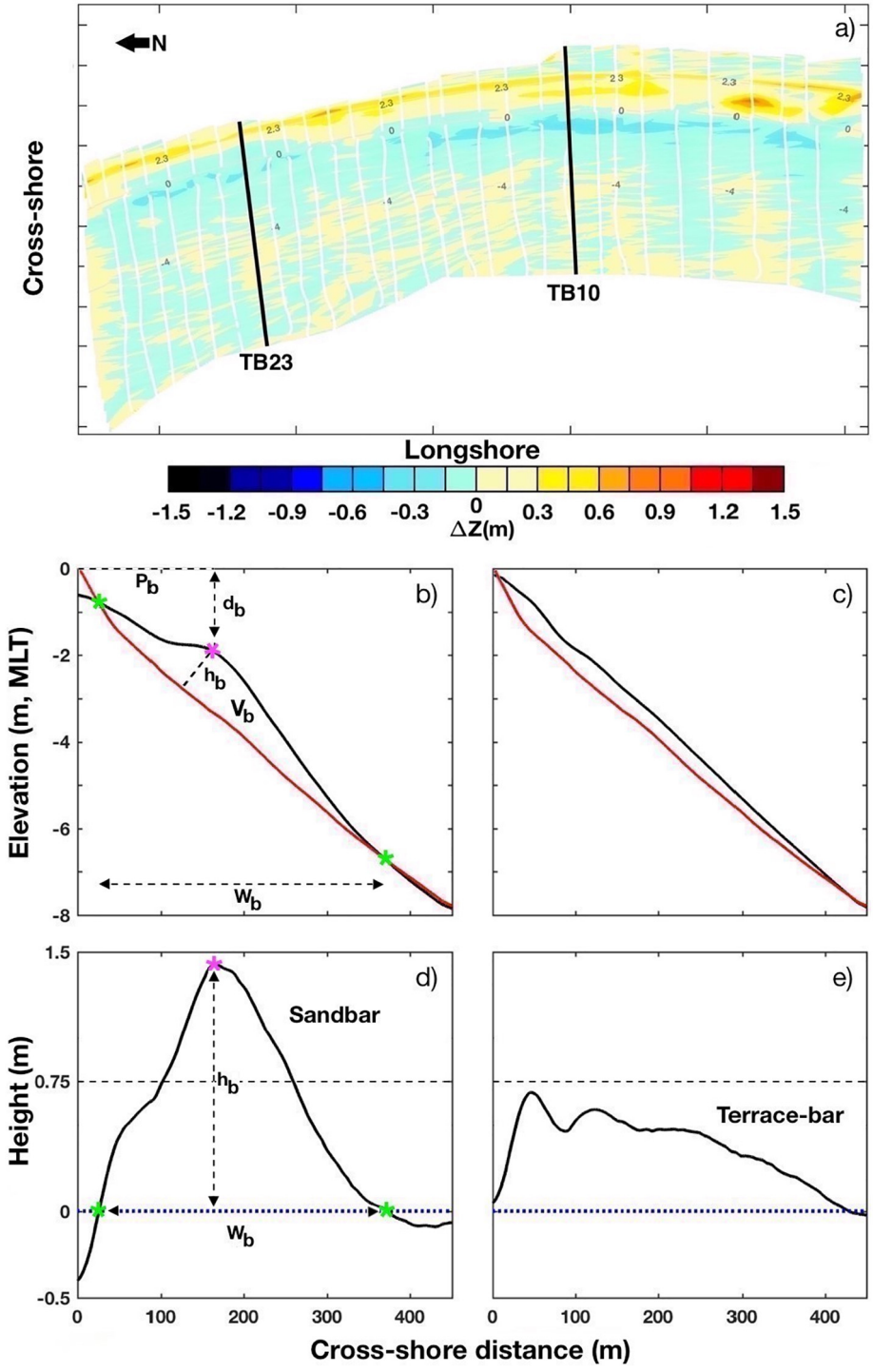

Fig. 2. (a) An example of a Digital Elevation Model (DEM) calculated from the measured 30 TB profiles (white lines); TB10 and TB23 are highlighted in black. (b and d) Schematic diagram of the main morphometric parameters of a sandbar: sandbar crest position (P_b; pink star), depth (d_b), height (h_b) and sandbar width (W_b; distance between the green stars) and volume (V_b), obtained plotting a typical instantaneous profile (black line) against the unbarred reference profile from September 2014 (red line). (c and e) refer to the terrace-bar case.

vertical errors and limitations on data acquisition across the surf zone are provided in Ruiz de Alegria-Arzaburu et al. (2017).

2.3. Sandbar morphometrics

In order to analyse the spatio-temporal variability of the subtidal sandbar morphology, five morphometric parameters were extracted from the measured TB profiles following the works of Ruessink and Kroon (1994) and Di Leonardo and Ruggiero (2015), which were: the sandbar crest height (h_b), depth (d_b) and cross-shore position (P_b), and sandbar width (W_b) and volume per linear metre (V_b) (Fig. 2). Each TB profile was first linearly interpolated at 0.1 m cross-shore and plotted against the unbarred reference profile from September 2014. Thus, all morphometric parameters were defined relative to the position of the reference profile. W_b was defined as the cross-shore distance between the intersecting points of the instantaneous profile with the unbarred reference profile, and V_b corresponds to the area confined between both profiles (Fig. 2b and d). A threshold value of $h_b > 0.75$ m was used to define a sandbar; hence, terrace-bars would be features with $h_b \leq 0.75$ m (Fig. 2d and e).

2.4. Nearshore wave measurements

Wave data were gathered hourly over the three-year period from August 2014 to August 2017 using a 1 MHz ADCP (Nortek AWAC) located 2500 m offshore from the beach, at a water depth of 20 m (Fig. 1). Time-series of significant wave heights (H_s), wave peak periods (T_p) and wave directions (α) were obtained. In order to characterise the seasonal wave variability over the three-year period, the wave parameters were monthly averaged and their standard deviations calculated. Joint probability density functions (PDF) between H_s and T_p were also determined for periods of high (November–April) and low wave-energy (May–October) over the study period.

3. Results

3.1. Wave conditions

The waves presented a clear seasonal pattern over the three-year study period, although significant interannual variability was encountered (Fig. 3A, B and C). The monthly-averaged waves were typically shorter (T_p of 9 s) and smaller ($H_s < 0.7$ m) between May and October, and longer ($T_p > 13$ s) and larger ($H_s > 1.3$ m reaching 2 m) between November and April. During El Niño 2015–2016 winter, the high-energy wave condition ($H_s > 4$ m, $T_p \approx 17$ s) lasted longer than during the preceding and succeeding winters (till April rather than February–March) (Ruiz de Alegría-Arzaburu and Vidal-Ruiz, 2018). The most energetic condition on 2016–2017 happened during an individual storm in late January 2017, which lasted ≈4 days and reached maximum H_s of 4.6 m and T_p of 17 s during a high neap tide; thus, this event presented conditions of similar wave energy as during the El Niño winter.

The joint PDFs between H_s and T_p for the energetic wave periods from November to April show significant differences between the winters of 2015–2016 and the others, being the most probable conditions of 1.0 m and 12 s in 2014–2015, 1.6 m and 13 s in 2015–2016, and 1.2 m and 12 s in 2016–2017 (Fig. 3b', d' and f'). In contrast, and as indicated in Ruiz de Alegría-Arzaburu and Vidal-Ruiz (2018), the low-wave energy periods presented similar joint PDFs over the study period, being the most common waves of 0.7 m and 9 s (Fig. 3a', c', e' and g'). In 2016, however, lesser variations in H_s happened compared to the other periods (Fig. 3e'). The wave direction ranged between 260 and 280° over the time series, but a slight shift toward 260–270° occurred

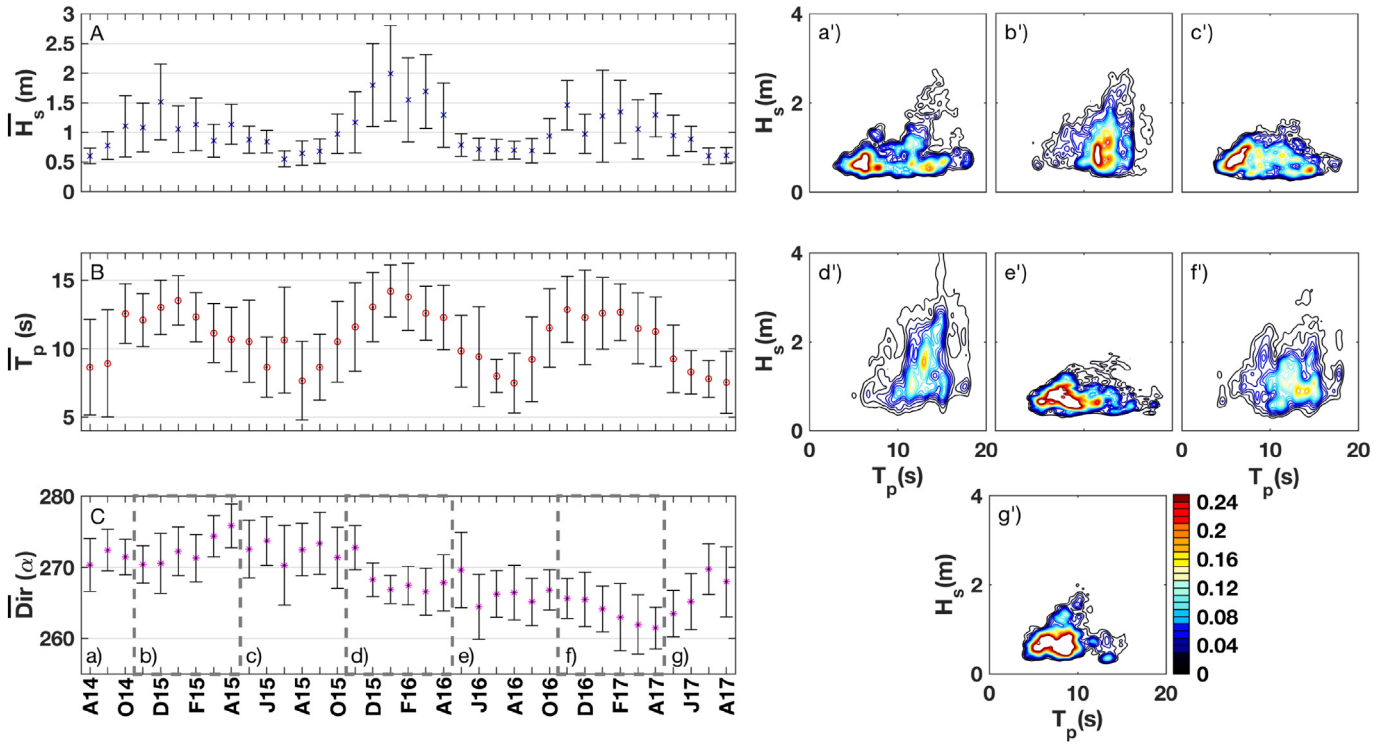

Fig. 3. Time-series of monthly-averaged significant wave heights, Hs, peak wave periods, Tp, and wave directions, Dir, from August 2014 to August 2017, and their standard deviations (vertical bars) (left panels A to C). The right panels present the joint probability density functions (PDFs) between Hs and Tp for the periods of May–October (a', c', e', g') and November–April (b', d', f') each year (dashed boxes on panel C). Low-energy wave conditions dominate in summer and present little variations, while high-energy waves occur between October and April.

after November 2015 (till the 2017 summer), while the dominating wave direction was 270–280° prior to that period (Fig. 3C).

3.2. Cross-shore sandbar evolution

Two representative TB profiles were selected from the mid-southern (TB10) and northern (TB23) beach (Fig. 2a), and their temporal evolution was analysed between August 2014 and August 2017 using the unbarred September 2014 profile as a reference (Figs. 4 and 5). During the first year, from August 2014 to August 2015 (previous to El Niño winter), the summer profiles remained unbarred, and a berm was present in the upper beach. In November 2014, a small sandbar was identified slightly below the mean low-tide level (MLT; 0-m elevation) in co-existence with a berm. By January 2015 the sandbar was well-developed and located at a depth of 1.7 m, and 150 m and 145 m offshore the reference shoreline in the southern (TB10, Fig. 4) and northern (TB23, Fig. 5) sections, respectively. The sandbar built-up and spread toward the shore after January, and by May 2015, it welded the shoreline, reincorporating its sediment onto the subaerial beach (Figs. 4 and 5).

Similar to the previous year, in November 2015 the sandbar formed close to the MLT level, in co-existence with the berm (Figs. 4 and 5). The energetic El Niño winter waves between November 2015 and January 2016 (Fig. 3) moved the sandbar offshore to depths of 2 m and distances of 145 m and 160 m in the southern and northern sections (Figs. 4 and 5). Between January and February 2016, the incoming waves were highly energetic (Fig. 3), and the sandbar migrated toward deeper depths reaching 2.5 m at a distance of 190 m in both sections; and presented steeper crests in the northern than in the southern beach (Figs. 4 and 5).

The milder wave conditions after May and during the 2016 summer (Fig. 3) induced the flattening of the sandbar. Part of the sandbar migrated onshore and welded to the shoreline during the spring, while considerable amounts of sediment remained at depths of 2.5–3.5 m (distances of 120–180 m) as a terrace-bar (Figs. 4 and 5). In November 2016, a subtidal sandbar reformed around 1.7 m depth, and its crest was steeper in the northern than in the southern beach section. During the 2016–2017 winter, the sandbar migrated up to 190 m offshore, gaining sediment, and reaching 3 m depth by January 2017 (Figs. 4 and 5). During the less energetic wave conditions after February 2017 (Fig. 3), the sandbar migrated onshore, partially welding the lower intertidal beach and gradually spreading its sediment toward the subaerial section. By August 2017, a significant amount of sediment remained in the lower subtidal section at the northern beach as a terrace-bar feature (Figs. 4 and 5).

3.3. Seasonal sandbar cycles

The beach was unbarred in August 2014, and the subaerial section accreted while the subtidal beach slightly eroded ($\Delta Z = \pm 0.3$ m). In November 2014, the sandbar formed slightly below MLT level, associated with partial subaerial erosion (Fig. 6). The subaerial erosion continued over the winter ($\Delta Z = -1$ m), and contributed to the sandbar accretion and offshore migration by January 2015. Between January and February 2015, the sandbar became an alongshore uniform ridge, losing its three-dimensional configuration or rhythmicity. The sandbar propagated onshore and welded to the intertidal beach by May 2015, reincorporating sediment onto the subaerial section.

Similar to the previous year, the sandbar formed in November 2015 close to the MLT level in the northern beach, and farther offshore in the southern section. The energetic El Niño 2015–2016 winter waves caused large morphological change ($\Delta Z = \pm 1.5$ m), eroding the subaerial beach and accreting the subtidal section. This contributed to the sandbar accretion at 1.5–3.9 m depth and its offshore migration till February 2016 (Fig. 6). By May 2016, the sandbar migrated onshore and presented alongshore rhythmicity (crest depths varying between 0.8 and 2.5 m alongshore). This contributed to the partial accretion of the

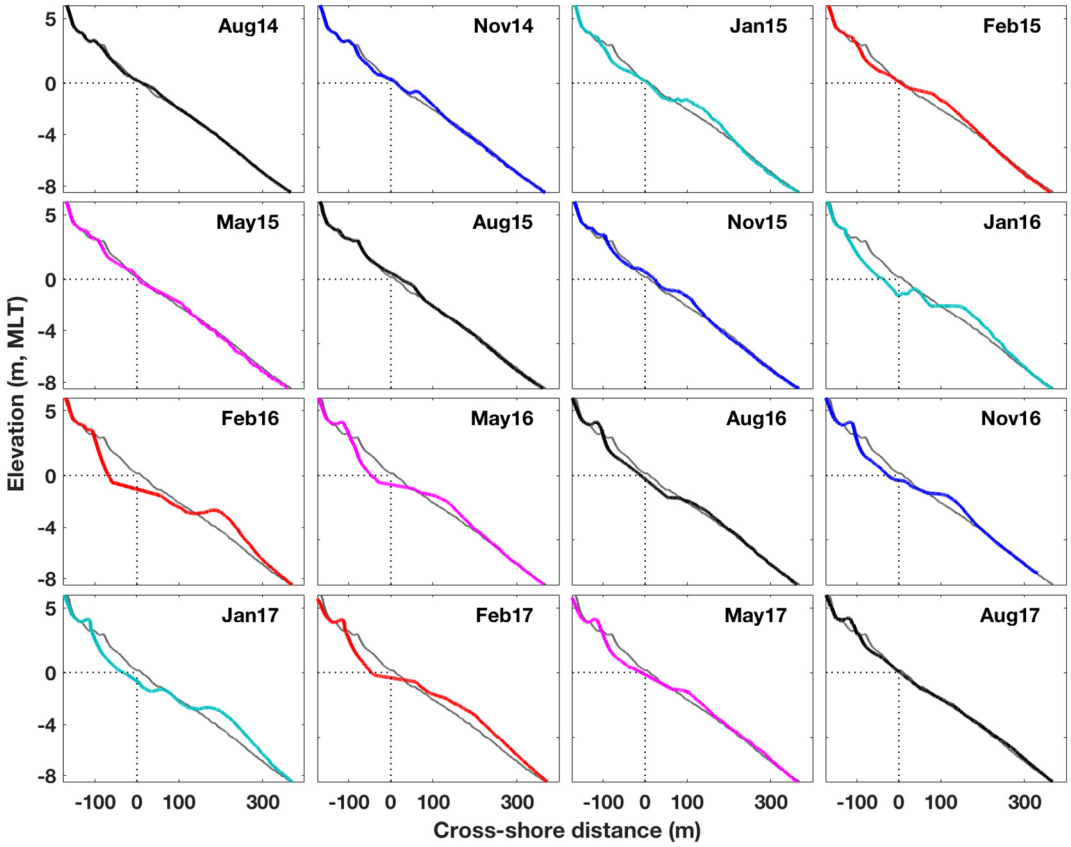

Fig. 4. Temporal evolution of TB10 (mid-southern beach) from August 2014 to August 2017 (coloured profiles) relative to the unbarred September 2014 reference profile (gray profile).

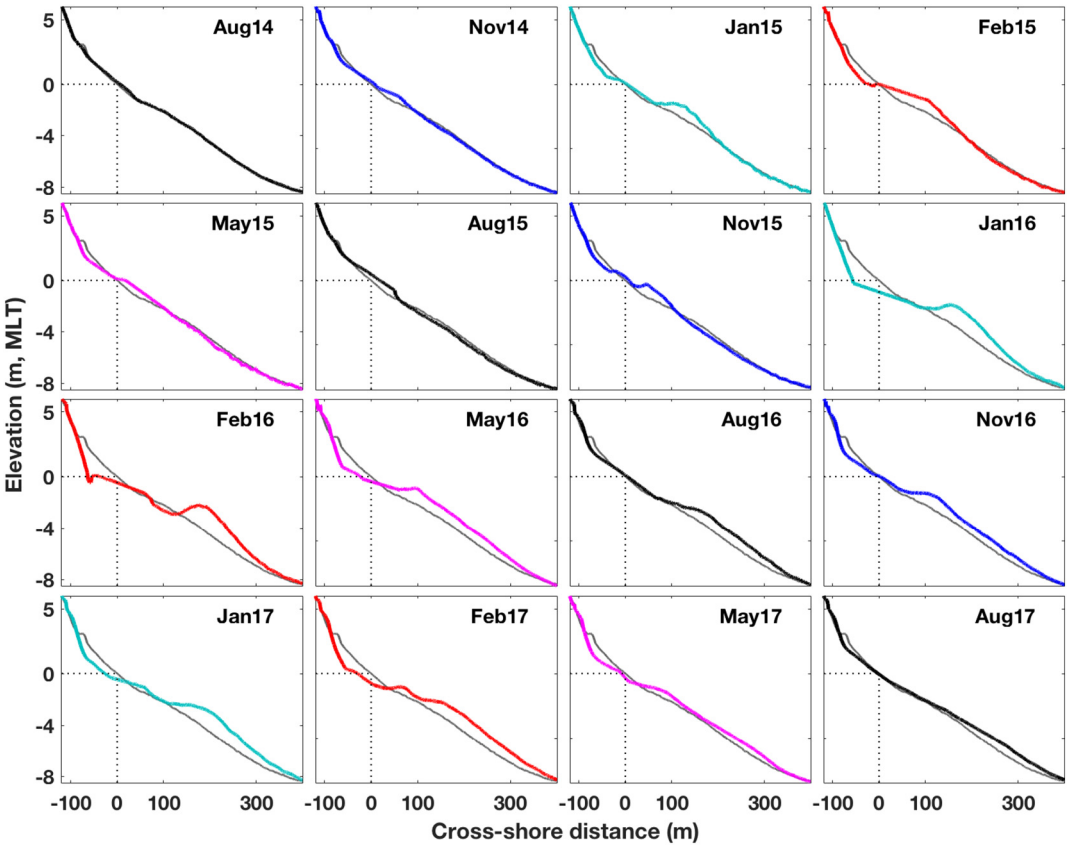

Fig. 5. Temporal evolution of TB23 (northern beach) from August 2014 to August 2017 (coloured profiles) relative to the unbarred September 2014 reference profile (gray profile).

inner subtidal beach, but the sandbar was unable to completely weld to the intertidal section. Part of the sandbar welded to the shoreline over the 2016 summer, contributing to partial subaerial recovery. Another part, however, formed a terrace-bar that flattened and propagated offshore up to depths of 2.5–3.6 m (Fig. 6).

The sandbar rebuilt in November 2016 around 1–2.5 m depth, partly with the sediment contained in the terrace-bar, and also with sand that eroded from the intertidal beach (Fig. 6). During the 2016–2017 winter, the subaerial beach eroded and the subtidal accreted ($\Delta Z \pm 1$ m). In January 2017, the sandbar was well formed and alongshore uniform, and after February it started migrating onshore, partially accreting the inner subtidal beach. By May 2017, the sandbar split into two sections: one migrated onshore up to depth of 1.5–2 m, and the other part remained at 2–4 m depth. Over the summer, the inner part of the sandbar welded to the shoreline and reincorporated its sediment onto the subaerial section, but large amounts of sand persisted at ~5 m depth by August 2017 in the form of a terrace-bar (Fig. 6).

3.4. Storm-driven sandbar migration

A single swell storm-event in late January 2017 caused the equivalent magnitude of offshore sandbar movement as during the El Niño 2015–2016 winter (Figs. 6 and 7). Prior to the storm, the beach presented an unusual morphological condition for January. The sandbar migrated onshore between November 2016 and early January 2017, becoming highly rhythmic and locating near the MLT level (Fig. 7). The storm with maximum H_s of 4.6 m, T_p of 14–17 s and an incident wave angle of 260° hit the beach on the 22nd of January and triggered a rapid offshore sandbar movement. The sandbar migrated a distance of 100 m and 145 m offshore up to 3 m depth in the southern and northern sections, respectively. During the seaward migration, the sandbar reshaped from rhythmic to an alongshore uniform configuration, and gained significant amounts of sand originated from the subaerial beach erosion.

3.5. Temporal variability of sandbar morphometrics

Temporal changes of sandbar morphometry were analysed from August 2014 to August 2017 based on alongshore averaged parameters such as sandbar crest positions, $\overline{P}_b$, depths, $\overline{d}_b$, and heights, $\overline{h}_b$, and sandbar widths, $\overline{W}_b$, and volumes, $\overline{V}_b$. The variability of these parameters was then related to the averaged significant wave height for the periods between morphological measurements, $\overline{H}_s$. Three complete annual cross-shore sandbar migration cycles are herein described into detail (Fig. 8).

Cycle I corresponded to pre-El Niño conditions (August 2014–August 2015). The sandbar formed in November 2014 at a distance of 50 m from the reference shoreline and 0.7 m depth, it was 0.8 m high and 95 m wide and contained ~35 m^3m^{-1} of sediment. During the energetic wave conditions (up to $\overline{H}_s \approx 1.3$ m) it migrated offshore reaching its maximum distance of 109 m and 1.5 m depth by January 2015; and contained ~75 m^3m^{-1} of sand and was 1 m high and 150 m wide (Fig. 8). Between January and February 2015, the sandbar moved slightly onshore to a distance of 97 m and 1.2 m depth, barely increasing its height to 1.1 m but gaining sediment ($\overline{V}_b = 88$ m^3 m^{-1}) and reaching its maximum width of 157 m. During the milder wave conditions after February ($\overline{H}_s$ of 1 m), the sandbar migrated onshore to a distance of 62 m from the reference shoreline and a depth of 0.8 m, and gradually decreased its volume (to 62 m^3 m^{-1}) and width (to 140 m), stabilizing its height to 1 m by April, and eventually welded to the shoreline by May 2015. The beach was unbarred over the 2015 summer (Fig. 8).

During *cycle II* (August 2015–August 2016), which included the El Niño winter, the sandbar formed in November near the shoreline, at

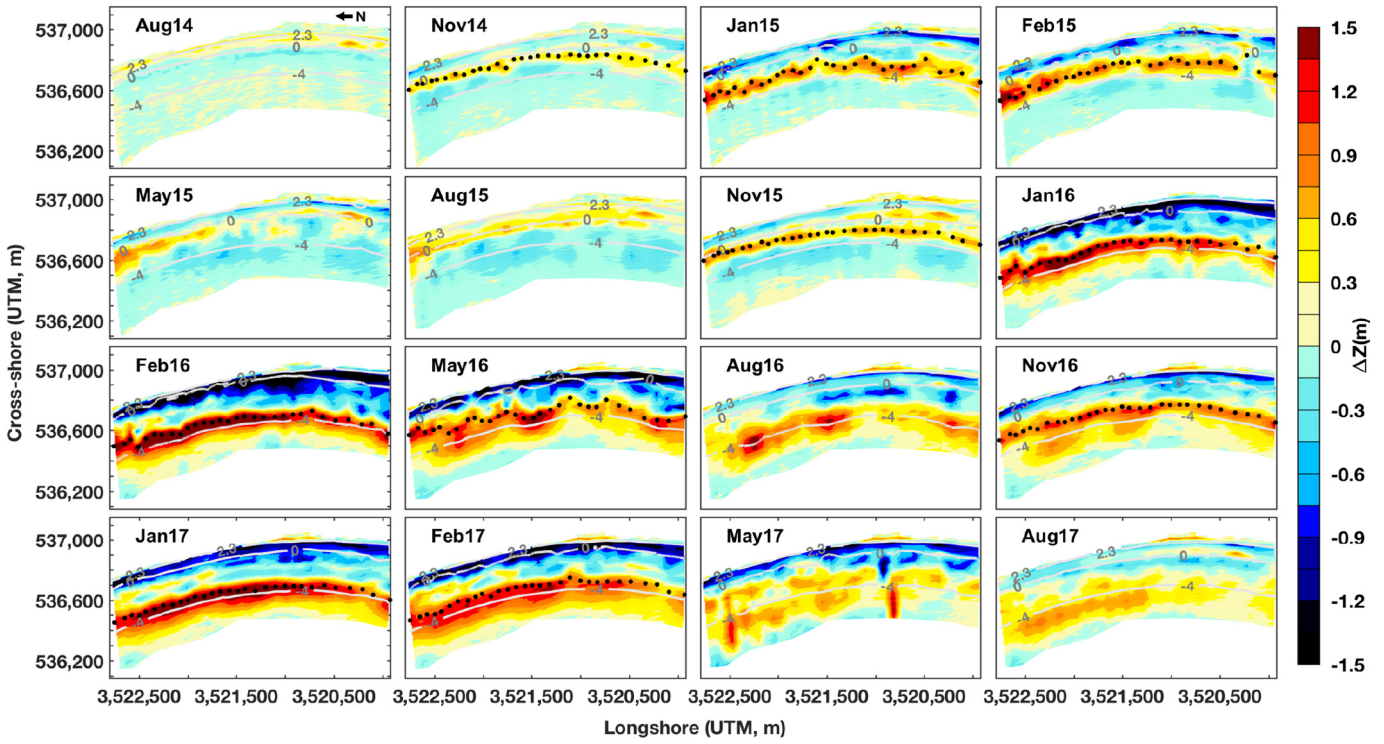

Fig. 6. Sandbar crest locations (black dots) overlaid the summer (Aug), autumn (Nov), winter (Jan, Feb) and spring (May) cumulative morphological changes from August 2014 to August 2017. The 0-m, 2.3-m and −4-m contour lines correspond to the mean low-tide level, upper intertidal limit and mid-subtidal zone, respectively.

0.9 m depth and 72 m offshore from the reference shoreline, it was 0.9 m high, 100 m wide and contained ~50 $m^3\ m^{-1}$ of sediment. The wave conditions during the winter were more energetic than in the previous year ($\overline{H_s}$ = 1.6–2 m), which induced a larger offshore sandbar migration. Thus, the sandbar reached a maximum distance of 183 m and depth of 2.6 m by February 2016, had a volume of 172 $m^3\ m^{-1}$ and was 1.4 m high and 249 m wide (Fig. 8). The wave energy decreased between February and May 2016 (from $\overline{H_s}$ of 2 m to 1 m) favouring the onshore sandbar migration to a distance of 125 m and to shallower depths of 1.8 m, reducing its $\overline{V_b}$ and $\overline{h_b}$ considerably (to 148 $m^3\ m^{-1}$ and 1 m), and increasing its $\overline{W_b}$ to 280 m. In June 2016, the sandbar was 0.8 m high and 288 m wide, and migrated slightly offshore to a distance of 137 m and depth of 2.3 m, decreasing its volume (134 $m^3\ m^{-1}$) and turning into a terrace-bar by July (Fig. 8). Over the 2016 summer a terrace-bar existed at distances between 165 and 185 m and depths of 2.5–3.5 m, and gradually decreased its volume (85–110 $m^3\ m^{-1}$), height (0.6–0.7 m) and width (246–275 m) while partially transferring sediment onto the subaerial beach.

In *cycle III* (August 2016–August 2017), the sandbar reformed in November farther offshore and deeper (distance of 120 m and depth of 1.7 m). It was 1 m high, 282 m wide and had 123 $m^3\ m^{-1}$ of sand, which suggested that the sediment contained in the terrace-bar contributed to the sandbar build-up. The first half of the winter (November to early January) presented mild wave conditions ($\overline{H_s}$ < 1.1 m) that favored onshore sandbar migration to a distance of 73 m and depths of 0.9 m, while it widened (from 282 to 305 m) and reduced its volume (111 $m^3\ m^{-1}$) and height (0.8 m) (Fig. 8). A large swell storm in late January (Jnn17; $\overline{H_s}$ of 2 m in Fig. 8) induced a rapid offshore sandbar movement of 120 m, placing the sandbar at a distance of 193 m and 3 m depth, and nearly doubling its $\overline{V_b}$ (from 111 to 197 $m^3\ m^{-1}$), increasing its $\overline{h_b}$ to 1.1 m and decreasing its $\overline{W_b}$ to 281 m (steepening). After the storm (in February), the sandbar moved slightly onshore (25 m), to a distance of 168 m and depth of 2.7 m, and widened ($\overline{W_b}$ = 3 19 m) but decreased its volume ($\overline{V_b}$ = 195 $m^3\ m^{-1}$) and flattened ($\overline{h_b}$ = 0.8 m). During the subsequent mild wave conditions ($\overline{H_s}$ < 1 m), the sandbar reduced its $\overline{V_b}$ (103 $m^3\ m^{-1}$), $\overline{h_b}$ (0.6 m) and $\overline{W_b}$ (270 m) turning the sandbar into a terrace-bar at a depth of 3.9 m and distance of 203 m by March (Fig. 8). By May the terrace-bar stabilized its $\overline{V_b}$, $\overline{h_b}$ and $\overline{W_b}$ and moved slightly onshore to a distance of 170 m and 3.2 m depth. The mild wave-energy conditions over the 2017 summer ($\overline{H_s}$ < 0.7 m) placed the terrace-bar at a distance of 220 m and depth of 4.6 m by August, and it became smaller and narrower ($\overline{h_b}$ = 0.4 m; $\overline{V_b}$ = 75 $m^3\ m^{-1}$; $\overline{W_b}$ = 280 m), suggesting that part of its sand was transferred onto the subaerial beach (Fig. 8).

3.6. Spatial variability of sandbar morphometrics

The cross-shore variability of the alongshore averaged sandbar morphometrics was analysed for the three annual cycles (Fig. 9). During *cycle I*, an increase of all morphometric parameters occurred during the high wave-energy period (November 2014 to February 2015). By January, the sandbar reached maximum distances of 110 m and depths of 1.5 m while the maximum sandbar crest heights (1.2 m) and volumes (75 $m^3\ m^{-1}$) happened by February. The sandbar migrated landwards near to its location of origin by April, and minimum values of $\overline{d_b}$ = 0.8 m, $\overline{h_b}$ = 0.9 m, $\overline{W_b}$ = 140 m and $\overline{V_b}$ = 60 $m^3\ m^{-1}$ were obtained (Fig. 9).

The morphometric parameters linearly increased with the cross-shore distance during *cycle II* (November 2015 to February 2016) too, but at a higher rate than in the previous cycle. The sandbar reached a maximum distance of nearly 190 m by February 2016 and presented $\overline{d_b}$ = 2.6 m, $\overline{h_b}$ = 1.4 m and $\overline{V_b}$ = 172 $m^3\ m^{-1}$. The sandbar persisted two months longer than in cycle I (until June rather than April), and in June, it was located at a distance of 140 m, even farther than in January the previous year. Thus, the sandbar was unable to reach a similar position as its origin in November, instead, it stabilized at $\overline{d_b}$ = 1.9–2.3 m, decreasing its volume (and height) and flattening between April and June (Fig. 9).

During *cycle III* the sandbar formed in November at a similar depth (1.7 m) and cross-shore distance (120 m) as where it was located in May in *cycle II* (Fig. 9). Contrary to the expected, the sandbar migrated

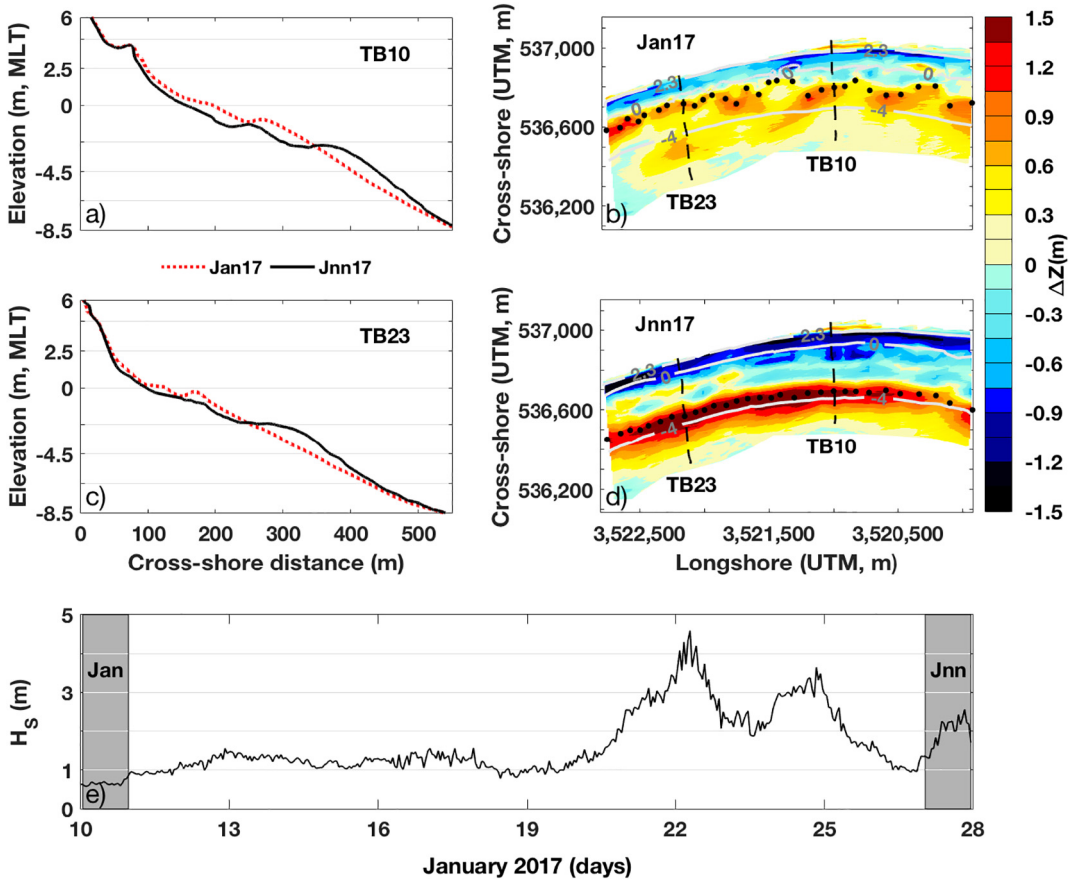

Fig. 7. Storm-driven offshore sandbar migration during the 21–25 January 2017 event. The top left panels show the profile change before (dashed red lines) and after (full black lines) the storm for TB10 and TB23. The top right panels present the cumulative morphological change before (Jan17) and after (Jnn17) the storm. The time series of significant wave height (H_s) during the storm and between the periods of morphological measurements (in gray) is presented in the bottom panel.

onshore between November and early January, locating it at a similar depth (0.9 m) and distance (70 m) as its origin in the previous cycles but containing twice as much as sand. Associated with the storm in late January (Jnn in Fig. 9), the sandbar migrated 120 m seaward, locating at a similar position as in February in cycle II (distance of 190 m) but slightly deeper ($\overline{d_b} \approx 3$ m). The sandbar migrated slightly onshore to a distance of 170 m by February but it flattened ($\overline{h_b}$<0.75 m) and widened, becoming a terrace-bar after March (Fig. 9).

4. Discussion

Morphological measurements of high temporal resolution (monthly) collected over three years, from August 2014 to August 2017, allowed a detailed analysis on the variability of sandbar crest positions, depths and heights, and sandbar widths and volumes relative to the incident wave forcing on a single-barred beach in Baja California. Prior studies showed strong seasonality in the morphological beach evolution, directly related to the incoming wave forcing (Ruiz de Alegria-Arzaburu et al., 2017). The cross-shore sandbar movement was highly modulated by the incident wave conditions (Ranasinghe et al., 2004; Ojeda et al., 2011), and in accordance with other studies (Shepard, 1950; Komar, 1974; Van Enckevort and Ruessink, 2003; Di Leonardo and Ruggiero, 2015; Splinter et al., 2018; Cheng and Wang, 2018), the sandbar migrated offshore during periods of energetic waves and onshore during calm wave conditions (Ruiz de Alegría-Arzaburu and Vidal-Ruiz, 2018). The recovery capability of the subaerial beach depended completely on the full attachment of the sandbar to the shoreline over the spring, which did not happen after the energetic El Niño 2015–2016 winter (Ruiz de Alegría-Arzaburu and Vidal-Ruiz, 2018). Here, the morphometric characteristics of the sandbar were analysed in order to understand its propagating patterns across the beach, prior, during and after the El Niño event.

The beach followed the accretionary morphological beach state sequence described by Wright and Short (1984) during the complete onshore sandbar migration cycle in 2015, prior to El Niño. At the end of that winter (in February), the beach presented a longshore bar-trough state, which turned into a low-tide terrace by the end of spring (in May). Thus, the beach became unbarred in summer while a berm was built in the upper beach, following the seasonal bar–berm model (Shepard, 1950; Komar, 1974). The sandbar formed in November (h_b = 0.8 – 0.9 m) at depths of 0.7–0.9 m and distance of 50–72 m, migrated offshore (to 1.5 m depth and distance of 109 m) during the winter (up to $\overline{H}_s \approx 1.3$ m) and landward during the lower energy conditions over the spring ($\overline{H}_s < 1.0$ m), to a similar location and depth as origin (62 m and $h_b = 0.8$), until it welded to the shoreline by May. These cross-shore migration patterns suggest that the sandbar migrates toward a wave height dependent equilibrium, following the breakpoint hypothesis (Dean, 1973; Sallenger et al., 1985; Dally, 1987; Plant et al., 1999). As wave energy increases, the sandbar migrates offshore in direction of an equilibrium position, very possibly driven by the undertow. However, the accretionary beach state sequence was not repeated in the following two years (after El Niño), and large differences in the geometry (width, height and volume) and magnitude of sandbar displacement (position and depth) were encountered between the different annual cycles.

Sandbars occasionally split into an onshore propagating feature and an offshore migrating feature, and some other times, inner and outer

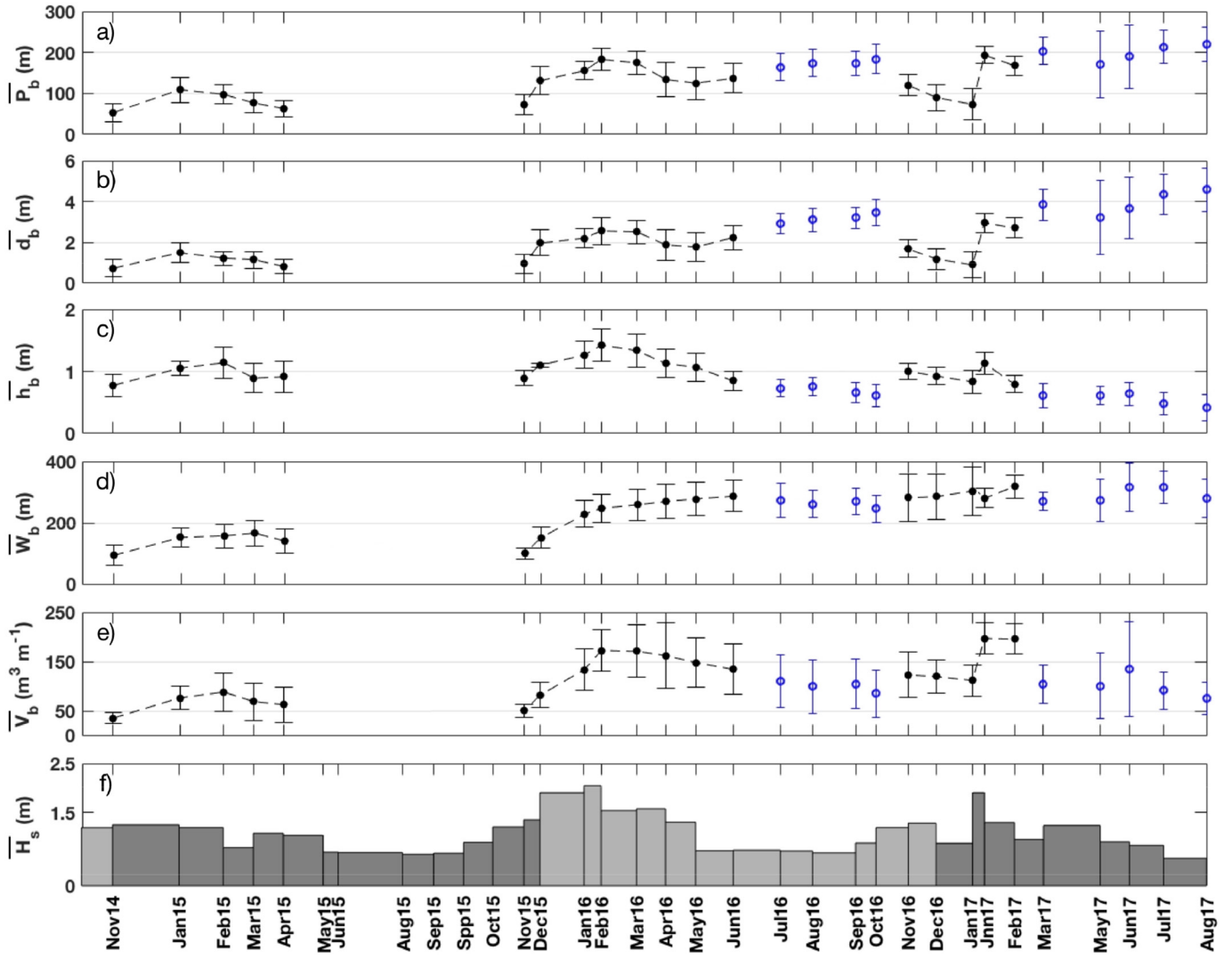

Fig. 8. Time-series of alongshore averaged sandbar morphometric parameters from October 2014 to August 2017. (a) ($\overline{P}_b$): sandbar crest positions. (b)($\overline{d}_b$): sandbar crest depths. (c) ($\overline{h}_b$): sandbar crest heights. (d) ($\overline{W}_b$): sandbar widths. (e) ($\overline{V}_b$): sandbar volumes. The black dots represent averaged values for sandbars and blue circles for terrace-bars, and the vertical lines are the standard deviations. (e) ($\overline{H}_s$): averaged significant wave height between periods of morphological measurements. The gap between measurements indicates an unbarred beach configuration.

bars merge (Plant et al., 1999). The incidence of higher wave energy during the El Niño winter ($\overline{H}_s$ = 1.6–2 m) propagated the sandbar 74 m farther than in the previous winter, up to a distance of 183 m and depth of 2.6 m, and with twice the volume (172 $m^3\ m^{-1}$). During the milder wave conditions in spring ($\overline{H}_s$ < 1.0 m), the sandbar migrated onshore, but stabilized at a distance of 125 m and 1.8 m depth, with large amount of sand ($\overline{V_b}$ = 148 $m^3\ m^{-1}$). Thus, the inability of the beach to reach the dynamic equilibrium during the lower wave energy period after the El Niño winter, is attributed to the large amount of sediment contained in the sandbar (twice the amount of the year before). The sandbar volume continuously decreased over the 2016 spring; part of the sandbar propagated landwards, and the other part became a terrace-bar (h_b < 0.75 m) that flattened over the summer ($\overline{d}_b$ = 2.5–3 m). In agreement with Plant et al. (1999), the sandbar divided into a shoreward propagating feature that contributed to partial subaerial recovery, and an offshore migrating and flattening terrace-bar over the summer. These findings suggest that the sandbar rebuilt in November 2016, with the input of terrace-bar sediment, and was located farther offshore (120 m) and deeper (1.7 m) than in previous years.

Although onshore sandbar movements are generally associated with the spring and summer seasons, this behavior can also occur anytime under moderately energetic wave condition (Plant et al., 1999; Pape et al., 2010). Landward sandbar propagation was measured during a low-wave energy period ($\overline{H}_s$ < 1.1 m) at the beginning of the 2016–2017 winter, which placed the sandbar at the location of its origin ($\overline{P}_b$ = 73 m; $\overline{d}_b$ = 0.9 m; $\overline{h}_b$ = 0.8 m; $\overline{V_b}$ = 111 $m^3\ m^{-1}$). Thus, the lowering of wave energy caused the disruption of the erosional morphological beach state sequence expected during the winter (Wright and Short, 1984). Nevertheless, this morphological beach state reseted with the impact of a subsequent extreme storm (Larson and Kraus, 1992; Ruessink et al., 2007; Ojeda et al., 2011) that caused a rapid seaward sandbar propagation of 120 m, placing it at a distance of 193 m and 3 m depth ($\overline{h}_b$ = 1.1 m; $\overline{V_b}$ = 197 $m^3\ m^{-1}$). Interestingly, the offshore sandbar displacement induced by this extreme storm was of similar magnitude to the reached at the end of the El Niño winter (~190 m from the reference shoreline), and in both cases, the sandbar migrated onshore during the subsequent milder wave period. Contrary to this behaviour, many multi-barred beaches lack intra-annual correlation between sandbar migrations and incident wave forcing, and instead,

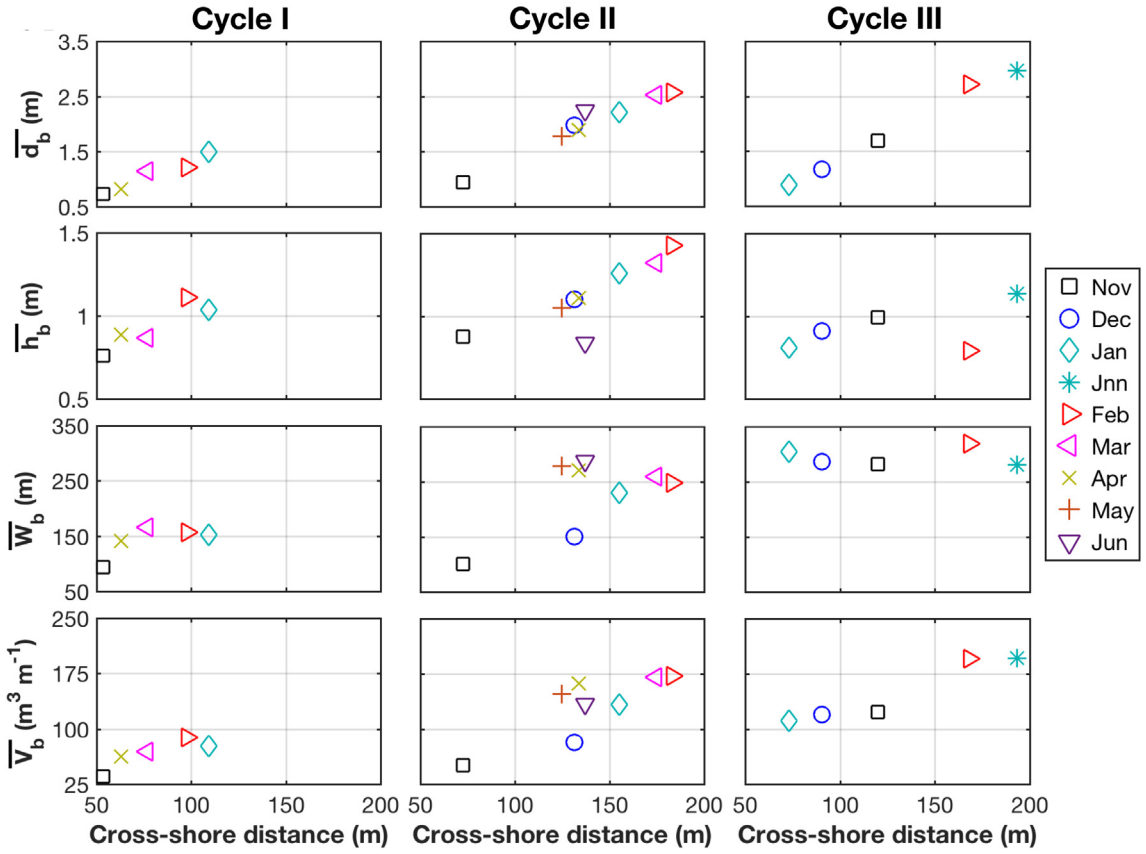

Fig. 9. Cross-shore distribution of the alongshore averaged morphometric parameters: sandbar crest depths ($\overline{d_b}$); top panels) and heights ($\overline{h_b}$); second top) and, sandbar widths ($\overline{W_b}$); third top panels) and volumes ($\overline{V_b}$); bottom panels) per migration cycle: Cycle I (August 2014–August 2015, left panels), Cycle II (August 2015–August 2016, middle panels) and Cycle III (August 2016–August 2017, right panels).

they present interannual variability consisting of a net offshore migration (NOM) over periods from a few years to decades, and a final sandbar degeneration phase at the outer nearshore margin (e.g. Ruessink and Kroon, 1994; Plant et al., 1999; Shand et al., 1999).

Four seasonal sandbar migration stages were identified in the studied single-barred beach: (*1*) generation in autumn (November) at lower depths than 1 m; (*2*) offshore migration during large winter waves ($\overline{H}_s$ > 1.3 m; until February); (*3*) onshore migration during milder waves over the spring ($\overline{H}_s$ < 1.0 m; March to April); and during May–June: (*4a*) weld to the subaerial beach resulting in an unbarred summer configuration; or (*4b*) terrace-bar formation and flattening during the summer (sand transference toward the subaerial beach). Option (*4a*) occurred when an offshore sandbar equilibrium distance of ~110 m and 1.5 m depth was reached, while (*4b*) took place when the sandbar migrated greater offshore distances of up to ~190 m and located at deeper depths (2.6–3 m; almost twice than in *4a*). The sandbar tended to evolve toward an equilibrium position during the seasonal cycle (e.g. Plant et al., 2001; Cheng and Wang, 2018), but was unable to reach its dynamic equilibrium in (*4b*). This supports the idea that offshore/onshore sandbar migration distances are not only associated with the incident wave energy, but also with the preceeding morphological conditions (Plant et al., 1999; Pape et al., 2010).

5. Conclusions

Sandbar morphometric variations were studied over three annual cycles (August 2014 to August 2017) at the single-barred Ensenada Beach, located in the northwestern Baja California peninsula in Mexico. Changes in sandbar migration patterns associated with the 2015–2016 El Niño anomaly and a highly energetic storm were analysed. The sandbar migrated toward a wave height dependent equilibrium, following the breakpoint hypothesis. After the El Niño winter, the beach was unable to reach the dynamic equilibrium during the low-wave energy period, which was attributed to the large sandbar volume (twice the amount of the year before). Consequently, the sandbar divided into a shoreward propagating feature, that contributed to partial subaerial recovery, and a terrace-bar feature that flattened and migrated offshore over the summer.

A period of mild wave conditions during the 2017 winter favored the landward migration of the sandbar, placing it at its dynamic equilibrium location onshore (near its generation point). But the impact of a subsequent extreme storm reseted the morphology and triggered a rapid offshore sandbar migration. The sandbar displacement of the individual energetic storm was very similar to the observed at the end of the El Niño winter, in both cases, the sandbar reached a maximum cross-shore distance of ~190 m; beyond the dynamic equilibrium. After these events, the sandbar migrated onshore during the subsequent milder wave period, but was unable to weld to the shoreline, and instead, a terrace-bar feature was formed.

In summary, four seasonal sandbar migration stages were identified: (*1*) generation in November at $\overline{d}_b$ < 1 m; (*2*) offshore migration over the winter until February ($\overline{H}_s$ > 1.3 m); (*3*) onshore migration from March to April ($\overline{H}_s$ < 1.0 m); and during May–June: (*4a*) weld to the subaerial beach (unbarred beach); or (*4b*) terrace-bar formation and flattening over the summer. Option (*4a*) occurred when an offshore sandbar equilibrium distance of ~110 m and 1.5 m depth was reached, while (*4b*) took place when the sandbar migrated greater offshore distances of up to ~190 m and located at deeper depths (2.6–3 m; almost twice than in *4a*). Consequently, the capabilities of the sandbar to reach shallow waters ($\overline{d}_b$<1 m) and weld to the subaerial beach will depend on its distance relative to the dynamic equilibrium point, but also, on the amount

of sand contained by the sandbar and the duration of the mild wave condition period.

Acknowledgments

The contribution of all field assistants and the Morphodynamics research group (MORDICS; www.mordics.org) is acknowledged, especially the technical support provided in the field by Ernesto Carsolio, Julio López, Tadashi Kono and Eduardo Gil. The authors are grateful to CONACyT for the PhD grant provided to J.A.V.R. and for the funding provided through the CB-2014-238765 project.

References

Aagaard, T., Davidson-Arnott, R., Greenwood, B., Nielsen, J., 2004. Sediment supply from shoreface to dunes: linking sediment transport measurements and long-term morphological evolution. Geomorphology 60 (1), 205–224. https://doi.org/10.1016/j.geomorph.2003.08.002.

Aagaard, T., Greenwood, B., Hughes, M.G., 2013. Sediment transport on dissipative, intermediate and reflective beaches. Earth Sci. Rev. 124, 32–50. https://doi.org/10.1016/j.earscirev.2013.05.002.

Aleman, N., Certain, R., Robin, N., Barusseau, J.-P., 2017. Morphodynamics of slightly oblique nearshore bars and their relationship with the cycle of net offshore migration. Mar. Geol. 392, 41–52. https://doi.org/10.1016/j.margeo.2017.08.014.

Anthony, E.J., Vanhée, S., Ruz, M.H., 2006. Short-term beach- dune sand budgets on the North Sea coast of France: sand supply from shoreface to dunes and the role of wind and fetch. Geomorphology 81, 316–329. https://doi.org/10.1016/j.geomorph.2006.04.022.

Birkemeier, W.A., 1984. Time scales of nearshore profile changes. Paper Presented at 19th International Conference on Coastal Engineering. American Society of Civil Engineers, New York.

Blossier, B., Bryan, K.R., Daly, C.J., Winter, C., 2016. Nearshore sandbar rotation at single-barred embayed beaches. J. Geophys. Res. Oceans 121, 2286–2313. https://doi.org/10.1002/2015JC011031.

Cheng, J., Wang, P., 2018. Dynamic equilibrium of sandbar position and height along a low wave energy micro-tidal coast. Cont. Shelf Res. 165, 120–136. https://doi.org/10.1016/j.csr.2018.05.004.

Coco, G., Murray, A.B., 2007. Patterns in the sand: from forcing templates to self-organization. Geomorphology 91, 271–290. https://doi.org/10.1016/j.geomorph.2007.04.023.

Cohn, N., Ruggiero, P., de Vries, S., García-Medina, G., 2017. Beach growth driven by intertidal sandbar welding. Paper Presented at 8th International Conference on Coastal Dynamics. Denmark, Helsingør.

Dally, W.R., 1987. Longshore bar formation -surf beat or undertow? Proceedings Coastal Sediments. 87. ASCE, pp. 71–86

Dean, R.G., May, 1973. Heuristic Models of Sand Transport in the Surf Zone. Proceedings of the Conference on Engineering Dynamics in the Surf Zone, Sydney.

Di Leonardo, D., Ruggiero, P., 2015. Regional scale sandbar variability: observations from the U.S. Pacific Northwest. Cont. Shelf Res. 95, 74–88. https://doi.org/10.1016/j.csr.2014.12.012.

Dubarbier, B., Castelle, B., Marieu, V., Ruessink, B.G., 2015. Process-based modeling of cross-shore sandbar behavior. Coast. Eng. 95, 35–50.

Fernández-Mora, A., Calvete, D., Falqués, A., de Swart, H.E., 2015. Onshore sandbar migration in the surf zone: new insights into the wave-induced sediment transport mechanisms. Geophys. Res. Lett. 42, 2869–2877. https://doi.org/10.1002/2014GL063004.

Grunnet, N.M., Hoekstra, P., 2004. Alongshore variability of the multiple barred coast of Terschelling, The Netherlands. Mar. Geol. 203, 23–41. https://doi.org/10.1016/S0025-3227(03)00336-0.

Henderson, S.M., Allen, J.S., Newberger, P.A., 2004. Nearshore sandbar migration predicted by an eddy-diffusive boundary layer model. J. Geophys. Res. 109, C06024. https://doi.org/10.1029/2003JC002137.

Hoefel, F., Elgar, S., 2003. Wave-induced sediment transport and sandbar migration. Science 299, 1885–1887. https://doi.org/10.1126/science.1081448.

Holman, R.A., Bowen, A.J., 1982. Bars, bumps, and holes: models for the generation of complex beach topography. J. Geophys. Res. 87, 457–468. https://doi.org/10.1029/JC087iC01p00457.

Holman, R.A., Lalejini, D.M., Holland, T., 2016. A parametric model for barred equilibrium beach profiles: two-dimensional implementation. Coast. Eng. 117, 166–175. https://doi.org/10.1016/j.coastaleng.2016.07.010.

Hsu, T.J., Elgar, S., Guza, R.T., 2006. Wave-induced sediment transport and onshore sandbar migration. Coast. Eng. 53, 817–824. https://doi.org/10.1016/j.coastaleng.2006.04.003.

Komar, P.D., 1974. Beach Processes and Sedimentation. (429 pp.). Prentice-Hall, Englewood Cliffs, NJ.

Larson, M., Kraus, N.C., 1992. Dynamics of longshore bars. Paper Presented at 23rd International Conference on Coastal Engineering. American Society of Civil Engineers, Venice, Italy.

Lippmann, T.C., Holman, R.A., 1990. The spatial and temporal variability of sand bar morphology. J. Geophys. Res. 95 (C7), 11575–11590. https://doi.org/10.1029/JC095iC07p11575.

Lippmann, T.C., Holman, R.A., Hathaway, K.K., 1993. Episodic, nonstationary behavior of a double bar system at Duck, North Carolina, U.S.A., 1986–1991. J. Coast. Res. SI 15, 49–75.

Mariño-Tapia, I.J., O'Hare, T.J., Russell, P.E., Davidson, M.A., Huntley, D.A., 2007. Cross-shore sediment transport on natural beaches and its relation to sandbar migration patterns: 2. Application of the field transport parameterization. J. Geophys. Res. 112, C03002. https://doi.org/10.1029/2005JC002894.

Masselink, G., Austin, M., Scott, T., Poate, T., Russell, P., 2014. Role of wave forcing, storms and NAO in outer bar dynamics on a high-energy, macro-tidal beach. Geomorphology 226, 76–93. https://doi.org/10.1016/j.geomorph.2014.07.025.

Ojeda, E., Guillén, J., Ribas, F., 2011. Dynamics of single-barred embayed beaches. Mar. Geol. 280, 76–90. https://doi.org/10.1016/j.margeo.2010.12.002.

Ostrowski, R., Pruszak, Z., Zeidler, R.B., 1991. Multi-scale nearshore and beach changes. Paper Presented at 22nd International Conference on Coastal Engineering. American Society of Civil Engineers, Delft, The Netherlands https://doi.org/10.1061/9780872627765.161.

Pape, L., Plant, N.G., Ruessink, B.G., 2010. On cross-shore migration and equilibrium states of nearshore sandbars. J. Geophys. Res. 115, F03008. https://doi.org/10.1029/2009JF001501.

Phillips, M.S., Harley, M.D., Turner, I.L., Splinter, K.D., Cox, R.J., 2017. Shoreline recovery on wave-dominated sandy coastlines: the role of sandbar morphodynamics and nearshore wave parameters. Mar. Geol. 385, 146–159. https://doi.org/10.1016/j.margeo.2017.01.005.

Plant, N.C., Holman, R.A., Freilich, M.H., Birkemeier, W.A., 1999. A simple model for interannual sandbar behaviour. J. Geophys. Res. 104, 15755–15776. https://doi.org/10.1029/1999JC900112.

Plant, N.G., Freilich, M.H., Holman, R.A., 2001. Role of morphologic feedback in surf zone sandbar response. J. Geophys. Res. 106 (C1), 973–989. https://doi.org/10.1029/2000JC900144.

Price, T.D., Ruessink, B.G., Castelle, B., 2014. Morphological coupling in multiple sandbar systems – a review. Earth Surf. Dyn. 2 (1), 309–321. https://doi.org/10.5194/esurf-2-309-2014.

Ranasinghe, R., Symonds, G., Black, K., Holman, R., 2004. Morphodynamics of intermediate beaches: a video imaging and numerical modelling study. Coast. Eng. 51 (7), 629–655. https://doi.org/10.1016/j.coastaleng.2004.07.018.

Ruessink, B.G., Kroon, A., 1994. The behaviour of a multiple bar system in the nearshore zone of Terschelling, the Netherlands: 1965–1993. Mar. Geol. 121, 187–197. https://doi.org/10.1016/0025-3227(94)90030-2.

Ruessink, B.G., Wijnberg, K.M., Holman, R.A., Kuriyama, Y., Van Enckevort, I.M.J., 2003. Intersite comparison of interannual nearshore bar behavior. J. Geophys. Res. 108, 3249. https://doi.org/10.1029/2002JC001505.

Ruessink, B.G., Coco, G., Ranasinghe, R., Turner, I.L., 2007. Coupled and noncoupled behavior of three-dimensional morphological patterns in a double sandbar system. J. Geophys. Res. 112, C07002. https://doi.org/10.1029/2006JC003799.

Ruessink, B.G., Pape, L., Turner, I.L., 2009. Daily to interannual cross-shore sandbar migration: observation from a multiple sandbar system. Cont. Shelf Res. 29, 1663–1677. https://doi.org/10.1016/j.csr.2009.05.011.

Ruessink, B.G., Blenkinsopp, C., Brinkkemper, J.A., Castelle, B., Dubarbier, B., Grasso, F., Puleo, J.A., Lanckriet, T., 2016. Sandbar and beach-face evolution on a prototype coarse sandy barrier. Coast. Eng. 113, 19–32. https://doi.org/10.1016/j.coastaleng.2015.11.005.

Ruggiero, P., Walstra, D.J.R., Gelfenbaum, G., Van Ormondt, M., 2009. Seasonal-scale nearshore morphological evolution: field observations and numerical modelling. Coast. Eng. 56, 1153–1172. https://doi.org/10.1016/j.coastaleng.2009.08.003.

Ruiz de Alegría-Arzaburu, A., Vidal-Ruiz, J.A., 2018. Beach recovery capabilities after El Niño 2015–2016 at Ensenada Beach, Northern Baja California. Ocean Dyn. (6), 749–759 https://doi.org/10.1007/s10236-018-1164-6.

Ruiz de Alegria-Arzaburu, A., García-Nava, H., Gil-Silva, E., Desplán-Salinas, G., 2015. A morphodynamic comparison of walled and non-walled beach sections, Ensenada beach, Mexico. Paper Presented at 8th International Conference on Coastal Sediments, San Diego, California https://doi.org/10.1142/9789814689977_0018.

Ruiz de Alegria-Arzaburu, A., Vidal-Ruiz, J.A., García-Nava, H., Romero-Arteaga, A., 2017. Seasonal morphodynamics of the subaerial and subtidal sections of an intermediate and mesotidal beach. Geomorphology 295, 383–392. https://doi.org/10.1016/j.geomorph.2017.07.021.

Sallenger, A.H., Holman, R.A., Birkemeier, W.A., 1985. Storm-induced response of a nearshore-bar system. Mar. Geol. 64, 237–257. https://doi.org/10.1016/0025-3227(85)90107-0.

Senechal, N., Coco, G., Castelle, B., Marieu, V., 2015. Storm impact on the seasonal shoreline dynamics of a meso- to macrotidal open sandy beach (Biscarrosse, France). Geomorphology 228, 448–461. https://doi.org/10.1016/j.geomorph.2014.09.025.

Shand, R.D., Bailey, D.G., Shepherd, M.J., 1999. An inter-site comparison of net offshore bar migration characteristics and environmental conditions. J. Coast. Res. 15, 750–765.

Shepard, F.P., 1950. Beach cycles in southern California. Beach Erosion Board (Technical Memo 20). US Army Corps of Engineering, Washington DC.

Short, A.D., 1999. Handbook of Beach and Shoreface Morphodynamics. John Wiley and Sons, Chichester, UK.

Smit, M.W.J., Reniers, A.J.H.M., Stive, M.J.F., 2012. Role of morphological variability in the evolution of nearshore sandbars. Coast. Eng. 69, 19–28. https://doi.org/10.1016/j.coastaleng.2012.05.005.

Splinter, K.D., Gonzalez, M.V.G., Oltman-Shay, J., Rutten, J., Holman, R., 2018. Observations and modelling of shoreline and multiple sandbar behaviour on a high-energy mesotidal beach. Cont. Shelf Res. 159, 33–45. https://doi.org/10.1016/j.csr.2018.03.010.

Tătui, F., Vespremeanu-Stroe, A., Ruessink, B.G., 2016. Alongshore variability of cross-shore bar behavior on a nontidal beach. Earth Surf. Process. Landf. 41 (14), 2085–2097. https://doi.org/10.1002/esp.3974.

Thiébot, J., Idier, D., Garnier, R., Falqués, A., Ruessink, B.G., 2012. The influence of wave direction on the morphological response of a double sandbar system. Cont. Shelf Res. 32, 71–85. https://doi.org/10.1016/j.csr.2011.10.014.

Van de Lageweg, W.I., Bryan, K.R., Coco, G., Ruessink, B.G., 2013. Observations of shoreline–sandbar coupling on an embayed beach. Mar. Geol. 344, 101–114. https://doi.org/10.1016/j.margeo.2013.07.018.

Van Enckevort, I.M.J., Ruessink, B.G., 2003. Video observations of nearshore bar behaviour. Part 1: alongshore uniform variability. Cont. Shelf Res. 23, 501–512. https://doi.org/10.1016/S0278-4343(02)00234-0.

Van Maanen, B., de Ruiter, P.J., Coco, G., Bryan, K.R., Ruessink, B.G., 2008. Onshore sandbar migration at Tairua Beach (New Zealand): numerical simulations and field measurements. Mar. Geol. 253, 99–106. https://doi.org/10.1016/j.margeo.2008.05.007.

Walstra, D.J.R., Ranasinghe, R., Roelvink, J.A., Ruessink, B.G., 2012. On bar growth and decay during interannual net offshore migration. Coast. Eng. 60, 190–200. https://doi.org/10.1016/j.coastaleng.2011.10.002.

Wright, L.D., Short, A.D., 1984. Morphodynamic variability of surf zones and beaches: a synthesis. Mar. Geol. 56, 93–118. https://doi.org/10.1016/0025-3227(84)90008-2.

Wright, L.D., Short, A.D., Green, M.O., 1985. Short-term changes in the morphodynamics states of beaches and surf zones: an empirical predictive model. Mar. Geol. 62, 339–364.

SHORELINE VARIABILITY RELATED TO SANDBAR MORPHOMETRICS ON A SINGLE-BARRED BEACH IN NW BAJA CALIFORNIA

JESÚS ADRIÁN VIDAL-RUIZ[1], AMAIA RUIZ DE ALEGRIA-ARZABURU[1*]

1. *Instituto de Investigaciones Oceanológicas, Universidad Autónoma de Baja California, 22860 Ensenada, México. adrian.vidal@uabc.edu.mx; amaia@uabc.edu.mx. *corresponding author.*

Abstract: Surfzone sandbars contain large amount of sediment that is usually transferred to the subaerial beach during low-energy wave conditions. This study investigates the relation between shorelines and sandbar positions and volumes on a single-barred beach in NW Baja California (Mexico). Four years (August 2014 to September 2018) of monthly topographic and bathymetric measurements and hourly wave data were used for this purpose. Shorelines and sandbar volumes were inversely correlated and evolved in phase. Maximum shoreline progradation occurred when the beach was unbarred. Largest sandbar volumes were associated with major shoreline retreats that took place during high-energy wave conditions. The magnitude of shoreline progradation during the low-energy wave period depended on the offshore sandbar location at the end of the preceding high-energy wave period.

Introduction

Beaches are very dynamic, experience dramatic spatio-temporal changes at different scales (Wright and Short 1984) and, understanding their cross-shore and alongshore morphological response to the wave action is a highly complex time-dependent phenomenon (e.g. Hanson and Kraus 1989; Larson and Kraus 1995). From a management perspective, there is an urgent need to understand the long-term behavior of beaches to enable the assessment of whether they are stable, or progressively either eroding or accreting. Ideally, long-term frequent (monthly or quarterly) and longshore distributed accurate beach profile data are needed, but often such data are only available over the short-term. Consequently, the evaluation of the stability of beaches is often undertaken based upon the interpretation of shoreline variabilities over the time (e.g., Miller and Dean 2004; Ruiz de Alegria-Arzaburu et al. 2010).

Coastal managers have relied on observations of the location of historic shorelines and their variability in time to evaluate coastal retreat and define management strategies (Smith and Zarillo 1990; Morton 1991; Boak and Turner 2005; Davidson and Turner 2009). Beach erosion and deposition, however, is a highly three-dimensional phenomenon, thus, determining these changes from one-dimension data (i.e. shorelines) is not necessarily correct (Morton et al. 1993). Surfzone sandbars contain large amounts of sediment and, in some

beaches, their cross-shore movement is highly modulated by the incoming wave energy (Shepard 1950; Komar 1974). That is the case of Ensenada Beach (NW Baja California), where the subaerial recovery completely depends on the onshore migration of the subtidal sandbar and weld to the shoreline (Ruiz de Alegria-Arzaburu and Vidal-Ruiz 2018).

This study investigates the correlation between the 0.5 m shoreline (above mean low low-tide level) and the morphometric variability of the surfzone sandbar (i.e. position and volume) over a four-year period. If good correlation between the shoreline position and sandbar location and geometry is encountered, a behavioral type model (e.g. Davidson and Turner 2009; Blossier et al. 2017; Splinter et al. 2018) could be used to predict sandbar morphometrics in relation to the incident wave conditions, and to ultimately envisage the capabilities of recovery of the subaerial beach after the impact of storms.

Methods

Morphological data consisting of shoreline positions and sandbar morphometrics were obtained from August 2014 to September 2018 along nearly 3,000 m of beach length in Ensenada Beach. In addition, nearshore wave conditions were measured and the total energy flux was calculated for the study period.

Field site

Ensenada, is a single-barred intermediate and mesotidal beach located in the northwestern Pacific coast of the Baja California peninsula in Mexico (Figure 1).

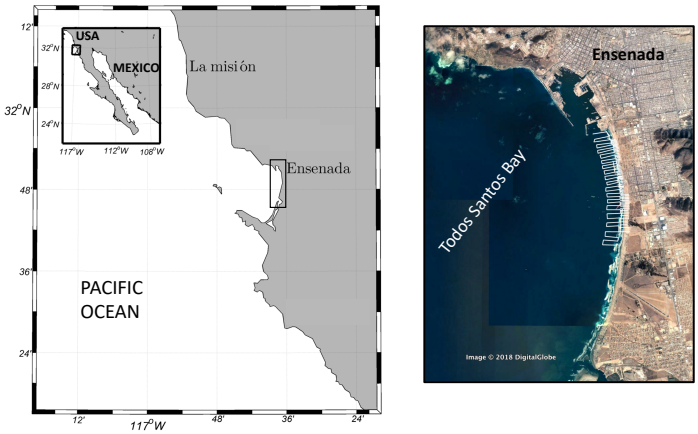

Fig. 1. Location of Ensenada Beach within Todos Santos Bay in NW Baja California, Mexico (right panel). The white lines on the aerial image represent measured topo-bathymetric profiles (left panel).

The beach is made of medium sand (D_{50} of 0.25 mm) and has a gently sloping beachface (tanß of 0.025). The incoming yearly averaged wave conditions are of medium-energy, characterized by significant wave height, H_s, of 1m with an associated peak wave period, T_p, of 11 s and shore normal incidence. The beach presents high seasonality in response to the incident wave conditions, and cross-shore sediment transport dominance over the longshore (Ruiz de Alegria-Arzaburu et al. 2017).

Nearshore waves

Hourly wave conditions were measured at 20 m depth using a bottom mounted acoustic Doppler current profiler, and data collected since October 2013 indicate highly seasonal wave incidence (Ruiz de Alegria-Arzaburu and Vidal-Ruiz 2018). Low-energy wave conditions (T_p of 9 s and $H_s < 0.7$ m) prevail between May and October, while longer ($T_p > 13$ s) and larger ($H_s > 1.3$ m reaching 2 m) waves exist between November and April (Figure 2). High-energy wave conditions occurred during the El Niño 2015–2016 winter (Hs>4 m, Tp ≈ 17 s; Figure 2) (Ruiz de Alegria-Arzaburu and Vidal-Ruiz 2018).

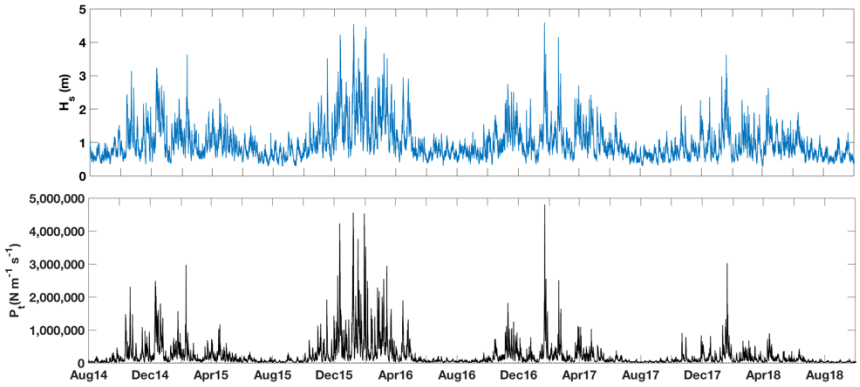

Fig. 2. Time-series of significant wave height (H_s; top panel) and the total energy flux (P_t; bottom panel) from August 2014 to November 2018 at Ensenada Beach.

Shoreline extraction

Monthly shorelines were extracted from 50-m spaced 61 topographic profiles measured along the nearly 3,000 m beach length. Details on the methods to collect the topographic data and calculate subaerial volumes are provided in Ruiz de Alegría-Arzaburu et al. (2017). The 0.5-m contourline above the mean low low-tide level was considered an adequate shoreline because of being well correlated with intertidal and total subaerial beach volumes (Figure 3). The averaged shoreline was calculated for the 4-year study period, and this was subtracted to all measured shorelines, in order to calculate the evolution of temporarily de-meaned shorelines.

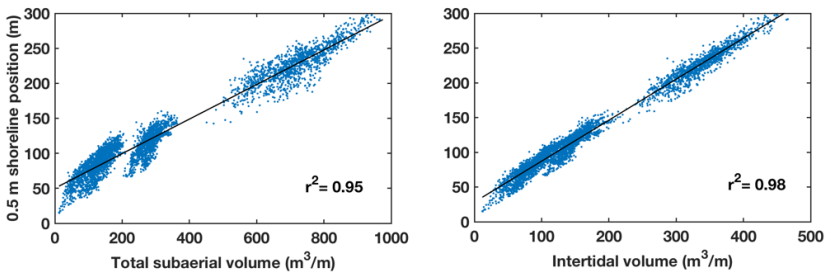

Fig. 3. Linear regression of the 0.5-m shoreline position *vs* total and intertidal beach volumes from August 2014 to August 2017.

Sandbar morphometrics

Monthly measured bathymetric data comprised 100-m spaced profiles (see Figure 1) measured until the depth of closure (around 10 m). Sandbar crest cross-shore positions and volumes per linear meter were calculated from the profiles over the 4-year period using the September 2014 survey as reference. Further details on the methods to collect the bathymetric data and extract the morphometric parameters are provided in Ruiz de Alegría-Arzaburu et al. (2017) and Ruiz de Alegría-Arzaburu and Vidal-Ruiz (2018).

Results

Alongshore-averaged shorelines and sandbar volumes

Shoreline positions and sandbar volumes were alongshore-averaged and de-meaned over the 4-year period between August 2014 and September 2018 (Figure 4). Sandbar volumes and shoreline positions were found to be inversely correlated. Sandbar volumes increased and shorelines retreated during the energetic wave conditions (Figures 2 and 4). In contrast, sandbar volumes diminished during the spring and summer mild wave conditions (Figure 2), allowing the progradation of the shoreline (Figure 4). The largest shoreline progradation occurred when the beach was unbarred, while the largest shoreline retreat took place after the energetic El Niño 2015-2016 winter (Figures 2 and 4). The degree of similarity between the de-meaned shoreline positions and sandbar volumes was investigated through a cross-shore correlation analysis, and best correlations were obtained with a lag of 0 (Figure 4).

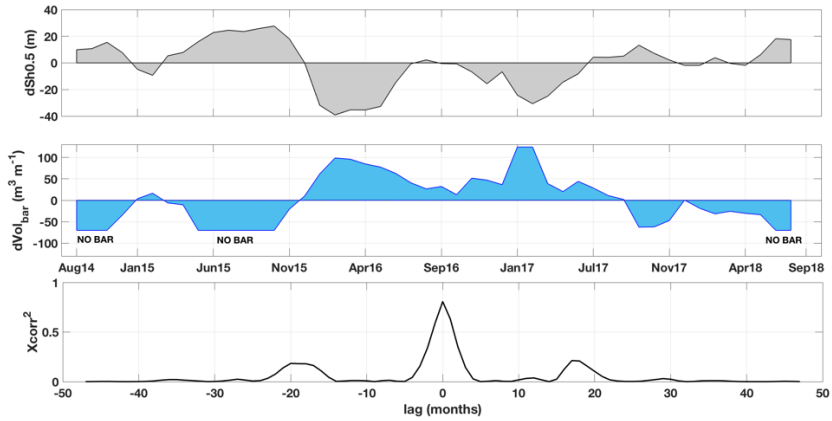

Fig. 4. Alongshore-averaged de-meaned 0.5-m shoreline (upper panel) and de-meaned sandbar volume (middle panel) evolution from August 2014 to September 2018. The cross-correlation of both variables for the same period of time is presented in the bottom panel.

Spatio-temporal variability of shoreline and sandbar positions

Figure 5 presents the temporal evolution of de-meaned shoreline positions for the 4-year study period. During the first year (August 2014 to August 2015), shoreline progradation (summer) and retreat (winter) were of similar magnitude.

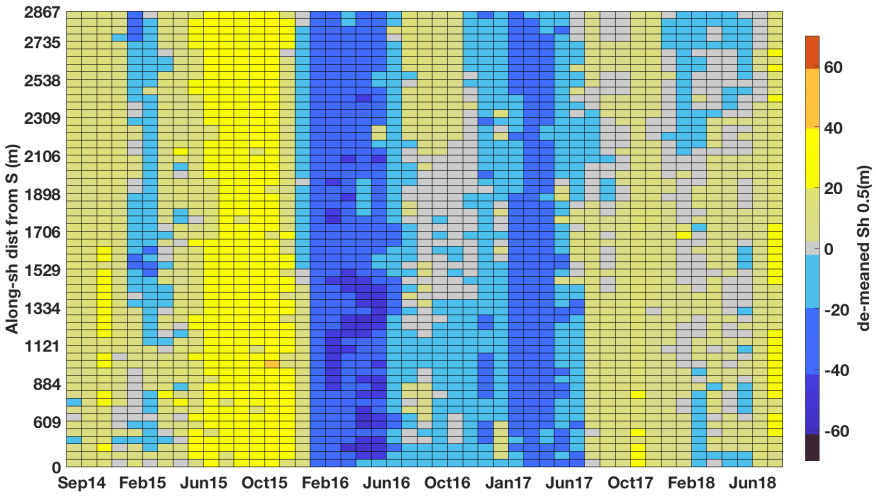

Fig. 5. Temporal evolution of de-meaned 0.5-m shoreline positions from August 2014 to September 2018.

The largest shoreline retreat occurred during the 2015-2016 El Niño winter, and over the following summer, the shoreline was unable of progradating like it did in 2015 (Figure 5). Overall, cross-shore shoreline displacements were quasi-uniform alongshore. During the energetic El Niño winter, however, the shoreline retreated more in the southern half than in the northern half of the beach. Consequently, the shoreline progradation during the following summer was larger in the northern beach (Figure 5).

The alongshore variability of sandbar crest positions (relative to the reference shoreline, 0-m) is represented in Figure 6 for the 4-year study period. Significant alongshore variations in the cross-shore sandbar crest positions exist. During the first year (August 2014 to August 2015), the sandbar migrated offshore in winter and onshore in summer, becoming an unbarred beach by the 2015 summer. The largest offshore sandbar crest displacements occurred during the El Niño 2015-2016 winter (Figure 6). During the 2016 summer, significant landward sandbar migrations occurred only at some specific locations (1,100 m, 1920 m and 2,700 m alongshore). The most evident onshore sandbar displacement occurred at the beginning of the 2017 winter (most clearly at the northern section), but it rapidly migrated offshore after the incidence of an

energetic storm in late January 2017 (Figure 2). The sandbar was able to weld to the shoreline in September 2018, and the beach became unbarred.

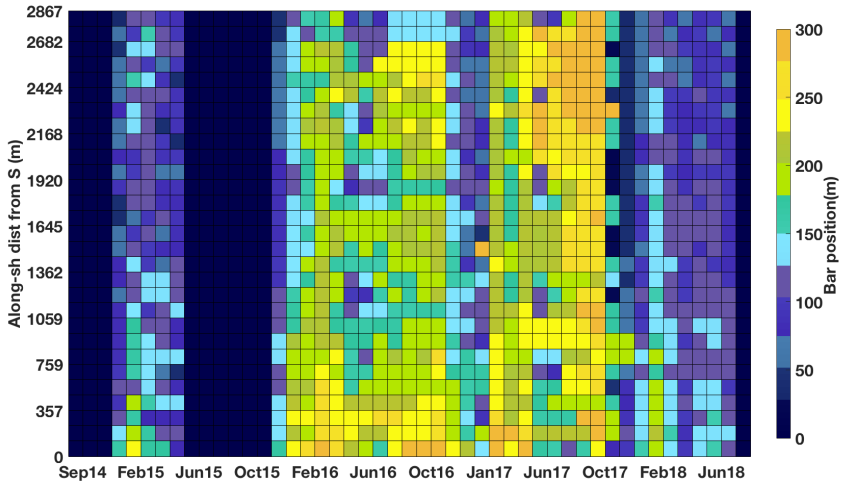

Fig. 6. Temporal evolution of cross-shore sandbar crest position (offshore distance from the September 2014 reference shoreline) from August 2014 to September 2018. Unbarred beach conditions correspond to 0-m bar positions (reference shoreline).

Conclusion

Sandbar volumes and shoreline positions were inversely correlated, and evolved in phase. Maximum shoreline progradation occurred when the beach was unbarred, associated with low-energy wave conditions. In contrast, largest sandbar volumes were obtained during major shoreline retreats associated with high-energy wave conditions. The energetic El Niño 2015-2016 winter induced higher shoreline retreat in the southern beach and the sandbar displaced farther offshore. Consequently, the shoreline progradation was smaller than in the northern beach during the subsequent summer. Thus, the magnitude of shoreline progradation during the low-energy wave period depended on the offshore sandbar location at the end of the preceding high-energy wave period.

Acknowledgements

The contribution of the MORDICS group (http://mordics.org) is acknowledged. The authors are grateful to CONACyT for the funding provided through CB-2014-238765 and for the PhD scholarship provided to J.A.V-R.

References

Blossier, B., Bryan, K.R., Daly, C.J., Winter, C. (2017). "Shore and bar cross-shore migration, rotation, and breathing processes at an embayed beach.", *Journal of Geophysical Research Earth Surface*, 122, 1745–1770.

Boak, E. H. and Turner, I. L. (2005), 'Shoreline definition and detection: a review', *Journal of Coastal Research* 21(4), 688–703.

Davidson, M. A. and Turner, I. L. (2009), 'A behavioral template beach profile model for predicting seasonal to interannual shoreline evolution', *Journal of Geophysical Research-Earth Surface* 114.

Hanson, H. and Kraus, N. (1989), "GENESIS - generalized model for simulating shoreline change." *Tech. Report CERC-89-19 USAE-WES*, Coastal Engineering Research Centre, Vicksburg, Miss.

Komar, P. D. (1974), "Beach Processes and Sedimentation". Englewood Cliffs, NJ: 519 Prentice-Hall, 429pp.

Larson, M. and Kraus, N.C., (1995). "Prediction of cross-shore sediment transport at different spatial and temporal scales.", *Marine Geology*, 126 (1–4), 111–127.

Miller, J. K. and Dean, R. G., (2004). "A simple new shoreline change model", *Coastal Engineering*, 51(7), 531–556.

Morton, R. A. (1991), 'Accurate shoreline mapping: past, present, and future', *Coastal Sediments'91* 1, 997–1010.

Morton, R.A., Leach, M.P., Paine, J.G., Cardoza, M.A., (1993). "Monitoring beach changes using GPS surveying techniques", *Journal of Coastal Research* 9(3), 702–720.

Ruiz de Alegria-Arzaburu, A., Pedrozo-Acuña, A., Horrillo-Caraballo, J.M., Masselink, G. and Reeve, D. (2010). "Determination of wave-shoreline

dynamics on a macrotidal gravel beach using Canonical Correlation Analysis", *Coastal Engineering*, 57, 290–303.

Ruiz de Alegria-Arzaburu, A., Vidal-Ruiz, J.A., García-Nava, H., Romero-Arteaga, A., (2017). "Seasonal morphodynamics of the subaerial and subtidal sections of an intermediate and mesotidal beach.", *Geomorphology*, 295, 383–392.

Ruiz de Alegría-Arzaburu, A., Vidal-Ruiz, J.A., (2018). "Beach recovery capabilities after El Niño 2015–2016 at Ensenada Beach, Northern Baja California.", *Ocean Dynam*ics, 6, 749–759.

Shepard, F.P., (1950). "Beach cycles in southern California." *Beach Erosion Board (Technical Memo 20)*. Washington DC: US Army Corps of Engineering.

Smith, G. L. and Zarillo, G. A. (1990), 'Calculating long-term shoreline recession rates using aerial photographic and beach profiling techniques', *Journal of Coastal Research* 6(1), 111–120.

Splinter, K.D., Gonzalez, M.V.G., Oltman-Shay, J., Rutten, J., Holman, R., (2018). "Observations and modelling of shoreline and multiple sandbar behaviour on a high-energy meso-tidal beach.", *Continental Shelf Research*, 159, 33–45.

Wright, L.D., Short, A.D., (1984). "Morphodynamic variability of surf zones and beaches: a synthesis. ", *Marine Geology*, 56, 93–118.